UNIVERSITÉ DE STRASBOURG

ÉCOLE DOCTORALE DES SCIENCES CHIMIQUES

UMR 7200-Laboratoire d'Innovation Thérapeutique

THÈSE

présentée par

Iuliia KARPENKO

soutenue le **16 octobre 2014**

pour obtenir le grade de

Docteur de l'Université de Strasbourg

Discipline / Spécialité : Chimie biologique thérapeutique

Conception, synthèse et évaluation de sondes fluorescentes et de radioligands TEP des récepteurs de l'ocytocine et de la vasopressine.

THÈSE dirigée par :

HIBERT Marcel	Professeur, Université de Strasbourg

RAPPORTEURS :

ACHER Francine	Docteur, Université Paris Descartes
RENARD Pierre-Yves	Professeur, Université de Rouen

AUTRES MEMBRES DU JURY :

DURROUX Thierry	Docteur, Université de Montpellier, INSERM
BOLZE Frédéric	Docteur, Université de Strasbourg
BONNET Dominique	Docteur, Université de Strasbourg

List of content

Remerciements

Au terme de ce travail je tiens à remercier chaleureusement le Prof. Marcel Hibert, mon directeur de thèse, de m'avoir confié ce sujet passionnant. Je te remercie pour ton enthousiasme, ton positivisme et ta foi en moi, pour tout ce que tu m'as appris ainsi que pour le temps que tu m'as consacré. Je remercie tout particulièrement le Dr. Dominique Bonnet pour m'avoir encadré tout au long de ma thèse. Merci pour ta disponibilité, tes conseils précieux qui m'ont fait avancer à grands pas, merci d'avoir toujours été un exemple du chercheur que je veux devenir.

Je tiens à remercier le Dr. Francine Acher, le Prof. Pierre-Yves Renard, le Dr. Thierry Durroux et le Dr. Frédéric Bolze qui me font le très grand honneur de juger ce travail.

Je remercie particulièrement le Dr. Thierry Durroux qui m'a accueilli au sein de son équipe de l'Institut de Génomique Fonctionnelle. Je vous remercie pour le temps que vous m'avez consacré et pour vos conseils éclairés (de s'arrêter, d'analyser et de réfléchir !). Mes pensées vont à toute la communauté des Montpelliérains : le Dr. Bernard Mouillac, le Dr. Christiane Mendre, le Dr. Jean-Philippe Pin, le Dr. Sébastien Granier. Je remercie le Dr. Damien Maurel pour ces explications et formations et ces encouragement pour mon futur post-doc ! Je pense également à ceux qui sont devenus mes amis pendant ce temps (toujours court !) à Montpellier et qui ont rendu mon séjour inoubliable : Amandine, Thiéric, Sarah, Elvira, Iulia (oui, on est au moins deux !), Walid, Abdarazak.

Le travail présenté dans ce manuscrit est le fruit de nombreuses collaborations que j'aimerais saluer ici. Merci à tout l'équipe Biophotonique des interactions moléculaires et cellulaires de l'UMR 7213 et tout particulièrement au Dr. Andrey Klymchenko pour tous ces conseils et tout ce qu'il m'a appris (la spectroscopie, la microscopie confocale et FLIM, les temps de vie et beaucoup d'autre)! Je remercie également les membres de la Plate-forme de Chimie Biologique Intégratif de Strasbourg, notamment le Dr. Pascal Villa, Christel Valencia et Sophie Gioria. Mes remerciements vont également au Dr. Aline Nonat et au Dr. Loïc Charbonnière du Laboratoire d'Ingénierie Moléculaire Appliquée à l'Analyse qui nous ont faits bénéficier du nouveau complexant du Tb et qui m'ont accueillis au sein de son laboratoire pour les études spectrales. Mes pensées vont à l'équipe de radiochimie du Dr. Thierry Billars et à l'équipe de neurochimie dirigé par le Prof. Luc Zimmer.

Je tiens à remercier chaleureusement tous les membres du Laboratoire d'Innovation Thérapeutique pour m'avoir si aimablement accueilli. Il m'a été très agréable de travailler en compagnie de Stéphanie, Pierre, Elsa, Maria, Corinne, Jeff. Je tiens à les remercier pour leur soutien, les petits moments joyeux et leurs conseils ainsi que leur aide dans mes synthèses. Merci beaucoup à Steph qui m'a amélioré tous mes rendements ☺!

Je souhaiterais remercier toute l'équipe du service commun d'analyse : le Dr. Patrick Wehrung, Pascale Buisine, Cyril Antheaume, le Dr. Justine Viéville.

Je veux dire un énorme merci à nos secrétaires Françoise et Marianne pour leur disponibilité et leur aide !

Un énorme merci à mon Papa et à ma Maman pour leurs soutien, amour et conseils dans les moments difficiles.

Merci à mes amis qui ont toujours été là pour moi : ma meilleure colloc Marianna, Sergii, Lesia, Marian, Katya, Ira, Alex (merci pour m'avoir ouvert le monde de la culture et de l'art !), Maria, Dasha et beaucoup d'autres… Je m'abstiens de les nommer tellement la liste est longue.

Je suis très heureuse et chanceuse d'avoir pu partager ces moments avec Dmytro, qui est toujours là pour moi, même s'il est loin. Merci de m'avoir écouté et supporté, merci pour tes conseils précieux et tes encouragements dans les moments difficiles !

To my Dmytro

List of abbreviations

- 5-SFX – 6-(fluorescein-5-carboxamido)hexanoic acid, succinimidyl ester
- Ac – acetyl
- AC – accessory nucleus
- ACN – acetonitrile
- ACTH – adrenocorticotropic hormone
- ASD – autism spectrum disorders
- ATP – adenosine triphosphate
- AVP – arginine vasopressin
- AVPR – arginine vasopressin receptor
- B_{max} – maximum density of receptors
- Bn – benzyl
- Boc – *tert*-butyloxycarbonyl
- BSA – bovine serum albumin
- BST – bed nucleus of the stria terminalis
- BTSA – *N*,*O*-bis(trimethylsilyl)acetamide
- CA - *Cornu Ammonis*
- cAMP – cyclic adenosine monophosphate
- CBT – carbetocin
- CNS – central nervous system
- CT – computed tomography
- DAG – diacylglycerol
- DBU – 1,8-diazabicycloundec-7-ene
- DCM – dichloromethane
- DIC – *N*,*N'*-diisopropylcarbodiimide
- DIEA – *N*,*N*-diisopropylethylamine
- DMAP – 4-dimethylaminopyridine
- DMF – *N*,*N*-dimethylformamide
- DNA – deoxyribonucleic acid
- DOPC – dioleoyl phosphatidyl choline
- EC_{50} – half maximal effective concentration
- EOB – end of bombardment
- EOS – end of synthesis
- eq. – equivalent
- *eV* – electron volt
- FCS – fluorescence correlation spectroscopy
- Fmoc – fluorenylmethyloxycarbonyl
- FRET – Förster resonance energy transfer
- GABA – *gamma*-aminobutyric acid
- GDP – guanosine diphosphate
- GFP – green fluorescent protein
- GPCR – G protein-coupled receptor
- GTP – guanosine triphosphate
- HBTU – *O*-(benzotriazol-1-yl)-*N,N,N′,N′*-tetramethyluronium hexafluorophosphate
- HOBt – 1-hydroxybenzotriazole hydrate
- HPLC – high-performance liquid chromatography
- HTS – high-throughput screening
- IP – intraperitoneal injection
- IV – intravenous injection
- IC_{50} – half maximal inhibitory concentration
- IP3 – inositol triphosphate
- K_d – dissociation constant
- K_i – inhibition constant
- logD – distribution-coefficient
- Mmt – 4-monomethoxytrityl
- mp – melting point
- MPS – methylphenylsulfide
- MRI – magnetic resonance imaging
- MS – mass spectroscopy
- MTBSTFA – *N*-*tert*-butyldimethylsilyl-*N*-methyltrifluoroacetamide
- Mtt – 4-monomethyltrityl
- NHS – *N*-hydroxysuccinimide
- NIR – near infrared
- NMP – 1-methyl-2-pyrrolidinone
- NR – Nile red
- OT – oxytocin
- OTR – oxytocin receptor

- PAMPA-BBB – parallel artificial membrane permeability assay for blood-brain barrier passage
- PDB – Protein Data Bank
- PEG – polyethylene glycol
- PET – positron emission tomography
- PG – protecting group
- Pip – piperidine
- pK_a –logarithmic acid dissociation constant
- PVN – hypothalamic paraventricular nucleus
- Py – pyridine
- PyBOP – benzotriazol-1-yl-oxytripyrrolidinophosphonium hexafluorophosphate
- QY – quantum yield
- r.t. – room temperature
- SON– supraoptic nucleus
- SPPS – solid-phase peptide synthesis
- SQ – squaraine
- SQpeg – core-pegylated squaraine
- S^{t}Bu – *tert*-butylthio
- TAS – taste receptor
- TBDMS – *tert*-butyldiphenylsilyl
- TFA – trifluoroacetic acid
- THF – tetrahydrofuran
- TIS – triethylsilane
- TM – transmembrane helix
- TMS – trimethylsilyl
- TNBS – 2,4,6-trinitrobenzenesulfonic acid
- TR-FRET – time-resolved FRET
- Tris – tris(hydroxymethyl) aminomethane
- Ts – tosyl
- US – ultrasound
- UV – ultraviolet
- wt – wild-type

Résumé de thèse

Introduction

Les récepteurs couplés aux protéines G de l'ocytocine (OTR) et de la vasopressine (V_1aR) sont connus pour être impliqués dans la modulation de comportements sociaux complexes comme l'amour, l'attachement mère-enfant et adulte-adulte, l'altruisme, la générosité, la confiance.[1,2,3]

Depuis quelques années le système OT a été proposé comme une cible thérapeutique potentielle pour le traitement des troubles du spectre autistique (TSA), qui sont des troubles du développement humain caractérisés par des difficultés d'interaction sociale avec des comportements restreints et répétitifs. D'après les études conduites par les groupes d'Angela Sirigu et d'Eric Hollander, l'amélioration des interactions sociales a été observée lorsque l'ocytocine sous forme d'un spray nasal a été administrée chez les autistes.[4,5]

Afin d'étudier le rôle des récepteurs de l'ocytocine et de la vasopressine dans le développement des troubles du spectre autistique, de mieux comprendre leur pharmacologie et aussi d'établir de nouveaux tests de liaison sur les récepteurs sauvages, nous avons envisagé de développer des outils de détection et d'imagerie des récepteurs OTR et V_1aR *in vitro* et *in vivo*.

Pour caractériser la distribution d'OTR et de V_1aR *in vivo*, la tomographie par émission des positons (TEP) et une technique de choix. La détermination non-invasive de la distribution des récepteurs de l'OT et de l'AVP à l'aide de la TEP sera idéale pour faire la corrélation entre la densité et la distribution des récepteurs et les disfonctionnements cognitifs chez les patients avec TSA. De plus, des radioligands TEP sélectifs permettraient d'étudier *in vivo* la distribution et le métabolisme des nouveaux candidats cliniques ciblant OTR et V_1aR.

D'autre part, il est difficile d'imaginer une technique plus performante pour étudier les interactions ligand-récepteur *ex vivo* que la fluorescence. Grace à son caractère non-invasif et non-destructif, sa haute vitesse de réponse et sa versatilité, la fluorescence est couramment utilisée pour étudier l'architecture et le fonctionnement des RCPG. Nous avons envisagé de développer des sondes fluorescentes pour les récepteurs fusionnés au SNAP et également

[1] T. R. Insel, L. J. Young, Nat. Rev. *Neurosc*. **2001**, *2*, 129–36.
[2] M. Kosfeld, M. Heinrichs, P. J. Zak, U. Fischbacher, E. Fehr, *Nature* **2005**, *435*, 673–6.
[3] S. Israel, O. Weisel, R. P. Ebstein, G. Bornstein, *Psychoneuroendocrinology* **2012**, *37*, 1341–4.
[4] E. Andari, J.-R. Duhamel, T. Zalla, E. Herbrecht, M. Leboyer, A. Sirigu, *PNAS* **2010**, *107*, 4389–94.
[5] E. Anagnostou, L. Soorya, W. Chaplin, J. Bartz, D. Halpern, S. Wasserman, A. T. Wang, L. Pepa, N. Tanel, A. Kushki, E. Hollander, *Mol. Autism* **2012**, *3*, 16.

pour les récepteurs sauvages afin de valider le test de liaison TR-FRET sur OTR et aussi développer un test de liaison « non-radioactif » sur les récepteurs non-modifiés. Finalement, le dernier objectif de thèse était de développer un test de liaison « multicouleur » afin de tester en parallèle l'affinité de ligands sur plusieurs récepteurs.

Partie I. Radiotraceurs TEP pour les récepteurs de l'ocytocine OTR et de la vasopressine $V_{1a}R$

Les objectifs de la première partie de ma thèse ont été d'obtenir les premiers radioligands TEP efficaces pour les récepteurs OTR et V_1aR marqués ^{11}C et ^{18}F.

Nous avons synthétisé et caractérisé trois précurseurs déméthylés pour le marquage avec $[^{11}C]CH_3$ afin d'obtenir les analogues ^{11}C des médicaments déjà testés chez l'homme (Figure R1).

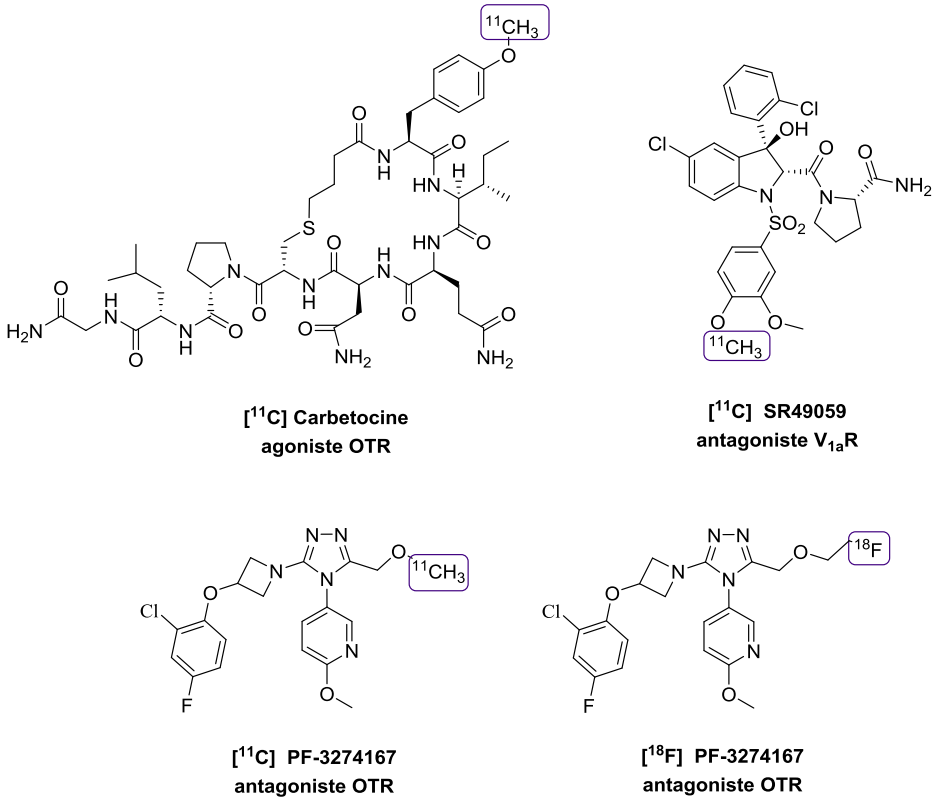

Figure R1. Radioligands envisagés pour les récepteurs de l'OT et de l'AVP.

Un précurseur, notamment celui de PF-3274167 a été marqué au ^{11}C par l'équipe du Dr. Thierry Billard (CERMEP, Bron) et ces études préliminaires sur les coupes de cerveau de rats ont été effectuées dans le groupe du Prof. Luc Zimmer (CERMEP, Bron). Bien que l'accumulation de la radioactivité dans les coupes de cerveau a bien été observée (Figure R2), les études de compétition avec le ligand froid ont montré que le marquage n'était malheureusement pas spécifique aux récepteurs de l'ocytocine. Cela peut être expliqué soit par l'affinité insuffisante du radioligand soit par de fortes interactions non-spécifiques.

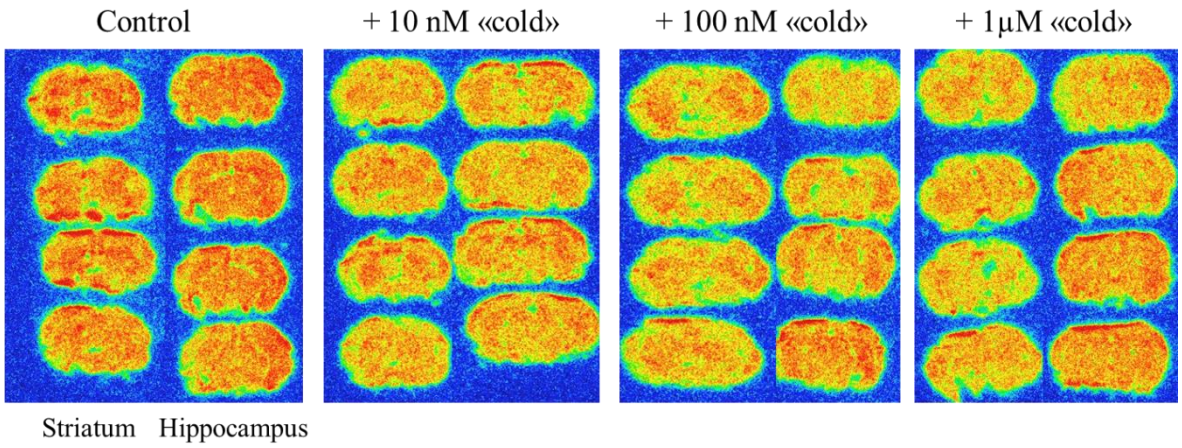

Figure R2. Autoradiographie sur les coupes de cerveau de rats avec [^{11}C]PF-3274167.

Ensuite, nous avons introduit un atome de fluor via la chaine latérale de PF-3274167 qui a rendu le ligand encore plus sélectif et affin pour OTR (Figure R1). L'analogue « chaud » ^{18}F, synthétisé par l'équipe du Dr. Thierry Billard à partir du précurseur tosylé **1.34** (Figure R3), a été capable de distinguer les régions du cerveau de rats avec des densités différentes d'OTR. L'optimisation de la procédure du marquage au ^{18}F ainsi que des études complémentaires du radioligand se poursuivent au centre d'imagerie CERMEP.

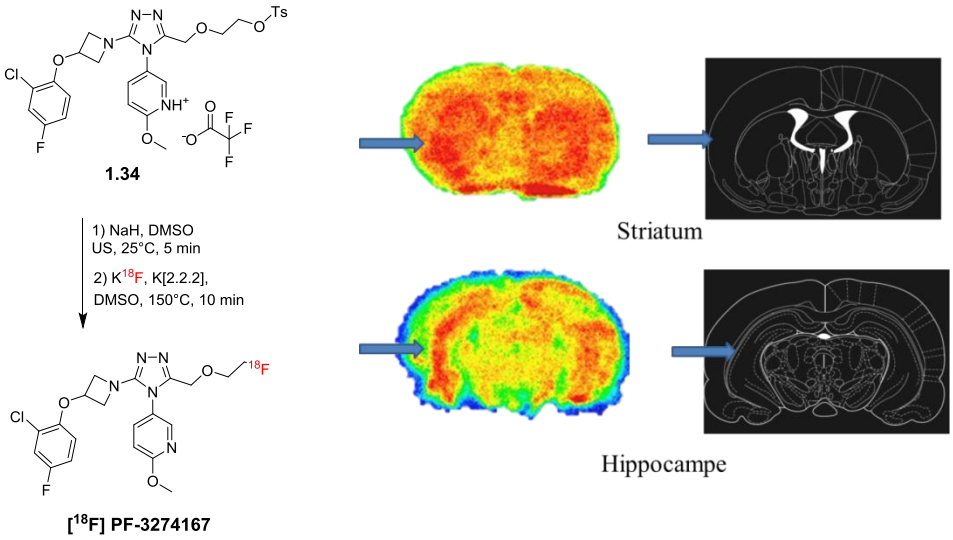

Figure R3. Radiosynthèse de [^{18}F] PF-3274167 et autoradiographie préliminaire sur les coupes de cerveau de rats.

Nous envisageons d'utiliser les radioligands développés pour étudier la distribution et le niveau d'expression d'OTR dans le modèle des macaques amoureux, développé par le groupe du Dr. Jean-René Duhamel (Institut des Sciences Cognitives de Lyon), et chez l'homme en collaboration avec le Dr. Angela Sirigu de l'Institut des Sciences Cognitives de Lyon.

Partie II. Sondes fluorescentes pour le récepteur de l'ocytocine OTR

Considérant les avantages de la fluorescence dans le suivi des interactions ligand-récepteur, nous avons envisagé de synthétiser des ligands fluorescents pour le récepteur de l'ocytocine d'une part pour établir un test de liaison TR-FRET sur OTR et, d'autre part, pour contribuer à la découverte de méthodes alternatives de suivi de liaison, particulièrement sur les récepteurs sauvages.

Chapitre 1. Sondes fluorescentes pour les études de liaison

Etudes de liaison par TR-FRET

La découverte de nouveaux ligands de RCPG nécessite l'utilisation de méthodes de criblage robustes et fiables pour caractériser les interactions ligand-récepteur. Le transfert

d'énergie par résonance de type Förster en temps résolu (TR-FRET) est une technique de choix qui combine les avantages du FRET classique (détection uniquement de la partie du ligand liée au récepteur ; possibilité de quantifier la liaison) avec la détection en temps résolu grâce à l'utilisation des complexes du Tb (III) comme donneurs d'énergie (Figure R4). Le principe des mesures en temps résolu est d'appliquer un délai entre le pulse d'excitation et la détection de l'émission afin de soustraire la fluorescence autocellulaire et augmenter le rapport signal sur bruit. La technique puissante de TR-FRET apporte des bénéfices pour le criblage à haute débit des RCPG sur une surface cellulaire.[6]

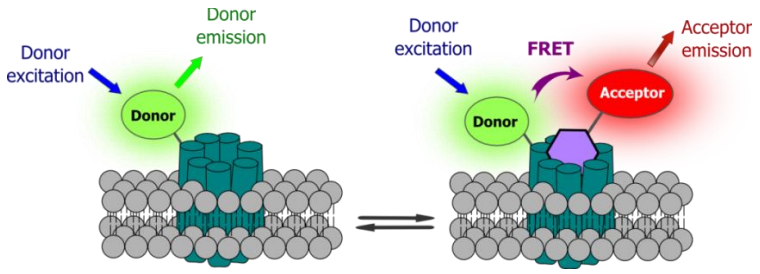

Figure R4. Principe de la détection de liaison ligand-récepteur par TR-FRET.

Ligands luminescents marqués au Tb(III)

Lors des dernières années, les complexes luminescents des lanthanides ont attiré un fort intérêt pour l'analyse biomédicale et l'imagerie à cause de leurs propriétés photophysiques exceptionnelles.[7] Le trait le plus remarquable de l'émission des lanthanides est leur temps de vie extrêmement long qui peut atteindre plusieurs millisecondes pour les complexes du Tb (III). Cet avantage est couramment utilisé dans les tests de criblage et dans l'imagerie en temps résolu, notamment les tests TR-FRET.

Pour avoir une alternative aux ligands marqués au Lumi4-Tb®, généralement utilisés dans les tests de liaison TR-FRET, nous avons synthétisé un conjugat de l'agoniste peptidique d'OTR, la carbétocine, avec un complexe du Tb développé précédemment par le groupe du Dr. Loïc Charbonnière de l'ECPM, Strasbourg[8] (Figure R5). Le test de liaison radioactive a confirmé une bonne affinité de la sonde luminescente pour le récepteur cible. Les études

[6] Degorce, F.; Card, A.; Soh, S.; Trinquet, E.; Knapik, G. P.; Xie, B. *Curr. Chem. Genomics* **2009,** *3*, 22-32.
[7] K. Hanaoka, *Chem. Pharm. Bull.* **2010**, *58*, 1283–1294.
[8] K. Nchimi-Nono, K.D. Wegner, S. Lindé, A. Lecointre, L. Ehret-Sabatier, S. Shakir, N. Hildebrandt, and L. J. Charbonnière, Org. Biomol. Chem. **2013**, *11*, 6493–6501.

photophysiques du ligand ont montré que ses propriétés spectrales ont satisfait tous les critères pour être utilisé comme donneur du FRET dans le test de liaison TR-FRET.

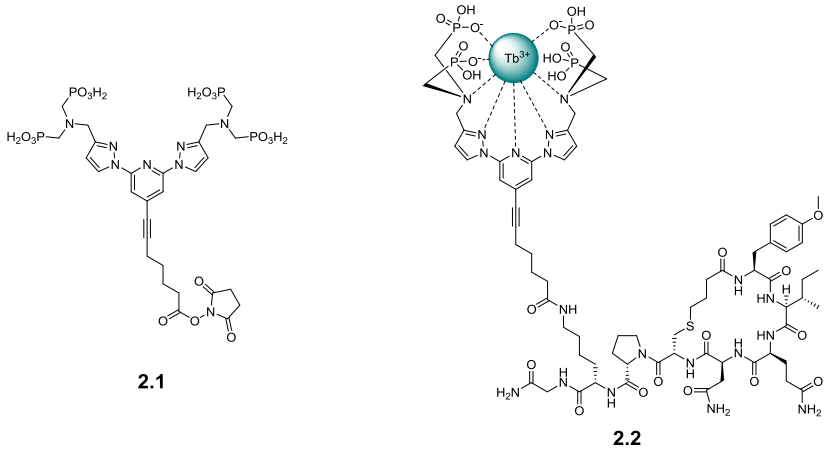

Figure R5. Le complexant du Tb (III) **2.1** et son conjugat avec la carbetocin **2.2**.

Premiers ligands fluorescents sélectifs OTR

Le prérequis pour le développement du test de liaison TR-FRET sur OTR est d'avoir des ligands fluorescents qui gardent les propriétés pharmacologiques du ligand non-marqué. A ce jour, les seules sondes fluorescentes pour étudier OTR sont des ligands peptidiques avec une stabilité limitée dans le milieu biologique. De plus, ces ligands ne sont pas sélectifs car ils se fixent également sur les récepteurs de la vasopressine

En introduisant les marqueurs fluorescents DY647 et la fluorescéine sur l'antagoniste OTR non-peptidique PF-3274167 via des chaines PEG de longueurs différentes, nous avons obtenu les premiers ligands fluorescents sélectifs OTR, qui possèdent de plus une forte affinité pour le récepteur.

Les ligands fluorescents nous ont permis de développer et de valider le test de liaison TR-FRET pour OTR. Cette méthode représente un outil efficace pour accélérer la découverte de ligands du récepteur cible.

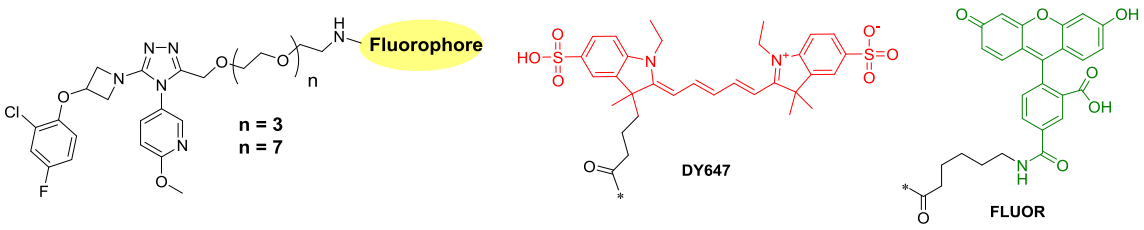

Figure R5. Dérivés fluorescents de PF-3274167.

Ligands turn-on pour les récepteurs natifs

Bien que la technique TR-FRET soit une approche efficace pour suivre la liaison ligand-récepteur dans des conditions homogènes, son inconvénient vient de la nécessité de modifier la structure du récepteur avec un donneur ou un accepteur de FRET. En effet, l'introduction de la GFP ou du SNAP-tag peut altérer la fonction du récepteur ou encombrer le site orthostérique. Il s'ensuit qu'il y a une forte demande pour une méthode homogène qui permettrait la détection et le suivi des interactions avec les récepteurs non-modifiés (sauvages).

En collaboration avec l'équipe du Dr. Andrey Klymchenko (LBP, Illkirch), nous avons proposé une approche turn-on pour étudier la liaison des ligands aux récepteurs. Cette méthode utilise des ligands fluorogènes, c'est-à-dire des molécules qui ne fluorescent pas dans l'eau mais qui fluorescent (« turn on ») lors de la fixation du ligand au récepteur qui permet à la sonde fluorescente d'interagir avec la membrane cellulaire lipidique (Figure R6).

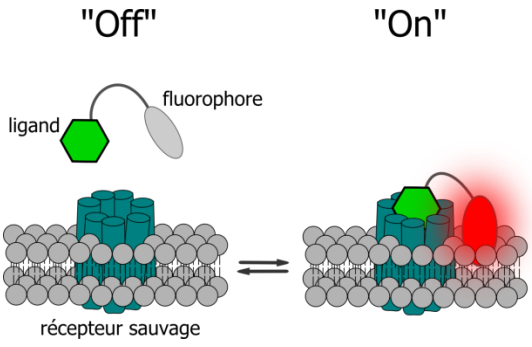

Figure R6. Principe de la détection de liaison ligand-récepteur par l'approche turn-on.

Ligands turn-on basés sur le Nile Rouge

Pour construire les premiers sondes fluorescentes turn-on pour OTR nous avons décidé de greffer un marqueur fluorogène Nile Rouge, qui est connu pour être non-fluorescent dans l'eau mais qui fluoresce fortement dans les membranes cellulaires, au ligand OTR peptidique la carbétocine via la chaine PEG8 hydrosoluble (Figure R7).

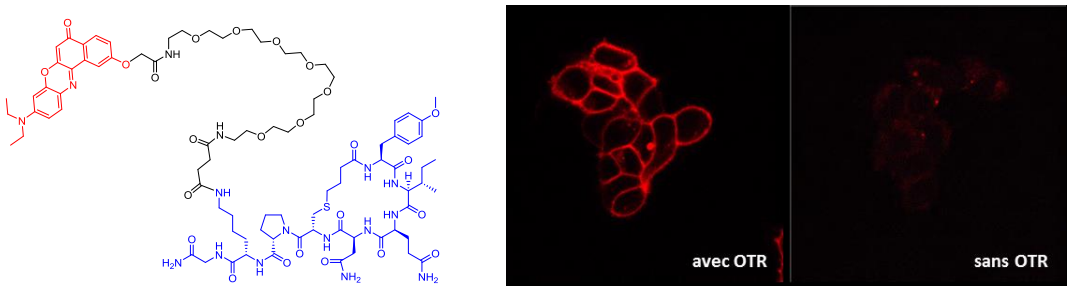

Figure R7. Structure du ligand turn-on basé sur le Nile Rouge et les images des cellules exprimant OTR.

Les propriétés fluorescentes de la sonde obtenue ont été similaires aux propriétés du fluorophore Nile Rouge. Le rendement quantique de la fluorescence augmente fortement quand le milieu aqueux est remplacé par un milieu apolaire. En même temps le maximum de fluorescence se déplace vers le bleu, ce qui a rendu l'effet turn-on encore plus important (≈ facteur 1000 entre l'eau et le dioxane). La chaine PEG joue un rôle très important pour diminuer les interactions non-spécifiques de la sonde avec les membranes cellulaires et les protéines plasmatiques.

La sonde turn-on nous a permis de visualiser les OTR sauvages sur les membranes de cellules vivantes dans des conditions homogènes sans aucun bruit de fond (Figure R7). De plus, nous avons montré que les sondes turn-on présentent une bonne alternative aux méthodes radioactives pour rapidement estimer le nombre de récepteurs sur la surface cellulaire.[9]

Ligands turn-on basés sur la squaraine

Etant encouragés par les premiers résultats des études cellulaires des sondes turn-on basées sur le Nile Rouge, nous nous sommes focalisés sur le développement de sondes turn-on qui

[9] Karpenko, I. A.; Kreder, R.; Valencia, C.; Villa, P.; Mendre, C.; Mouillac, B.; Mély, Y.; Hibert, M.; Bonnet, D.; Klymchenko, A. S. *Chembiochem* **2014**, *15*, 359–363.

absorbent et émettent dans la région proche infrarouge (PIR). Les avantages de travailler dans le PIR sont l'absence de l'autofluorescence cellulaire, la diminution de la diffraction de la lumière et la meilleure pénétration dans les tissus biologiques.

Nous étions intéressés par la classe des fluorophores « squaraines ». Grace à sa brillance exceptionnelle, au caractère spectral PIR et à leur synthèse directe, les squaraines sont couramment utilisées dans les domaines de la chimie des matériaux. Les exemples d'application des squaraines dans les études biologiques sont limités, principalement à cause de leur instabilité en présence de nucléophiles forts.

Nous avons montré que les squaraines du type « arylidenes » présentent une excellente stabilité dans le milieu biologique (protéines plasmatiques) et sont de plus caractérisées par une bonne stabilité photochimique. Ces propriétés nous ont permis de considérer les squaraines-arylidenes comme des fluorophores PIR prometteurs possédant un caractère fluorogène pour les études des RCPG.

Nous avons synthétisé une sonde fluorescente basée sur la squaraine pour l'OTR en utilisant toujours comme ligand peptidique la carbétocine (Figure R8). La sonde a été appliquée à la visualisation d'OTR fusionné à la GFP sur la membrane cellulaire avec une excellente sensibilité (Figure R8). La colocalisation des images dans le canal « squaraine » avec les images dans le canal « GFP » ainsi que la substitution de la sonde avec un excès de la carbétocine non-marquée nous ont permis de conclure que la fixation du ligand fluorescent sur la membrane était spécifique à OTR. Bien que le turn-on entre l'eau et le dioxane soit seulement de 7 fois, il était suffisant pour obtenir des images confocales sans aucun bruit de fond dans les conditions homogènes. De plus, la stabilité photochimique de la sonde basée sur la squaraine était nettement meilleure que celle de la sonde analogue marquée au Nile Rouge.

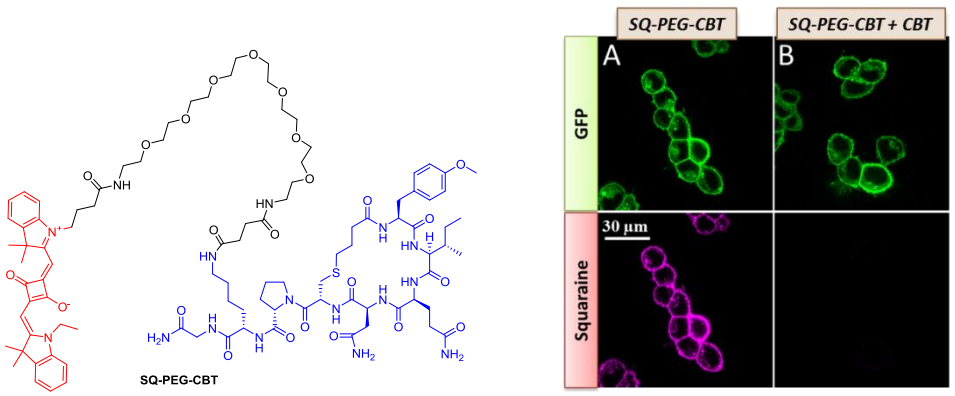

Figure R8. Structure du ligand turn-on basé sur la squaraine et images des cellules exprimant OTR fusionné à la GFP.

Squaraines-dimère comme un nouveau concept des sondes fluorogènes

Bien que les premiers résultats avec les sondes turn-on sur la base de la squaraine soient prometteurs, nous avons cherché à améliorer son turn-on entre l'eau et le dioxane. Nous avons proposé une approche de squaraine-dimères avec des interactions du type π-stacking entre les deux fluorophores. Dans les solvants apolaires qui solvatent bien la squaraine, le dimère existe sous forme « désagrégée » fluorescente, tandis que dans l'eau la conformation avec le π-stacking prédomine ce qui cause la perte de la fluorescence (Figure R9).

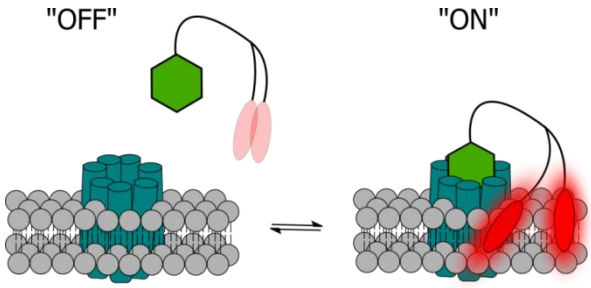

Figure R9. Principe de la détection de liaison ligand-récepteur avec les squaraine-dimères.

Il a été envisagé de séparer deux squaraines par des chaines PEG3 qui sont assez courtes pour tenir les fluorophores proches l'un de l'autre et assez long pour éviter la désactivation photochimique par collision. Afin de diminuer les interactions non-spécifiques avec les membranes cellulaires, nous avons testé deux approches : 1) insérer un acide aminé hydrosoluble dans la chaine PEG latérale et 2) rajouter les petites chaines PEG sur la squaraine.

Trois dérivés de la carbétocine avec des dimères différents ont été synthétisés et évalués dans les solvants organiques et sur les cellules exprimant OTR fusionné à la GFP (Figures R10 et R11).

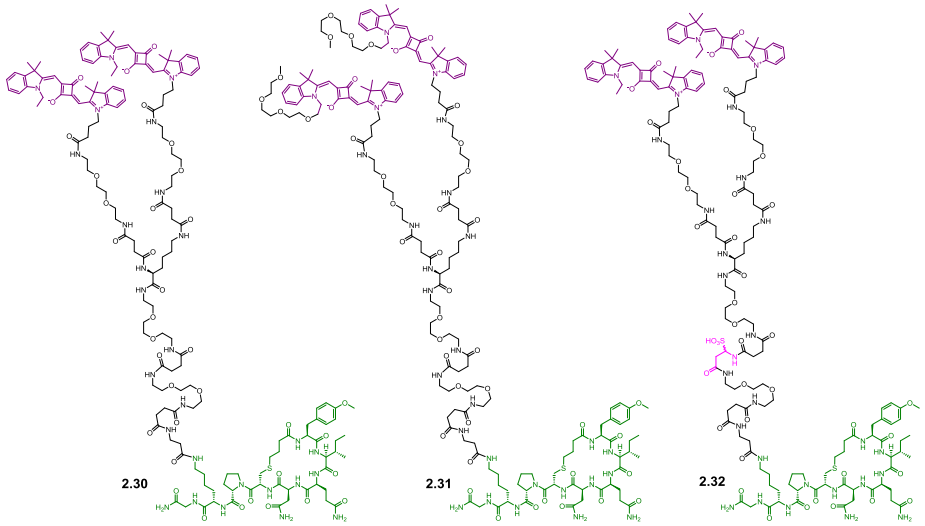

Figure R10. Structures de trois squaraine-dimères.

Il s'est avéré que la sonde la plus efficace était le squaraine-dimère modifié avec les chaines PEG. Son turn-on entre l'eau et la dioxane de 80 fois, sa brillance exceptionnelle (absorbance molaire autour de 600 000 $M^{-1}cm^{-1}$) et l'absence d'interactions non-spécifiques nous ont permis de considérer la sonde comme un outil très prometteur pour le développement du test de liaison turn-on sur les récepteurs sauvages, qui est actuellement en cours.

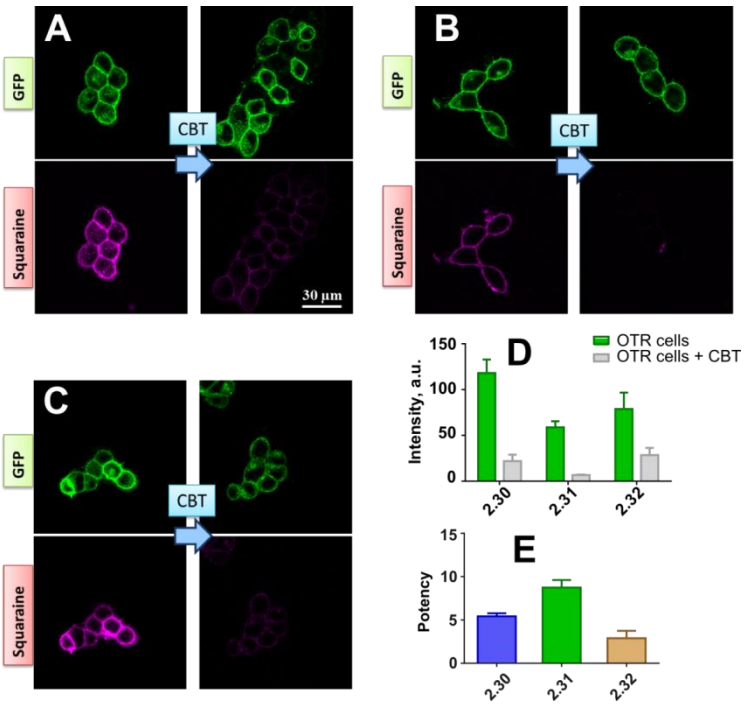

Figure R10. Images des cellules GFP-OTR avec 10 nM de 2.30 (A), 100 nM de 2.31 (B) et 10 nM de 2.32 (C) avant et après l'addition de la carbétocine non-modifiée. L'intensité de la fluorescence membranaire avant et après l'ajout de la carbetocin (D) et la sensitivité des sondes (E).

Chapitre 2. Sondes fluorescents pour les études de sélectivité

Développement du test de liaison TR-FRET multicouleur

La caractérisation pharmacologique d'un ligand de RCPG inclue 1) la détermination de son affinité pour le récepteur cible (constante de dissociation K_d ou constante d'inhibition K_i) et 2) l'investigation de sa sélectivité vis à vis d'autres RGPG. Ces mesures demandent la mise en œuvre d'essais de liaison multiples pour caractériser un seul ligand.

Une alternative est de conduire plusieurs tests de liaison dans un seul essai en utilisant les canaux de détection différents et d'obtenir à la fois l'information sur l'affinité du ligand pour le récepteur cible et sa sélectivité. Cette approche est techniquement possible sachant que les bandes d'émission du cryptate de Tb (III) peuvent servir pour exciter différents fluorophores dont la fluorescence est détectée avec des filtres optiques différents. La quantité des canaux de détection parallèles n'est limitée que par la largeur des spectres de fluorescence des accepteurs utilisés et par les filtres optiques disponibles.

Nous avons décidé de valider l'approche « multicouleur » sur un système modèle de trois RCPG (apéline ApelinR, dopamine D_3R et vasopressine V_2R) en utilisant trois filtres d'émission commerciaux : vert (520 nm), orange (605 nm) et rouge (665 nm).

Les étapes d'essai multicouleur sont les suivantes : 1) mélanger trois types de cellules chacun exprimant un récepteur d'intérêt (marqué avec le donneur du TR-FRET) ; 2) incuber les cellules avec un mélange de trois ligands fluorescents sélectifs pour chacun des récepteurs (« vert » pour D_3R, « orange » pour V_2R et « rouge » pour ApelinR) et détecter trois FRET différents ; 3) ajouter le ligand à tester ; 4) mesurer les changements du FRET dans chaque canal causés par compétition entre les ligands fluorescents et le ligand à tester (Figure R11).

Les ligands fluorescents sélectifs pour ApelinR (marqué avec le fluorophore rouge DY647) et pour D_3R (marqué avec le fluorophore vert fluorescéine) ont été précédemment développés au laboratoire. Notre travail a donc consisté à concevoir et synthétiser un ligand « orange » sélectif de V_2R. Trois fluorophores différents ont été greffés sur le ligand benzazepine de V_2R, et parmi eux le DY-590 s'est avéré le plus efficace en raison de sa forte brillance, sa compatibilité avec le filtre optique orange et sa contamination minimale dans les autres filtres utilisés.

La validation du test multicouleur est actuellement en cours dans le groupe du Dr. Thierry Durroux à IGF, Montpellier.

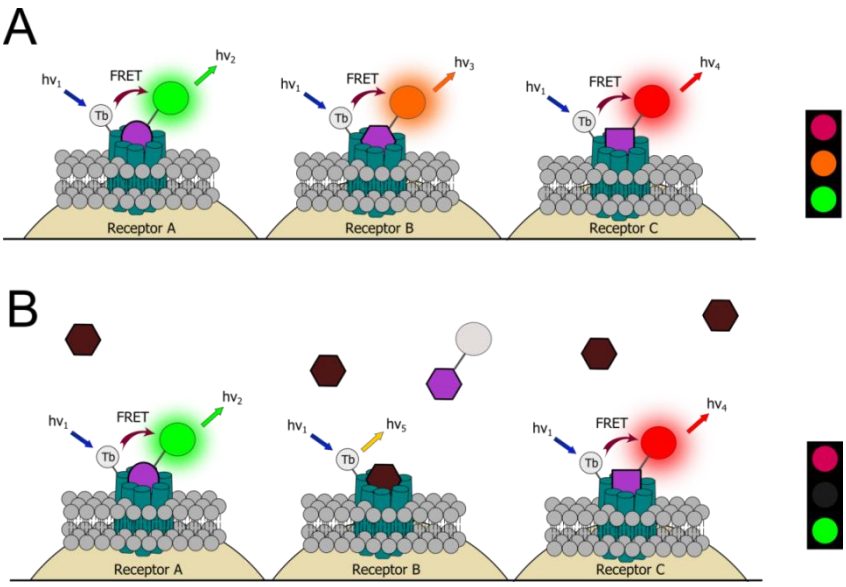

Figure R11. Principe du test de liaison « multicouleur » sur trois récepteurs (A : en absence du ligand à tester ; B : après l'ajout du ligand à tester).

Conclusion et perspectives

Les objectifs majeurs de mes recherches doctorales étaient de développer des outils de détection et d'imagerie des récepteurs de l'ocytocine et de la vasopressine *in vitro* et *in vivo* afin, d'une part de mieux comprendre leur rôle dans les troubles du spectre autistique (TSA) et d'autre part, d'accélérer la découverte des agonistes centraux d'OTR pour le traitement de TSA.

Au cours de ma thèse, j'ai contribué au développement de quatre précurseurs pour le radiomarquage au ^{11}C et ^{18}F, dont deux ont été marqués et étudiés sur les coupes de cerveau de rats. Nous espérons que les radioligands efficaces permettront de faire l'imagerie translationnelle de la souris à l'homme pour mieux comprendre la répartition des récepteurs OTR et leurs fonctions au niveau central.

Parmi les résultats de notre collaboration sur les ligands fluorescents pour OTR sont le développement des premiers ligands sélectifs OTR et la découverte des ligands turn-on rouges et proche infra-rouges. Les ligands sélectifs OTR ont été utilisés pour valider le test de liaison TR-FRET sur OTR. Notre futur objectif est de développer le test de liaison sur les récepteurs sauvages en utilisant le meilleur ligand turn-on à savoir la squaraine-dimère pégylée.

Finalement, j'étais heureuse d'être impliquée dans projet de développement du test de liaison « multicouleur », qui devrait permettre d'accélérer la découverte de nouveaux ligands des RCPGs, notamment des récepteurs de l'ocytocine et de la vasopressine.

Introduction: the world of GPCRs

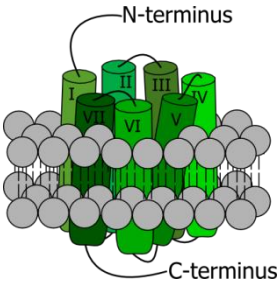

1. G protein – coupled receptors (GPCRs)

G protein-coupled receptors (GPCRs) constitute the largest family of transmembrane proteins in humans (Rosenbaum et al., 2009). They play a major role in the regulation of physiological processes, serve to ensure the intercellular communication and the perception of information from the outside world. Thanks to GPCRs we can see the beauty of nature, smell lilies of the valley and taste our morning croissant.

The classical role of a GPCR is to receive a signal from an extracellular mediator and by conformational changes that provoke interactions with intracellular proteins, activate the cellular response. The extracellular information can be mediated by hormones and neurotransmitters, small organic molecules, proteins or glycoproteins, protons, ions and even photons.

Since GPCRs are involved into a majority of physiological functions including central nervous system processes, they are implicated in many diseases. As a result about 40% of current market drugs target GPCRs (Filmore, 2004). This consideration explains the extremely high interest which is paid to the thematic of GPCR structure and functioning by the actual scientific society.

1.1. Structural characteristics of GPCRs

G protein-coupled receptors are integral membrane proteins which are constituted of seven peptide helices (20 to 35 hydrophobic amino-acid residues) linked by three extracellular and three intracellular loops formed by hydrophilic amino-acids (Ji et al., 1998; Figure 1A). Extracellular N-terminal segment (from 7 to 600 amino-acids) and intracellular C-terminal segment (from 12 to 360 amino-acids) are less conserved in length among GPCR representatives.

The first steps toward the understanding of the GPCR structure were made in 1980s with the purification of the β2-adrenergic receptor (Shorr and Heald, 1982), sequencing of the gene encoding the bovine rhodopsin receptor (Nathans and Hogness, 1983) and cloning of the β2-adrenergic hamster receptor (Dixon et al., 1986). Already at that time it was suggested that the β2-adrenergic and the rhodopsin receptors possessed multiple membrane-spanning regions. 7-helices three-dimensional structures were then proposed by Marcel Hibert (Hibert et al., 1991) and Joyce Baldwin (Baldwin, 1993), but almost ten year passed before their confirmation by

solving the three-dimensional crystal structure of the bovine rhodopsin receptor at 2.8 Å (Palczewski, 2000).

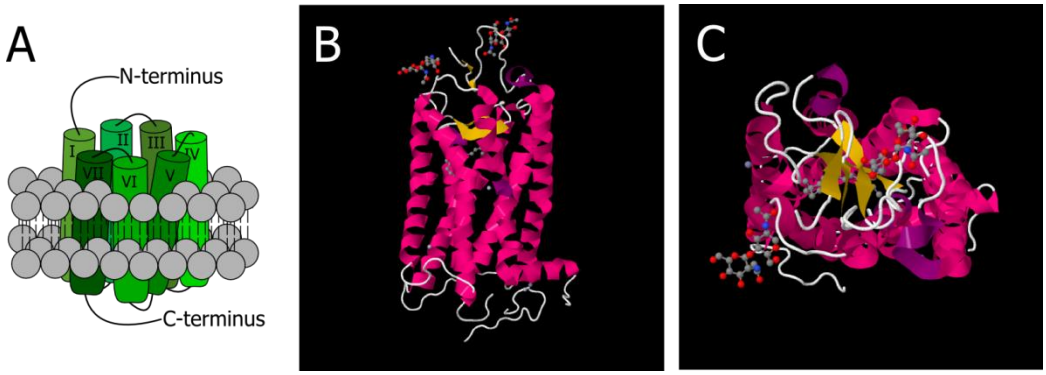

Figure 1. Schematic representation of the tri-dimensional structure of a GPCR (A). Face (B) and extracellular (C) views of the first structure of the bovine rhodopsin receptor (PDB: 1F88). α-Helices are presented in pink, β-sheets in yellow.

The crystal structure of the bovine rhodopsin receptor (Figure 1, B and C) displays the arrangement of seven transmembrane hydrophobe helices to form the corpse of the receptor and to define the central pocket. This pocket is closed by the extracellular E2 loop to shield the cofactor retinal which is covalently attached to the transmembrane helix 7 (TM7). The rhodopsin receptor is particular among the GPCRs because its activation is performed by the action of light. The absorption of photon by 11-*cis*-retinal leads to its isomerization to all-*trans*-retinal, which provokes the conformational changes of the receptor and activates its response.

Soon after the discovery of the rhodopsin receptor structure, the structures of other GPCRs were solved. Nowadays, 22 receptors are crystalized and their structures are available from the Protein Data Bank (Yang and Zhang, 2014).

It should be noticed that the majority of these structures were obtained for receptors in their inactive states, whereas significant affords are made today to get crystal structures of fully active or agonist-bound GPCRs in order to better understand their functional architecture. Nowadays active-state structures are available for the rhodopsin receptor (Park et al., 2013), human $B_{2A}R$ (Rasmussen et al., 2011; Rosenbaum et al., 2011), turkey $B_{1A}R$ (Warne et al., 2008), human $A_{2A}R$ (Xu et al., 2011a), the neurotensin receptor (Egloff et al., 2014), human CHRM2 (Kruse et al., 2013), the human 5-HT_{2B} receptor (Wacker et al., 2013), the human P2Y12 receptor (Zhang et al., 2014) and human FFAR1 (Srivastava et al., 2014).

1.2. Classification of GPCRs

GPCRs are encoded by more than 800 genes in human genome (Fredriksson et al., 2003). ≈ 500 of known GPCRs are chemosensory, 100 are still orphans, i.e. lacking endogenous ligands (Chung et al., 2008).

Historically GPCRs were divided into six families according to the A-F clan system (Attwood and Findlay, 1994; Kolakowski, 1994). Some families in A-F system do not exist in humans, for example fungal pheromone receptors which were attributed to the clan D.

To overcome the disadvantaged of the A-F system, mainly the high homological difference between human and non-human GPCRs, a GRAFS family system was established in 2003 (Fredriksson et al., 2003). The GRAFS classification singles out five human GPCR families based on their structural homology: glutamate (G), rhodopsin (R), adhesion (A), frizzled/taste2 (F) and secretin (S). Only the largest rhodopsin receptor family is divided into four groups with 13 subbranches.

- The *glutamate receptor family* consists of 15 members. Among them are 8 metabotropic glutamate receptors, two GABA receptors, one calcium-sensing receptor and taste receptors. These receptors are characterized by long N termini rich in Cys residues (with the exception of GABA receptors), which contain ligand-binding sites. This receptor family corresponds to clan C in the ancient system.
- *Rhodopsin receptor family* corresponds to clan A. It is the largest and the most diverse GPCR family (701 members). The common feature for the receptors of this family is the presence of NSxxNPxxY motif in TMVII and the DRY motif or D(E)-R-Y(F) between TMIII and IL2. In contrast to other GPCRs, rhodopsin-like receptors do not possess long N termini (with the exception of few members). In most cases, ligands bind to the receptors of the rhodopsin family within a cavity, formed by their helices (Baldwin, 1994). Glycoprotein binding receptors present, however, an exception: their orthosteric binding sites are situated in the N termini.
- *Adhesion receptors* (24 members) are isolated in a distinct family due to the fusion of transmembrane domains with adhesion-like domains in the N terminus. Their N termini are variable in size but generally long, rich in proline residues and glycosylation sites. These GPCRs are believed to participate in cell adhesion, whence comes their name (Stacey et al., 2000).

- *Frizzled/taste2 receptor family* combines two clusters of the frizzled receptors and the TAS2 receptors, based on their common fragments IFL in TMII, SFLL in TMV and SxKTL in TMVII, which were not found in any other GPCR. The frizzled receptors control cell development and proliferation. They possess 200-amino acid N termini with conserved Cys residues. The TAS2 receptors are characterized by a very short N terminus and surprisingly do not display high homology which the TAS1 receptors, which belong to the glutamate receptors family. They are mostly expressed in tongue and palate epithelium, however little is known about their function.
- *Secretin receptors* (with 15 members) correspond to clan B in the previous classification. Their endogenous ligands are large peptides which are bound to the 60-80 amino acids Cys-rich N terminal domain. In contrast to hormones, the ligands of the secretin receptors family act mainly in a paracrine manner.

1.3. GPCR signaling

In the absence of ligands GPCRs exist in a conformational equilibrium between their active forms (when the transduction of the signal is realized) and the inactive forms. Thus, every receptor has its natural, "basal", activity.

The result of the ligand-receptor interaction depends on the nature of the ligand. Binding to an antagonist does not influence the conformational equilibrium however protects the receptor binding site from binding of an endogenous ligand (Figure 2). Ligands which have higher affinities for the inactive form are called inverse agonists. Their binging provokes the displacement of the equilibrium toward the inactive conformation and the decrease in the receptor activity. Finally, an agonist is a ligand which displays higher affinity for the receptor in its active conformation. The receptor-agonist interaction shifts the equilibrium toward the activated form and induces intracellular response.

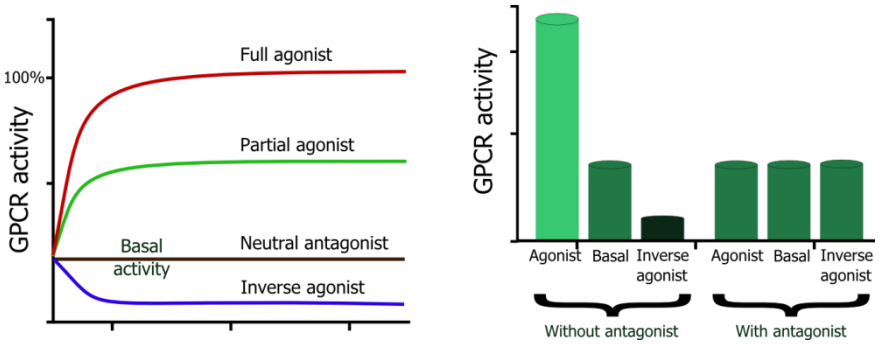

Figure 2. Schematic representation of the action of different ligands on a GPCR.

The agonist-induced receptor activation results in a motion of the helices and conformational changes of the receptor. These changes promote the activation of a heterotrimeric G protein (after which the receptors were named) by binding of the latter to the GPCR (Figure 3).

G proteins belong to the GTPase family (Roux and Cottrell, 2014). They consist of three subunits: β- and γ-, which are stably dimerized and α-subunit. G protein activation results in a release of guanosine diphosphate (GDP), which is bound to the α-subunit in the inactive state, and a consequent binding of guanosine triphosphate (GTP). The latter event induces the dissociation of the α-subunit. Both α- and βγ-subunits in their dissociated forms are able to activate intracellular cascade via the action of different effectors which produce second messengers.

G proteins are classically divided into 4 families, based on their α-subunits: $G\alpha_s$, $G\alpha_{i/o}$, $G\alpha_{q/11}$ and $G\alpha_{12/13}$ (Cabrera-Vera et al., 2003). The $G\alpha_s$ family is known to activate adenylate cyclase (effector) which produces cyclic adenosine monophosphate cAMP (second messenger). On the contrary, $G\alpha_{i/o}$ proteins inhibit the activity of adenylate cyclase, decreasing the cAMP production. $G\alpha_{q/11}$ proteins induce the hydrolysis of phosphatidylinositol phosphates by phospholipase C (effector) into two second messengers, inositol trisphosphate (IP3) and diacylglycerol (DAG). IP3 liberation leads to the intracellular Ca^{2+} mobilization and the activation of protein kinase C. Finally, G proteins of the $G\alpha_{12/13}$ family are involved in Rho family GTPase signaling.

It has been discovered that βγ-subunit (Gβγ) is also involved into the cellular signaling. It interacts directly with adenylate cyclase, GPCR kinase 2, phospholipase C, phosphoinositide 3-kinase γ and N-type calcium channels (Lin and Smrcka, 2011).

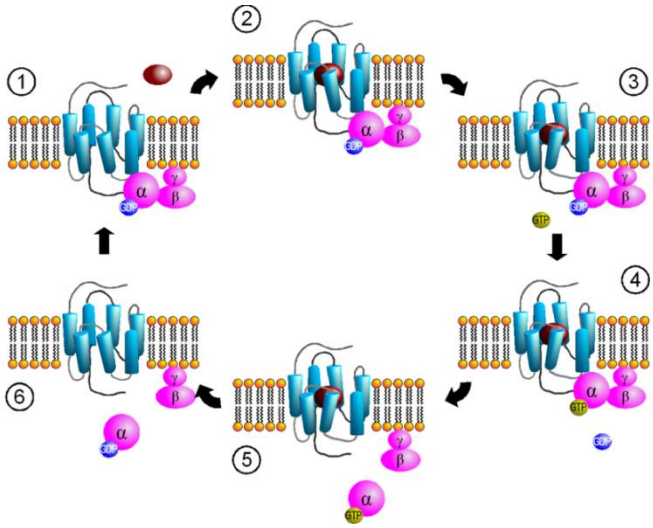

Figure 3. A simplified scheme of a G protein-mediated GPCR signaling.

Finally, multiple GPCRs have been recently shown to initiate cellular signaling pathways independently from G proteins (Drake et al., 2006; Rajagopal et al., 2005). The signal transduction can be instead mediated by G protein-coupled receptor kinases (Marrero et al., 1995) and β-arrestins (Lefkowitz and Shenoy, 2005).

β-Arrestins are also known to be responsible for the receptor desensitization (the attenuation of the receptor-mediated cellular response). The GPCR desensitization starts from the phosphorylation of the receptor by GPCR kinases (Premont and Gainetdinov, 2007). Binding of β-arrestins to the phosphorylated receptors induces the uncoupling of GPCRs from their G proteins and internalization of the receptors in endosomes. After internalization, GPCRs are either recycled back to the cell surface or undergo degradation in lysosomes (Roux and Cottrell, 2014).

Recent discoveries challenged the simple "one ligand–one GPCR–one signaling pathway" model (Wang, 2013). It has been shown that different agonists can provoke slightly different active conformations of the receptor leading to binding to different G proteins (Urban et al., 2007; Zheng et al., 2010). This phenomenon, called the functional selectivity, is highly important for drug discovery, since almost always only a certain pathway is implicated into the target disease.

In addition, GPCR are known to be able to oligomerize in native tissues. The pharmacology of homo- and heteromers can be completely different from those of monomeric receptors. Recent studies highlighted the critical role of GPCR heteromers in

pathophysiological processes and proposed them as important drug targets (Rozenfeld and Devi, 2010).

2. The oxytocin and the vasopressin GPCRs

Few GPCRs could boast of being so exciting and attractive for neuroscientists as the oxytocin (OTR) and the vasopressin (AVPR) GPCRs – the receptors of attachment, social recognition and love (Meyer-Lindenberg et al., 2011). It is now evident that OTR and AVPR play a crucial role in social cognition and behavior which established there receptors as emerging targets for the treatment of mental diseases, especially autism spectrum disorders.

The oxytocin and the vasopressin receptors belong to the rhodopsin family of GPCRs. Three human vasopressin receptors – V_2R (Birnbaumer et al., 1992), $V_{1a}R$ (Thibonnier et al., 1994) and $V_{1b}R$ (Sugimoto et al., 1994) – and the only one oxytocin receptor OTR (Kimura et al., 1992) were cloned at the beginning of 1990s. The four receptors have 36 to 46% overall sequence similarity (Ocampo Daza et al., 2012), mainly in the region of transmembrane helices.

2.1. The oxytocin receptor

Human OTR is a 389-amino acid protein with a molecular mass of 40 – 45 kDa, calculated on the basis of the "core" amino-acid sequence. It plays an important role of uterine contractions during parturition and of milk ejection.

The endogenous ligand binding site was proposed to be located in a cleft formed by a ringlike arrangement of transmembrane helices (Gimpl and Fahrenholz, 2001). It was also demonstrated that the N terminus and the first and the second extracellular loops played an important role for peptide agonist binding and selectivity (Postina et al., 1996).

OTR is known to act mainly via $G\alpha_{q/11}$ signaling pathway. It stimulates the activity of phospholipase C and induces the Ca^{2+} release from intracellular stores (by the action of IP3) as well as activates protein kinase C (with diacylglycerol). However, in neurons OTR can be coupled with $G\alpha_{i/o}$ protein (Gravati et al., 2010), causing antiproliferative effects.

The oxytocin receptors in mammals are distributed mainly in myoepithelial cells of the mammary glands (Grigor'eva and Golubeva, 2010). In addition, they are found in vascular endothelium (Thibonnier et al., 1999), kidney epithelium (Arpin-Bott et al., 2002), heart (Gutkowska et al., 1997), but also in the regions of central nervous system: hypothalamus, anterior pituitary, cortex (Grigor'eva and Golubeva, 2010).

2.2. The vasopressin V_{1a} receptor

$V_{1a}R$ is one of the three major receptor types for arginine vasopressin, which can be found in the liver, kidney, vasculature and in the brain (Caldwell et al., 2008). It is responsible for the vasoconstriction of blood vessels. The receptor is composed of 418 amino acids and displays sequence homology of 45%, 36% and 45% with human $V_{1b}R$ (Sugimoto et al., 1994), V_2R and OTR (Thibonnier et al., 1994), respectively.

It has been shown that the N terminal juxtamembrane segment together with Glu^{54} and Arg^{46} played an important role in the agonist binding (Hawtin et al., 2005). The physiological action of $V_{1a}R$ is ensured by $G\alpha_{q/11}$ proteins which together with $G\beta\gamma$ activate phospholipase C (Caldwell et al., 2008).

2.3. The vasopressin V_{1b} receptor

The V_{1b} receptor (sometimes called V_3R (Holmes et al., 2003)) is a 424-amino acid membrane integral protein, which is well known for its important role in antidiuresis, contraction of vascular smooth muscle and stimulation of hepatic glycogenolysis (Sugimoto et al., 1994). It has the highest degree of similarity with the other members of the OTR/AVPR family (45% with OTR, 39% with V_2R and 45% with $V_{1a}R$).

$V_{1b}R$ signaling appears to involve several G proteins, depending on the receptor expression and the concentration of the agonist (Thibonnier et al., 1998). Classically, $V_{1b}R$ activation was associated with the $G\alpha_{q/11}$ signaling (Sugimoto et al., 1994). Other signalization pathways peculiar to $V_{1b}R$ include $G\alpha_s$ and $G\alpha_i$, which result in the production of DNA and cAMP in ACTH-secreting tumors (Thibonnier et al., 1997).

In addition to the $V_{1b}R$ peripheral expression in the pancreas and the adrenal gland, this receptor was found in rodent and human brain, predominantly in the dorsal one-third of pyramidal cells of the CA2 region of the hippocampus (Stevenson and Caldwell, 2012).

2.4. The vasopressin V_2 receptor

The V_2 receptor is mainly localized in the kidney, where it plays a major role in water reabsorption (Birnbaumer et al., 1992).

The main difference between V_1R and V_2R is that the formers have multiple glycosylation sites at both N termini and extracellular loops, whereas the latter possesses glycosylation sites only at its N terminus (Holmes et al., 2003).

V_2R acts via $G\alpha_s$ signaling pathway, which involves the activation of adenylate cyclase (Birnbaumer, 2000). The increase of intracellular cAMP in the kidney induces the fusion of aquaporin-2-bearing vesicles with the apical plasma membrane of the collecting duct principal cells, increasing water reabsorption (Harris et al., 1994).

2.5. The endogenous ligands: oxytocin and vasopressin

Hormone oxytocin (OT) – the endogenous ligand of the oxytocin receptor – was the first peptide hormone to be sequenced and chemically synthesized (Du Vigneaud et al., 1953). Its name means "quick birth" and refers to the oxytocin uterotonic and milk-ejecting activity (Gimpl and Fahrenholz, 2001). OT is a nonapeptide with a disulfide bridge between Cys1 and Cys6 which forms a cycle of eight amino acids (Figure 4).

The structurally close "antidiuretic" hormone arginine vasopressin (AVP) controls cardiovascular homeostasis, renal water reabsorption and hormone secretion from the anterior pituitary (Koshimizu et al., 2012). It differs from OT by only two amino acids: Phe^3 instead of Ile^3 and Arg^8 instead of Leu^8 (Figure 4). The presence of the basic amino acid in position 8 is suggested to enhance binding to the vasopressin receptors, whereas Ile^3 is essential for stimulating OTR (Barberis et al., 1998).

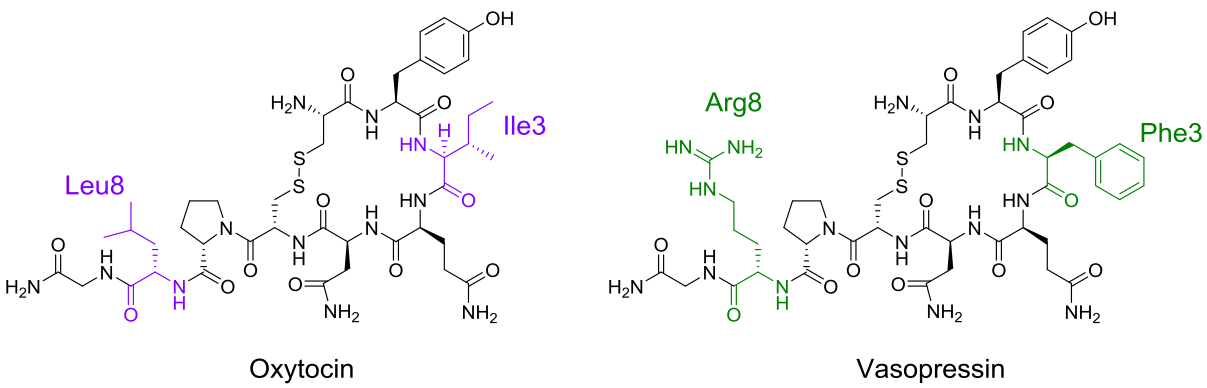

Figure 4. Chemical structures of oxytocin and vasopressin.

The genes encoding for OT and AVP are located on the same chromosome, separated by a DNA segment of 12 kilobases (Riddell et al., 1985). The neuropeptides are synthesized in the hypothalamic paraventricular nucleus (PVN), supraoptic nucleus (SON) and in the accessory nucleus (AC) (Farina Lipari and Valentino, 1993; Farina Lipari et al., 1995). OT synthesizing neurons were also found in the bed nucleus of the stria terminalis (BST), the medial amygdala, the dorsomedial hypothalamus and the locus coeruleus (Caffé and van Leeuwen, 1983; Caffé et al., 1987). In males, AVP is also produced in the amygdala and the bed nucleus of the stria terminalis (Francis et al., 2014). OT and AVP are transported by neurosecretion to the mammalian posterior and then released into the blood to act as hormones or they move to different regions of the central nervous system by cerebral spinal fluid (Neumann and Landgraf, 2012).

2.6. Central roles of oxytocin and vasopressin

There is growing evidence that oxytocin and vasopressin in addition to their well-studies peripheral actions modulate complex social behavior in rodents, non-human primates as well as in humans. OT is generally associated with positive sociality, such as mother-child and adult-adult attachment, trust, fidelity, altruism (Figure 5). AVP was historically considered as anxiogenic, which plays an important role in protection and species survival. Nowadays it became evident that the central role of AVP is more complex and depends on the concentration of the neuropeptide (Francis et al., 2014).

Parental behavior

The OT role in reproduction was discovered already a century ago, however only at the end of 1970s it became evident that the neuropeptide influences also the parental behavior. Pedersen and Prange discovered that central administration of OT to virgin rats stimulated their maternal behavior (Pedersen and Prange, 1979). Further studies in rodents showed that elevated levels of parental care correlated with higher OTR density in the central nervous system (CNS) and could be controlled by the antagonist administration both in females and in males (Bales et al., 2004; Champagne et al., 2001; Francis et al., 2002). Moreover, OTR knockout mice exhibited deficit in maternal care (Takayanagi et al., 2005). Interestingly, as was shown by Kendrich et al., in sheep OTR is more important in the initiation of maternal

care than in its maintenance (Kendrick et al., 1997). Already established maternal behavior was not altered by OTR disrupting lesions to the PVN or the antagonist administration.

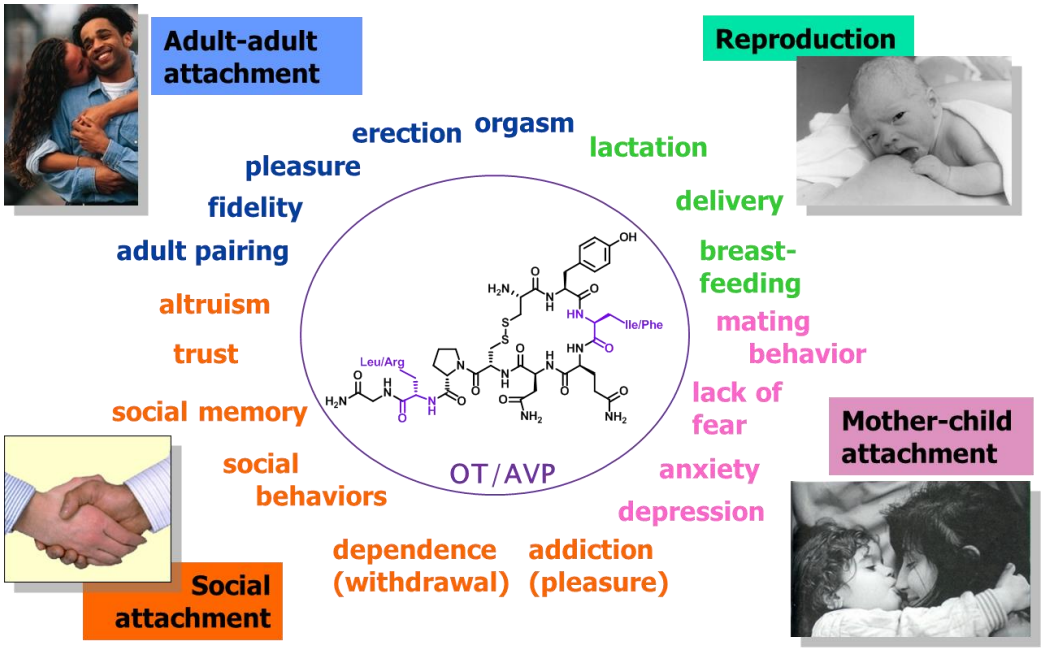

Figure 5. The roles of oxytocin and vasopressin.

Several studies were conducted in humans. It was demonstrated that the oxytocin plasma level during pregnancy is associated with maternal bonding, such as maternal care, gazing at the infant, touching and attachment (Feldman et al., 2007), and it can be increased by interaction of mothers with their children (Feldman et al., 2010). Low plasma OT concentration in mid pregnancy was associated with the risk of postpartum depression (Skrundz et al., 2011). Similar relationship between the OT plasma level and the paternal care was discovered. Thus, fathers who actively contacted with their newborns demonstrated higher plasma OT concentration that father who were less implicated in the concern for their infants (Feldman et al., 2010).

There are evidences that not only OT but also AVP plays an important role in the establishment and the regulation of maternal behavior by acting via the central V_{1a} receptors (Bisceglia et al., 2012). The density of $V_{1a}R$ in female mice was positively correlated with postpartum licking and grooming of pups (Curley et al., 2012), whereas the higher level of central V_{1a} receptors in monogamous male California mice in comparison to polygamous male white-footed mice made the formers more paternal and aggressive towards nest intruders (Bester-Meredith et al., 1999).

Human studies revealed that maternal sensitivity is associated with the V_{1a} receptor gene, particularly with the long RS3 allele: two copies of these alleles make mothers less sensitive than one or no copies (Bisceglia et al., 2012).

Affiliation

OT and AVP are known to assure the establishment and the control of social bonds in several mammalian species (Nephew, 2012). Several examples of gender difference in OT and AVP roles were described (Insel and Young, 2000). Thus, Insel et al. demonstrated that central OT administration in monogamous female prairie voles facilitated the development of partner preference, although in male prairie voles such effect was mediated by the centrally administrated AVP (Insel and Hulihan, 1995). The implication of V_{1a} receptors was proved by blocking pair bonding behaviors in male prairie voles with a selective V_{1a}R antagonist (Winslow et al., 1993). Interestingly, central OT, AVP or their antagonists administration to polygamous montane voles did not influence their social behavior (Insel and Shapiro, 1992).

There are evidences of positive correlation of OTR density with affiliation and sexual behavior in rodents and tamarin monkeys (Snowdon et al., 2010). Similarly, over-expression of V_{1a}R in the forebrain of male prairie voles facilitates pair bonding (Pitkow et al., 2001), which can be inhibited by the V_{1a}R antagonist injection (Lim and Young, 2004).

Oxytocin and vasopressin were suggested to facilitate pair formation in humans as well as in voles. As was shown by Grewen et al., the OT level in female but not in male humans increased during and after physical contacts with supportive partners (Grewen et al., 2005). It was even proposed to use plasma OT level as a biomarker of disbalanced relationships in female humans as well as AVP plasma level for the same detection in male humans (Taylor et al., 2010).

The intranasal OT administration in humans was shown to promote trust and prosocial behavior, especially as measured by experimental economic games (Baumgartner et al., 2008; Kosfeld et al., 2005). Intranasal AVP administration facilitated recognition of facial expressions in humans (Guastella et al., 2010), sexual cues in men (Guastella et al., 2011) and increased cooperative behavior in men in a social experiment (Rilling et al., 2011).

Aggression

Initially OT in the PVN was considered to display excitatory effects on the maternal aggression (Ferris et al., 1992), however according to recent studies in rats it was concluded that OT has mostly inhibitory effects (Consiglio et al., 2005). Multiparous rats, which are known to be more aggressive than primiparous dams, have lower OTR brain levels in comparison to primiparous dams (Nephew et al., 2009).

AVP in male mammals is known to display positive effects on the aggressive behavior. Studies in male hamsters revealed that the administration of V_{1a}R antagonist decreased aggression (Ferris and Potegal, 1988), while exogenous AVP in the anterior hypothalamus stimulated it (Caldwell and Albers, 2004).

Similarly to OT, AVP has inhibitory effects on maternal aggression in female mammals. Treatment of primiparous and multiparous dams with V_{1a}R antagonist increased maternal aggression, whereas treatment of multiparous dams with AVP decreased aggressive behavior (Nephew and Bridges, 2008). Similar results on the inhibitory role of AVP on female aggression were obtained in non-maternal female hamsters (Gutzler et al., 2010).

There are evidences that OT and AVP systems play a cooperative role on the aggression behavior. Studies in male mice revealed that disruption of the OTR gene decreased aggression (DeVries et al., 1997). Later Insel discovered that although OTR knockout mice did not show impairs in maternal and sexual behavior contrary to rats, such mice were significantly more aggressive than wild-type mice (Winslow and Insel, 2002). This inconsistency with previous OTR gene disruption studies was supposed to result from a compensatory increase in AVP in OTR knockout male mice (Nephew, 2012).

Depression and anxiety

Oxytocin and vasopressin V_{1a} receptors are known to be perspective targets for the treatment of mood disorders and postpartum depression (Nephew, 2012).

Animal studies revealed that peripheral OT had antidepressant effects in young and old rats (Arletti and Bertolini, 1987) and decreased anxiety in pregnant and lactating rats (Neumann et al., 2000). In contrast, elevated brain and plasma AVP levels in male rodents were evidenced to enhance depression and anxiety (Bosch et al., 2006), while V_{1a}R antagonists were shown to possess antidepressant activity (Ebner et al., 2002; Wigger et al., 2004). V_{1a} receptor knockout mice displayed lower levels of anxiety compared to wild type mice (Egashira et al., 2007). Interestingly, administration of a V_{1b}R selective antagonist was discovered to be anxiolytic in

rats (Griebel et al., 2002). The implication of central V_{1b} receptor in depression and anxiety was confirmed by studies on V_{1b}R knockout mice, which exhibited reduced aggressive behavior in comparison to wild-type mice (Wersinger et al., 2002)

In humans, low plasma OT level was correlated with depressive symptoms (Frasch et al., 1995; Heim et al., 2009), however nasal oxytocin administration influenced only specific types of depression. Thus, placebo-controlled study on patients with social anxiety disorder showed that treatment with OT improved mental representation in self, but the levels of symptoms reduction was the same as in placebo-treated patients (Guastella et al., 2009). Low plasma OT level during pregnancy increases risks of postpartum depression (Skrundz et al., 2011), whereas in women with high plasma OT concentration levels of postpartum anxiety are minimal (Uvnäs-Mobcrg et al., 1990).

The role of AVP in mood disorders was described in late 1970s (Gold et al., 1978). Elevated plasma AVP level was correlated with depression, specifically melancholic (van Londen et al., 1997) and suicidal (Inder et al., 1997), and anxiety (Goekoop et al., 2006). Interestingly, resilience against depression was associated with single nucleotide polymorphisms of the V_{1b}R gene in humans (Dempster et al., 2007; van West et al., 2004).

Learning and memory

Oxytocin and vasopressin were found to mediate recognition in several species. Thus, OTR knockout mice as well as wild-type mice treated with an OTR antagonist exhibited social amnesia (Ferguson et al., 2000; Lee et al., 2008). The effect can be reversed by OT treatment (Ferguson et al., 2001), which was explained by its action via the transmembrane protein CD38 (Jin et al., 2007). It was also discovered that the effect of OT in pair bonding and maternal care involves a recognition function (Campbell, 2008; D'Cunha et al., 2011).

Administration of vasopressin to wild type and V_{1a}R deficient rats (Engelmann et al., 1994; Landgraf et al., 1995), as well as the overexpression of V_{1a} receptors (Landgraf et al., 2003), were found to improve social memory and social discrimination abilities.

The data from human studies are consistent with animal studies results. Intranasal oxytocin was found to improve learning (Hurlemann et al., 2010) and social memory (Rimmele et al., 2009). Intranasal AVP analog DGAVP (desglycinamide-arginine-vasopressin) enhanced the memory performance and facilitated recall (Beckwith et al., 1987; Pietrowsky et al., 1988).

Autism spectrum disorders

Autism was firstly described by Leo Kanner in 1943 as a mental disorder with stereotyped repetitive movements and difficulties with social communication (Kanner, 1943). Currently this group of symptoms is known as autism spectrum disorders (ASD). ASD is a highly heterogeneous disorder, characterized by high level of anxiety, irritability, social deficits, restricted interests and repetitive behaviors (Francis et al., 2014). Until now there are no effective medications to treat ASD.

Recently oxytocin receptor was proposed as a potential target for the treatment of core ASD features: social deficits, language abnormalities and repetitive behaviors. In 2003 Hollander et al. performed a double-blind placebo-controlled study of the impact of IV OT on the repetitive behaviors in patients with ASD (Hollander et al., 2003). Patients showed a significant reduction in repetitive behaviors following four hours of oxytocin infusion in comparison to placebo infusion.

More recently a study conducted by Guastella et al. revealed that a single dose of intranasal oxytocin improved emotion recognition on the Reading the Mind in the Eyes Task in young people with ASD (Guastella et al., 2010).

The group of Angela Sirigu studied the impact of intranasal OT on the social interaction of ASD patients using Social Ball Tossing Game (Andari et al., 2010). In this game patients interacted with three fictitious partners, which were classified as “good”, “bad” and “neutral” according to the probability that this player would throw the ball to the examined patient. Whereas a healthy player prefers to send the ball to a “good” partner in order to get it back, for patients with ASD this choice is not evident. Under placebo treatment patients did not discriminate between the three partners, however oxytocin intake led ASD patients to send significantly more balls to the most socially cooperative partner. In the same study, it was described that intranasal OT increased patients’ gazing time on the socially informative region of the face, namely the eyes.

Anagnostou et al. performed the first long-termed study on the influence of intranasal OT on social cognition and functioning and repetitive behavior (Anagnostou et al., 2012). The six-week pilot study demonstrated improvements in social cognitions, in low order repetitive behaviors and in the quality of life – the core features of ASD.

Another long-termed case study of an ASD patient was described by Kosaka et al., 2012. Social communications and interactions of the patient were improved after 2 times per day

treatment with intranasal OT, whereas irritability and aggressive behavior were dramatically decreased.

Finally OT was also reported to enhance brain activity in young and adult patients with ASD (Domes et al., 2013; Gordon et al., 2013).

Research objectives

One of the main research axes of the laboratory consists in exploring the pharmacology of the oxytocin and the vasopressin receptors, their role in mental diseases namely autism spectrum disorders and in developing selective centrally active agonists for OTR as potential treatment of ASD.

In this context, the objective of my thesis is to develop detection and imaging tools to study the oxytocin and the vasopressin receptors both *in vivo* and *in vitro*.

To characterize the distribution of OTR and AVPR *in vivo,* positron emission tomography (PET) is an imaging technique of choice. The non-invasive determination of the distribution of OTR and $V_{1a}R$ using PET will be helpful to correlate the density of these receptors in different regions of the human brain with the observed cognitive dysfunctions in ASD patients. Moreover, selective radiotracers for the oxytocin and the vasopressin receptors could be used to study the distribution and metabolism of new drug candidates targeting these receptors.

For *ex vivo* studies of ligand-receptor binding it is hard to imagine a spectroscopy technique more powerful than fluorescence. Due to its non-invasive and non-destructive character, high detection speed and simplicity in utilization, fluorescence is widely used to study the architecture and functioning of GPCRs. We aimed at developing fluorescent probes for the detection of ligand-receptor interactions on both modified and wild-type OTRs with the idea to further establish a screening method on wild-type GPCRs without radioactive handle. Finally, we envisaged the development of a new "multicolor" binding approach in order to ameliorate the efficacy of the established luminescence time-resolved screening assay for GPCRs.

This work would never be possible without our kind collaborators:

- Dr. Andrey Klymchenko, Rémy Kreder, Dr. Mayeul Collot, Dr. Ludovic Richert, Romain Vauchelles from Laboratoire de Biophotonique et Pharmacologie, Université de Strasbourg.
- Dr. Thierry Durroux, Dr. Bernard Mouillac, Dr. Christiane Mendre, Thiéric Rodriguez, Amandine Falco from Institut de Génomique Fonctionnelle de Montpellier.
- Christel Valencia-Schmitt, Sophie Gioria, Dr. Pascal Villa from Plate-forme de Chimie Biologique Intégrative de Strasbourg (PCBIS, Illkirch)
- Dr. Aline Nonat, Dr. Loic Charbonnière from Laboratoire d'Ingénierie Moléculaire Appliquée à l'Analyse, Université de Strasbourg.
- Prof. Luc Zimmer and Dr. Thierry Billard from the Lyon Neuroscience Research Center and CERMEP-Imaging platform.
- Dr. Angela Sirigu and Dr. Jean-René Duhamel from Centre de Neuroscience Cognitive, Bron.

PART I. PET radiotracers for the oxytocin and the vasopressin V_{1a} receptors

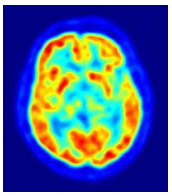

1. Positron emission tomography

1.1. Principles of positron emission tomography

Positron emission tomography (PET) is a non-invasive medical imaging technique that produces a three-dimensional image of functional processes in the body by the detection of radiolabeled biologically active molecules (radiotracers). The PET camera detects a pair of gamma quants formed as a result of an annihilation of a positron, emitted by a radiotracer, with an electron (Figure 6).

Unlike magnetic resonance imaging (MRI), X-ray computed tomography (CT), or ultrasound (US), which provide information on anatomy, PET experiments allow the study of metabolic or molecular events (Miller et al., 2008b). PET is a powerful and rapidly developing medical imaging technique, which due to its good resolution, picomolar sensitivity and accurate quantification is nowadays widely used in disease treatment monitoring in oncology, cardiology and neurology (Dunphy and Lewis, 2009; Van Heertum and Tikofsky, 2003; Murphy et al., 2008), studies of biochemical mechanisms in living tissues and drug development (Cunningham et al., 2005; Gee, 2003; Miller et al., 2008a).

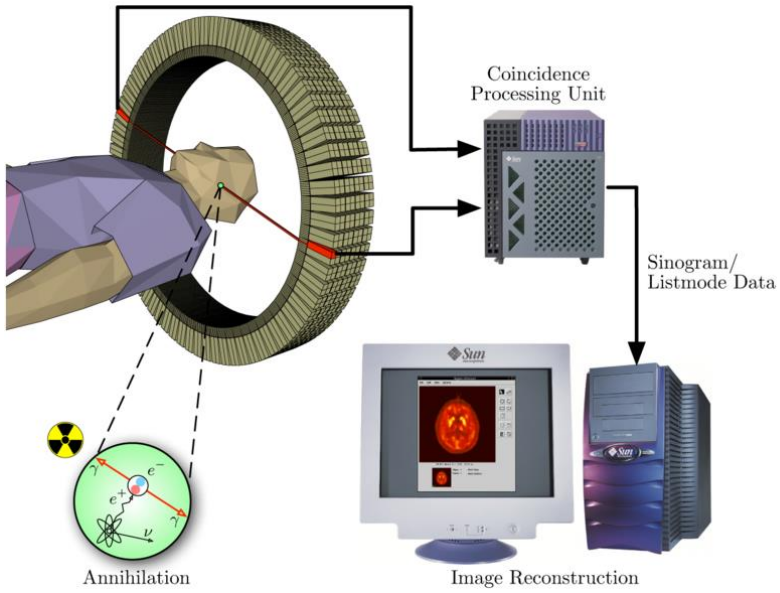

Figure 6. The processing principles of a positron emission tomograph commonly used in cancer diagnostics.

Beta(+)-emitting radionuclides, which are commonly used in PET to label bioactive molecules, are listed in Table 1. The choice of the radioisotope depends not only on the possibility of its introduction on the molecule, but also on the radioactive decay half-life,

which should be comparable with the time of the biological event of interest in order to obtain a good signal-to-noise ratio and avoid excessive irradiation (Li and Conti, 2010). Since the study of the ligand-receptor interaction at equilibrium requires several hours to a few days of incubation, the radionuclides such as ^{64}Cu, ^{89}Zr or ^{124}I could be used. On the other hand, since the detection of the distribution and metabolism of small organic molecules requires rapid repetitive scans, the ^{11}C or ^{18}F would be an isotope of choice. It should also be noticed that the short half-live of ^{11}C and especially ^{15}O and ^{13}N rules out its transportation, so the imaging site should be situated in close proximity to the radiolabelling site. Finally, the resolution of the PET images also depends on the nature of the nuclide, notably on the energy of the emitted positron: high energy positrons track for longer distances in the tissue before the annihilation, resulting in less accurate positional information, i.e. a lower spatial resolution. This is the reason why ^{18}F-labeled radiotracers generally give higher resolution images than ^{11}C-labeled radiotracers.

Table 1. Commonly used positron-emitting radionuclides in PET and their decay properties (from Li and Conti, 2010).

Radionuclide	*Half-life*	E_{max} *(β^+), KeV*	β^+ *decay , %*	*Chemistry*
^{76}Br	16.2 h	1310	54	Organic chemistry
^{11}C	20.3 min	961	100	Fast organic chemistry
^{64}Cu	12.8 h	656	19	Chelation chemistry
^{18}F	110 min	634	97	Fast organic chemistry
^{68}Ga	67.6 min	1899	89	Chelation chemistry
^{124}I	4.17 d	2100	23	Organic chemistry
^{13}N	9.97 min	1190	100	Fast organic chemistry
^{15}O	2.1 min	1732	100	Fast on-line gas phase chemistry
^{86}Y	14.7 h	3150	34	Chelation chemistry
^{89}Zr	78.4 h	897	23	Chelation chemistry

It is particularly important for biodistribution and pharmacokinetic studies to preserve the biological activity of the molecule of interest while introducing a radioactive PET tag. Since the ^{11}C isotope could replace the existing carbon in the molecule (for example by methylation

of the desmethyl precursor with [^{11}C]CH_3I) and ^{18}F is a classical isostere of hydrogen, these two radionuclides seem to be the best choice for pharmacological applications.

1.2. Applications of PET to drug discovery

Over the last few decades, PET has been increasingly used by the pharmaceutical industry to evaluate new drug candidates at a very early stage of the development. The principal areas of drug development that can be directly accessed by PET are biodistribution and drug occupancy studies (Cunningham et al., 2005).

The *biodistribution studies* aim to discover the pharmacokinetics, i.e. the fate of the drug from the moment of the administration into the human body until its complete elimination. The principal questions to answer are the speed of the delivery of the drug to its target tissue, the presence of undesirable accumulation in other tissues and organs, such as liver or kidneys, the blood-brain barrier penetration in the case of CNS drugs. For biodistribution studies the ideal radiotracer would be the direct analogue of the molecule of interest to ensure the preservation of all the pharmacological properties, which is the reason that ^{11}C chemistry is widely used.

The objective of *drug occupancy studies* is to characterize the interaction of the non-labeled drug candidate with its molecular target (receptor or enzyme), using a previously characterized highly selective radiotracer of different structure. The radiotracer is injected in trace dose, while the compound is administrated in increasing pharmacological doses. The ratio of the specifically bound and free radiotracer, called the *binding potential*, is equal in the simplest case to the ratio of the concentration of the available receptor binding sites to the dissociation constant of the radioligand (B_{max}/K_d). The decrease in the binding potential of the radioligand after the administration of the unlabeled drug correlates with the decrease in the receptor B_{max}, indicating the interaction of the drug with its molecular target.

The occupancy of the receptor by a drug activates a cascade of intracellular processes which are regulated by different second messengers. In order to overcome possible side effects, *characterizing the downstream biochemical consequences of drug actions* may be useful in determining the efficacy of drugs (Gee, 2003). For example, one can monitor changes in the glucose level with [^{18}F]fluorodeoxyglucose (Cooper et al., 1998), changes in

cerebral blood flow using [^{15}O]H_2O (Theodore, 2000) or probe a second messenger system directly (e.g. the cAMP cascade using [^{11}C]rolipram; Lourenco et al., 1999).

1.3. Criteria for an effective radioligand for a GPCR[10]

Several criteria should be fulfilled to obtain an "effective" radiotracer to study receptors *in vivo*. Some of the important properties could be already tested *in vitro* for the "cold" analogue, but for the other criteria the answer can be obtained only after PET scan analysis.

Among the so called "design criteria", one can mention:

- The appropriate target for the PET study. The concentration of the target receptor (B_{max}) in the tissue of interest should be high enough to detect the PET signal with a good signal to noise ratio ($B_{max}/K_d > 4$). The lowest possible concentration of the receptor is considered to be around 1nM (10 fmole/mg protein), otherwise the picomolar affinity of the radioligand is required. This explains the existence of dozens of good radiotracers for the dopamine transporter (B_{max} > 100 nM), but no effective one for the norepinephrine transporter (B_{max} = 5 nM).
- The high affinity and selectivity of the "cold" analogue for the target.
- The possibility of rapidly and effectively labeling the precursor and purifying the radiotracer. The time from production of the isotope to the injection of the purified radiotracer to the patient or animal should not exceed three half-lives of the radioisotope (thus 60 min for ^{11}C or 5 h for ^{18}F). This is why efficient labelling and purification procedures are very much required.
- The accessibility of the target and low non-specific binding of the tracer. For most radiotracers the accessibility of the target means the ability to cross the blood-brain barrier, which depends on many factors, but the most important one seems to be the lipophilicity (logD), as polar organic molecules are not able to cross the membrane. On the other hand, the extreme lipophilic character of the drug could lead to its non-specific binding to the brain membrane and plasma proteins. It is recommended to maintain the logD of the radiotracer between 1.5 and 3, but the

[10] Inspired by the Master 2 course "Medicinal Radiochemistry: Design and Development of New Radiotracers for *In Vivo* Imaging" by Prof. Tony Gee (King's College London), University of Strasbourg, 2013.

fulfillment of this criterion is not a guarantee for the appropriate *in vivo* distribution of the radiotracer.

The parameters which should be tested *in vivo* are the following:

- A high signal to noise ratio.
- An appropriate *in vivo* pharmacokinetics. Besides the blood-brain barrier passage and the absence of the non-specific interactions, another very important parameter to consider is the possible elimination of the radiotracer from the brain or tumor by ATP-dependent efflux pump P-glycoprotein, which transports lipophilic compounds usually with a cationic amine group and few aromatic rings (Hall and Pike, 2011).
- An absence of the labelled metabolites. It should be noticed that PET, like other molecular imaging techniques, does not provide information on the position of the radiotracer at a given moment in time, but on the emitted radioactivity. The latter could result from the specifically bound ligand as well as from the unbound ligand or from the labeled metabolite. It is preferable that the radioisotope is present in the part of the molecule that will be rapidly cleared from the tissue of interest.
- A sensitivity towards the target.

1.4. PET radiotracers for OT and AVP receptors

The non-invasive determination of the distribution of OTR and $V_{1a}R$ with PET would be helpful to correlate the density of the receptors in different regions of the human brain with the observed cognitive dysfunctions and to confirm the implication of OTR and $V_{1a}R$ in the development of mental diseases. Moreover, selective radiotracers for the oxytocin and the vasopressin receptors could be used to study the distribution and metabolism of new drug candidates targeting these receptors.

Several attempts to synthesize effective radiotracers for OT and AVP receptors have been described, but to date none of them has been successful.

The first reported PET radioligand for the oxytocin/vasopressin receptors family was the $V_{1b}R$ antagonist [^{11}C]SSR149415 (Figure 7), developed in 2010 by the group of Jacob Hooker (Schönberger et al., 2010). The *in vivo* and *in vitro* characterizations of the radiotracer in non-

human primates showed strong affinity of the molecule to plasma proteins and very minimal uptake of the radioactivity in the brain after the IV injection.

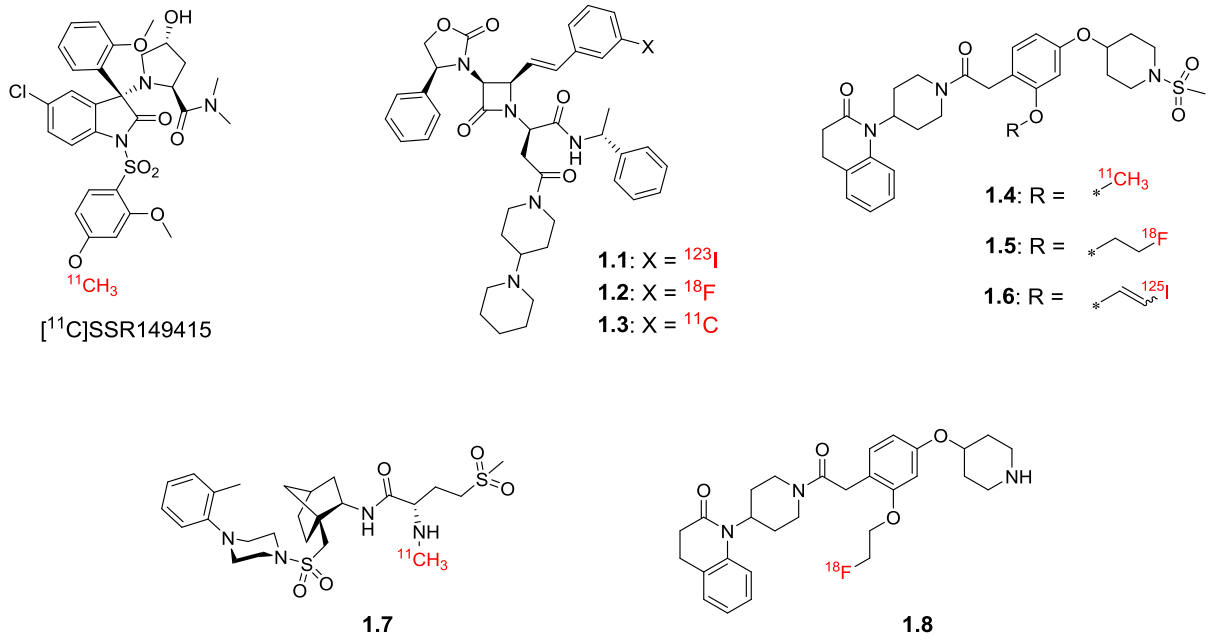

Figure 7. PET radiotracers for OT and AVP receptors developed to date.

$V_{1a}R$ selective antagonists **1.1**, **1.2** and **1.3** labeled with ^{123}I, ^{18}F and ^{11}C, respectively, were reported one year later (Fabio et al., 2011). Although the ligands presented subnanomolar affinity for the target receptor, excellent selectivity versus the other vasopressin receptors and high predicted blood-brain barrier permeability (by PAMPA-BBB test), the *in vivo* studies of the radiotracers have still not be published.

The first OTR radiotracers **1.4-1.6** were developed by the group of Mark Goodman in 2012 (Smith et al., 2012). These radiotracers allowed the researchers to obtain the first small molecule radioligand images of OTR and $V_{1a}R$ on rodent brain slices. However, none of the radioligands were convenient for the central PET investigations due to the insufficient uptake in the brain.

One year later the group published the synthesis and the evaluation of **1.7** – a ^{11}C derivative of L-368,899, an OTR antagonist which was previously reported to penetrate the blood–brain barrier (Smith et al., 2013a). The brain penetration was observed for the rat PET scans with **1.7**, but the specific uptake could be distinguished only by blocking the peripheral oxytocin receptors with a peptide OTR selective antagonist. However, no specific uptake was detected in a cynomolgus monkey model. According to the authors, the poor brain

accumulation could be explained either by the P-glycoprotein function or by the rapid metabolic demethylation leading to the loss of the radioactivity.

Finally, the ^{18}F-labeled OTR ligand **1.8** has recently been reported (Smith et al., 2013b). The PET imaging studies in rats showed that **1.8** reached the brain and accumulated in various regions, but washed out too rapidly for its adequate quantification and localization. *In vivo* PET imaging studies in a cynomolgus monkey revealed that the molecule had limited brain penetration. The authors suggested that the densities of OTR in the cynomolgus monkey brain are not high enough to afford a reliable PET signal using a biomarker with an affinity greater than 1 nM, or that they even do not exist.

In their following work, Goodman et al. investigated the neuroanatomical distribution of the oxytocin receptor in the male rhesus macaque brain by competitive binding autoradiography and localized the OTR mRNA by *in situ* hybridization (Freeman et al., 2014). Their results demonstrated that the OTR expression in the rhesus macaque brain is largely limited to the nucleus basalis of Meynert, pedunculopontine tegmental nucleus, the superficial gray layer of the superior colliculus, the trapezoid body and the ventromedial hypothalamus – the regions which are responsible for the processing of visual and auditory information and involved in social cognition. It is noteworthy that in rodents OTR is mostly expressed in the regions processing olfactory information (Ferguson et al., 2001).

Considering the growing interest in the role of OTR and $V_{1a}R$ in human social cognition and the existence of plenty of unanswered questions concerning the possibility of the PET detection of these receptors in the brains of mammalians and especially in man, the aim of our work was to develop efficient high-affinity radioligands for OT and V_{1a} receptors.

The preference was made for the ^{11}C analogues of the existing drugs which target OTR, as in such a case the time for the passage to the tests in human is considered to be reduced because of the already approved structure of the active compound.

2. [^{11}C] Carbetocin (CBT)

The oxytocin peptide analogue carbetocin (Figure 8), which has a similar binding profile for the oxytocin receptor but a much longer elimination half-live (85-100 min compared to 3 min for OT; Engstrøm et al., 1998), is approved for use in many countries for the control of postpartum intrauterine hemorrhage (Attilakos et al., 2010). Interestingly, although the OT is known to hardly pass the blood-brain barrier, several studies on the central effects of the carbetocin after its IV or IP injection have been published. For example, it was reported that CBT produced antidepressant-like changes in rat behavior, which were blocked by co-administration with the OTR antagonist atosiban (Chaviaras et al., 2010; Klenerova et al., 2009). In a recent study, it was shown that IP CBT was able to attenuate the negative emotional consequences of opioid withdrawal (anxiety, depressive-like behavior, reduction of sociability) in mice (Zanos et al., 2014).

In order to investigate the brain permeability of carbetocin and to follow its distribution after the IV injection, we envisaged the synthesis of its ^{11}C analogue by direct methylation of the desmethyl precursor **1.9** (Figure 8) with [^{11}C]CH_3I.

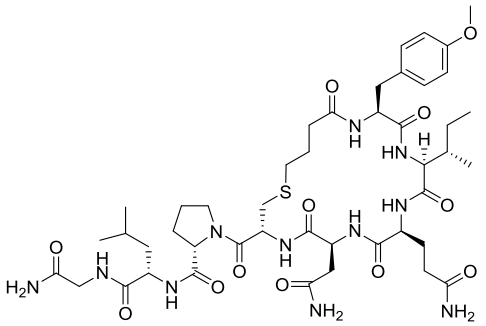

Carbetocin

OTR: K_i = 1.96 nM

V_{1a}R: K_i = 7.24 nM

V_2R: K_i = 61.3 nM

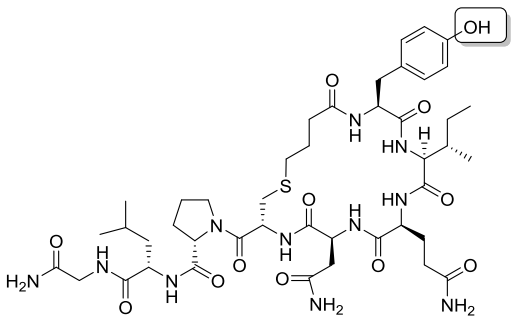

1.9

Figure 8. Carbetocin and its desmethyl precursor **1.9.**

The precursor **1.9** was obtained by manual Fmoc solid phase peptide synthesis (SPPS) following the slightly modified protocol described for the synthesis of the monocarba-oxytocin (Mayer and Heil, 1995). We firstly prepared the linear peptide chain **1.11** by alteration of the coupling steps of Fmoc-protected amino acids with HBTU and HOBt in DMF (with the exception of DIC/HOBt for the coupling of 4-bromobutyric acid) with the

cleavage of Fmoc protecting groups in 20% piperidine/DMF (Scheme 1). The completion of couplings and Fmoc cleavages was monitored with the ninhydrin test (Kaiser et al., 1970), the TNBS test (Hancock and Battersby, 1976) or the chloranil test (Mařík et al., 2003) as well as by analytical HPLC (minicleavages of the resin with TFA/H_2O 95/5).

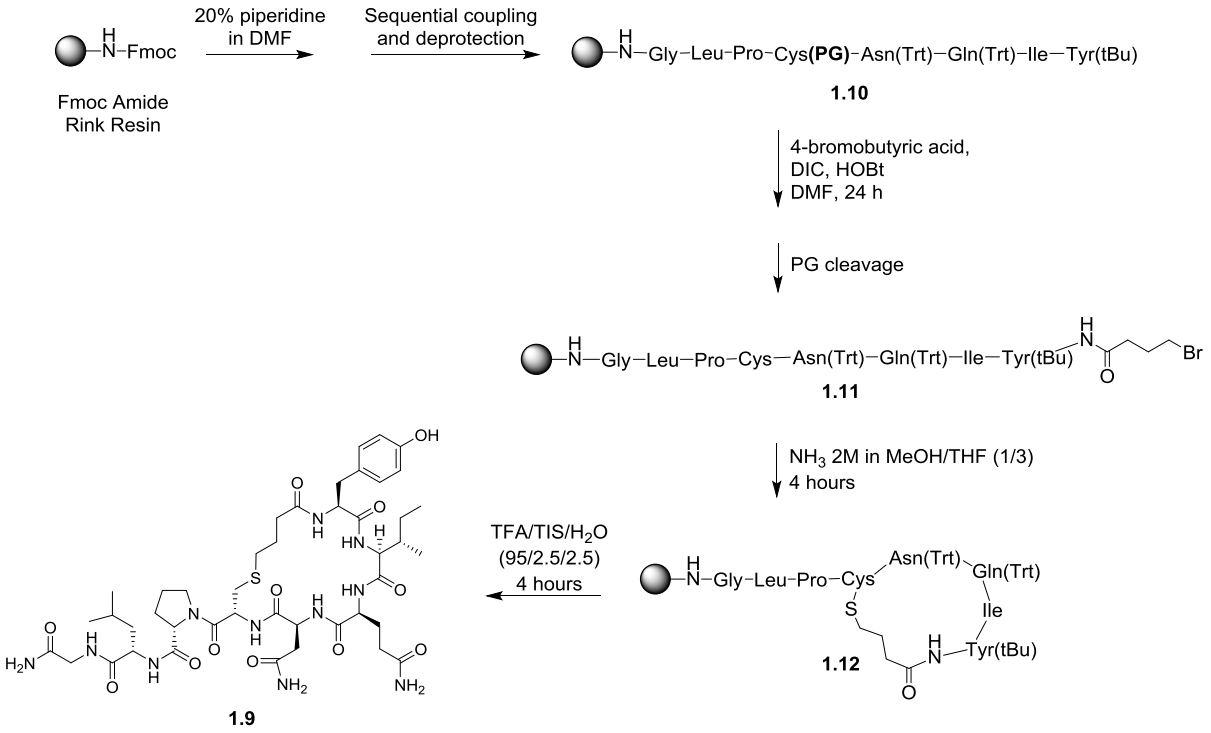

Scheme 1. Synthesis of the desmethyl precursor **1.9**.

Particular attention was paid to the choice of the Cys[6] protecting group (PG) as it should be labile enough to be easily removed prior to intramolecular cyclisation. First, the *S-tert*-butylsulfanyl protection was used, as it was reported to be orthogonal to Fmoc and Trt protecting groups and compatible with SPPS strategy (Ludolph et al., 2002). However, the desulfurization of Cys(S^{t}Bu) to alanine was observed during the reductive deprotection with tributhylphosphine (Scheme 2), as it has already been described for peptides of highly hydrophobic nature (the β-elimination process in the phosphonium intermediate followed by by reduction with the hydride donor triisopropylsilane is more favorable than the reaction with H_2O; Rijkers et al., 2005).

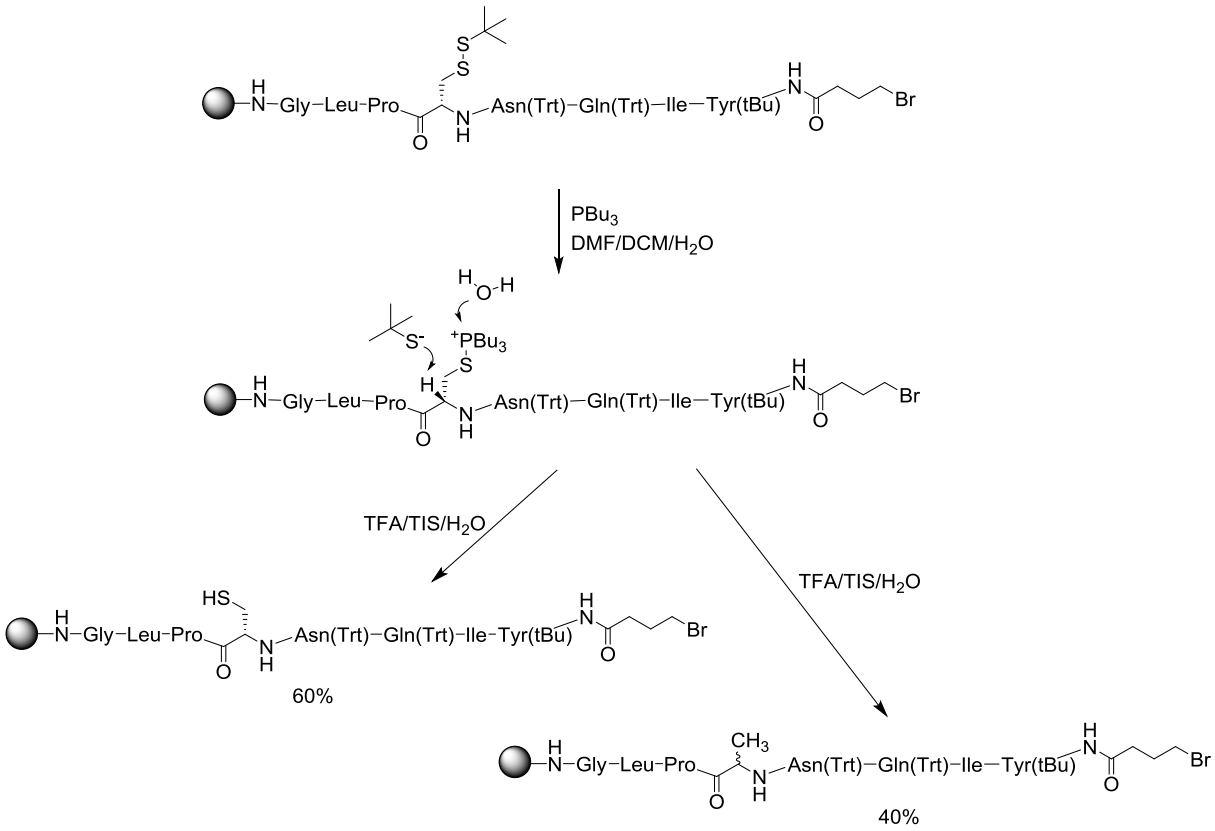

Scheme 2. Cleavage of the *S*-*tert*-butylsulfanyl protection group.

Thus, it was decided to use another protecting group for the cysteine, namely the 4-methoxyltrityl (Mmt; Barlos et al., 1996), which can be selectively cleaved under mild acidic conditions such as 2% of trifluoroacetic acid in DCM with 5% TIS (Beaino and Trifilieff, 2010). The deprotection was monitored by analytical HPLC (minicleavages of the resin with TFA/H_2O 95/5) and it was found that the Mmt group was completely removed after 6 cycles of deprotection (2 min each cycle).

The unprotected –SH group of the cysteine was then intramolecularly alkylated in the presence of 2M ammonia in methanol/THF mixture (Or et al., 1991). Finally, the cyclic peptide was cleaved from the solid phase in the mixture of TFA/TIS/H_2O (95/2.5/2.5) and purified by semi-preparative HPLC to give the target cyclic peptide in 22% overall yield.

The methylation of the precursor with [^{11}C]CH_3I should be fast (usually 5 min) and efficient in order to minimize the radioactivity loss due to the short half-decay time of ^{11}C and facilitate the purification of the target compound. We tested several alkylation conditions with "cold" CH_3I in DMF, which seems to be an optimal solvent as it solubilizes well all the compounds and can be directly injected into the HPLC, and found the best protocol for the

alkylation: in 5 min at 50°C in the presence of 20 eq of NaOMe the desmethyl precursor was fully converted to the carbetocin (Table 2).

Table 2. Conditions for the methylation of the precursor **1.9**.

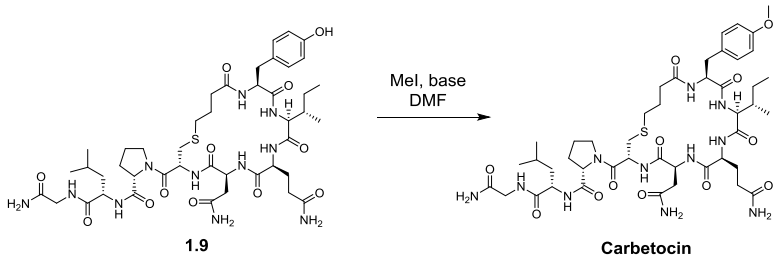

1.9 **Carbetocin**

Base	*20°C, 5 min*	*50°C, 5 min*
K_2CO_3	only traces of CBT	only traces of CBT
NaOMe	partial conversion	**total conversion**

The studies on the translation of the labelling protocol to the "hot" conditions are ongoing in the CERMEP Imaging Institute in Lyon in the group of Dr. Thierry Billard.

3. [^{11}C] Relcovaptan (SR49059)

The non-peptide selective V_{1a} receptor antagonist SR49059 (also known as relcovaptan, Figure 9) was developed by Sanofi-Synthélabo for the treatment of the Raynaud's disease (Hayoz et al., 2000), dysmenorrhea (Brouard et al., 2000) and preterm labour (Steinwall et al., 2005), but its studies were recently stopped in the phase II of clinical trials (Manning et al., 2012). Although no data on the brain permeability of SR49059 are available in the literature, it was reported that relcovaptan caused central effects after the IV injection, namely reversed the proconvulsive effects of AVP and OT (Loyens et al., 2012). Moreover, the presence of methoxy groups in SR49059 enables introduction of the ^{11}C label without changing the structure and the excellent pharmacological profile of the drug.

Among two methoxy groups, the one in para-position to the sulfonamide bond was chosen for the modification, as the corresponding starting material (guaiacolsulfonate) was commercially available.

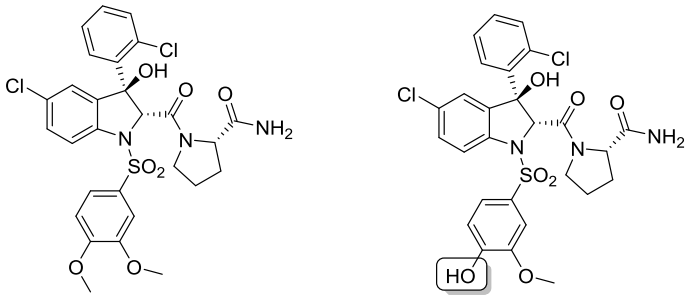

SR49059

$V_{1a}R$: K_i = 1.5 nM
$V_{1b}R$: K_i = 220 nM
V_2R: K_i = 275 nM
OTR: K_i = 130 nM

1.13

Figure 9. SR49059 and its desmethyl precursor **1.13.**

For the synthesis of the desmethyl precursor **1.13** we followed the synthetic route presented in Scheme 3, which was inspired by the synthesis of some related compound (Wagnon et al., 1992). The phenol protecting group is needed to be introduced at the very beginning and kept until the aldol reaction and should be stable in basic conditions.

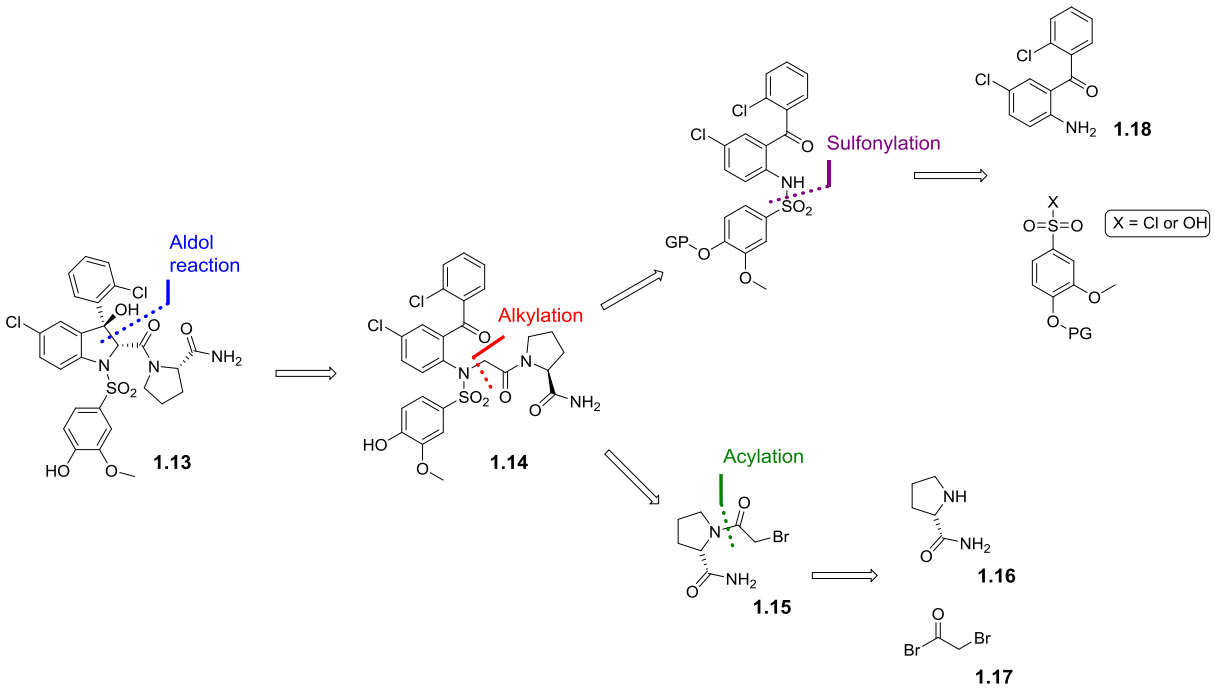

Scheme 3. Retrosynthetic analysis for the synthesis of the desmethyl precursor **1.13**.

It was decided to start the synthesis from the commercially available 4-hydroxy-3-methoxybenzenesulfonyl chloride **1.19** (Scheme 4).

First we tried to protect the phenolic OH with a TBDMS protecting group under standard conditions (TBDMS-Cl, NEt_3, DMAP, DCM), but it was revealed that **1.19** did not support treatment even with mild organic bases – significant amounts of by-products of polymeric nature were detected by HPLC. Thus, we used the base-free conditions of TBDMS group introduction, *viz.* *N*-methyl-*N*-(*tert*-butyldimethylsilyl)trifluoroacetamide in acetonitrile with catalytic amounts of TBDMS-Cl (Mawhinney and Madson, 1982) to get the protected compound **1.20** in almost quantitative yield.

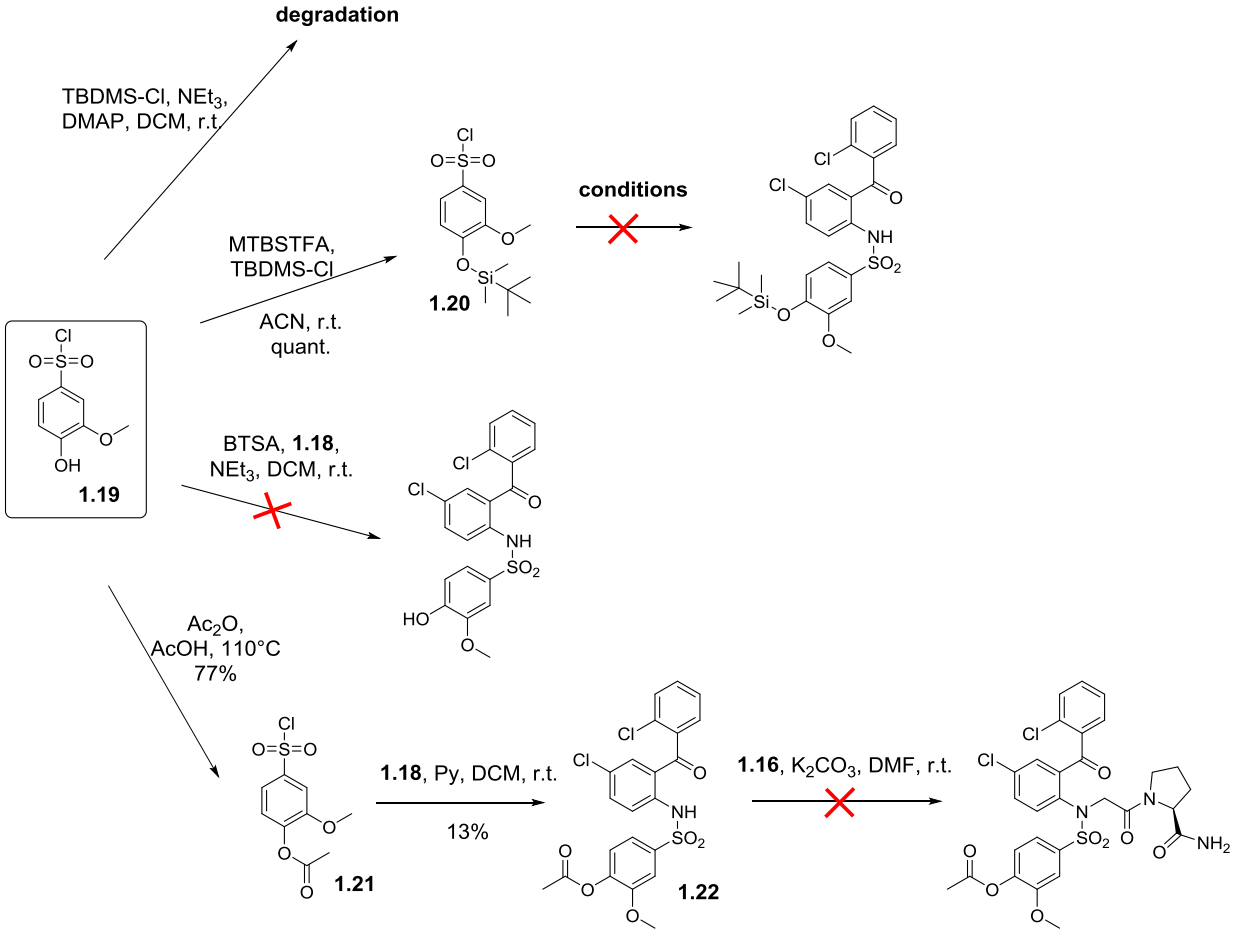

Scheme 4. Primary synthetic route started from 4-hydroxy-3-methoxybenzenesulfonyl chloride **1.19**.

However, we faced difficulties in performing the sulfonamide synthesis with compound **1.20**. Different basic and base-free conditions were tested (

Table 3), but they all resulted in instantaneous or slow degradation of **1.20** without any traces of new compounds (all the reactions were monitored by analytical HPLC with the detection at 220 nm and 254 nm and LC-MS). The explanation could be in the instability of the TBDMS protecting group under the treatment with organic bases and heating, however such a high lability is not usual.

Table 3. Sulfonamide formation from compound **1.20.**

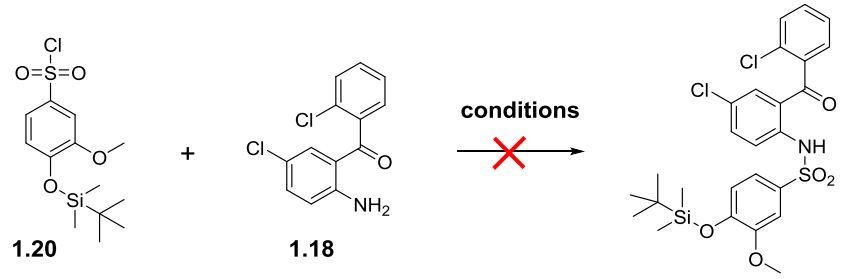

Conditions	*20°C*	*80°C*
pyridine / DMSO 1/2	degradation	n.d.
DIEA (5eq) / acetonitrile	no reaction	degradation
DIEA (5eq) / DMF	no reaction	degradation
K_2CO_3(5 eq) / DMF	slow degradation	degradation
HOBt (1 eq) / DIEA (3 eq) / DCM (Palakurthy and Mandal, 2011)	slow degradation	n.d.
In (1 eq) / ACN (Kim and Jang, 2007)	no reaction	slow degradation

We also failed to use trimethylsilyl (TMS) temporary protecting group (introduction with BTSA (*N*,*O*-bis(trimethylsilyl)acetamide; Levin et al., 2004)) to convert the starting benzenesulfonyl chloride **1.19** to the corresponding sulfonamide (Scheme 4).

Finally, we tested the acetate protecting group which can be also introduced under the base-free conditions (refluxing in Ac_2O/AcOH; Scheme 4). The protected benzenesulfonyl chloride **1.21** was obtained in good yield, however the protecting group was found to be too labile in basic conditions. The corresponding sulfonamide **1.22** was obtained in poor yield (13%) due to the Ac cleavage even in optimised mild conditions (10% of pyridine in DCM at r.t.), but during the next alkylation step the protecting group was completely lost and the desired compound was not detected.

Thus, it was concluded that 4-hydroxy-3-methoxybenzenesulfonyl chloride **1.19** was not suitable for the synthesis of the SR49059 desmethyl precursor. In order to get more flexibility in choice of the protecting group, we decided to start the synthesis from potassium guaiacolsulfonate **1.23** (Scheme 5).

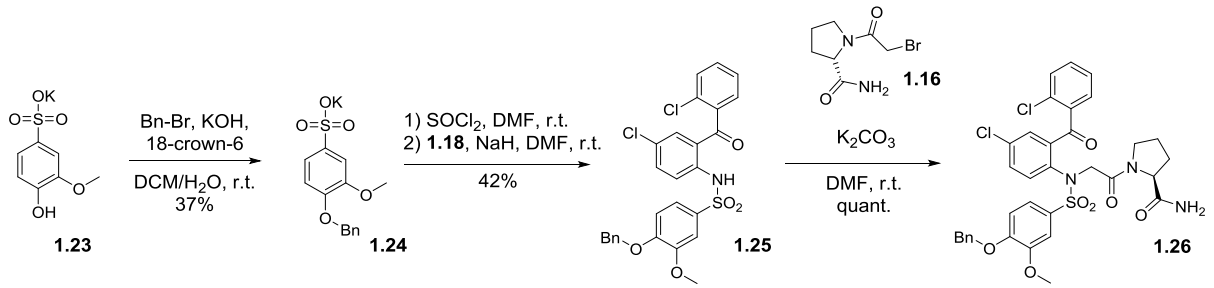

Scheme 5. Synthetic route started from potassium guaiacolsulfonate **1.23**.

To protect the potassium guaiacolsulfonate, the benzyl (Bn) protecting group was chosen for its excellent stability in the presence of bases and a possibility to be removed either by hydrogenolysis or by the action of Lewis acids. Taking into account that the started compound **1.23** was only soluble in water, we conducted the protection in heterogeneous conditions DCM/water under phase-transfer catalysis following the described protocol (Dziuba et al., 2011). 18-crown-6 was supposed to coordinate the potassium ion and thus to increase the concentration of the guaiacolsulfonate at the interface. Although, the yield of the reaction was moderate (37%), the accessibility of starting materials enabled us to continue the strategy. The benzyl guaiacolsulfonate **1.24** was then engaged into the two-step sulfonamide formation (via the corresponding sulfochloride) to afford **1.25** in 42% overall yield. The latter was alkylated with 1-bromoacetyl-2-(*S*)-pyrrolidinecarboxamide **7** (prepared according to Villhauer et al., 2002) in the presence of potassium carbonate in DMF to yield quantitatively the target compound **1.26**.

Different conditions for the cleavage of the benzyl protecting group were tested (Table 4). The treatment of **1.26** with methyl phenyl sulfide in TFA (Kanamori et al., 2011) surprisingly leaded to a complete rupture of the sulfonamide bond. The yield of the hydrogenation over Pd/C under atmospheric pressure strongly depended on the quantity of the catalyst used. The reaction carried out with 0.1 eq. of Pd/C was too slow, but when the quantity of catalyst was increased to 0.5 eq. reductive dechlorination occurred. The optimal conditions were found to be 0.3 eq of Pd/C and the desired compound **1.14** was isolated in 62% yield.

Table 4. Conditions for the cleavage of the Bn protection in **1.26.**

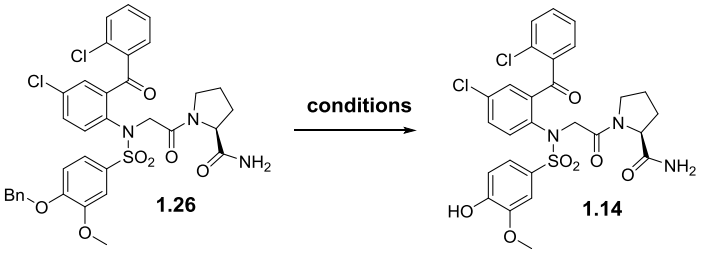

Conditions	*Overnight yield (analyzed by HPLC)*
8 eq. MPS in TFA, 20°C (Kanamori et al., 2011)	0% (sulfonamide bond rupture)
0.1 eq. Pd/C in EtOAc, 20°C, 1 atm.	22% (conversion not total)
0.5 eq. Pd/C in EtOAc, 20°C, 1 atm.	68% (partial dechlorination)
0.3 eq. Pd/C in EtOAc, 20°C, 1 atm.	**90%**

The last step of the synthesis of the desmethyl precursor **1.13** implicated the intramolecular cyclisation of **1.14** by Aldol reaction (Scheme 6). The described conditions for the synthesis of SR49059 were DBU in MeOH at -10°C (Wagnon et al., 1992). We tested some other cyclisation conditions, *viz*. K_2CO_3 in MeOH or in DMF, tBuOK in DMF, as well as the influence of the temperature (-10°C, 25°C and 50°C) and found that the full conversion of the starting material **1.14** was achieved by its treatment with DBU in MeOH at 25°C.

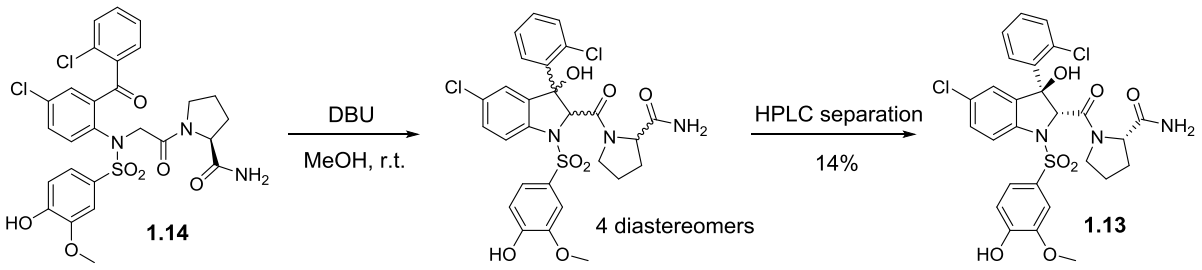

Scheme 6. Intramolecular cyclisation of **1.14.**

Four diastereomers were detected by analytical HPLC as a result of the cyclisation. Two of them resulted from the new bond formation, however, the two others were supposed to be formed after the racemization of the prolinamide under the DBU treatment.

The principal question was how to identify the target diastereomer in the mixture. Unfortunately, 1D and 2D NOESY studies did not show any characteristic correlations neither for the commercial SR49059 nor for the mixture of diastereomers. We decided to find the

target isomer by methylation of its phenolic hydroxyl and comparison of the retention time of resulted compound with that of SR49059. Thus, the diastereomeric mixture was roughly separated by semi-preparative HPLC which allowed us to get three fractions with major compounds II, III and IV (Figure 10). We treated all fractions with MeI in the presence of an excess of K_2CO_3 in DMSO at 70°C and found that the major compound from the fraction II gave SR49059 under methylation. The target diastereomer was purified by semi-preparative HPLC and characterized by RMN and LC-HRMS.

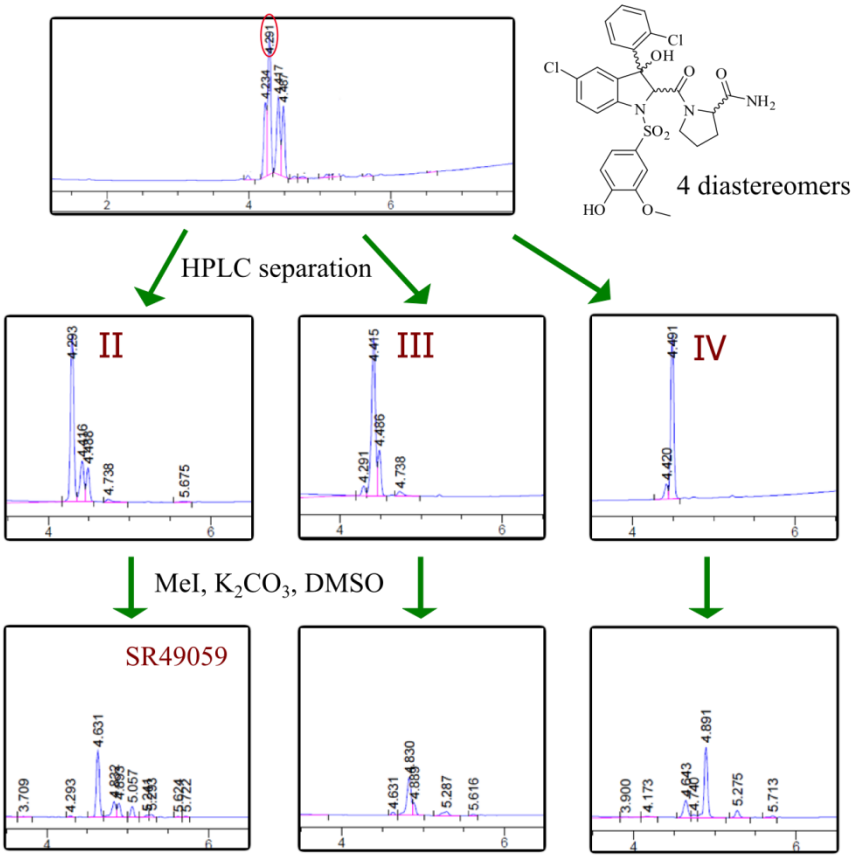

Figure 10. Separation of the diastereomers of **1.13.**

The radiomethylation studies on the precursor of SR49059 are ongoing in the CERMEP Imaging Institute in Lyon in the group of Dr. Thierry Billard.

3. [^{11}C] PF-3274167

The triazole oxytocin receptor antagonist PF-3274167 (Figure 11), published in 2010 by Pfizer research group (Brown et al., 2010), attracted our attention due to its excellent pharmacological profile, high oral bioavailability and good CNS penetration (Borthwick, 2010). Moreover, it seemed that the synthesis of its desmethyl precursor **1.27** should be rather straightforward, as the triazole formation was the last step according to the proposed synthetic route (Brown et al., 2006).

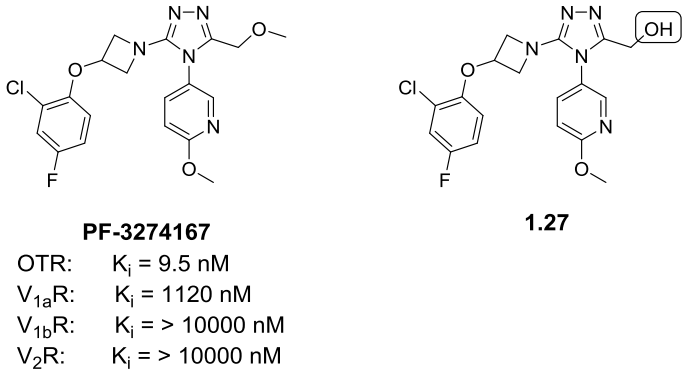

Figure 11. PF-3274167 and its desmethyl precursor **1.27.**

The synthesis of the desmethyl precursor **1.27** started from the thiourea **1.28** (Scheme 7), which was obtained in excellent yields (90% for 3 steps) according to the described protocol (Brown et al., 2006). It was converted to the corresponding *S*-methylisothiourea by treatment with methyl iodide in the presence of potassium carbonate and engaged into the acid-catalyzed condensation with OH-protected hydroxyacetic acid hydrazide **1.31**, which was synthesized from methyl glycolate in two steps. Again, we supposed that the benzyl protecting group would be the most appropriate for the hydroxyl protection. The desired benzyl protected triazole **1.32** was isolated in 41% yield (two steps).

The protecting group was readily cleaved by treatment with boron trichloride in dichloromethane at ice-water temperature (Polucci et al., 2013) to afford the desmethyl precursor **1.27** in 90% yield.

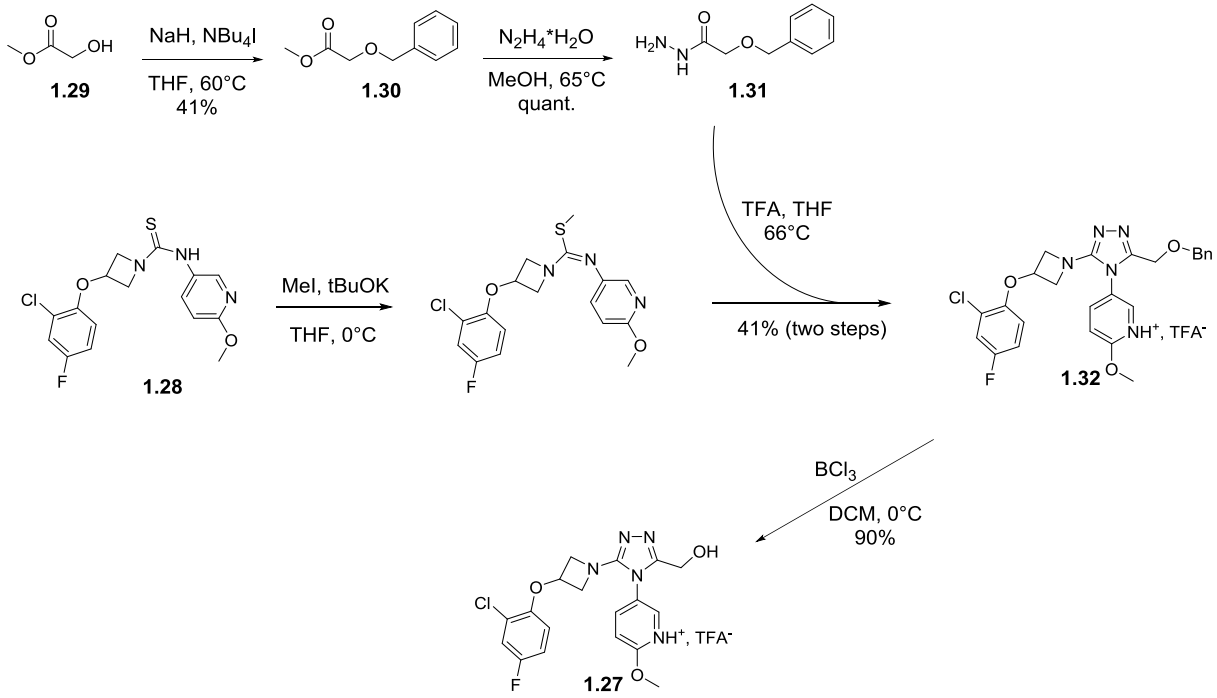

Scheme 7. Synthesis of the desmethyl precursor of PF-3274167.

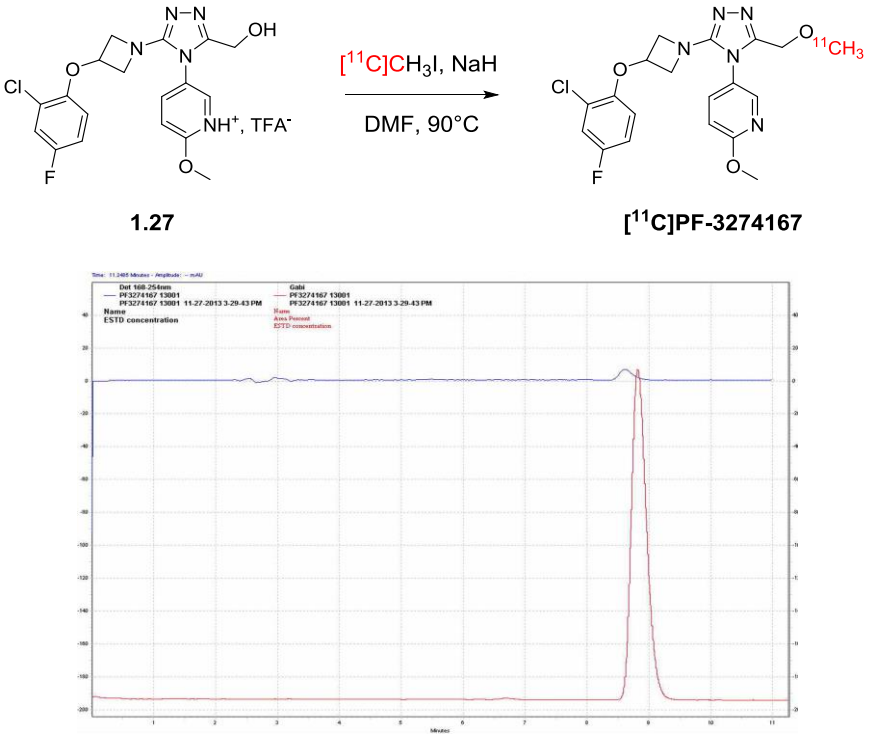

Figure 12. Radiolabelling of **1.27** and the quality chromatogram of final [^{11}C]PF-3274167 (UV absorbance at 254 nm in blue and radioactivity in red)

The introduction of the ^{11}C label was performed in the CERMEP Imaging Institute in Lyon by the group of Dr. Thierry Billard. The precursor **1.27** was treated for 5 min at 90°C with [^{11}C]CH_3I in DMF in the presence of NaH. The radiolabeled compound was produced in good radiochemical yield (71%, EOB), >95% radiochemical and chemical purity and specific activity (EOS) of 28.9 GBq/µmol (Figure 12).

Then, the distribution of [^{11}C]PF-3274167 in rat brain (striatum and hippocampus) was evaluated by semiquantitative autoradiography by the group of Prof. Luc Zimmer (Lyon Neuroscience Research Center, Lyon and CERMEP-Imaging platform). The autoradiograms, obtained by incubation of brain slices with 10 nM of [^{11}C]PF-3274167, revealed the accumulation of the radioactivity in the selected brain regions (Figure 13). However, no decrease in the binding level was detected after the competition with "cold" PF-3274167, indicating that the distribution of the radiotracer in rat brain was not specific to the oxytocin receptors. The absence of the specific binding could be explained by either low density of the receptors and thus non-sufficient affinity of the probe (a B_{max}/K_d ratio of at least 4 is required for an optimal PET binding), or by an unexpectedly high lipophilicity of PF-3274167, which caused strong non-specific interactions.

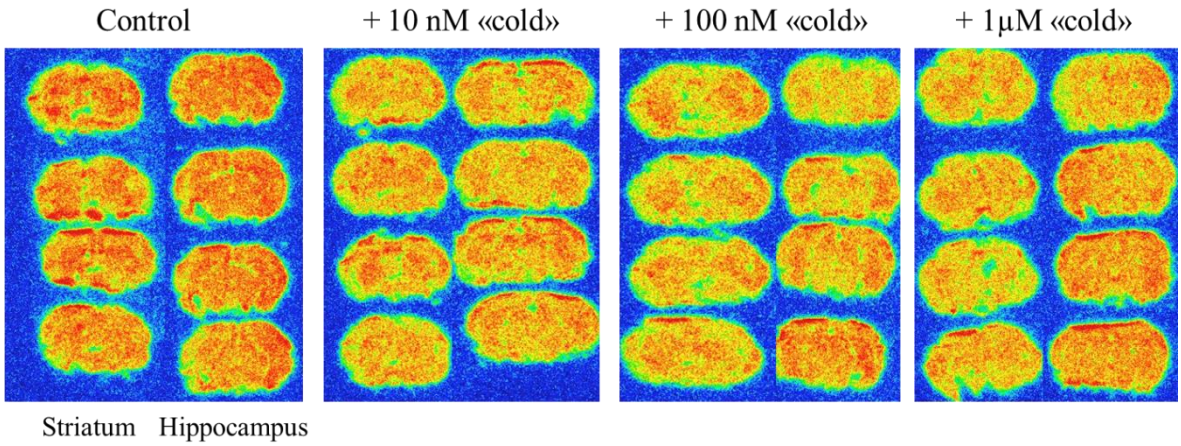

Figure 13. *In vitro* autoradiograms of rat brain sections incubated with [^{11}C]PF-3274167 and after competition with cold PF-3274167.

4. [^{18}F] derivative of PF-3274167

^{18}F radionuclide is often considered as preferable over ^{11}C for PET due to its optimal radioactivity decay half-live and the highest resolution of images of all the available positron emitters (Miller et al., 2008b).

We aimed to develop a ^{18}F derivative of PF-3274167 that would retain the high affinity and selectivity of the parent ligand. It was decided to substitute the lateral methoxy group in the molecule by a fluoroethoxy group (Figure 14). Thus the ^{18}F label will be introduced by nucleophilic substitution of the corresponding tosylate **1.34**.

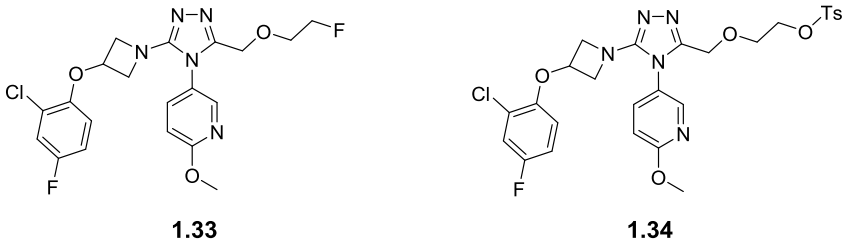

Figure 14. Fluorinated derivative of PF-3274167 **1.33** and its precursor **1.34.**

The synthesis of the precursor **1.34** started from the already obtained scaffold **1.27** (Scheme 8). Firstly, the hydroxyl group of **1.27** was alkylated with benzyl 2-bromoethyl ether in the presence of KOH in DMF to afford **1.36**. Then, the Bn protecting group was cleaved in mild conditions by treatment with boron trichloride in DCM at -78°C and finally the liberated hydroxyl was tosylated to give the target precursor **1.34** in good yield.

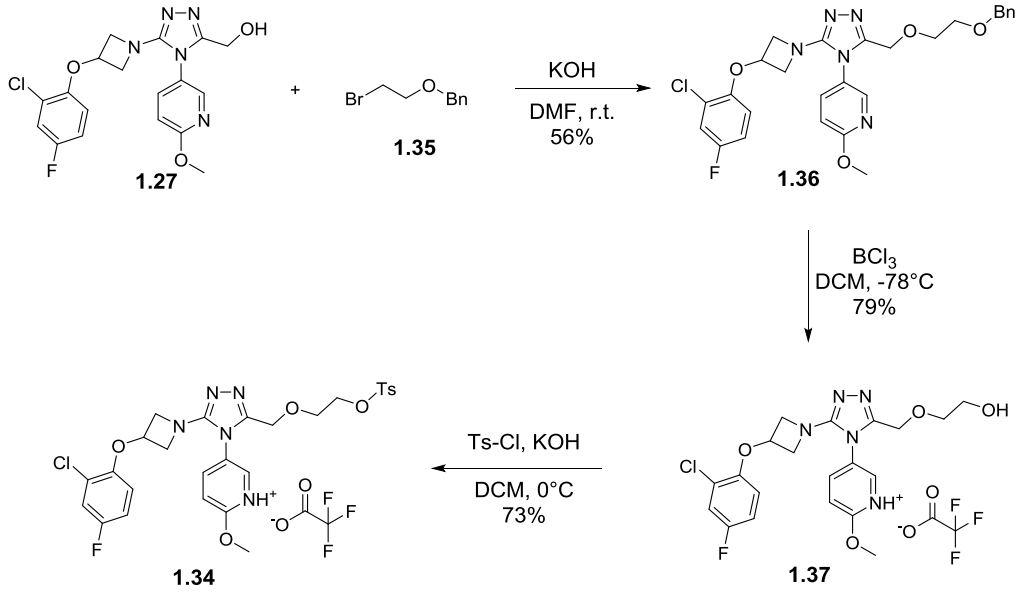

Scheme 8. Synthesis of the precursor **1.34** for ^{18}F labelling.

We also prepared the "cold" fluorinated compound **1.33** by alkylation of **1.27** with 1-fluoro-2-tosylethane **1.39** (Scheme 9).

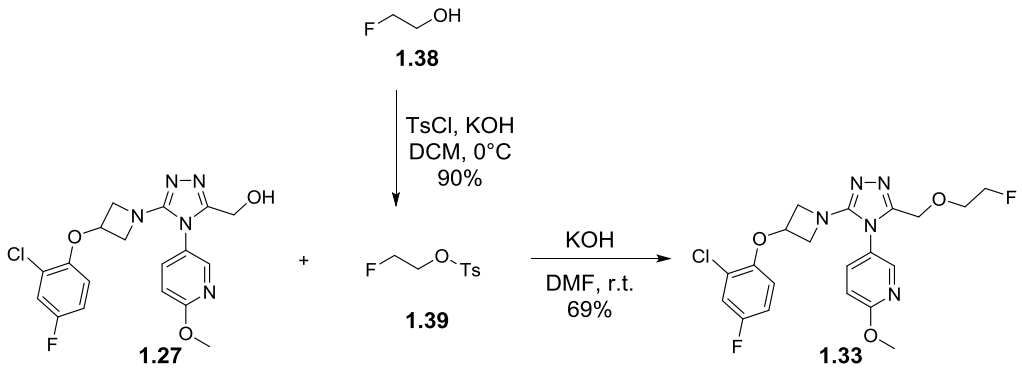

Scheme 9. Synthesis of the "cold" **1.33**.

Surprisingly, the affinity of **1.33** for the oxytocin receptor (investigated at PCBIS, Strasbourg) was not only retained, but improved in comparison to the parent PF-3274167 (Table 5). The functional activity tests by measurement of intracellular calcium release confirmed the preservation of the antagonistic character of the ligand (IC_{50} = 1 nM).

Table 5. Physico-chemical and pharmacological properties of PF-3274167 and **1.33.**

	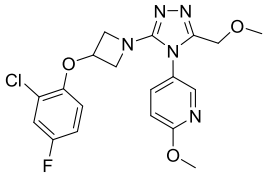 PF-3274167	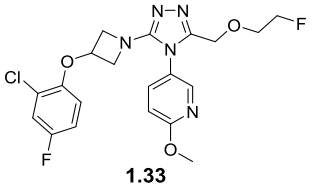 1.33
Molar mass, g/mol	419.84	451.85
Lipophilicity (logD)*	2.42	2.58
K_i OTR (nM)	9.5	1.6
K_i V_{1a}R (nM)	1120	>1000
K_i V_{1b}R (nM)	>10000	>1000
K_i V_2R (nM)	>10000	nd

* log D was calculated using online ChemAxon physico-chemical property predictor

The radioactive labelling with ^{18}F was performed by the group of Dr. Thierry Billard under classical conditions for the nucleophilic substitution with F^- (Scheme 10). Firstly, the precursor **1.34** was rapidly treated with sodium hydride in order to eliminate the TFA salt (which is not compatible with $^{18}F^-$ because of the relatively high pK_a of the latter). Then, the fluorination was performed with [^{18}F]KF in DMSO in the presence of Kryptofix® 2.2.2. Although, the radiochemical and chemical purity of **[^{18}F]1.33** was very high (>95%), the radiochemical yield of the reaction (EOB) was less than 1%. As it was confirmed afterwards, the precursor **1.34** was not stable in its neutral form, probably due to the rapid intermolecular nucleophilic substitution of the OTs by the pyridine nitrogen.

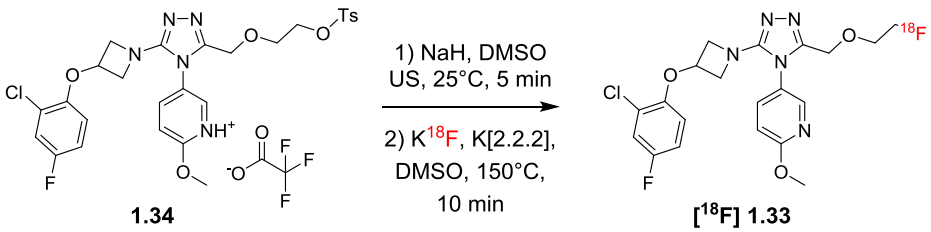

Scheme 10. Radiolabelling of **1.34** with ^{18}F.

Despite the poor radiochemical yield, we were able to perform preliminary autoradiography studies in rat brains. The non-homogenous accumulation of the radioactivity

in striatum and hippocampus, OTR-rich regions (Figure 15) allowed us to suppose that **[^{18}F]1.33** could bind specifically to the oxytocin receptors in rat brains. However these data are preliminary and further studies are indispensable. Particularly, it will be crucial to evaluate the specificity and the selectivity of this binding before envisaging a transfer to *in vivo* experiments (e.g. microPET studies).

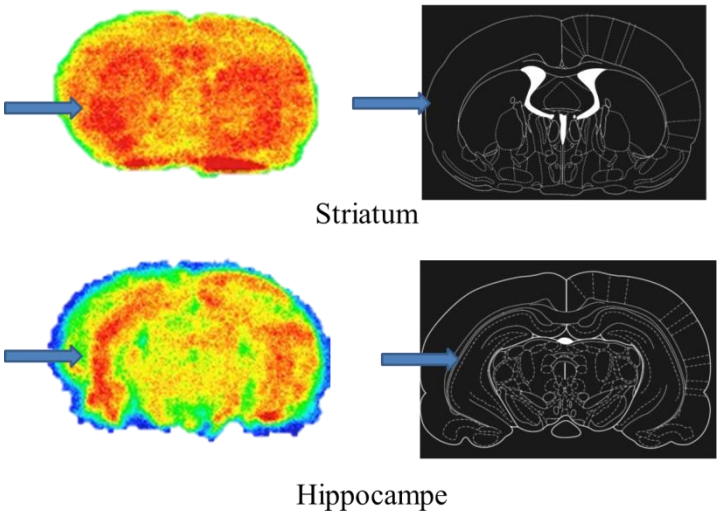

Figure 15. *In vitro* autoradiograms of rat brain sections incubated with **[^{18}F]1.33**.

To improve the radiochemical yield of the synthesis of **[^{18}F]1.33** we decided to perform a two-steps radiolabelling procedure starting from the desmethyl precursor **1.27** (Scheme 11).

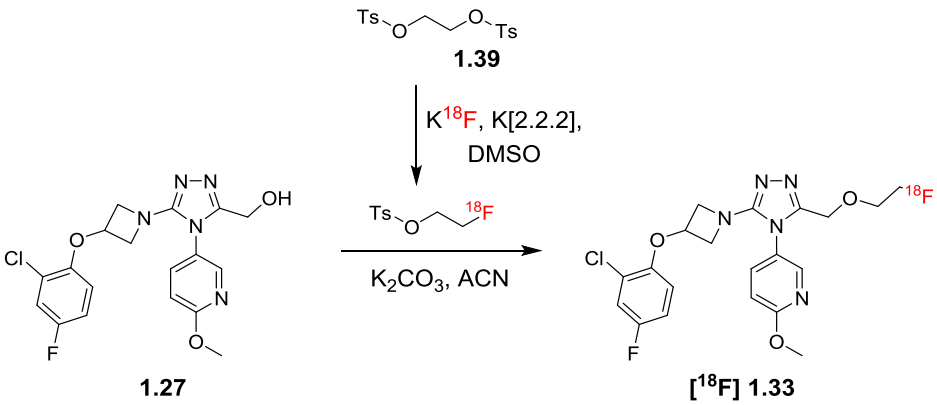

Scheme 11. Two-step labelling procedure for the introduction of ^{18}F.

The optimization of the two-step radiolabelling procedure and the validation of the sequence are ongoing.

5. Conclusion and perspectives

The objective of the first part of my research project was to develop effective PET radiotracers for the oxytocin and the vasopressin V_{1a} receptors. With such tools in hand, it will be possible to study the distribution of these receptors in the non-human primate brains and in men and to answer the question, is there a correlation between the distribution or the expression level of OTR and $V_{1a}R$ and cognitive dysfunctions, such as autism.

We synthesized and fully characterized three precursors for [^{11}C]CH_3 labelling to produce ^{11}C analogues of drugs, already approved in humans. One of them, [^{11}C]PF-3274167, has already been studied by autoradiography in rat brain slices, however, the detected binding was not specific.

A fluorine atom was then introduced in OTR antagonist PF-3274167 via the lateral fluoroethoxy group, which turned the ligand even more potent and selective. The corresponding "hot" ^{18}F radiotracer was able to distinguish the regions with different OTR density by autoradiography in rat brain slices; the optimization of the labelling method as well as further autoradiography and PET studies are ongoing.

We envisage using the developed radiotracers to study the distribution and the expression level of the oxytocin receptors in the "enamored" macaque model developed by the group of Dr. Jean-René Duhamel in the Institute of Cognitive Science in Lyon.

PART II. Fluorescent probes for the oxytocin and the vasopressin receptors

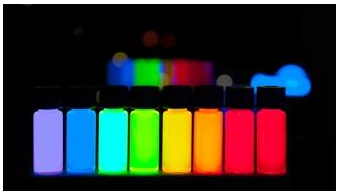

Introduction to fluorescence

During last few decades there has been a remarkable growth in the use of fluorescence to study biological objects. This technique became nowadays one of the most commonly used in chemical and molecular biology to investigate cellular events at the molecular level as well as in medical diagnostics to perform tissue and whole animal imaging.

Luminescence in general refers to an emission of light by a substance after its excitation with light of higher energy (Lakowicz, 2006). If the emission is resulted from the first singlet excited state (S_1), such a phenomenon is known as *fluorescence* (Figure 16A). The basic fluorescence parameters are the *absorption* and *the emission maxima* (λ_{max} abs and λ_{max} fluo, respectively) and their difference, which is called *the Stock shift* (Figure 16B). The ability of a fluorophore to absorb light of a given wavelength is known as *the extinction coefficient* (ε). *The luminescence quantum yield* (QY) denotes the percentage of the absorbed energy which is emitted after the vibrational relaxation and nonradiative deexcitation processes. Finally, the product of the extinction coefficient and the quantum yield gives *the brightness* – an important characteristic of a fluorophore.

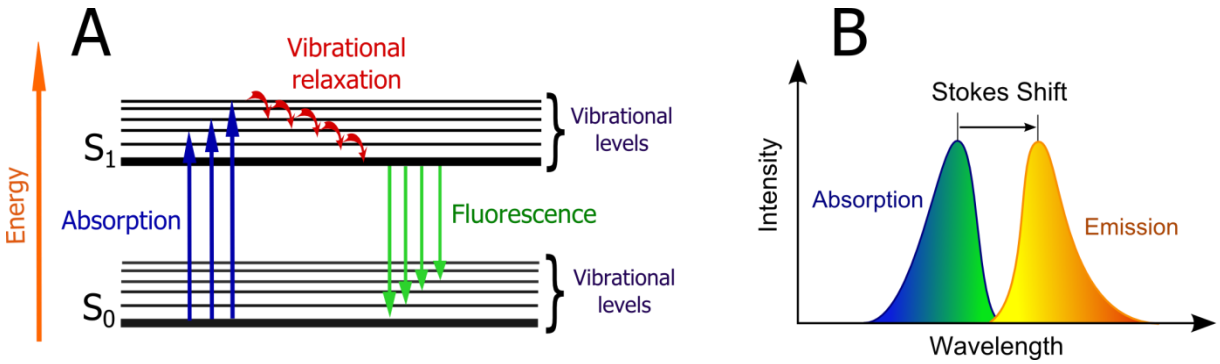

Figure 16. (A) A simplified representation of the Jablonski diagram of molecular energy levels. (B) A schematic representation of absorption and emission spectra.

Among the advantages of the fluorescence detection in comparison to other molecular imaging techniques one can point out the ultra-high sensitivity, which reaches the absolute limit of single molecules, the high speed of response (up to 10^{-8} – 10^{-10} s), limited only by the speed of photophysical processes, considerable spatial resolution allowing for the detection of molecular interactions, and finally the non-destructive and non-invasive character which makes this technique suitable for biological and medical application (Demchenko, 2009).

As a consequence, fluorescence is proven to be a versatile tool for a large range of applications, such as cellular imaging (Wombacher and Cornish, 2011), immunofluorescence assays (Fritschy and Hartig, 2001), measurement of an analyte concentration inside the cell (Wang et al., 2012; Yang et al., 2013), studies of protein folding and dynamics (Michalet et al., 2006; Royer, 2006), following biomolecular interactions (Deshayes and Divita, 2013; Loving et al., 2010), detection and quantification of ligand-receptor interaction (Ma et al., 2014; Sridharan et al., 2014).

Fluorescence methods to study ligand-receptor binding

The utility of fluorescent ligands for the study of GPCRs has been recognized for several decades (Kuder and Kieć-Kononowicz, 2008). They allowed the visualization and localization of receptors in cells and tissues (Leopoldo et al., 2009), the studies of conformational changes following an agonist binding (Harikumar et al., 2005), the real-time monitoring and quantification of ligand-receptor binding (Sridharan et al., 2014).

Two major requirements to fluorescent ligands to study GPCRs are the preservation of the pharmacological profile of the ligand modified with a fluorescent probe (which in the case of biogenic amines, for example, is always greater than the native ligand) and the ability to distinguish the specifically bound fraction of the ligand from the free and the non-specifically bound ones.

Approaches to obtain a fluorescence response from the ligand-receptor binding event include:

1. *Separation of bound and free ligand*. If fluorescence of the label is not sensitive to the changes in the environment, such fluorescent ligands can be used as a replacement of radioactive tracers in binding assays. This requires the mechanical separation of the bound fraction from the unbound one and the quantification of fluorescence from each fraction (Shi et al., 2005). However in comparison to radioactive labelling such an alternative fluorescence approach suffers from several drawbacks. First, the fluorescence of small organic probes could be rarely absolutely independent of environmental changes. In most cases small fluctuations of quantum yield and/or fluorescence maximum are present which lowers the precision of the measurement. Then, one should notice that fluorescence is not an absolute parameter which can be easily quantified. The use of fluorescent standards in identical instrumental conditions

is required to get any quantitative information from the fluorescence emission. After all, the measurement could be affected by the cellular autofluorescence, not mentioning the fact that fluorescence detection is rather less sensitive compared to the radioactive one.

2. *Membrane staining by fluorescence microscopy* is apparently the oldest approach to detect a ligand-to-receptor binding (Melamed et al., 1976). It was widely used to visualize different GPCRs at the cell surface, however the method lacks for the information on the mechanism of the interaction and the receptor activation. Moreover, the accurate quantification of the binding by fluorescence microscopy becomes difficult because of cellular autofluorescence, ligand-induced receptor internalization and non-specific binding to the cell membrane.
3. *Flow-cytometry* is based on measuring fluorescence of the whole cell only when it passes through the narrow fluid path of the cytometer. This allows the statistical quantification of the light emitted from cells in homogenous conditions which is then correlated with the amount of the bound ligand (Waller et al., 2004). However, the approach is limited to the investigation of high-affinity interactions, which do not require high ligand concentration resulting in a fluorescence background.
4. *Fluorescence correlation spectroscopy (FCS).* The idea of FCS is to detect fluctuations in fluorescence of the ligand caused by diffusion changes by binding to the receptor. The ability of the correlation spectroscopy to track free and bound ligands in the same solution enables the time-dependent binding measurement under homogenous conditions (Briddon and Hill, 2007). However, the measurement could be complicated by various diffusion times got for the same ligand's fraction due to the binding to oligomeric receptors or the non-specific interactions.
5. *Fluorescence anisotropy or polarization* is widely used to determine ligand-receptor dissociation constants. The method is based on the detection of changes in ligand's rotational motion by analyzing the polarization of the emitted light. The unbound ligand undergoes rapid rotation in the solution which results in unpolarized fluorescence even when illuminated with linearly-polarized light. However, if the rotation is hampered by the receptor binding, the fluorescence of the ligand becomes partially polarized. The approach does not require separation of the unbound ligand and is easily applicable to high-throughput screening (HTS) using fluorescence plate reader with polarization detection (Albizu et al., 2007; Lee, 2000). The only limitation of the

method is that the obtained anisotropy signal represents the average value of the system, so a significant portion of the ligand should be bound to the receptor in order to get a reliable signal.

6. *FRET- and TR-FRET-based assays.* The principle of FRET (Förster resonance energy transfer) is based on the non-radiative photon transfer from an excited donor fluorophore to an acceptor fluorophore, causing the fluorescence emission of the latter (Figure 17A). This results in an increased Stocks shift and in a receptor-specific fluorescence signal of the acceptor, which emits light only in the close proximity to its donor (Figure 17C). The main requirements for the efficient FRET is the distance between the fluorophores, which should not exceed 10 nm, and the overlap of the fluorescence spectrum of the donor with the absorption spectrum of the acceptor (Figure 17B). The FRET-based assay is performed in homogenous conditions, as no separation of the unbound and bound ligand fractions is necessary, and is easily amenable to HTS.

   The use of rare-earth lanthanides with long emission half-lives as donor fluorophores enabled the recent development of a time-resolved modification of the resonance energy transfer (TR-FRET). The important feature of the lanthanide emission is an extremely long luminescence lifetime (Berezin and Achilefu, 2010), which makes possible the application of the delay between the excitation pulse and the detection of the donor fluorescence, thus completely eliminating the short-lived cellular fluorescence. This powerful combination of FRET with time-resolved detection resulted in the development of the Tag-lite® technology with great advantages in terms of flexibility, rapidity, user friendliness, and easy miniaturization (Cottet et al., 2013; Zwier et al., 2010).

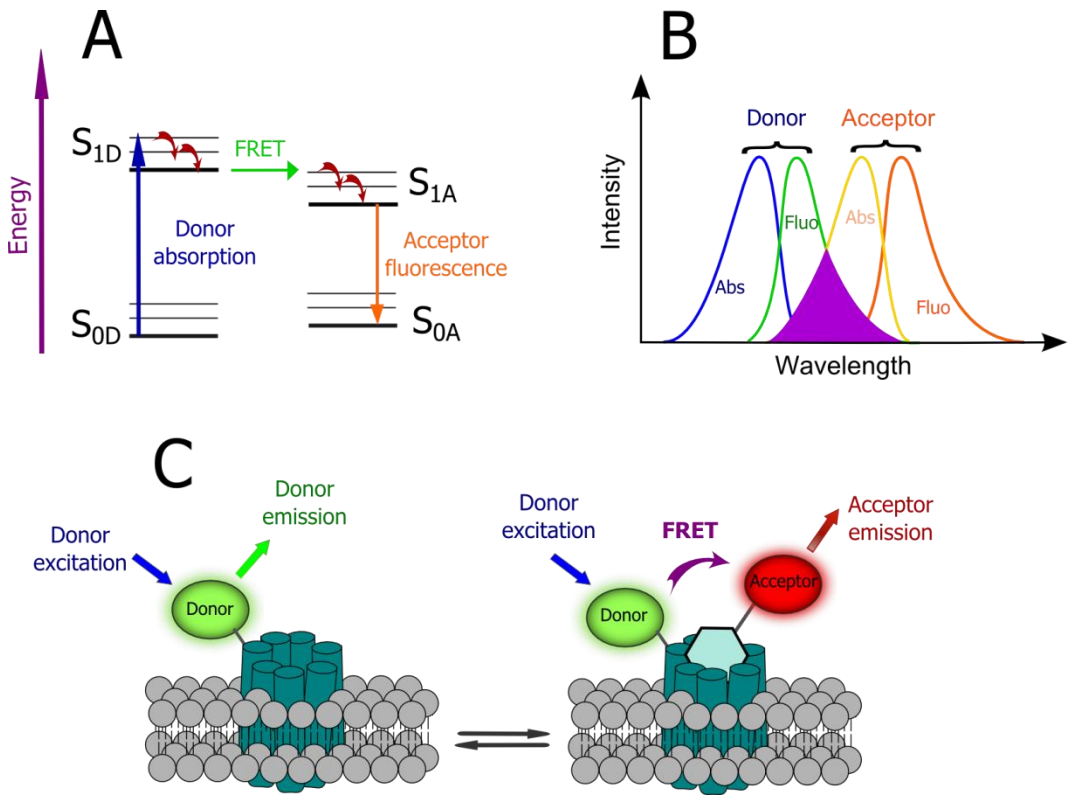

Figure 17. (A) Jablonski diagram of FRET. (B) Spectral conditions of FRET. (C) FRET detection of ligand-receptor interactions.

Considering the importance of fluorescence to study G protein-coupled receptors, we aimed to develop fluorescent ligands for the oxytocin receptor that could serve to establish TR-FRET based screening assay for OTR and on the other hand, contribute to the discovery of alternative methods for HTS on GPCR, especially those which can be performed with non-modified receptors.

Chapter 1. Fluorescent probes for binding studies

Fluorescent ligands for TR-FRET assays

1. Tb (III)–labeled ligands

During the past few decades luminescent lanthanide complexes have attracted considerable interest for biomedical analysis and imaging because of their exceptional photophysical properties (Bünzli, 2010; Hanaoka, 2010). Their large Stocks shift preserves lanthanide complexes from self-quenching, whereas line-like emission enables multicolor detection assays. Maybe the most important feature of the lanthanide emission is an extremely long lifetime caused by the ligand-to-metal charge transfer mechanism of luminescence (Figure 18; Berezin and Achilefu, 2010). Free lanthanides are not capable of absorption of photons due to the forbidden nature of 4f-4f transitions. The organic ligand plays a role of an antenna by capturing of a photon and transferring it by intersystem crossing via the first excited triplet state T_1 to the 4f* excited state of the Tb (III). The 4f orbitals of lanthanides are effectively shielded by the filled 5p and 6s orbitals from the quenching by the oxygen which results in very long (up to milliseconds for Tb (III)) luminescence lifetimes.

This advantage is widely used in time-resolved screening assays and time-gated imaging, the idea of which is to employ a delay between the excitation pulse and the detection in order to eliminate any background fluorescence of small organic dyes and cellular constituents and to extremely increase the signal-to-noise ratio.

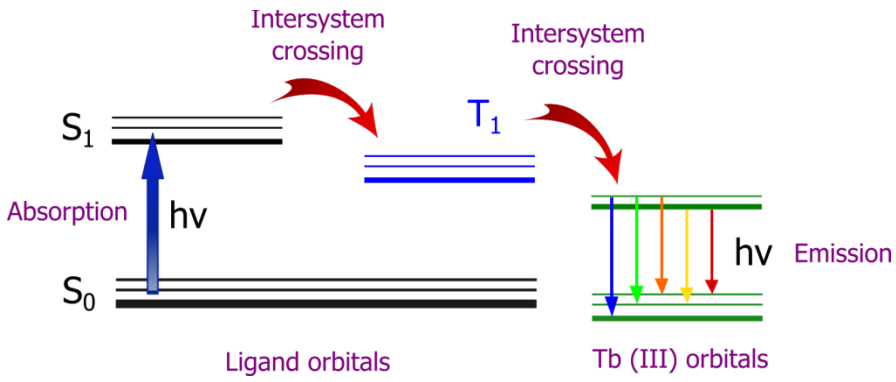

Figure 18. Principle of the Tb (III) luminescence.

Recently, a new class of luminescent Tb (III) chelates with a nonadentate cage constructed around a bis-pyrazolyl–pyridine framework **2.1** was developed by the group of Dr. Loic Charbonnière (Figure 19; Nchimi-Nono et al., 2013). The described complex possesses an excellent solubility and photostability in water (due to the absence of water molecules in the

coordination sphere), which together with a good extinction coefficient of 13 000 $M^{-1}\times cm^{-1}$ (330 nm) and a quantum yield of 25% in water allowed us to consider the complex as a prominent candidate for cellular applications.

We suggested the synthesis of the time-resolved luminescent probe for the oxytocin receptor by coupling **2.1** to the OTR peptide agonist carbetocin (Figure 19).

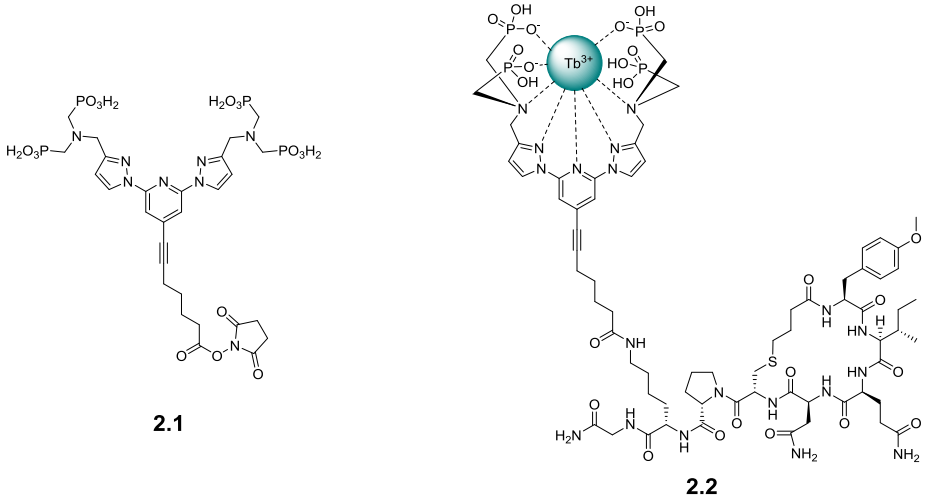

Figure 19. Bis-pyrazolyl–pyridine Tb (III) ligand **2.1** and the target conjugate with carbetocin **2.2**.

To functionalize carbetocin, it was decided to introduce a Lys residue at the position 8, following the previously described approach for oxytocin analogues (Terrillon et al., 2002).

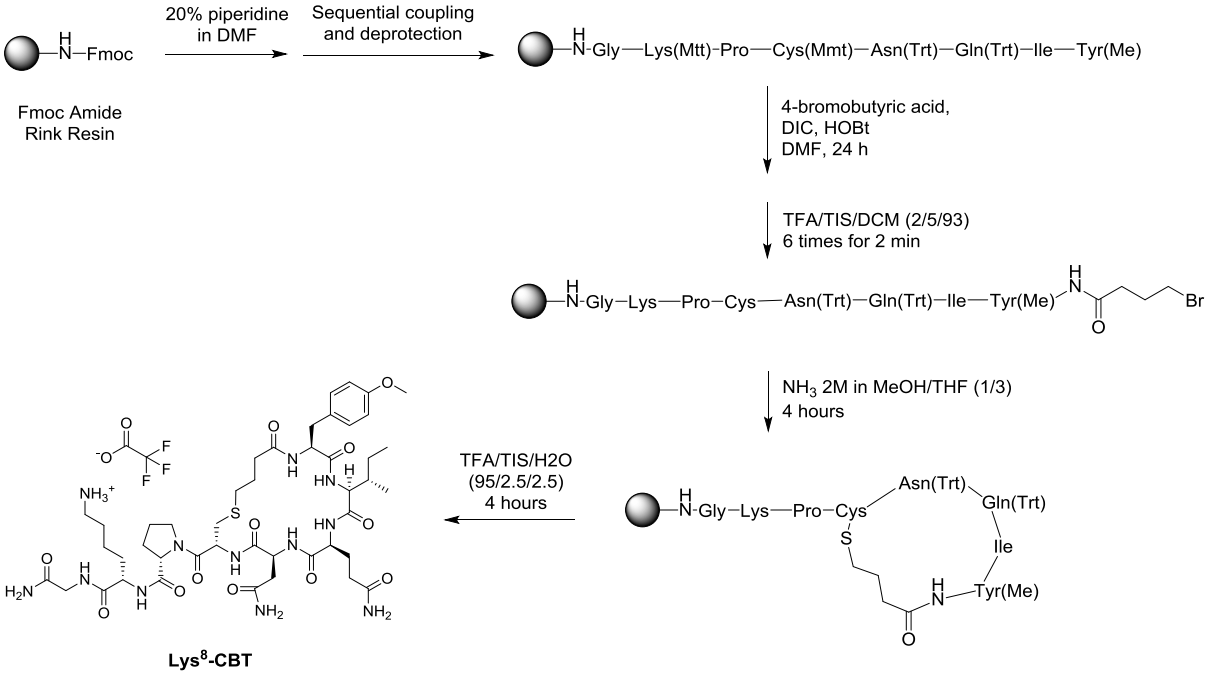

Scheme 12. Synthesis of Lys[8]-CBT.

The solid-phase peptide synthesis of Lys[8]-CBT (Scheme 12) was carried out following the same protocol as for the synthesis of desmethyl carbetocin (Part I, Scheme 1), except the use of Fmoc-Lys(Mtt)-OH instead of Fmoc-Leu-OH in the position 8 and Fmoc-Tyr(Me)-OH instead of Fmoc-Tyr(Boc)-OH in the position 2.

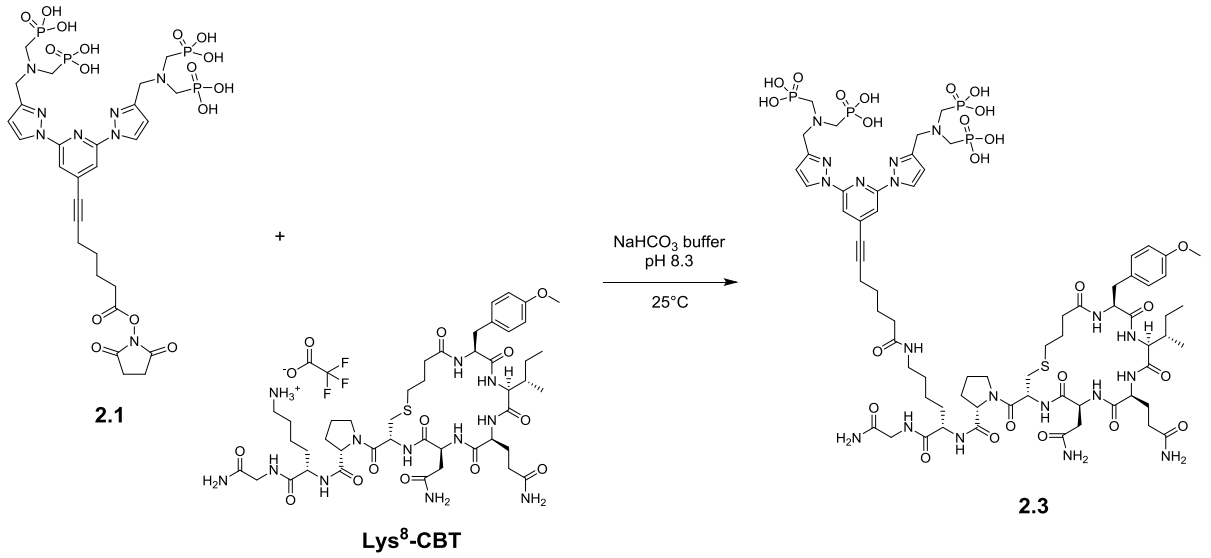

Scheme 13. Synthesis of the conjugate **2.3.**

The conjugation between Lys[8]-CBT and the Tb (III) ligand **2.1** was performed in sodium bicarbonate buffer with a pH of 8.3 and the progress of the reaction was monitored by HPLC-MS (Scheme 13). The crude product was purified by semi-preparative HPLC.

To follow the interaction of the peptide conjugate **2.3** with Tb^{3+} in aqueous solution, spectrophotometric and luminescence titration experiments were performed with the help of Dr. Aline Nonat from IPHC, Strasbourg. In aqueous solution at neutral pH, the free chelate showed a strong absorption band at 254 nm and a less intensive one at 322 nm corresponding to electronic transitions within the bis-pyrazolyl-pyridine core (Figure 20B). Upon addition of the metal ion (with an increment of 0.1 equivalent), due to orbital interactions of the ligand with Tb^{3+}, a new absorption band at 272 nm appeared at the expense of the band at 254 nm. At the same time, the band at 322 nm shifted bathochromically to 337 nm with a decrease in intensity up to the point of 1:1 stoichiometry.

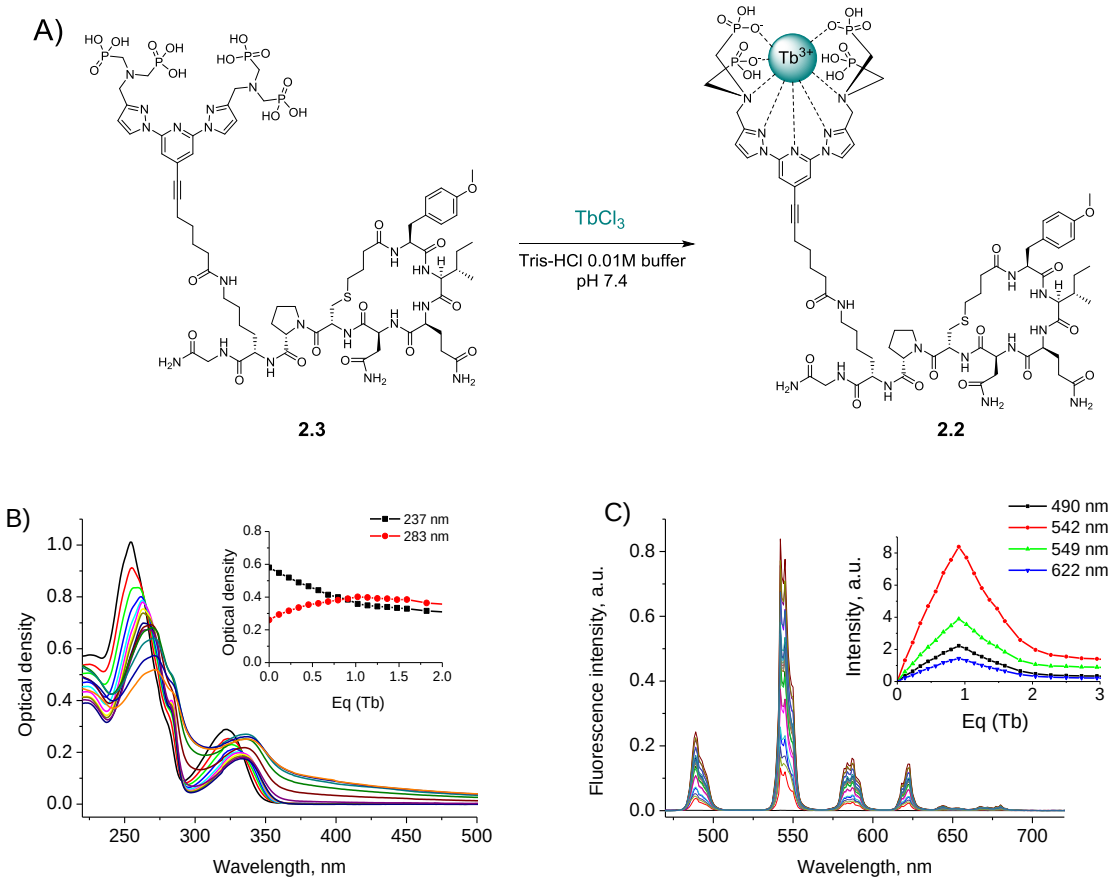

Figure 20. Formation of the complex **2.2**

(A) Scheme of the reaction. (B) Absorption spectra of the aqueous solution of **2.3** titrated with $TbCl_3$. (B, inset) Evolution of the absorption intensity measured at 237 and 283 nm. (C) Emission spectra of the aqueous solution of **2.3** titrated with $TbCl_3$. (C, inset) Evolution of the emission intensity measured at 490, 542, 549 and 622 nm.

Excitation at 330 nm produced characteristic for Tb (III) complex emission bands at 489 nm, 544 nm, 585 nm, and 622 nm (Figure 20C). Up to the addition of 1 equivalent of Tb^{3+}, the intensity of all emission bands increased, while with an excess of the lanthanide salt, the luminescence intensity decreased due to the formation of non-luminescent complexes.

The analysis of the evolution curves (Figure 20B, inset and Figure 20C, inset) allowed us to correct the concentration of the stock solution of **2.2**, previously determined by gravimetry. The inflection points correspond to the luminescent complex with 1:1 stoichiometry, as it was shown preciously for similar complexes that coordination of successive Tb^{3+} ions resulted in the luminescence decrease. Thus, in the inflection points the quantity of **2.2** in the titrated solution became equal to the quantity of the added titrant.

The complex **2.2** was prepared by mixing equimolar quantities of **2.3** and $TbCl_3$ in 0.01 M Tris-HCl buffer pH 7.4. From the obtained solution of **2.2** with known concentration we calculated its extinction coefficient according to the Beer–Lambert law (1), which gave the value of 13900 $M^{-1}\times cm^{-1}$ (at 333 nm):

(1) $\varepsilon = {}^{A}/_{(c \times l)}$ where ε is the extinction coefficient, A – absorbance, l – distance the light travels through the material.

The formed complex **2.2** was freeze dried and purified by semi-preparative HPLC (eluted with acetonitrile / triethylammonium acetate buffer pH 7).

The spectroscopic properties of the isolated compound **2.2** are summarized in Table 6. The absorption spectrum of the Tb (III) complex displays a strong band at 263 nm and a less intensive one at 332 nm, corresponding to the transitions within the bis-pyrazolyl-pyridine core. Excitation at 330 nm results in a characteristic emission of the Tb (III) complex with maxima at 489, 544, 585 and 622 nm. The luminescence quantum yield of **2.2** measured in 0.01 M Tris/HCl buffer was around 17%. The emission is characterized by monoexponential kinetics with a lifetime of 2.74 ms in water. The hydration number (number of water molecules in the coordination sphere), estimated as described previously (Beeby et al., 1999), was close to zero, indicating that the metal inside the cage is well-protected from the non-radiative deactivation.

Table 6. Spectroscopic properties of **2.2** in aqueous solution.

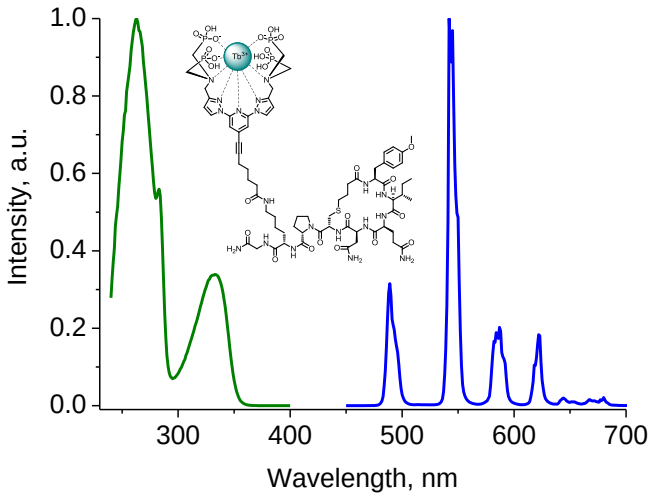

Absorption [a]		Emission			
λ_{abs}, nm	ε [b], $M^{-1}\times cm^{-1}$	τ (H_2O) [c], ms	τ (D_2O) [c], ms	ϕ [d]	q [e]
263, 333	13900 (333 nm)	2.74	3.26	16.7%	-0.01 ≈ 0

[a] In 0.01 M Tris–HCl buffer at pH = 7.4. [b] Molar absorption coefficient. [c] Luminescence lifetime. [d] Luminescence quantum yield. [e] Number of water molecules in the coordination sphere.

The radioligand binding assay performed by Dr. Christiane Mendre and Dr. Bernard Mouillac in the Institut de Génomique Fonctionnelle (Montpellier) revealed high affinity (11 nM) of the Tb (III) luminescent complex **2.2** for the oxytocin receptor.

To evaluate the capacity of the luminescent probe **2.2** to detect the oxytocin receptor it was decided to perform time-resolved FRET experiments with the GFP (green fluorescent protein)- labeled OTR on living cells (assays were conducted at PCBIS, Illkirch with the help of Sophie Gioria). The suspensions of HEK293 cells, stably expressing OTR fused to GPF, were distributed in 96-well plates and incubated with increasing amounts of **2.2** for 30 min at room temperature. In order to have control conditions, the same incubations were performed with HEK293 cells expressing the wild-type OTR (wtOTR cells) and in HEPES buffer without cells. The fluorescence of GFP was read at 510 nm after the time-gated laser excitation of **2.2** at 337 nm. The results presented in Figure 21A showed that although **2.2** possessed nanomolar affinity for OTR, no reliable FRET to GFP was detected. Then we carried out kinetic experiments in GFP-OTR cell suspensions on a spectrofluorometer, but still the specific signal detected at 515 nm after adding the solution of **2.2** to GFP-OTR cells was very weak (Figure 21B). Moreover, the same experiment on wtOTR cells resulted in a week positive signal which could be explained by the residual luminescence of Tb complex at

515 nm (Figure 21C). Thus, it was concluded that FRET was not efficient between the OTR ligand **2.2** and the GFP, probably due to the remoteness of the fluorescent protein from the ligand binding site (as it was explained above, the distance of maximum 10 nm between a donor and an acceptor is required for an efficient FRET).

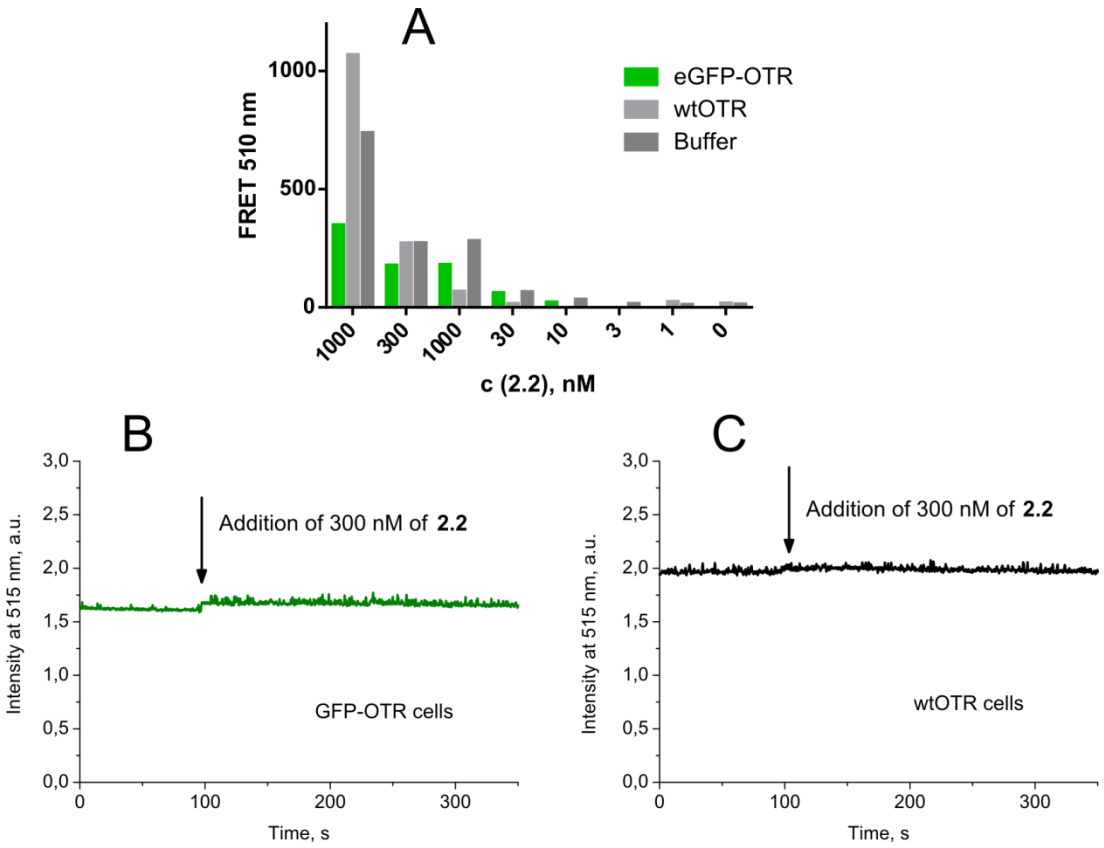

Figure 21. (A) Results of binding experiments on GFP-OTR and wtOTR cells. (B) Kinetic experiments on GFP-OTR cells. (C) Kinetic experiments on wtOTR cells.

2. First selective non-peptide fluorescent probes for the oxytocin receptor

The discovery of potent and selective ligands for G protein-coupled receptors requires the use of robust and reliable screening methods to characterize ligand-receptor interactions. Time-resolved Förster resonance energy transfer (TR-FRET) is a technique which combines the advantages of classical FRET with the use of long-emitting lanthanides, thus enabling the study of ligand-receptor interactions in "wash-free" conditions with minimal background fluorescence due to the time-gated detection. This powerful combination provides significant benefits for high-throughput screening of GPCRs at the cell surface (Degorce et al., 2009).

To date, the only fluorescent probes for the oxytocin receptor are peptide OT analogues that have poor bioavailability (short half-life in plasma, poor blood-brain barrier penetration and rapid clearance) (Mouillac et al., 2008). Moreover, although few reported peptide fluorescent ligands showed good selectivity for OTR versus the vasopressin receptor family (Corbani et al., 2011), they still possessed nanomolar affinity for the receptors V_{1a} and V_{1b}.

We aimed to develop selective high-affinity non-peptide OTR ligands to validate the TR-FRET based assay for OTR in order to accelerate the discovery of new small organic ligands for the target receptor.

Our strategy was to introduce fluorescent dyes (fluorescein and DY-647, which are commonly used in TR-FRET applications) onto one of the most selective high-affinity non-peptide OTR antagonists, PF-3274167 (Brown et al., 2010; Figure 22). It was decided to elongate its methoxymethyl moiety with two PEG chains of different lengths starting from the previously obtained desmethyl precursor **1.27**.

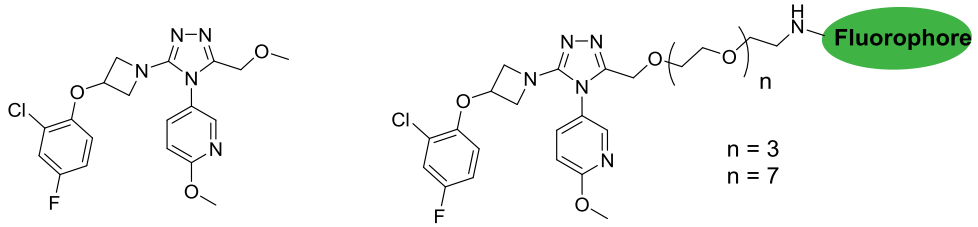

PF-3274167

OTR: K_i = 9.5 nM
V_{1a}R: K_i = 1120 nM
V_{1b}R: K_i = > 10000 nM
V_2R: K_i = > 10000 nM

Figure 22. PF-3274167 and its fluorescent derivatives.

The synthesis of PEG chains started with the tosylation of commercially available tetraethylene glycol **2.4** and octaethylene glycol **2.5** (Scheme 14) under the treatment with KOH in dichloromethane (Sekiguchi et al., 2010). Then, one of the tosyl groups was substituted by di-*tert*-butyl-iminodicarboxylate to afford protected amines **2.8** and **2.9**. It was found previously in the laboratory (unpublished data) that alkylation with bromides of long PEG chains resulted in better yields that alkylation with tosylates, so it was decided to convert **2.9** to the corresponding bromide **2.10**.

The previously synthesized desmethyl PF-3274167 derivative was alkylated either with **2.8** or with **2.10** chains in the presence of KOH in DMF to give after the cleavage of terminal Boc protecting groups **2.11** and **2.12** in 60% and 30% yield, respectively (two steps).

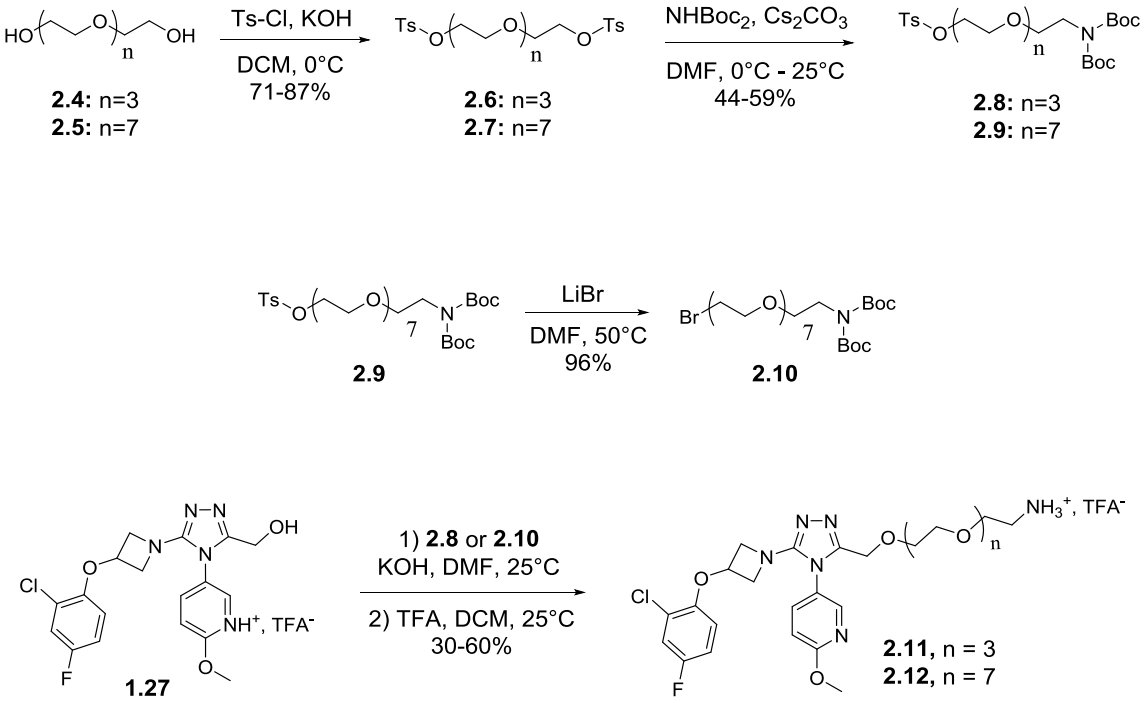

Scheme 14. Synthesis of amines **2.11** and **2.12.**

Having the amino precursors derived from PF-3274167 in hand, we performed the incorporation of fluorescein and DY-647 using commercially available *N*-hydroxysuccinimide esters of 6-(fluorescein-5-carboxamido)hexanoic acid (5-SFX) or DY-647 (DY-647-NHS-ester) in DMSO in the presence of the Hünig's base (Scheme 15). The obtained fluorescent compounds **2.13**-**2.16** were isolated by semi-preparative reverse-phase HPLC. Their identity was confirmed by HRMS and their purity was determined by analytical HPLC.

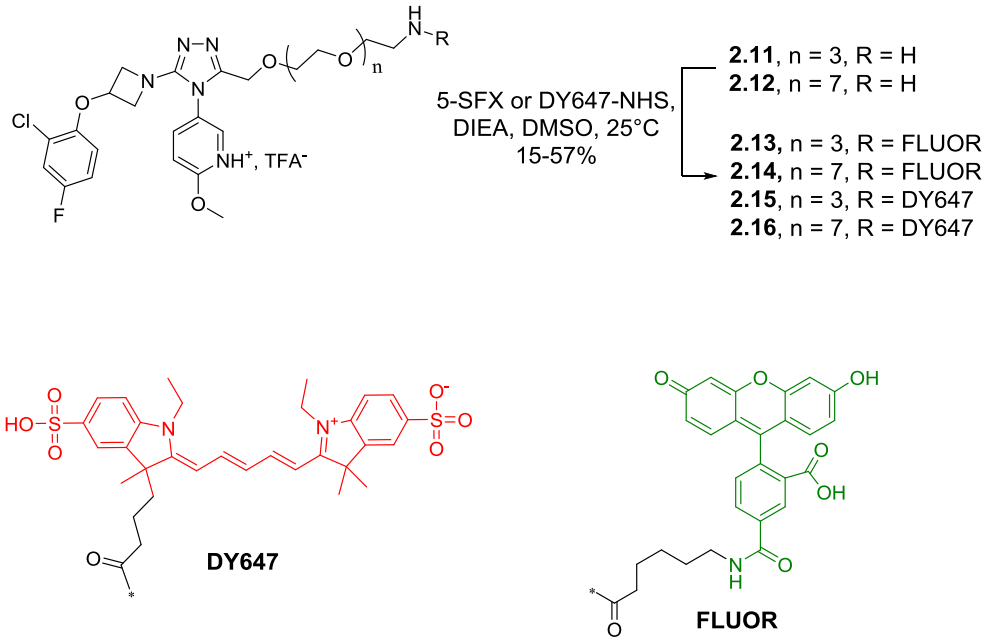

Scheme 15. Synthesis of fluorescent derivatives of PF-3274167.

The spectroscopic properties of fluorescent compounds **2.13-2.16** were studied in Tag-lite® labelling medium, which is commonly used in TR-FRET binding assays. The absorption and the fluorescence maxima of all compounds were found to be very close to those of the parent dyes fluorescein and DY-647 (Table 7).

Table 7. Physicochemical and spectroscopic properties of fluorescent compounds **2.13-2.16**.

Compound	HPLC, T_r (min)	Molecular formula	MS calculated	MS found (HR-MS)	Fluorophore	λ_{max} (nm) [a]	
						Absorption	Emission[b]
2.13	4.38	$C_{53}H_{55}ClFN_7O_{13}$	526.6843[d]	526.6855[d]	Fluorescein	498	524
2.14	4.39	$C_{61}H_{71}ClFN_7O_{17}$	614.7368[d]	614.7391[d]	Fluorescein	498	524
2.15	3.94	$C_{58}H_{70}ClFN_8O_{13}S_2$	1205.4255[c]	1205.4251[c]	DY-647	651	665
2.16	3.97	$C_{66}H_{86}ClFN_8O_{17}S_2$	691.2691[d]	691.2696[d]	DY-647	651	665

[a] The absorption and the emission parameters were measured in Tag-lite® labelling medium. [b] The excitation wavelength was set to 470 nm for fluorescein derivatives and to 620 nm for DY-647 derivatives. [c] For $[M+H]^+$. [d] For $[M+2H]^{2+}/2$.

The affinities of fluorescent ligands were evaluated in collaboration with the group of Dr. Thierry Durroux (IGF, Montpellier) by TR-FRET binding experiments using the ligands as

acceptors of the resonance energy transfer and the SNAP-tagged oxytocin receptors labelled with terbium cryptate Lumi4-Tb as FRET donor (Xu et al., 2011b). The TR-FRET efficiency was measured as a ratio of the acceptor fluorescence at 665 nm (DY-647) or 520 nm (fluorescein) and the donor luminescence (Lumi4-Tb) at 620 nm. According to the obtained results, all fluorescent ligands possessed nanomolar affinity for the oxytocin receptor (Table 8), close to those of the parent OTR ligand PF-3274167, indicating that the introduction of the rather bulky fluorophores did not influence the interaction of the ligands with the receptor, regardless of the length of the spacer and the nature of the fluorophore. Indeed, no difference in dissociation constants was observed between the triazole derivatives with the PEG chains of 4 and 8 units. The possible explanation is that the PEG4 spacer was already long enough to hold away the fluorophore from the receptor binding pocket.

Table 8. Dissociation constants of **2.13**-**2.14** determined by saturation TR-FRET experiments and the representative curves for **2.13**.

Compound	Binding, TR-FRET (K_d, nM)			
	OTR	$V_{1a}R$	$V_{1b}R$	V_2R
PF-3274167	9.5	1120	>1000	>1000
2.13	1.59 ± 0.38	>1000	>1000	>1000
2.14	2.05 ± 0.58	>1000	>1000	>1000
2.15	1.59 ± 0.39	>1000	>1000	509 ± 122
2.16	1.86 ± 0.51	>1000	>1000	353 ± 82

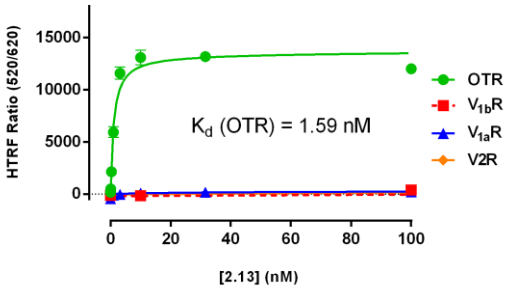

The selectivities of the fluorescent OTR ligands were investigated in the TR-FRET based assay on the three subtypes of the vasopressin receptor family known to have the highest homology (≈ 25%) with the oxytocin receptor (Gimpl and Fahrenholz, 2001). All the fluorescent probes derived from PF-3274167 showed excellent selectivity versus the vasopressin receptors with almost no affinity for the V_{1b} and V_{1a} subtypes (Table 8). Surprisingly, introduction of the fluorophore onto PF-3274167 not only maintained its ability to bind to the oxytocin receptor, but increased its affinity by one order of magnitude and drastically improved the ligand selectivity versus the $V_{1a}R$. Interestingly, both PF-3274167 derivatives **2.15** and **2.16** labelled with DY-647 presented submicromolar affinity to the vasopressin V_2 receptor (509 and 353 nM, respectively), suggesting that the red fluorophore displayed a cooperative role in the binding to V_2R.

To evaluate the relevance of the fluorescent OTR ligands in the TR-FRET screening assay the competition experiments were performed. It was decided to use probes **2.13** and **2.15** with shorter PEG linker and to test the affinities of oxytocin itself (Barberis et al., 1999), of the linear peptide OTR antagonist OTA (Terrillon et al., 2002) and of the non-peptide OTR antagonist **31a** (from Frantz et al., 2010). The affinity constants found in the competition experiments with both fluorescein- and DY-647- derived tracers were in good accordance with the previously reported data from the radioligand binding assay (Table 9). By contrast, inhibition constant estimated for agonist OT was found higher than the dissociation constant estimated by radioactive binding assays, whatever the tracers used. Such differences in the estimation of the affinity of a ligand has already been reported and can be explained by the existence of positive or negative binding cooperativity of the ligand depending on the agonist or antagonist character of the tracer (Durroux, 2005).

Table 9. Inhibition constants of oxytocin, OTA and **31a** on OTR when using compounds **2.13** and **2.15** as tracers and a representative curve for the competition of **2.13** with **31a**.

Tracer	Binding, K_i (nM)[a]		
	Competitor		
	OT	OTA	**31a**
2.13	9.53 ± 1.57	0.67 ± 0.07	6.22 ± 1.63
2.15	6.60 ± 1.70	0.45 ± 0.01	6.60 ± 1.27
Literature	0.79	0.21	27.8 ± 0.8

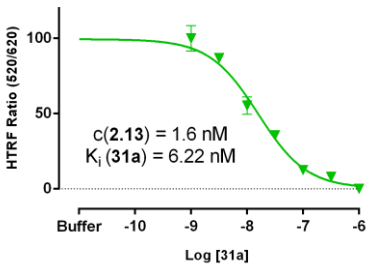

In summary, we have designed and synthesized the first selective non-peptide fluorescent ligands for the oxytocin receptor. These probes have found applications for the development of TR-FRET based assays readily amenable to high-throughput screening for OTR. These assays will be useful to accelerate the discovery of novel small organic ligands of the target receptor and to gain a better understanding of its role in the modulation of social behavior.

Turn-on fluorescent probes for native G protein-coupled receptors

1. Turn-on Nile red-based probes for OTR (Karpenko et al., 2014)

TR-FRET is a powerful homogeneous technique which allows for rapid discovery of small organic ligands of GPCRs, however its major drawback is in the requirement of the receptor labelling by a FRET donor or acceptor via the SNAP fusion protein. Although SNAP-tag, derived from the 20 kDa DNA repair protein O^6-alkylguanine-DNA alkyltransferase (Gautier et al., 2008), is smaller than OTR (mammary OT receptor is a 65-kDa protein; Gimpl and Fahrenholz, 2001), it could however influence the accessibility of the receptor binding pocket and the equilibrium between the active and the inactive receptor conformations and may not be representative of the physiological receptor behavior. Thereby, there is a strong demand for a homogenous screening method which allows the detection and quantification of ligand-receptor interactions and do not require the GPCR structural modification.

In the context of the development of a screening method on the wild-type GPCRs we turned our attention to the fluorogenic or so-called "turn-on" fluorescent dyes: the molecules which are not fluorescent in water but which turn on the fluorescence upon changing of local environment. Such turn-on systems are widely used in biological sensing, enabling direct quantification of an analyte without removal of unreacted probe and providing the possibility of *in-vivo* monitoring of molecular interactions (Grimm et al., 2013; Lavis and Raines, 2008; Nadler and Schultz, 2013).

Only few GPCR ligands bearing fluorogenic dyes have been reported to date (Sridharan et al., 2014). In addition, they suffer from limited efficacy due to non-specific interactions (Berque-Bestel et al., 2003; Lacivita et al., 2009) or from the requirement to perform studies on isolated membranes and not living cells (Krieger et al., 2008). Moreover, all these examples were limited to blue dyes, while red dyes are advantageous for cellular studies due to lower sample photo-damage, light scattering and auto-fluorescence.

Among known red fluorogenic dyes, Nile Red (NR; Figure 23) is probably the best representative, featuring excellent sensitivity to solvent polarity (Greenspan and Fowler, 1985) and being successfully applied to study apolar environment in micelles (Datta et al., 1997), lipid nanoparticles (Jores et al., 2005) and biomembranes (Kucherak et al., 2010).

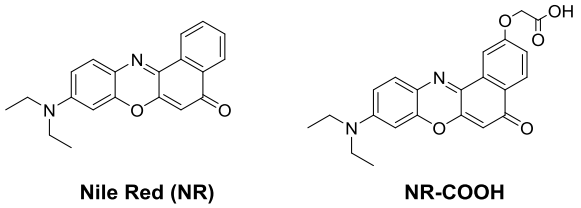

Figure 23. Nile Red fluorogenic dye and its carboxylic acid derivative.

Our strategy was to link the NR fluorophore via a sufficiently long PEG spacer to the oxytocin receptor ligands: Lys^{8}-CBT and a non-peptide OTR/V_{1a}R antagonist EP, developed in the laboratory (Bonnet et al., 2014). In this case, ligand-receptor interaction would change the fluorophore environment from aqueous to apolar, thus turning on the fluorescence (Figure 24).

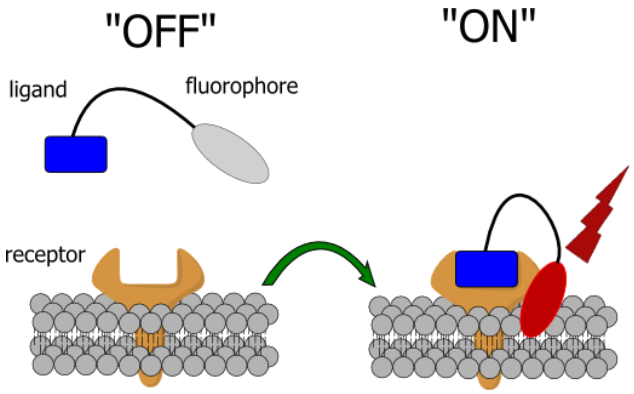

Figure 24. Principle of the turn-on detection of GPCRs.

The synthesis of the PEG chain for the Lys^{8}-CBT turn-on derivative started from the previously described difunctionalized PEG8 chain **2.9** (Scheme 16). The tosyl group was substituted by azide under the classical conditions and the latter was quantitatively reduced to free amino group by treatment with polymer-bound triphenylphosphine in the presence of water in THF. The resulting mono-protected PEG8 diamine **2.18** was coupled to the carboxylic acid Nile red derivative NR-COOH, synthesized by the group of Dr. Andrey Klymchenko (Figure 23; Kashida and Asanuma, 2012), to afford the compound **2.19**. In the latter the Boc protecting groups were removed by treatment with trifluoroacetic acid, and the liberated amino group was converted to the carboxylic acid by reaction with succinic anhydride. Finally, **2.21** was coupled to Lys^{8}-CBT to afford the desired fluorescent probe NR-PEG-CBT.

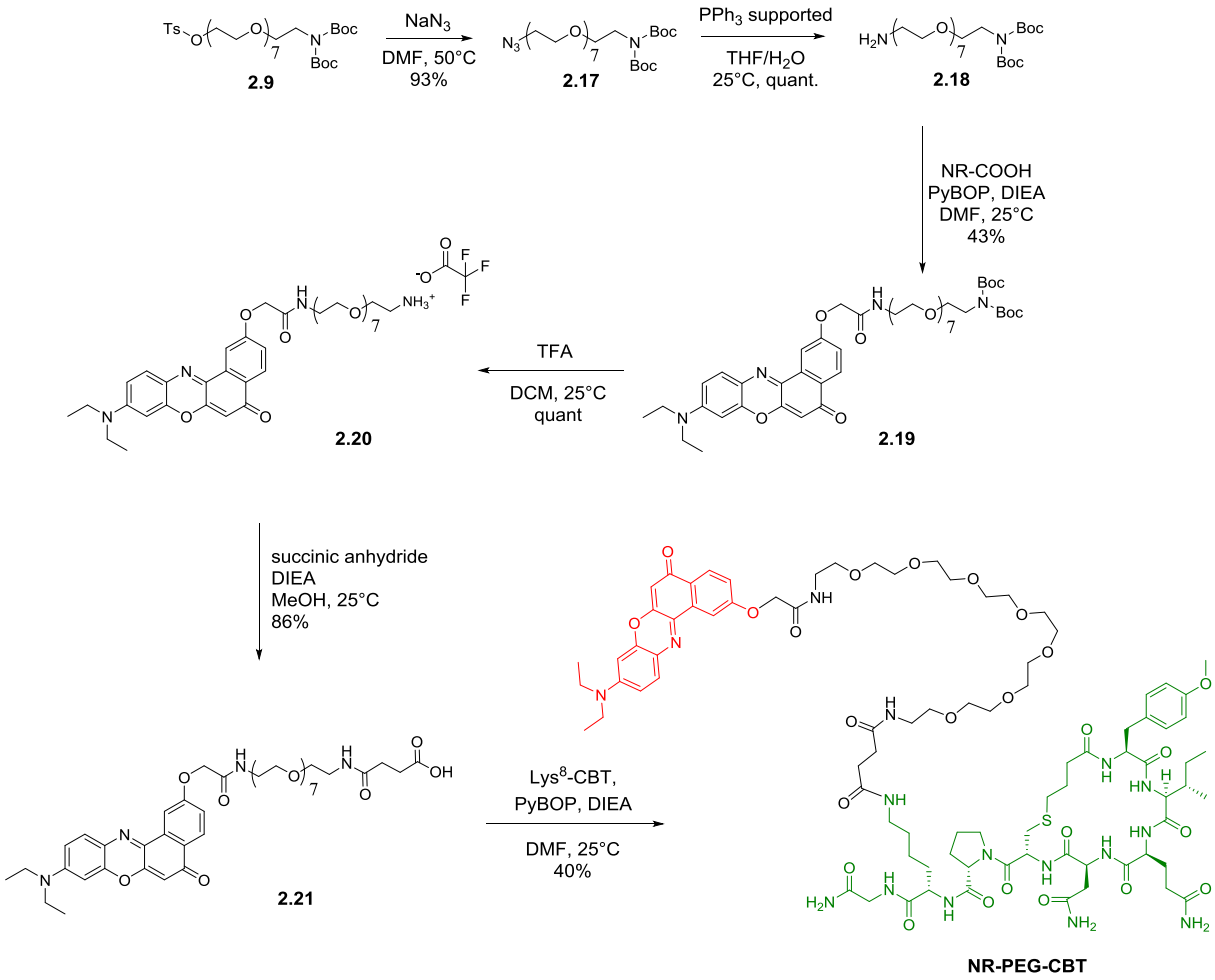

Scheme 16. Synthesis of NR-PEG-CBT.

Next, we alkylated the non-peptide OTR ligand EP, which was synthesized in the laboratory by Dr. Elsa Pflimlin, with the previously described PEG8 protected amino-bromide chain **2.10** (Scheme 17). The Boc protecting groups were removed in trifluoroacetic acid and resulting amine **2.22** was coupled to NR-COOH to afford the non-peptide fluorescent OTR ligand NR-PEG-EP.

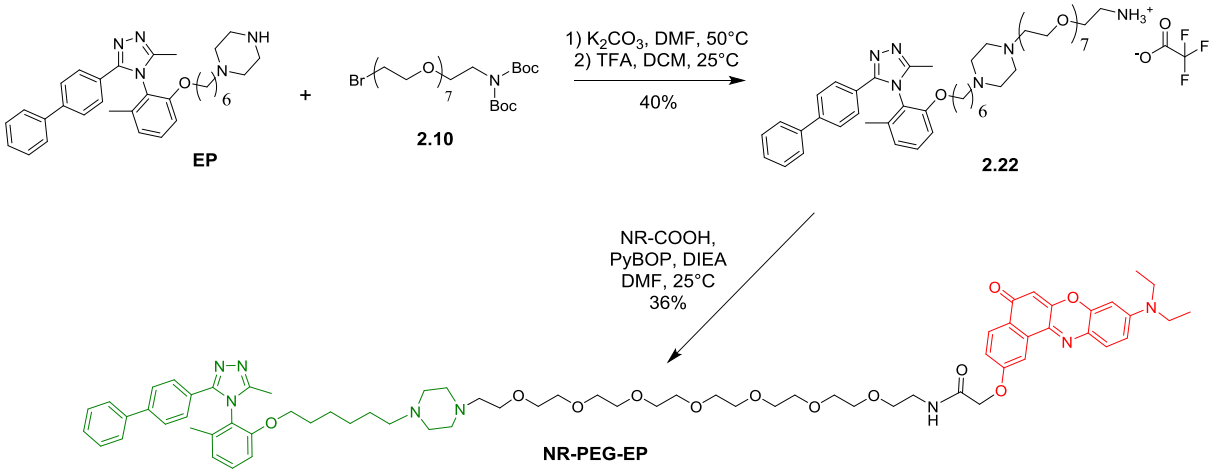

Scheme 17. Synthesis of NR-PEG-EP.

To investigate the importance of the PEG spacer, the analogue of NR-PEG-CBT without PEG was obtained by direct coupling of NR-COOH to Lys^8-CBT (Scheme 18). Finally, a conjugate of Lys^8-CBT with a classical non-fluorogenic dye *p*-Lissamine® Rhodamine B (LRh-CBT) was synthesized as a control.

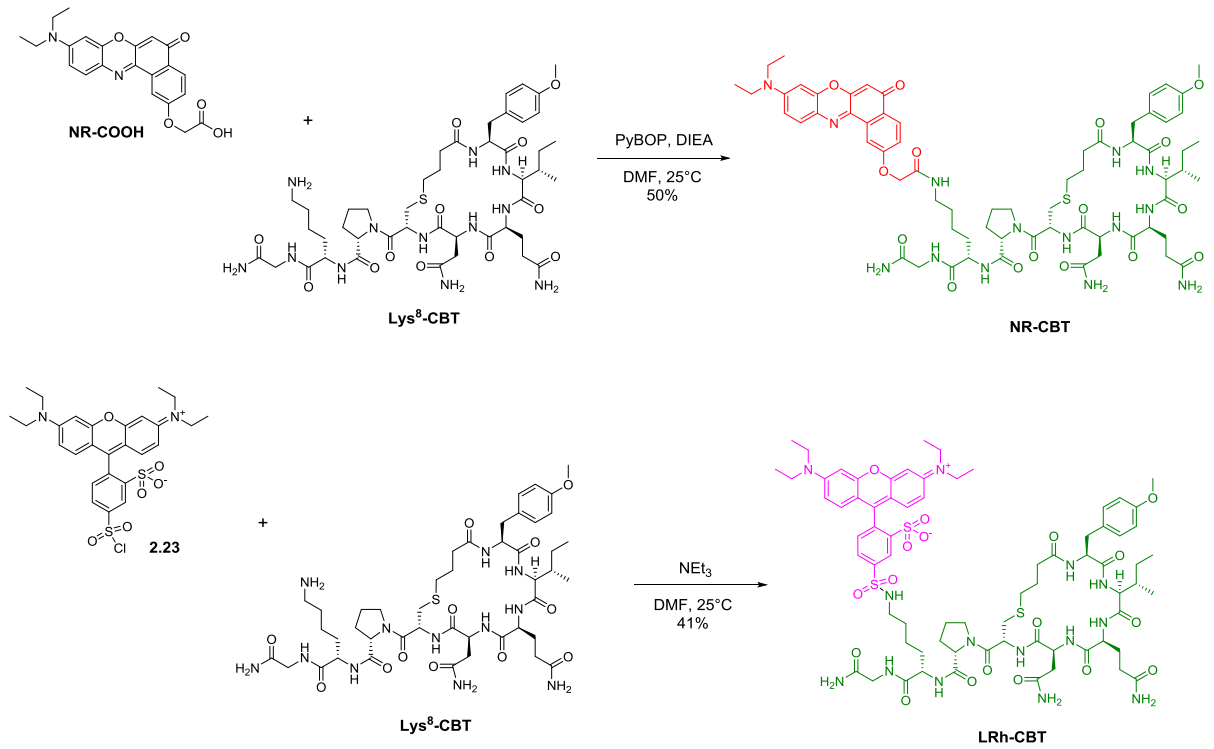

Scheme 18. Synthesis of NR-CBT and LRh-CBT.

The binding affinities of the NR-labeled CBT derivatives were determined by competition experiments against [^{3}H]-AVP by Dr. Bernard Mouillac and Dr. Christiane Mendre (IGF, Montpellier). Both NR-PEG-CBT and NR-CBT showed high affinity for the oxytocin receptor (K_i = 0.54 and 0.55 nM, respectively; Table 10). In addition, the functional activities of NR-PEG-CBT and NR-CBT were evaluated by measurement of intracellular calcium release (Weill et al., 2011) by Christel Valencia (PCBIS, Strasbourg). While NR-CBT fully inhibited the oxytocin-induced calcium release in a dose-dependent manner, highlighting its antagonistic character (IC_{50} = 74 nM), NR-PEG-CBT was found to induce calcium release in a dose-dependent manner, showing its agonistic character (EC_{50} = 244 nM). These results demonstrate the crucial role of the linker between the pharmacophore and the fluorophore to preserve the functional activity of the ligand.

Table 10. Inhibition constants of NR-PEG-CBT and NR-CBT on OTR when using [^{3}H]-AVP as radiotracer and their functional activities. A representative curve for the competition of [^{3}H]-AVP with NR-PEG-CBT.

Compound	Binding (K_i, nM)	Functional activity
NR-PEG-CBT	0.54 ± 0.034	EC_{50} = 244 nM
NR-CBT	0.55 ± 0.022	IC_{50} = 74 nM

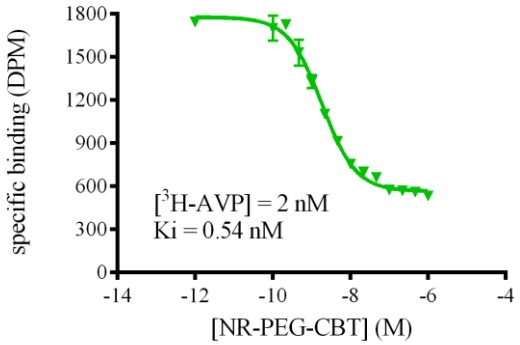

The turn-on properties of the fluorescent ligands were first studied in organic solvents of different polarities in collaboration with Dr. Andrey Klymchenko. For all the three NR conjugates (Table 11 and Figure 25), fluorescence spectra shifted to the blue region and fluorescence intensities increased with decrease in the solvent Reichardt polarity index (Reichardt, 1994) in line with the solvatochromism of NR and its derivatives (Jose and Burgess, 2006; Kucherak et al., 2010). As a result, a good correlation was observed between the quantum yield of the NR conjugates and the position of the emission maximum (Figure 25B). Remarkably, the change from polar aqueous environment to apolar 1,4-dioxane resulted in ~10^4-fold fluorescence enhancement at 580 nm.

Table 11. Photophysical properties of NR-PEG-CBT, NR-PEG-EP, NR-CBT and LRh-CBT.

Compound	Solvent	E_T30, kcal/mol [a]	ε_r [b]	λ_{max} abs, nm [c]	λ_{max} fluor, nm [d]	QY, % [e]
NR-PEG-CBT	1,4-Dioxane	36	2.3	526	584	60
	Acetone	42.2	21	535	608	48
	Acetonitrile	45.6	37.5	539	613	45
	Ethanol	51.9	24.55	551	626	33
	Methanol	55.4	33	555	631	25
	Water	63.1	80	597	657	3.7
	HBS	63.1	80	599	659	3.4
NR-CBT	1,4-Dioxane	36	2.3	524	584	59
	Acetone	42.2	21	534	606	48
	Acetonitrile	45.6	37.5	538	612	44
	Ethanol	51.9	24.55	552	627	32
	Methanol	55.4	33	555	632	24
	Water	63.1	80	592	656	2.7
	HBS	63.1	80	597	657	2.4
NR-PEG-EP	1,4-Dioxane	36	2.3	522	583	60
	Acetone	42.2	21	535	606	48
	Acetonitrile	45.6	37.5	538	614	43
	Ethanol	51.9	24.55	552	626	32
	Methanol	55.4	33	556	632	23
	Water	63.1	80	574	658	2.4
	HBS	63.1	80	aggregation	659	1.0
LRh-CBT	1,4-Dioxane	36	2.3	563	579	70
	Acetone	42.2	21	562	580	54
	Acetonitrile	45.6	37.5	561	580	44
	Ethanol	51.9	24.55	563	581	52
	Methanol	55.4	33	562	580	46
	Water	63.1	80	570	588	32
	HBS	63.1	80	570	588	32

[a] Reichardt polarity parameter. [b] Dielectric constant. [c] Position of the absorption maximum. [d] Position of the emission maximum. [e] Fluorescence quantum yield.

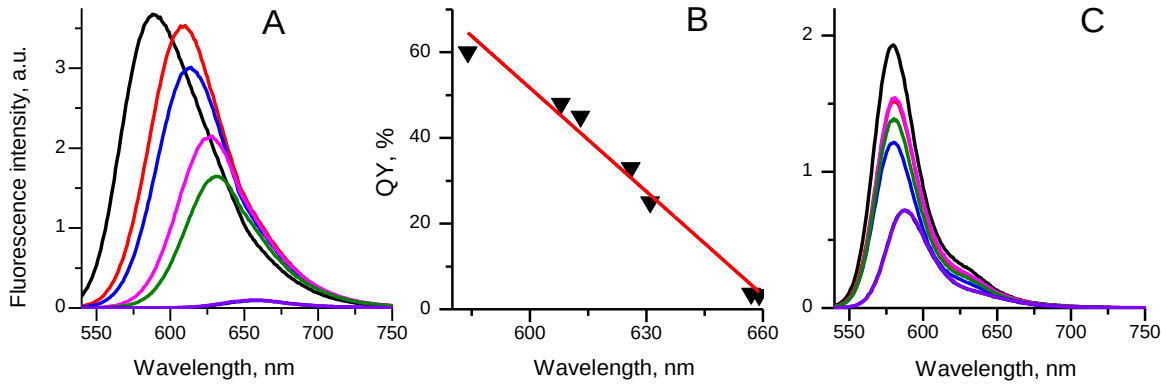

Figure 25. Fluorescence spectra of NR-PEG-CBT (A) and LRh-CBT (C) in 1,4-dioxane (black), acetone (red), CH_3CN (blue), EtOH (magenta), MeOH (olive), H_2O (navy) and HEPES buffer (violet) upon the excitation at 520 nm. Correlation between the fluorescence quantum yield and the fluorescence maximum for NR-PEG-CBT (B).

Turn-on ligands applied in cellular studies should exhibit minimal non-specific binding. As NR and its derivatives are known for their relatively high affinity for lipid membranes (Kucherak et al., 2010) and serum albumins (Davis and Birch, 1996), we decided to study the non-specific interactions of our ligands. In the presence of large unilamellar DOPC (dioleoylphosphatidylcholine) vesicles used as cell membrane models, we observed no change in the fluorescence spectrum for NR-PEG-CBT (Figure 26) and only a little intensity increase at 580 nm for NR-CBT, while NR-PEG-EP showed a blue shift (up to 620 nm) and an intensity increase typical for membrane binding, which was even stronger than for the parent NR-COOH dye. Very similar behavior was observed in the presence of bovine serum albumin (BSA) or blood serum. It thus appears that NR-PEG-EP, due to the high lipophilicity of the pharmacophore, binds non-specifically to DOPC membranes and serum proteins, which unfortunately rules out its application to the development of the turn-on screening assay. The CBT derivatives demonstrated low non-specific interactions, however the difference was clearly observed between the ligand with PEG spacer, which did not show any significant increase in the non-specific fluorescence, and NR-CBT. Thus the PEG spacer seems to enhance the hydrophilicity of the ligand, decreasing non-specific binding to lipid membranes and serum constituents, and making NR-PEG-CBT highly promising for cellular studies.

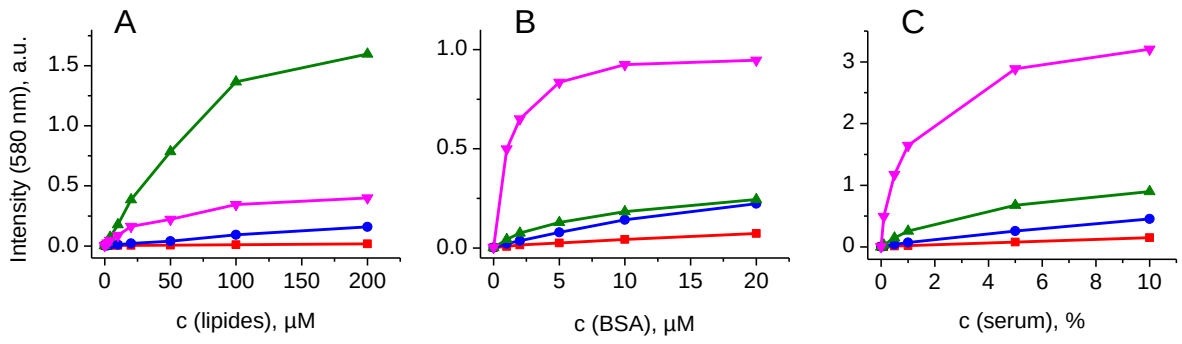

Figure 26. Fluorescence intensities at 580 nm as a function of the DOPC (A), BSA (B) or serum (C) concentration in HEPES buffer for NR-PEG-CBT (red), NR-CBT (blue), NR-PEG-EP (green) and NR-COOH (magenta).

The ligands were further evaluated for their ability to detect OTR in suspension of HEK293 cells overexpressing the oxytocin receptor (OTR+ cells). In the presence of unlabeled CBT as a competitor that saturates all receptors, the spectrum of NR-PEG-CBT displayed a very low intensity (Figure 27A, black) with the emission maximum corresponding to that in aqueous media (around 650 nm). In cells without the competitor (Figure 27A, red) we observed a 250-fold intensity increase at 580 nm, showing a receptor-specific turn-on response of the ligand. Remarkably, the blue-shifted maximum (585 nm) corresponded to a rather apolar environment (Kucherak et al., 2010), suggesting that after ligand-receptor interaction, the NR moiety protrude into the lipid environment of the receptor or into its hydrophobic allosteric binding site. Similar results were obtained with NR-CBT (Figure 27B), though the turn-on response was somewhat weaker (15-fold) as a result of the broader emission band in the presence of CBT. Thus, the turn-on response of the slightly more lipophilic NR-CBT is likely contaminated by non-specific binding to cell membranes. NR-PEG-EP due to its strong non-specific interactions was not able to distinguish the cells with and without available oxytocin receptors (Figure 27C). Finally, no significant spectral changes in the presence or the absence of OTR was either revealed for LRh-CBT, the analogue of NR-CBT with a non-fluorogenic dye (Figure 27D). Thus, the ligand bearing a classical fluorophore does not show a turn-on response upon binding to the receptor, as it remains always in the “on” state.

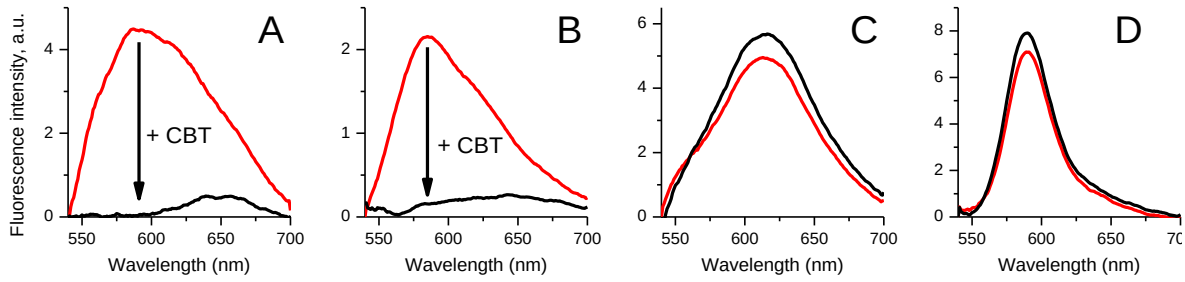

Figure 27. Fluorescence spectra of NR-PEG-CBT (A), NR-CBT (B), NR-PEG-EP (C) and LRh-CBT (D) at 10 nM concentration in suspensions of OTR+ cells in the absence (red) or the presence (black) of 1 µM of CBT.

Next, we performed confocal microscopy studies of adherent OTR+ and OTR- (wild-type HEK293) cells in the presence of the turn-on ligands. A clear fluorescence staining at the level of the plasma membranes in OTR+ cells was already observed at 20 nM concentration of NR-PEG-CBT or NR-CBT (Figure 28A-B), while in control OTR- cells the membrane fluorescence intensity was close to the auto-fluorescence level (Figure 28I-J). Moreover, both fluorescent ligands were readily substituted by the unlabeled CBT, which led to the decrease of the membrane staining (Figure 29). These results confirm that the developed ligands bind to the cell surface in a receptor-specific manner.

As for the non-peptide ligand NR-PEG-EP, it penetrated the cell membrane and stained the apolar intracellular constituents – only the nucleus remained uncolored (Figure 28C) – which can be easily explained by the high lipophilicity of the molecule. Naturally, the substitution experiments with the unlabeled CBT did not lead to the decrease in the membrane staining (Figure 29).

The comparative non-fluorogenic ligand LRh-CBT also showed a good membrane staining (Figure 28D) at low concentrations. However, in contrast to turn-on ligands, it presented non-negligible background fluorescence, particularly strong at higher ligand concentrations (Figure 28H) due to the fluorescence of the non-bound ligand in the cellular medium. These results show that although the turn-on response is not an obligatory property for imaging applications (Briddon et al., 2004), it improves the image quality by decreasing the background fluorescence.

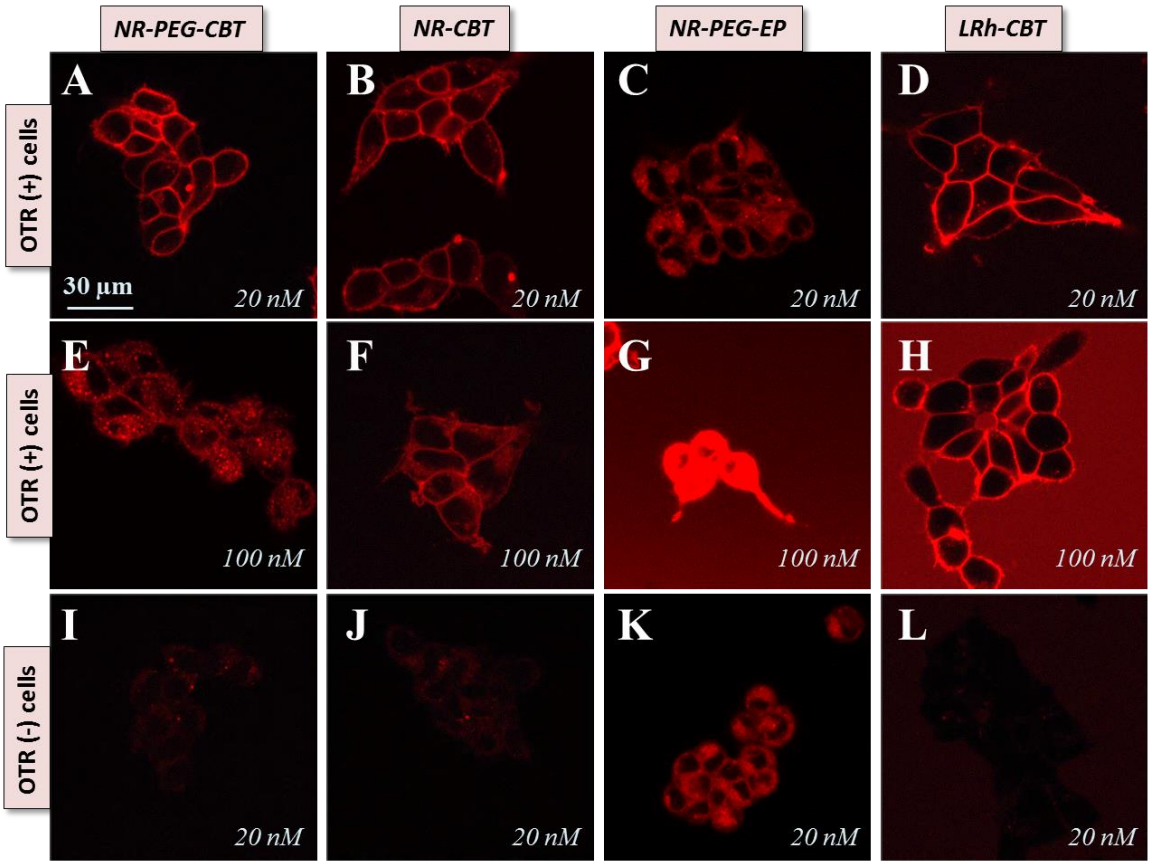

Figure 28. Confocal images of adherent OTR+ cells with 20 nM (A-D) and 100 nM (E-H) of NR-PEG-CBT, NR-CBT, NR-PEG-EP or LRh-CBT and images of OTR- cells (I-L) with 20 nM of NR-PEG-CBT, NR-CBT, NR-PEG-EP or LRh-CBT.

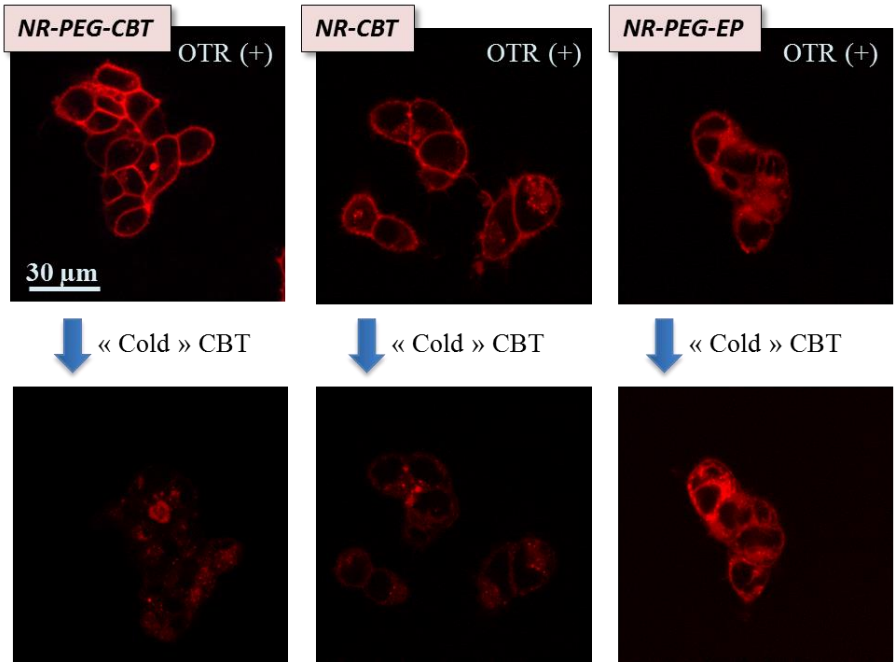

Figure 29. Confocal images of OTR+ cells with 20 nM of NR-PEG-CBT, NR-CBT or NR-PEG-EP and images of the same cells following the addition of 1 µM of CBT.

Incidentally, even in the presence of 10% serum (typically used concentration in the growth media for cell culture), no background fluorescence was observed at high ligand concentrations for both NR-PEG-CBT and NR-CBT (Figure 30). The latter property is crucial for the development of probes for *in vivo* imaging, as high non-specific fluorescence is known to be one of the main reasons of their failure.

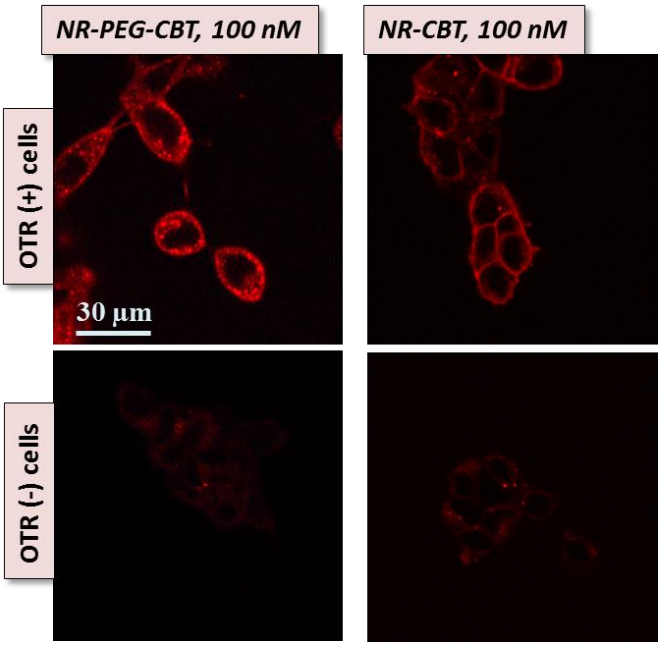

Figure 30. Confocal images of adherent OTR+ cells and OTR- cells in the presence of 100 nM of NR-PEG-CBT or NR-CBT in HBS with 10% v/v serum.

Microscopy data also revealed peculiar differences in the pharmacological profiles of two CBT derivatives. OTR is known to be rapidly internalized after agonist stimulation (Gimpl and Fahrenholz, 2001). As it can be seen from Figure 31, NR-PEG-CBT induced OTR internalization, while the ligand without spacer remains at the cell surface regardless the time of incubation. Moreover, the receptor internalization by NR-PEG-CBT became even faster at higher ligand concentrations (compare Figure 30 A and E, registered after 5 min of incubation at r.t.). Such a difference in behavior of two CBT derivatives is in accordance with their functional activity profiles, described above.

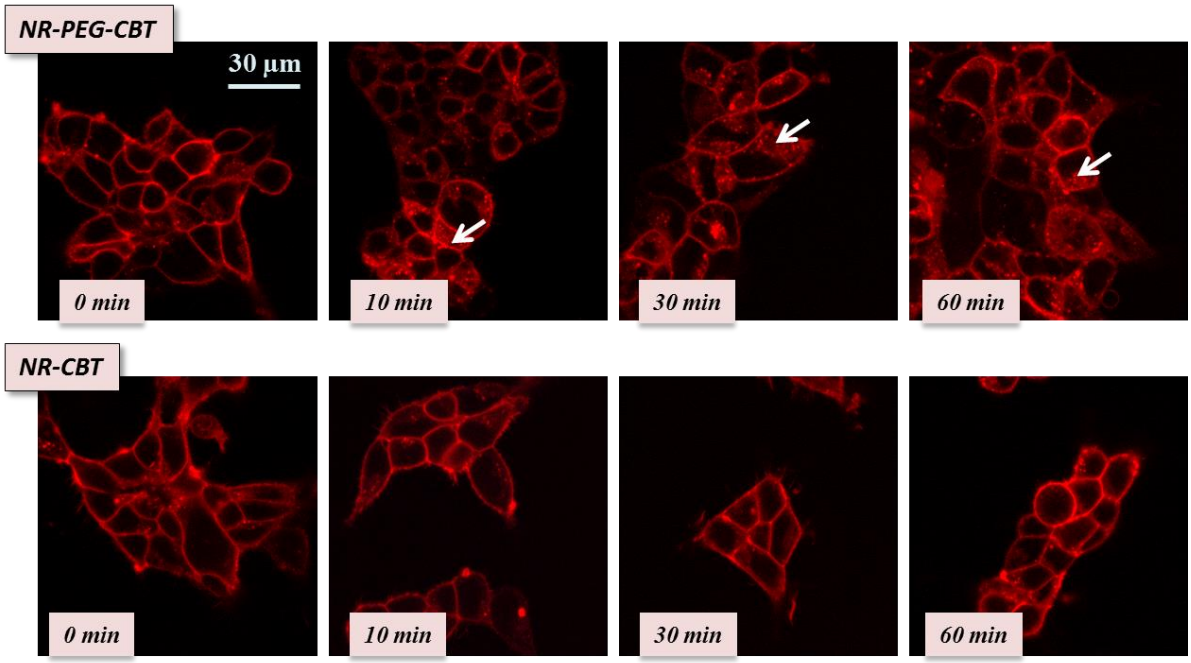

Figure 31. Internalization studies: OTR+ cells in the presence of 20 nM of NR-PEG-CBT or NR-CBT were incubated at 37°C and 5% of CO_2. Images were taken after 10, 30 and 60 min of incubation.

Finally, the successful turn-on ligand NR-PEG-CBT was evaluated as a tool to rapidly estimate the number of receptors available for ligand binding at the cell surface. At the moment, to quantify the receptors at the cell surface, one should use either radioligands (Parker et al., 2005) (which require protective equipment and result in radioactive waste) or fluorescently labeled antibodies (expensive specialized equipment is needed; Daly and McGrath, 2003). Moreover, in both techniques the washing step is unavoidable. Turn-on ligands present a simple and inexpensive alternative to the established methods.

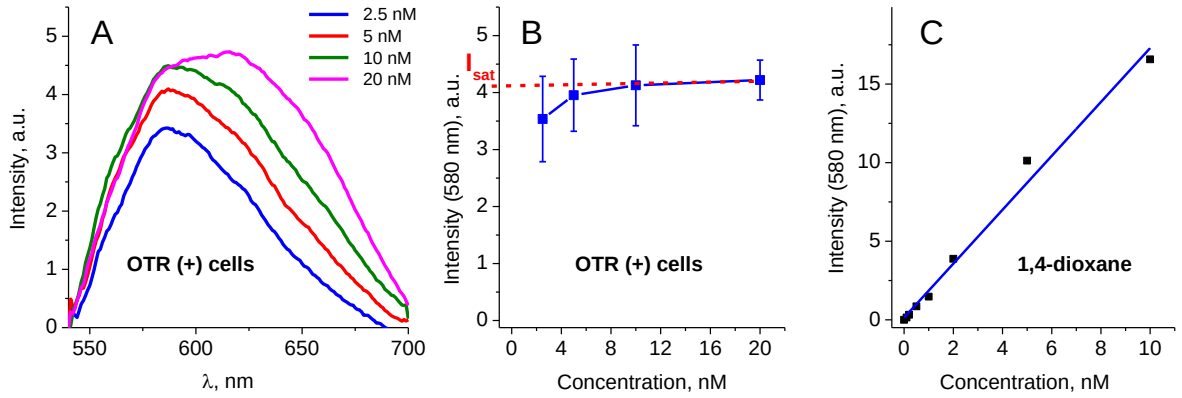

Figure 32. Receptor quantification: titration of OTR+ cells in HEPES buffer with NR-PEG-CBT (A) and the corresponding saturation curve for fluorescence intensity at 580 nm (B). Calibration curve for NR-PEG-CBT in 1,4-dioxane (C).

We performed the titration of the suspension (50 mln/mL) of OTR+ cells with NR-PEG-CBT. The experiment showed that all available receptors were saturated below 20 nM of the ligand (Figure 32A-B).

The fluorescence intensity is a semi-quantitative parameter that depends not only on the fluorophore concentration but also on its fluorescence quantum yield and on instrumental settings. Our turn-on system based on Nile Red allows the rough estimation of the fluorescence quantum yield, because this latter correlates with the position of the emission maximum (Figure 25B).

Being bound to the receptor, the ligand showed a fluorescence maximum at 585 nm (Figure 32A), very close to that observed in 1,4-dioxane, suggesting that the receptor-bound ligands may exhibit a quantum yield around 60% (Table 11). In cellular context, the quantum yield values could be slightly higher because of higher local viscosity, but this should only marginally affect the estimation. Using exactly the same instrumental settings as in the cellular measurements, we made a calibration curve of the fluorescence intensity vs. concentration of NR-PEG-CBT in 1,4-dioxane (Figure 32C). Based on this curve and the saturation intensity (I_{sat}) at 580 nm found in the titration experiments (Figure 32B), we calculated the concentration of fluorescent species (c_{fl}) and thus the number of available receptors (N):

I_{sat} (580 nm) = 4.13 ± 17% a.u. (calculated for 4 independent measurements) which corresponds to c_{fl} = 2.4 nM (from Figure 32C).

$N = c_{fl} \times N_a / c_{cell}$, where N_a is an Avogadro constant, c_{cell} is the concentration of the cells in the experiment.

$N = 2.4\times10^{-9}$ M $\times$ 6.022×10^{23} mol^{-1} / 50×10^{3} cell$\times L^{-1}$ = 29000 (± 5000) receptors/cell.

The obtained value was in good accordance with that determined by the group of Dr. Bernard Mouillac for the same cell line by the classical radioactive binding assay (46000 ± 8000 receptors/cell), which suggests the turn-on ligands as very promising alternative tools for receptor quantification without radioactive handle.

In conclusion, we developed first red turn-on ligand to study wild-type receptors without removal of the unbound ligand, which does not require expensive and time-consuming fluorescence techniques or the use of radiotracers. It is potentially interesting for development of high-throughput screening assay for GPCRs at the cell surface as well as for background free *in vivo* molecular imaging.

2. Turn-on squaraine-based probes for OTR

Being encouraged by the results of first cellular studies of Nile red-based turn-on probes we focused our attention on the development of near-infrared (NIR) fluorogenic probes for OTR. The advantage of excitation and detection in NIR region is a strong decrease of biomolecular autofluorescence and a diminished Rayleigh-Tyndall light scattering (Yuan et al., 2013). In addition the light penetration in biological tissues is strongly improved in the region of 600-900 nm allowing the *in vivo* application of fluorescent probes.

Squaraines were first reported in 1965 (Treibs and Jacob, 1965) but the actual interest for this class of dyes is still high due to their exceptional brightness, NIR spectral character and rather straightforward synthesis. Squaraines are products of condensation of squaric acid with two electron-rich moieties. Such a donor–acceptor–donor resonance stabilized zwitterionic structure causes sharp and intense absorption and emission bands, high quantum yields and large two-photon action cross-sections (Beverina and Salice, 2010). Since squaraines are generally non-fluorescent in water and highly fluorescent in apolar organic solvents, they are attractive candidates for the development of NIR turn-on probes for GPCRs.

The majority of squaraines could be referred to either arenes (Figure 33A, type A) or arylidenes (type B).

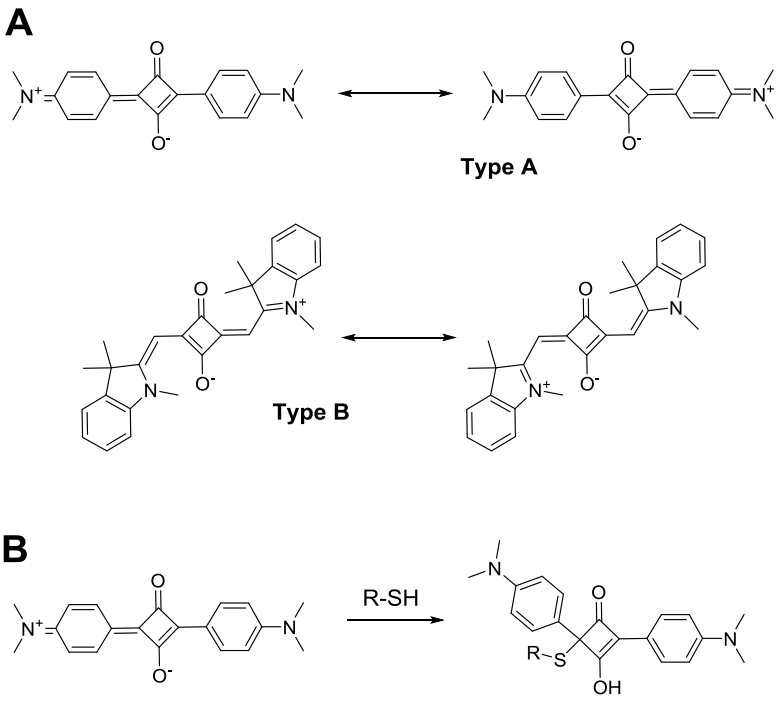

Figure 33. The simplest representatives of two types of squaraines (A) and the mechanism of the squaraine degradation under nucleophile attack (B).

Both types of squaraines found a broad application in the fields of two-photon absorbing materials (Chung et al., 2006; Scherer et al., 2002), organic solar cells (Lloyd et al., 2007; Silvestri et al., 2008) and sensitizers for photodynamic therapy (Rapozzi et al., 2010; Shafeekh et al., 2014). It has been discovered that the type A squaraines were unstable in biological medium due to the nucleophilic attack of thiols (cysteine or its derivatives) which led to the loss of conjugation and naturally, fluorescence (Figure 33B). Such property was used to quantify thiols (Ros-Lis et al., 2004) and cyanide (Ros-Lis et al., 2002) in acetonitrile/water mixtures as well as free low-molecular weight aminothiols in human plasma (Sreejith et al., 2008). Arunkumar and Smith introduced a general approach to overcome the lability of the type A squaraines in biological medium and to improve their solubility by incorporation of the dye inside a rotaxane structure (Arunkumar et al., 2005a).

However, to the best of our knowledge, the susceptibility of the type B squaraines to nucleophilic attack and their instability in biological media has never been reported. Moreover, they were successfully used to label DNA (Markova et al., 2012), to detect human and bovine serum albumins *in vitro* (Pisoni et al., 2013), to trace lysozyme-lipid interactions (Ioffe et al., 2007), and were shown to display a photosensitizing effect in cell cultures (Rapozzi et al., 2010; Shafeekh et al., 2014).

Thereby, it was decided to examine the potential of squaraines as turn-on probes for NIR detection of OTR by constructing the analogue of NR-PEG-CBT with the squaraine dye (Figure 34).

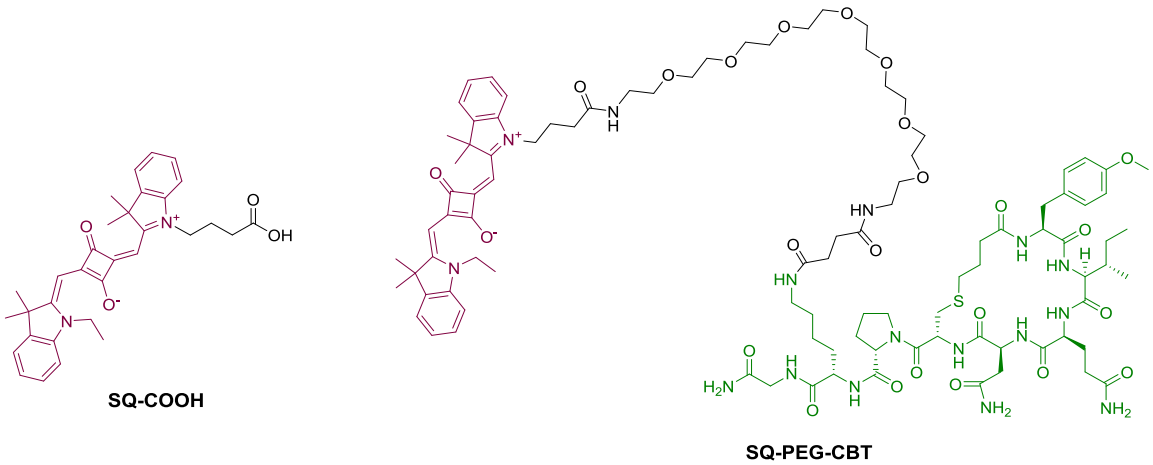

Figure 34. SQ-COOH and the target carbetocin derivative SQ-PEG-CBT.

The required squaraine carboxylic acid derivative SQ-COOH (Figure 34) was prepared by Rémy Kreder (LBP, Illkirch). The desired carbetocin derivative was synthesized in three steps starting by the condensation between SQ-COOH and commercially available PEG8 mono Boc-protected diamine **2.24** (Scheme 19). Deprotected amine **2.25** was converted to corresponding carboxylic acid **2.26** by treatment with succinic anhydride. Finally **2.26** was coupled with Lys^{8}-CBT to afford the target fluorescent probe SQ-PEG-CBT.

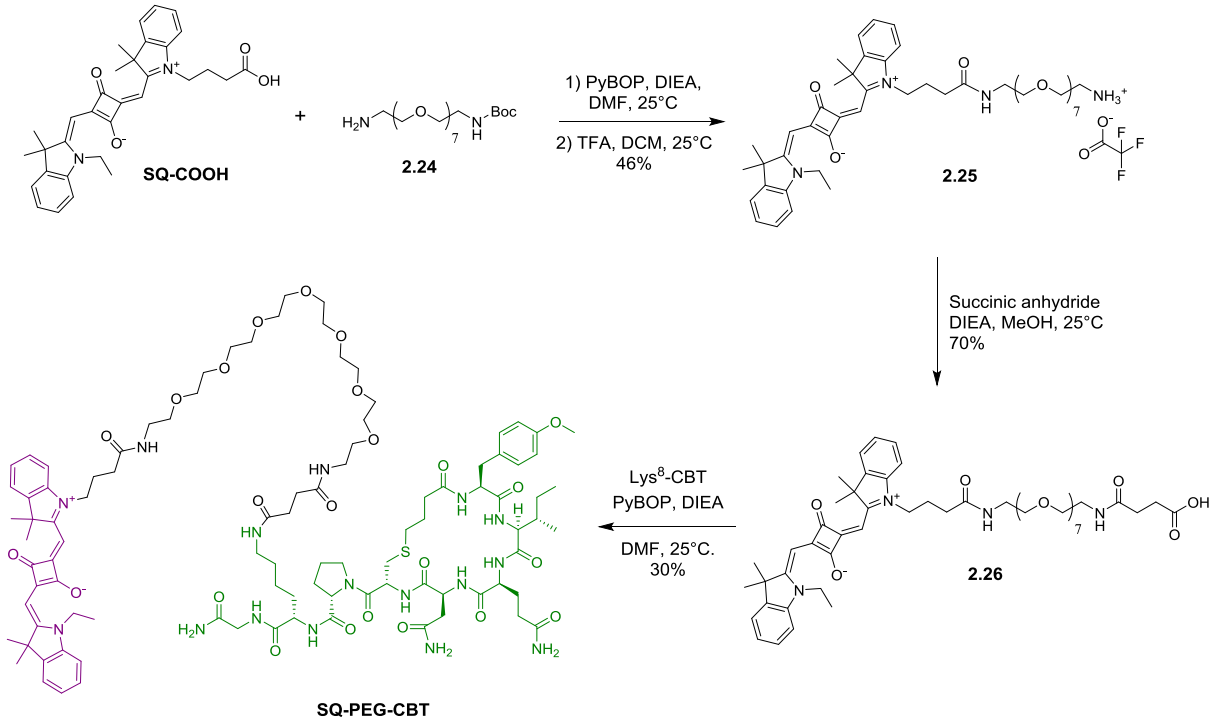

Scheme 19. Synthesis of SQ-PEG-CBT.

The evaluation of the affinity of SQ-PEG-CBT for the oxytocin receptor is in progress at PCBIS (Illkirch) by TR-FRET binding assay.

The spectroscopic properties of SQ-PEG-CBT, the parent dye SQ-COOH and SQ-COOH modified with a PEG8 chain (**2.26**) are listed in Table 12. All the squaraine derivatives were characterized by extremely high molar absorption coefficients (around 350 000 $M^{-1}\times cm^{-1}$ in dioxane compared to 38 000 $M^{-1}\times cm^{-1}$ for Nile red), negative solvatochromism (the absorption and the emission maxima shift to the blue with the increase in the solvent polarity; Figure 35A) and high quantum yields in apolar aprotic solvents. Surprisingly, in contrast to SQ-COOH, the carbetocin conjugate SQ-PEG-CBT displayed a fluorescence quantum yield of 10% in water, whereas the QY of **2.26** was intermediate between SQ-COOH and SQ-PEG-

CBT. This suggests that the low fluorescence quantum yield of SQ-COOH in water could result from its poor solubility and the formation of non-fluorescent aggregates.

Table 12. Spectroscopic properties of SQ-COOH, **2.26** and SQ-PEG-CBT.

Compound	Solvent	ε, $M^{-1}\times cm^{-1}$ [a]	λ_{max} abs, nm [b]	λ_{max} fluor, nm [c]	QY, % [d]
SQ-COOH	1,4-Dioxane	373 000	638	643	51
	Acetone	333 000	634	639	25
	Acetonitrile	228 000	632	638	6.4
	Ethanol	355 000	631	636	30
	Methanol	345 000	628	635	11
	Water	200 000	623	630	2.4
	HBS	157 000	623	630	2.9
2.26	1,4-Dioxane	332 000	638	645	50
	EtOAc	265 000	634	641	25
	DMF	352 000	640	648	25
	Glycerol	nd	637	645	35
	EtOH	344 000	632	638	20
	MeOH	330 000	629	636	10
	Water	282 000	626	635	5.0
SQ-PEG-CBT	1,4-Dioxane	308 000	639	644	51
	Acetone	227 000	635	641	13
	Acetonitrile	164 000	634	640	10
	Ethanol	355 000	632	637	25
	Methanol	301 000	629	636	13
	Water	199 000	628	636	8.6
	HBS	207 000	628	636	9.8

[a] Molar absorption coefficient. [b] Position of the absorption maximum. [c] Position of the emission maximum. [d] Fluorescence quantum yield.

Despite the non-negligible fluorescence in water which resulted in only 7-fold turn-on between water and 1,4-dioxane (at 655 nm), it was decided to continue the investigation of SQ-PEG-CBT as NIR turn-on probe.

The non-specific interactions of SQ-PEG-CBT were studied following the same approach as for Nile red derivatives. Titration of 1 µM solutions of SQ-COOH and SQ-PEG-COOH in HBS with DOPC liposomes and bovine serum confirmed the suggestion that the introduction of a long PEG chain decreases the non-specific binding of fluorescent probes to lipid membranes and plasma proteins (Figure 35B and C).

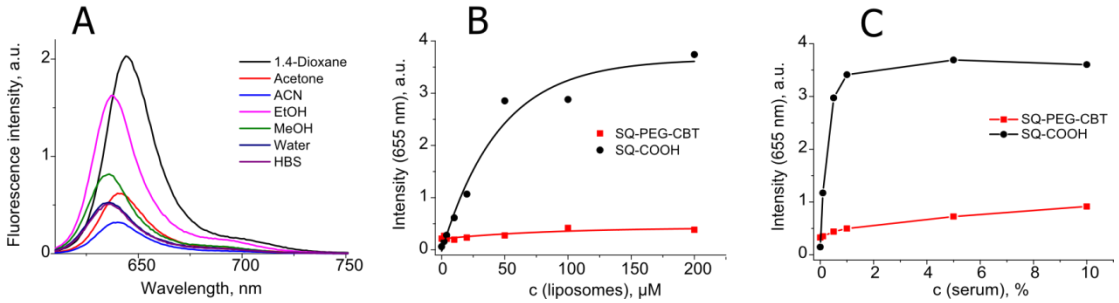

Figure 35. Fluorescence spectra of SQ-PEG-CBT in different solvents (A). Fluorescence intensity at 655 nm as a function of the liposomes (B) or serum (C) concentration in HBS.

To verify the stability of squaraine derivatives in biological medium, we incubated SQ-PEG-CBT and SQ-COOH at 1 μM concentration in 10% serum for 4 hours. No fluorescence loss was detected for both the carbetocin derivative or the parent dye, indicating that despite the binding of at least SQ-COOH to serum proteins (as evidenced by its strong fluorescence) no chemical degradation occurred (Figure 36A).

We also investigated the photostability of SQ-PEG-CBT in 1,4-dioxane, a solvent which mimics the polarity of NR and probably, SQ binding site in cells with OTR. Upon continuous excitation at 650 nm the fluorescence intensity of SQ-PEG-CBT decreased by 20% during first 20 min (which could be explained by absorption of the molecule on the cuvette) and then stabilized, confirming the good photostability of the dye (Figure 36B).

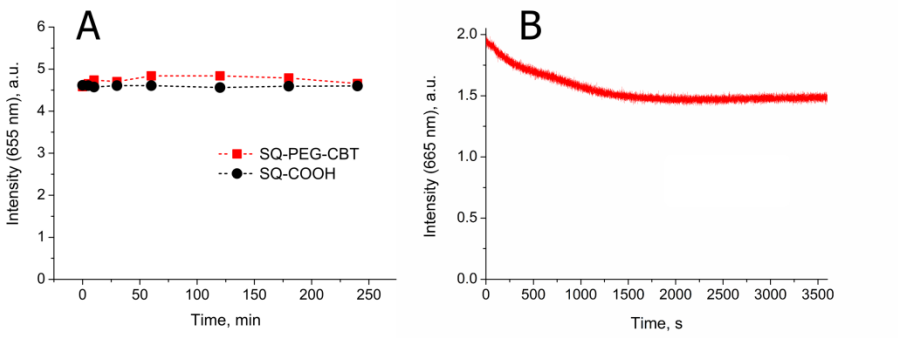

Figure 36. Stability of the squaraine derivatives in 10% serum (A) and photostability of SQ-PEG-CBT in 1,4-dioxane (B).

Next, confocal microscopy studies on cells expressing the oxytocin receptor fused to the green fluorescent protein (GFP-OTR cells) and on cells expressing the wild-type OTR (wtOTR cells) were performed (Figure 37). Due to its exceptional brightness, SQ-PEG-CBT

stained the cell membranes already at 10 nM concentration and 30% laser intensity. The images obtained in the "squaraine" channel (excitation at 635 nm, emission at 650-700 nm) were perfectly colocalized with the images recorded in the "GFP" channel (excitation at 488 nm, emission at 500-550 nm), which confirmed that the ligand was bound to the cells in a receptor-specific manner. Due to the turn-on properties of SQ-PEG-CBT, no background fluorescence was detected at higher concentrations of the fluorescent probe (Figure 37).

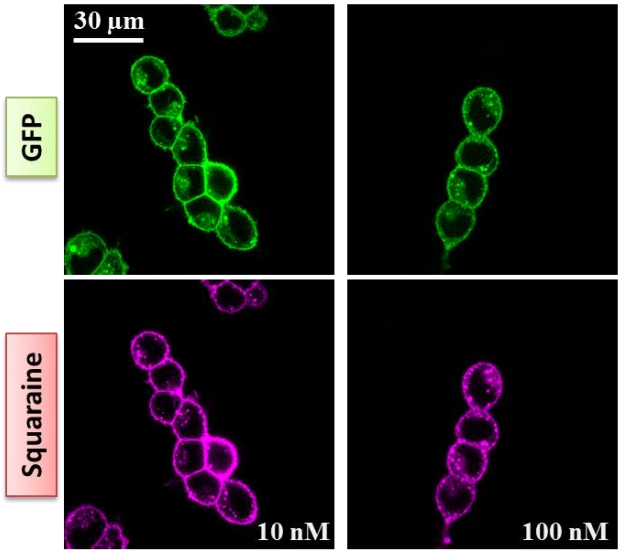

Figure 37. Confocal images of adherent GFP-OTR cells in the presence of 10 nM and 100 nM of SQ-PEG-CBT.

In the same manner we recorded fluorescence images of wtOTR cells in the presence of 10 nM of SQ-PEG-CBT and revealed the complete substitution of the membrane-bound probe in the presence of an access of unlabeled carbetocin (Figure 38).

To reveal the advantage of the photostability of the squaraine-based probe, photobleaching comparative experiments with NR-PEG-CBT were performed. GFP-OTR cells were stained with either 20 nM of NR-PEG-CBT or 20 nM of SQ-PEG-CBT and subjected to continuous laser irradiation (50 consecutive double-average scans). The intensities of two lasers (488 nm for NR and 635 nm for SQ) were adjusted in the way to get similar fluorescence intensities with the same photomultiplier gain. As it can be seen from Figure 39, NR-PEG-CBT lost from its intensity already after first scans, whereas SQ-PEG-CBT seemed to be highly photostable.

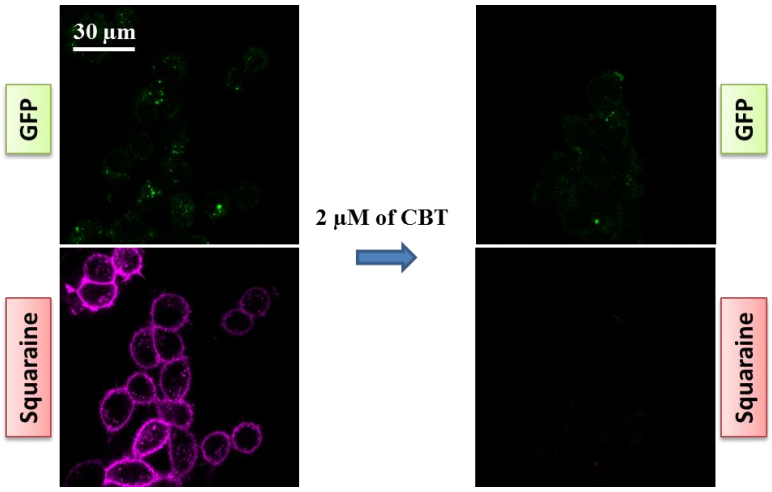

Figure 38. Confocal images of wtOTR cells with 10 nM of SQ-PEG-CBT before and after the addition of 2 µM of CBT.

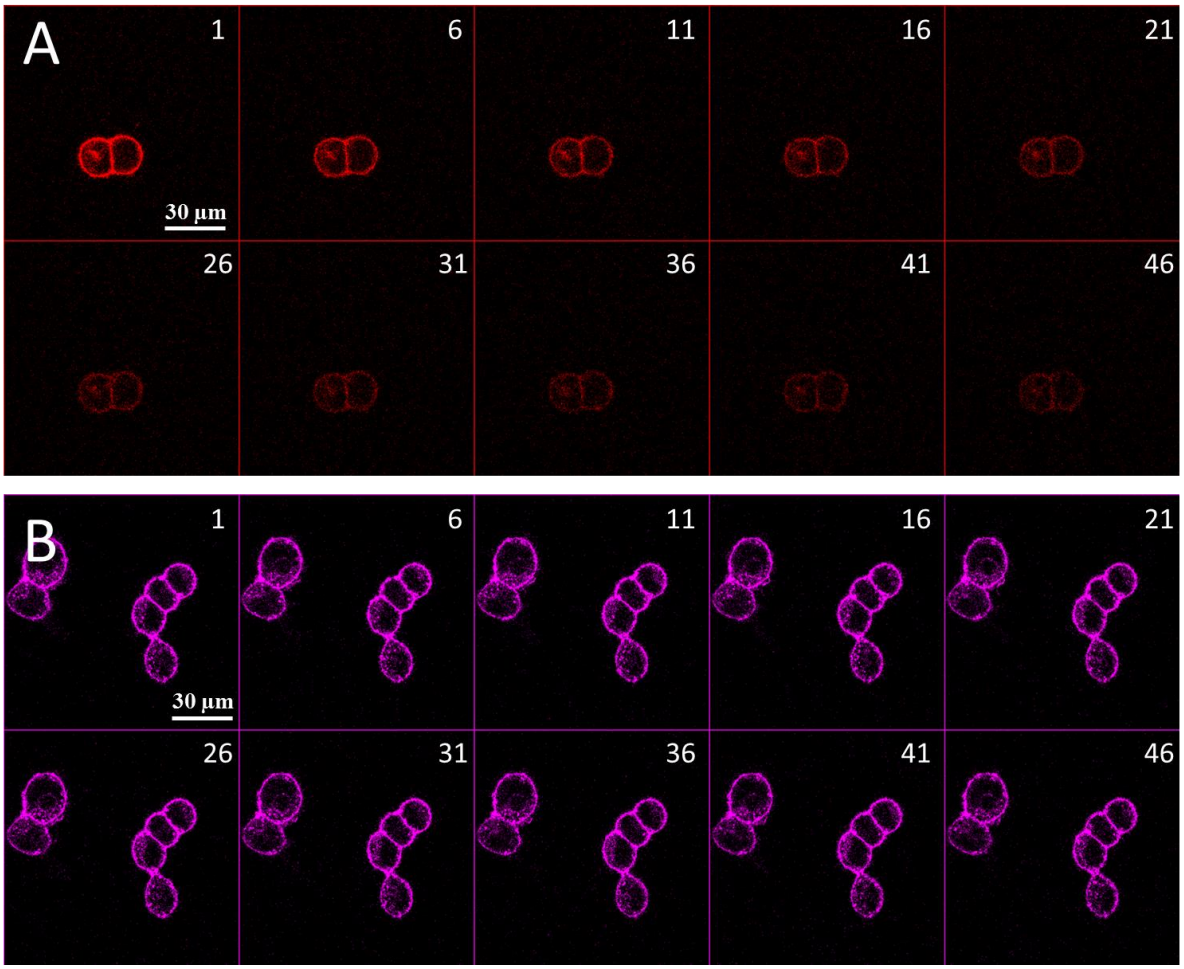

Figure 39. Photobleaching microscopy experiment with 20 nM NR-PEG-CBT (A) and SQ-PEG-CBT (B). 50 double-average scans were performed using the laser intensities which provided for equal fluorescence signal. Every 5th scan' results are presented.

Before starting the saturation experiments with the turn-on probe, we recorded its fluorescence spectra at 5 nM concentration in suspensions of wtOTR cells. An encouraging difference in fluorescence spectra with and without competitor was obtained (Figure 40A). Moreover, the fluorescence intensity in wtOTR cells in the presence of the competitor was very close to those obtained in buffer without cells, suggesting that the non-specific interactions of the probe were minimal.

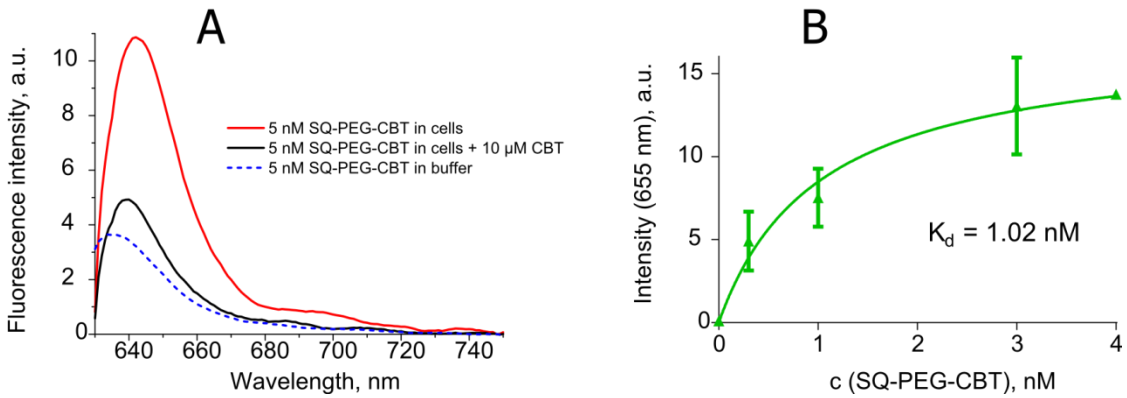

Figure 40. Fluorescence spectra of SQ-PEG-CBT in wtOTR cells with or without unlabeled competitor CBT (A). Saturation curve of SQ-PEG-CBT on wtOTR cells (B).

The preliminary saturation experiments were performed at PCBIS (Illkirch) with the help of Sophie Gioria. Fluorescence spectra of increasing concentrations of SQ-PEG-CBT in suspensions of wtOTR cells were recorded. The fluorescence intensity at 655 nm was plotted as a function of the dye concentration (Figure 40B). The dissociation constant K_d found in the turn-on saturation experiment was very close to those reported for non-modified carbetocin (1.96 nM; Engstrøm et al., 1998). The competition experiments with SQ-PEG-CBT are ongoing at PCBIS in order to validate the new turn-on binding assay.

3. Squaraine-dimers as a new concept of fluorogenic probes

Although the preliminary results of the saturation experiments with SQ-PEG-CBT were mostly reassuring, the problem of the residual fluorescence in water (QY of 10%) needed still to be solved. Since the possible explanation of the low fluorescence of SQ-COOH in water was the formation of aggregates (which is not convenient for pharmacological studies because it changes the effective ligand concentration), we envisaged the development of a water-soluble squaraine dimeric system with internal stacking between squaraines (Figure 41). Our hypothesis was that due to the low solubility of the squaraine core in aqueous solutions, the preferential form of the dye in water will be the one with stacked squaraines and quenched fluorescence, while in apolar solvents and likely in lipid membrane the solvation of squaraines will lead to their swinging and enhanced fluorescence. A similar approach was already reported for the development of Ca^{2+} probe based on the type A squaraine (Arunkumar et al., 2005b).

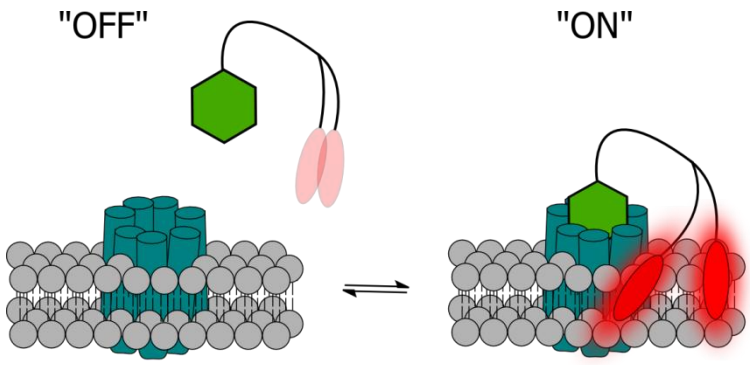

Figure 41. Principle of the turn-on detection using squaraine-dimers.

In addition to previously described SQ-COOH it was decided to use its pegylated analogue, developed by Dr. Mayeul Collot (LBP, Illkirch), in order to decrease the affinity of the probe for lipid membranes (Figure 42).

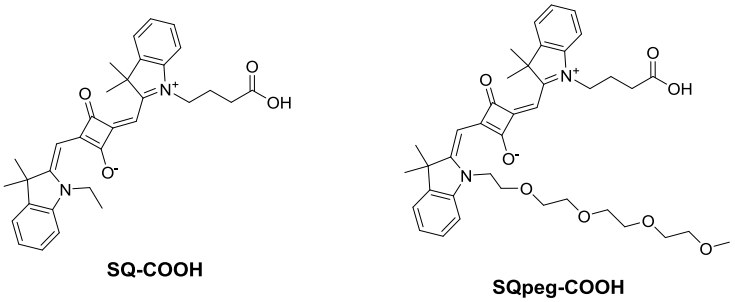

Figure 42. Chemical structures of two squaraine dyes.

It was envisaged to synthesize two dimeric derivatives of SQ-COOH and SQpeg-COOH (**2.27** and **2.28**, respectively) using PEG linkers of 8 and 3 units (Figure 43). To improve the water solubility of dimers, an α-sulfo-β-alanine moiety was introduced into **2.27** following the previously described approach (Romieu et al., 2008). Finally, the previously described monomer **2.26** would serve for the comparison.

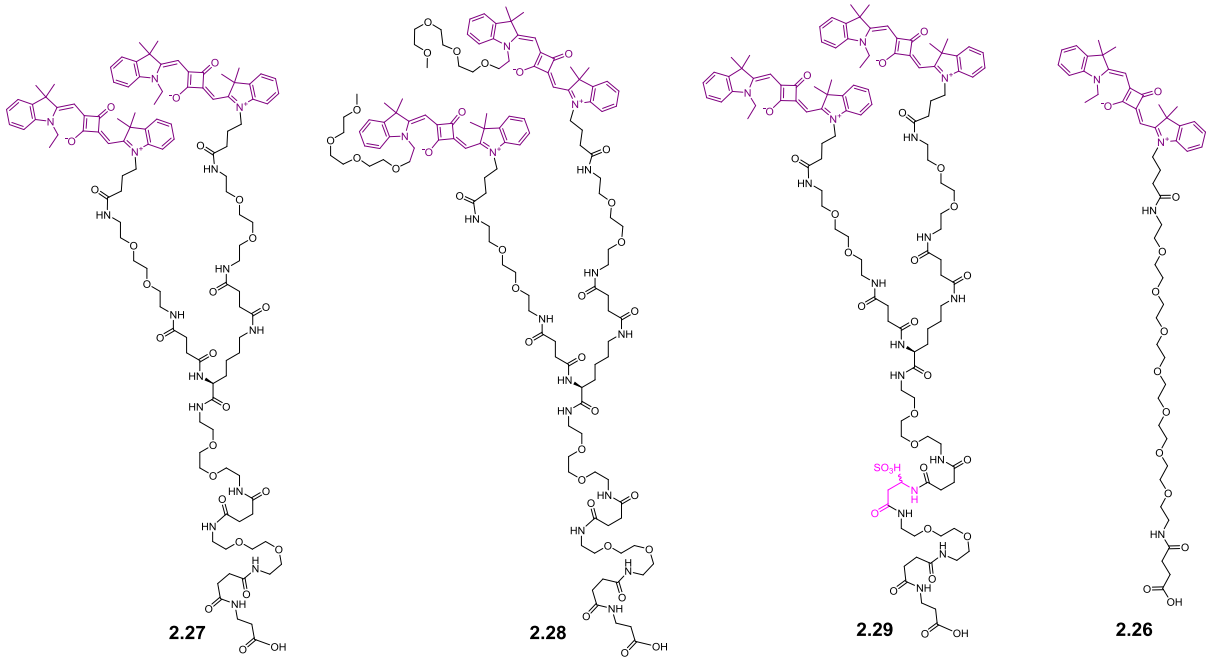

Figure 43. Structures of squaraine-dimers and the monomer of reference **2.26**.

The synthesis of squaraine-dimers was performed on solid phase starting from the commercially available Wang (*p*-alkoxybenzyl alcohol) resin (Scheme 20). First, β-alanine residue was introduced by activation with DIC in the presence of DMAP in DMF. Then, its deprotected amino group was coupled to Fmoc-NH-PEG3-COOH, obtained as previously described (Soriano et al., 2009). α-Sulfo-β-alanine amino acid was then incorporated in the case of the synthesis of **2.29** according to the described protocol (Romieu et al., 2008). The

subsequent coupling of the chains with Fmoc-NH-PEG3-COOH, Fmoc-Lys(Fmoc)-OH and again with Fmoc-NH-PEG3-COOH led to the formation of Fmoc-protected chains **2.30** and **2.31**, ready for coupling with SQ-COOH or SQpeg-COOH.

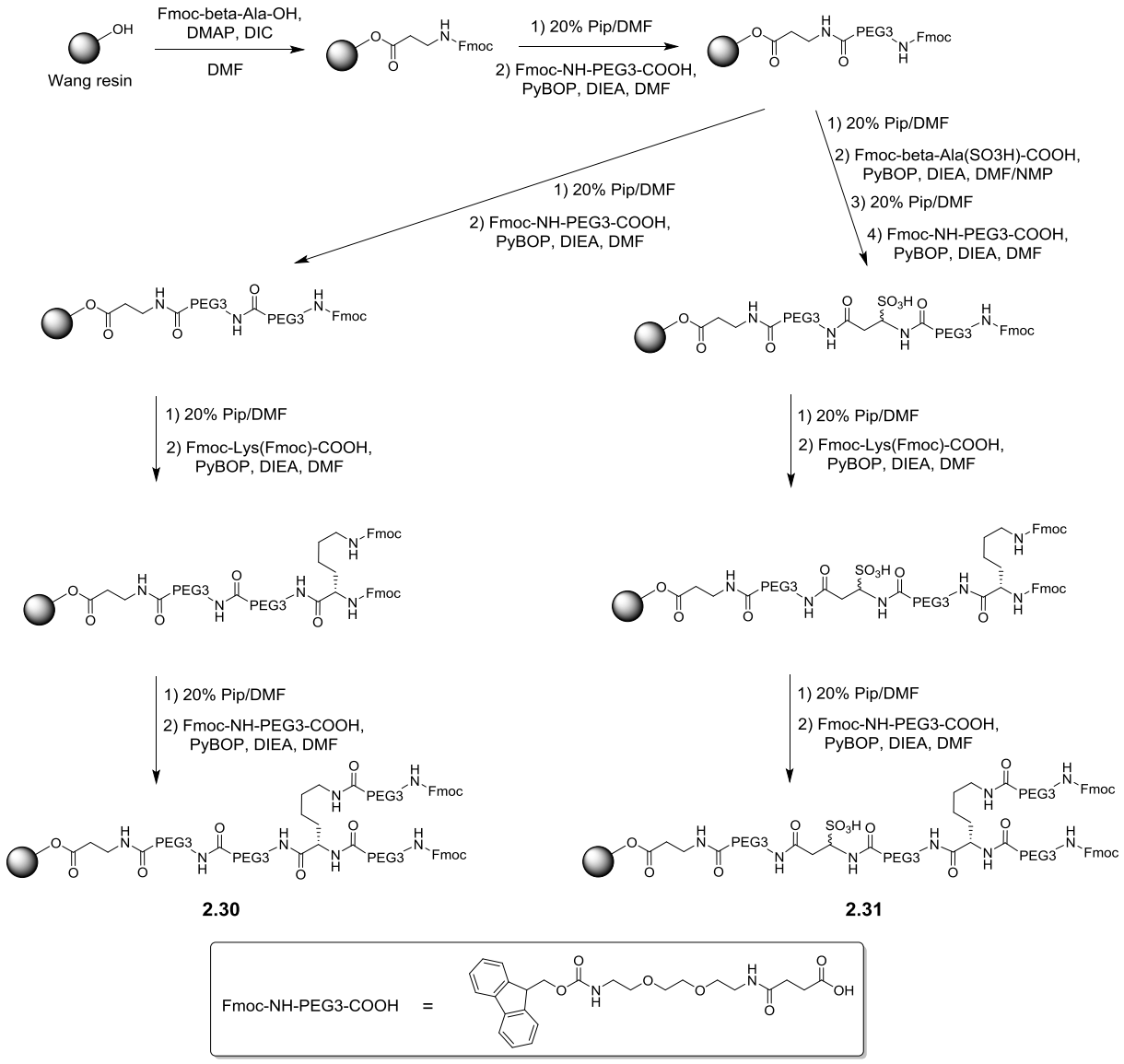

Scheme 20. Synthesis of branched chains **2.30** and **2.31**.

The introduction of the fluorophores on **2.30** and **2.31** was conducted on solid phase by activation with PyBOP in the presence of DIEA in DMF (Scheme 21 and Scheme 22). After completion of the couplings the chains were cleaved from the solid phase in concentrated TFA and purified by semi-preparative HPLC. The identity and the purity of fluorescent dimers **2.27**, **2.28** and **2.29** were confirmed by LC-HRMS.

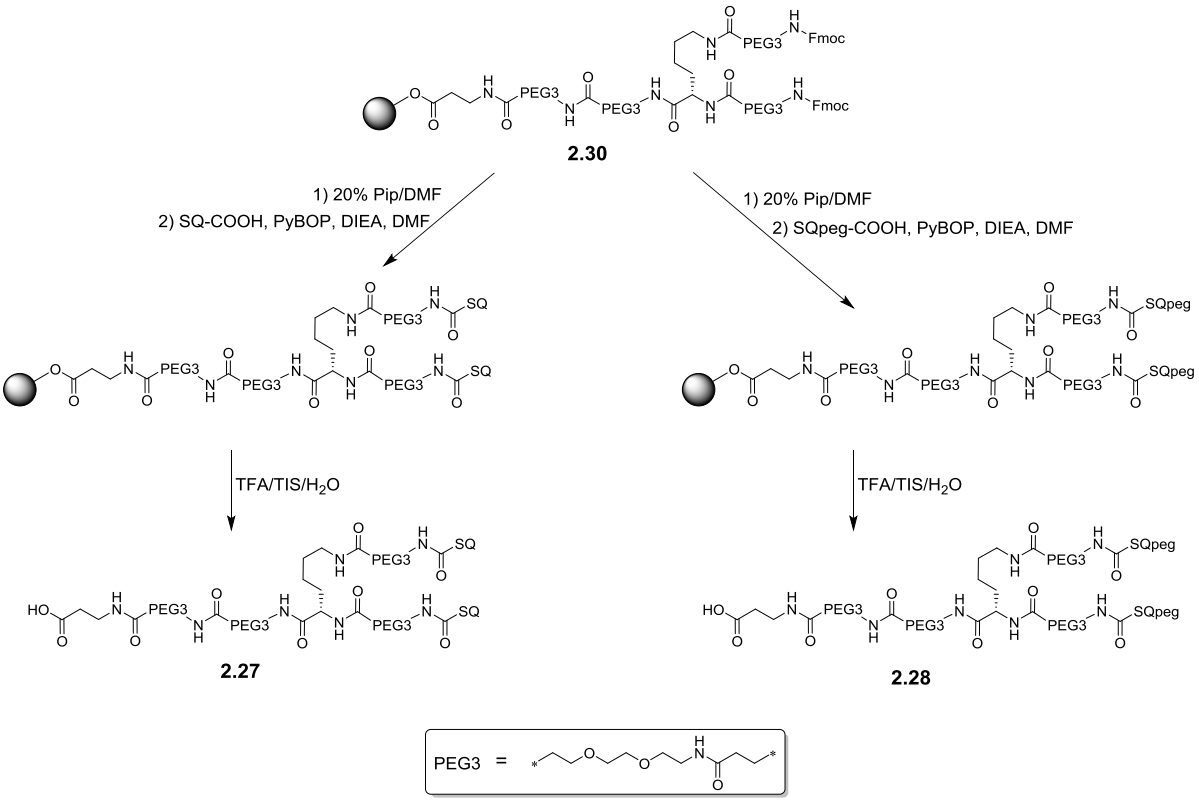

Scheme 21. Synthesis of **2.27** and **2.28**.

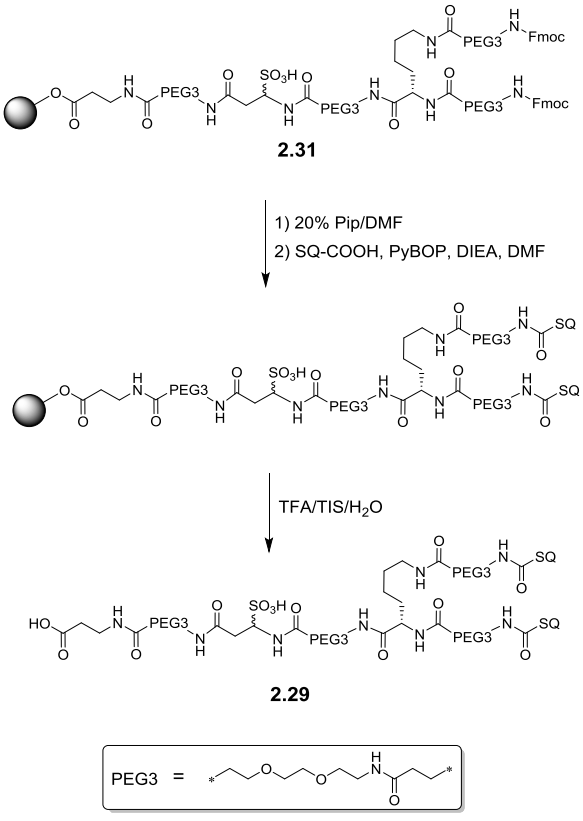

Scheme 22. Synthesis of **2.29**

The spectroscopic properties of squaraine-dimers and the monomer **2.26** were studied in solvents of different polarities (Table 13). The molar absorption coefficients (ε) of dimers reached 450 000 for the SQ and 330 000 for the SQpeg derivatives. Obviously, the obtained values did not double the ε of monomers, because the proximity of two squaraines creates the high "local concentration" of dyes which influences the attenuation. But in any case, such strong absorption coefficients could be compared with those of quantum dots – the brightest dyes known to date.

Table 13. Spectroscopic properties of **2.26**, **2.27**, **2.28** and **2.29**.

Compound	Solvent	Dielectric constant	ε, $M^{-1}\times cm^{-1}$ [a]	λ_{max} abs, nm [b]	λ_{max} fluor, nm [c]	QY, % [d]
2.26	1,4-Dioxane	2.3	332 000	638	645	50
	EtOAc	6.0	265 000	634	641	25
	Ethanol	25	344 000	632	638	20
	Methanol	33	330 000	629	636	10
	DMF	38	325 000	640	648	25
	Ethylene glycol	41	nd	635	643	38
	Glycerol	41	nd	637	645	35
	Water	80	282 000	626	635	5.0
2.27	1,4-Dioxane	2.3	364 000	638	647	22
	EtOAc	6.0	275 000	634	643	8.8
	Ethanol	25	434 000	632	640	14
	Methanol	33	463 000	629	638	6.3
	DMF	38	462 000	640	649	21
	Ethylene glycol	41	nd	635	644	24
	Glycerol	41	nd	637	646	39
	Water	80	nd	584	639	0.7
2.28	1,4-Dioxane	2.3	444 000	639	648	14
	EtOAc	6.0	326 000	636	645	11
	Ethanol	25	444 000	633	642	16
	Methanol	33	481 000	629	638	8.5
	DMF	38	450 000	641	651	22
	Ethylene glycol	41	nd	637	646	29
	Glycerol	41	nd	639	648	25
	Water	80	nd	587	640	0.4
2.29	1,4-Dioxane	2.3	263 000	638	647	28
	EtOAc	6.0	nd	635	643	4.0
	Ethanol	25	334 000	632	640	15
	Methanol	33	328 000	629	638	8.8

DMF	38	334 000	641	649	20
Ethylene glycol	41	nd	635	644	23
Glycerol	41	nd	637	646	39
Water	80	nd	584	639	0.5

[a] Molar absorption coefficient. [b] Position of the absorption maximum. [c] Position of the emission maximum. [d] Fluorescence quantum yield.

We were pleased to discover that the fluorescence quantum yields of squaraine-dimers in water were 10 times lower in comparison to the quantum yield of the monomer. At the same time the quantum yield in 1,4-dioxane decreased by a factor two when going from the monomer to dimers, possibly due to the presence of a collisional deactivation pathway. Taken together, the theoretical turn-on between water and 1,4-dioxane (at 655 nm) increased up to 35 for squaraine-dimers (in comparison, the calculated turn-on was 7-fold for the monomer **2.26**).

Of particular interest were the absorption spectra of squaraine-dimers in water. In contrast to the classical absorption spectrum of **2.26** (Figure 44A), the absorption spectra of all the three dimers differed from their excitation spectra, indicating the presence of non-fluorescent species. The absorption maxima of the dark species were blue shifted in comparison to the maxima of the fluorescent forms (584 nm and 623 nm, respectively). Based on the previously reported studies, we concluded that the non-fluorescent species corresponded to H-aggregates (Das et al., 1996). Whereas H-aggregates were predominant in aqueous solution at 200 nM concentration of **2.27** (Figure 45B), the absorption of the fluorescent form became quickly major when increasing quantities of MeOH were added to the water solution of the dye.

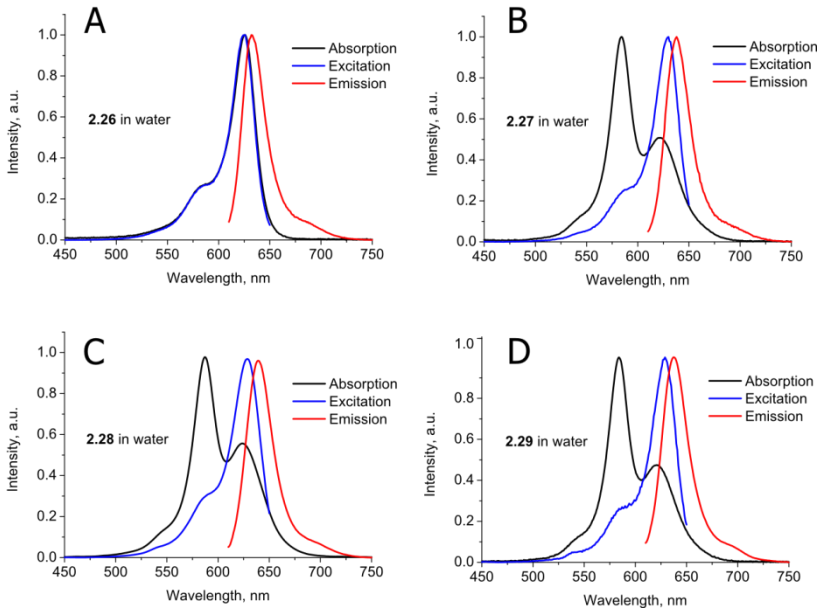

Figure 44. Absorption, excitation and fluorescence spectra of 200 nM **2.26** (A), **2.27** (B), **2.28** (C) and **2.29** (D) in water.

The absorption spectra of squaraine-dimers recorded in water at different concentrations of dyes (Figure 46) revealed the important difference in water solubility of three turn-on probes. Whereas the SQpeg derivative **2.28** and the SQ derivative with an α-sulfo-β-alanine moiety **2.29** displayed identical absorptions spectra regardless the concentration (in the range of 20 nm – 2 µM), a third red-shifted band appeared in the absorption spectra of **2.27** starting from 1 µM concentration. Such a band, which corresponds to a non-fluorescent form, could be referred to intermolecular aggregates which were formed clearly due to the lack of water solubility of **2.27**.

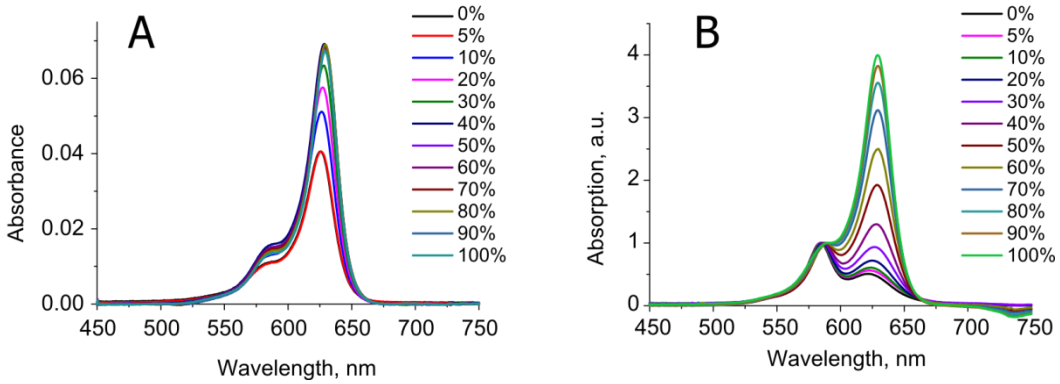

Figure 45. Absorption spectra of 200 nM **2.26** (A) and **2.27** (B) in increasing concentrations of MeOH in water.

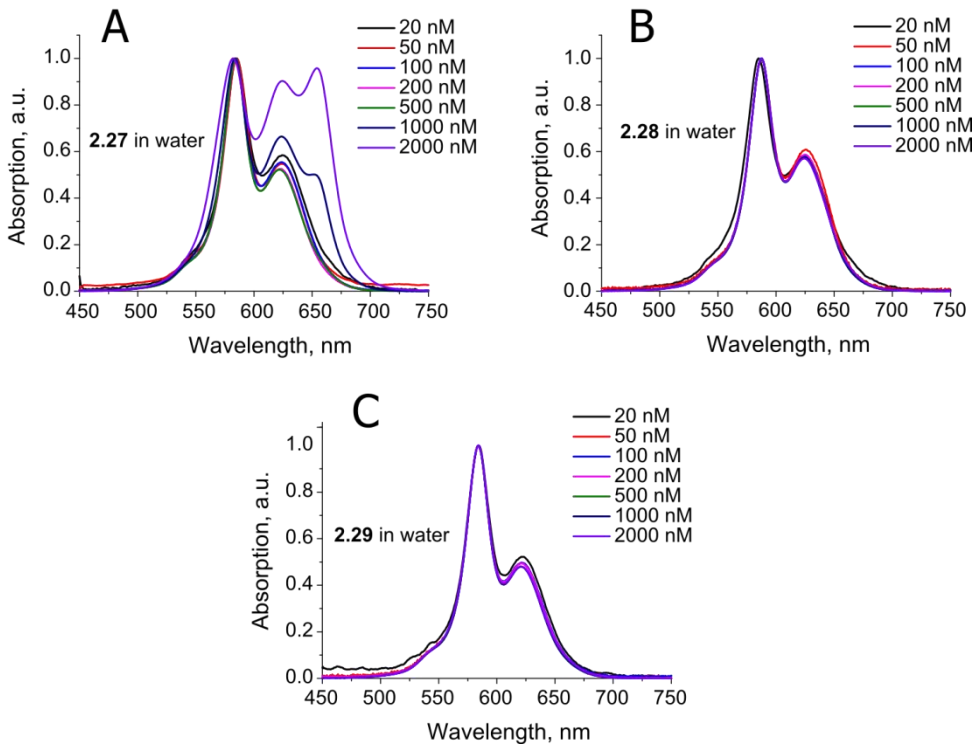

Figure 46. Absorption spectra of **2.27** (A), **2.28** (B) and **2.29** (C) at different concentrations in water.

Another important feature of the fluorescence of squaraine-dimers was the strong increase of quantum yields in viscous ethylene glycol and glycerol in comparison to non-viscous solvents like ethanol (Table 13). The quantum yield of **2.27** undergone 2.8-fold increase going from EtOH to glycerol whereas for the corresponding monomer **2.26** the increase was only 1.8-fold.

To characterize the nature of the fluorescence enhancement in viscous solvents we performed time-resolved experiments for **2.27** and its corresponding monomer **2.26** in a number of solvents. The results of these measurements are summarized in Table 14. The squaraine emission was in most cases characterized by biexponential kinetics, in accordance to previous studies (Chen et al., 1996). In non-viscous solvents (dioxane, ethanol, methanol) a clear tendency of mean decay time decrease with the increase in the solvent polarity was observed. The decay components were similar for the monomer and the dimer regardless the difference in their quantum yields (except for ethylene glycol in which the situation is not yet clear). Such a phenomenon can be explained by the presence of dark species in the case of the dimer **2.27** which decrease the quantum yield. The decay components in viscous media (ethylene glycol and glycerol) were slower than in polar non-viscous solvents in accordance to the difference in their quantum yields.

To deeply understand the time-resolved properties of squaraine-dimers further investigations are ongoing in LBP, Illkirch.

Table 14. Time-resolved decay parameters for **2.26** and **2.27**.

Comp.	Solvent	QY, % [a]	τ_1, ns [b]	α_1 [c]	τ_2, ns [b]	α_2 [c]	τ, ns [d]
2.26	1,4-Dioxane	50	0.36 ± 0.01	0.42	1.47 ± 0.01	0.58	1.00
	Ethanol	20	0.43 ± 0.04	0.18	0.70 ± 0.01	0.82	0.65
	Methanol	10	0.31 ± 0.01	1.00			0.31
	Ethylene glycol	38	0.31 ± 0.01	0.08	0.68 ± 0.00	0.92	0.65
	Glycerol	35	2.52 ± 0.01	1.00			2.52
2.27	1,4-Dioxane	22	0.86 ± 0.03	0.26	1.48 ± 0.01	0.74	1.32
	Ethanol	14	0.48 ± 0.01	0.58	0.74 ± 0.01	0.42	0.59
	Methanol	6.3	0.26 ± 0.03	0.76	0.37 ± 0.05	0.24	0.29
	Ethylene glycol	24	1.07 ± 0.03	0.72	1.48 ± 0.05	0.28	1.18
	Glycerol	39	0.68 ± 0.05	0.09	2.39 ± 0.01	0.91	2.24

[a] Fluorescence quantum yield. [b] Emission decay times. [a] Corresponding pre-exponential coefficients. [a] Mean emission decay times.

To explore the potency of squaraine-dimers in cellular studies, we coupled **2.27**, **2.28** and **2.29** to Lys^8-CBT in order to obtain conjugates **2.30**, **2.31** and **2.32** (Scheme 23). The purity and identity of the obtained probes were confirmed by LC-HRMS.

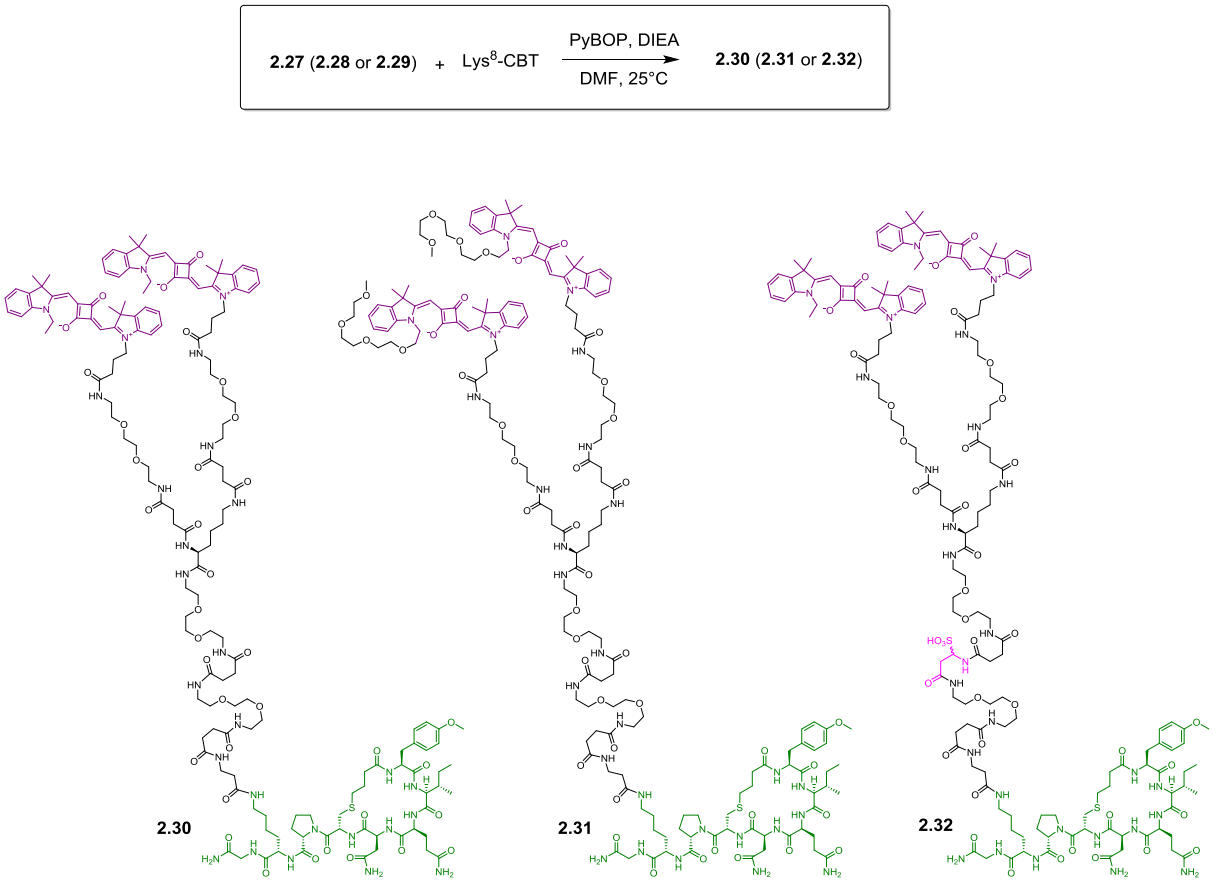

Scheme 23. Conjugation of squaraine-dimers to Lys[8]-CBT.

The spectroscopic properties of the obtained conjugates were similar to those of the parent dyes **2.27**, **2.28** and **2.29** (Table 15).

The non-specific interactions were studied according to the previously developed approach (Figure 47). Between the three CBT derivatives, **2.31** – the one with the pegylated squaraine – clearly displayed less non-specific binding to DOPC liposomes and BSA. This confirmed our suggestion of the influence of "lateral" PEG groups on non-specific interactions of squaraine-dimer.

Table 15. Spectroscopic properties of **2.30**, **2.31** and **2.32**.

Compound	Solvent	Dielectric constant	ε, $M^{-1}\times cm^{-1}$ [a]	λ_{max} abs, nm [b]	λ_{max} fluor, nm [c]	QY, % [d]
2.30	1,4-Dioxane	2.3	368 000	638	647	27
	Ethanol	25	451 000	632	640	16
	Methanol	33	433 000	629	638	8.4
	Water	80	nd	584	640	0.3
2.31	1,4-Dioxane	2.3	382 000	640	649	31

	Ethanol	25	426 000	633	642	16
	Methanol	33	413 000	631	640	8.2
	Water	80	nd	588	641	0.6
2.32	1,4-Dioxane	2.3	404 000	638	648	33
	Ethanol	25	447 000	632	640	15
	Methanol	33	449 000	629	638	6.5
	Water	80	nd	586	640	0.4

[a] Molar absorption coefficient. [b] Position of the absorption maximum. [c] Position of the emission maximum. [d] Fluorescence quantum yield.

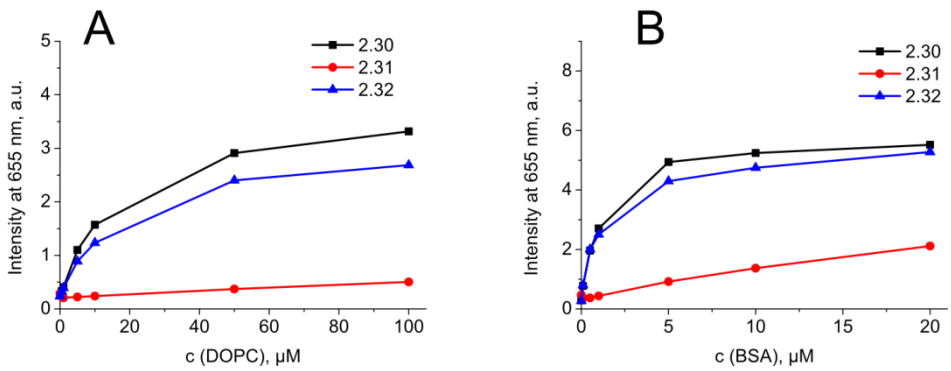

Figure 47. Fluorescence intensities **2.30**, **2.31** and **2.32** at 20 nM as a function of DOPC (A) or BSA (B) concentration in phosphate buffer.

The affinities of **2.30**, **2.31** and **2.32** for the oxytocin receptor were studied by TR-FRET binding assay, using squaraine-dimers as acceptors of the Lumi-4-Tb emission. Surprisingly, although SQ and SQpeg dyes were both well distant from the pharmacophore CBT, the pharmacological properties of corresponding probes were quite different. Whereas **2.31**, derived from the pegylated squaraine, displayed a classical binding profile which K_d of 41 nM, the affinities of **2.30** and **2.32** were found to be subnanomolar (Table 16). Moreover, the non-specific fluorescence in the case of **2.30** and **2.32** was important thus the precision of the obtained dissociation constants can be called in question. Such a difference in affinities can be explained by the cooperative effect of squaraine SQ, which interacts with the receptor allosteric pocket or lipid membranes close to the receptor binding site and decrease the dissociation constant of **2.30** and **2.32**. By pegylating the squaraine core we increased its shape, diminished the affinity to lipid membranes and probably changed the way it lays in the membrane bilayer or the receptor hydrophobic pocket. On the other hand, binding to lipid membranes close to the SNAP fusion protein can also result in FRET and explain the obtained

non-negligible fluorescence in the presence of 10 µM of CBT (non-specific binding). The additional competition experiments with SQ-derived dimers and non-labeled CBT to reveal the nature of high affinity of **2.30** and **2.32** are ongoing.

Table 16. Dissociation constants of **2.30**, **2.31** and **2.32** determined by saturation TR-FRET experiments and the representative curves.

Compound	Binding, K_d (nM)[a]
2.30	0.15 ± 0.06
2.31	41.3 ± 11.7
2.32	0.44 ± 0.01

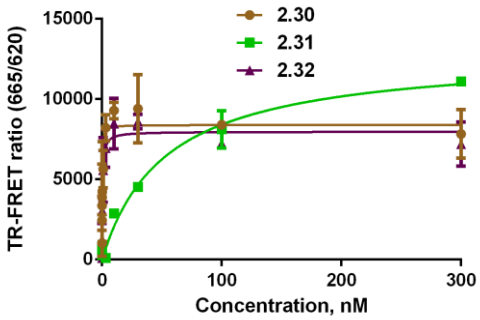

Confocal microscopy studies with squaraine-dimers were performed on adherent GFP-OTR cells. Due to the exceptional brightness of dimers and their high affinity for OTR, we were able to stain OTR at the cell surface with only 1 nM of **2.30** (Figure 48). Because of the turn-on character of squaraines, any background fluorescence was detected at 100 times higher ligand concentration. A clear colocalization between the "GFP" and the "squaraine" channels is seen from Figure 48. Moreover, the difference in the fluorescence intensity of different cells (explained by different OTR expression) was coherent with the fluorescence intensity in the "squaraine" channel.

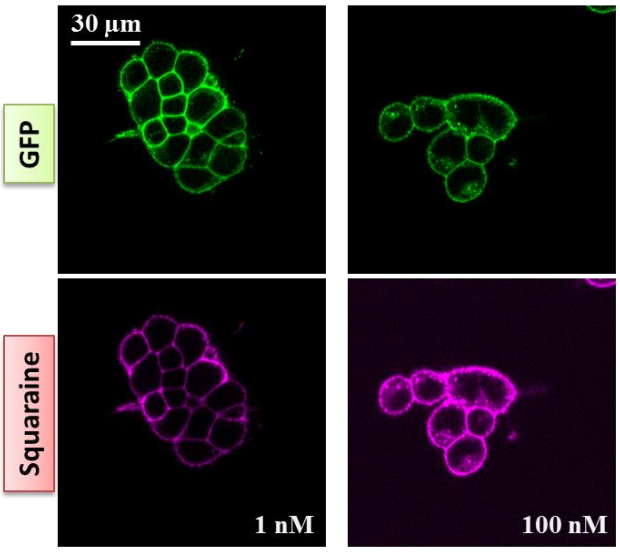

Figure 48. Confocal images of adherent GFP-OTR cells in the presence of 1 nM and 100 nM of **2.30**.

To compare the three turn-on dimers, a quantitative image analysis was performed. The working concentrations of 10 nM for **2.30** and **2.32** and 100 nM for **2.31** were chosen based on their affinities (in order to saturate most of the receptors). The average fluorescence intensities from cell membranes recorded in the "squaraine" channel (corrected by the average intensities in the "GFP" channel) are presented in Figure 49D. The green bars correspond to the total fluorescence and the grey bars to the non-specific fluorescence (recorded in the presence of an excess of the unlabeled competitor CBT). Although **2.30** was the brightest at the cell membrane, it also displayed a non-negligible non-specific fluorescence. By making the ratio between the total and the non-specific fluorescence (which we called the "potency" of the turn-on probe; Figure 49E), we showed that despite its less bright character, squaraine-dimer **2.31**, derived from the pegylated squaraine, was the most potent in detecting the oxytocin receptors at the surface of living cells.

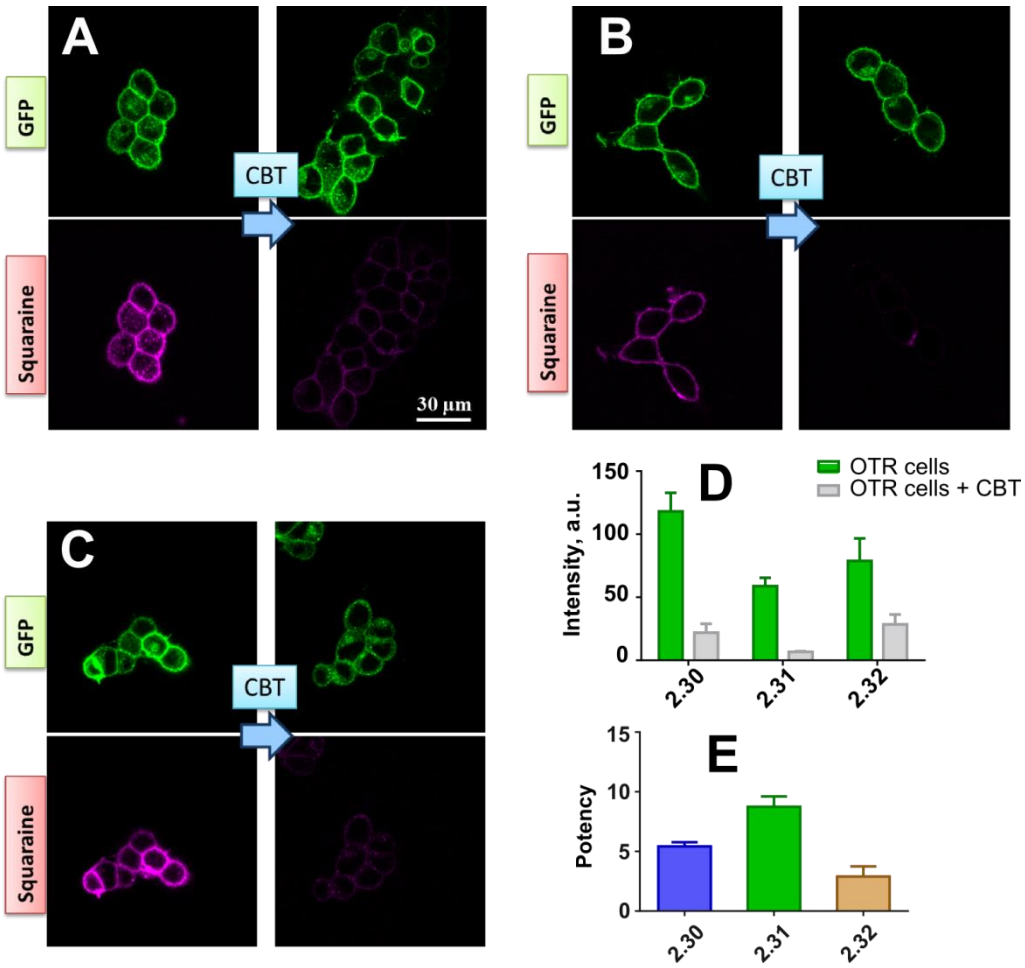

Figure 49. Confocal images of GFP-OTR cells with 10 nM of **2.30** (A), 100 nM of **2.31** (B) and 10 nM of **2.32** (C) before and after the addition of 2 µM of CBT. Average fluorescence intensity from the cell surface before and after the addition of CBT (D) and the sensitivity of probes (ratio between specific and non-specific membrane fluorescence; E).

The FLIM studies were then conducted on adherent wtOTR cells in order to investigate the fluorescence lifetimes of squaraine-dimers bound to OTR. As it can be seen from Figure 50, the mean lifetimes for all the three CBT-derived probes were around 2.4 ns and close to the values obtained in glycerol (Table 14). Thus, the lifetimes of squaraines are much more sensitive to the viscosity of the medium than to its polarity, in contrast to the sensitivity of Nile red derived probes.

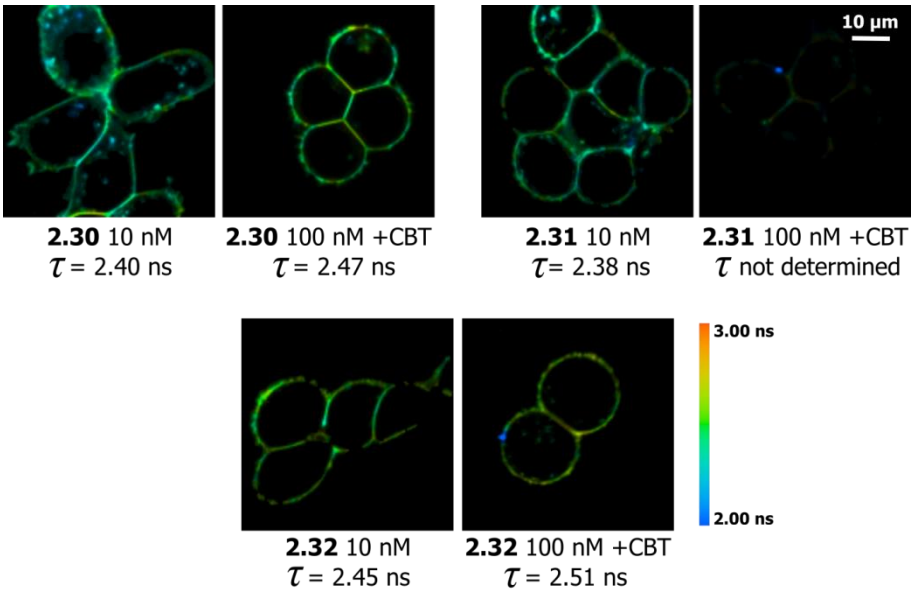

Figure 50. Lifetime images of **2.30**, **2.31** and **2.32** at the surface of attached wtOTR cells.

In conclusion, we developed a new type of NIR photostable fluorogenic probes based on the "dimer" approach. Among the three evaluated probes, the one derived from the pegylated squaraine was found to be the most potent in sensing OTR at the cell surface with high sensitivity and reduced non-specific binding to the lipophilic cell constituents.

Conclusion and perspectives

The objective of the part of my thesis presented above was the design and the synthesis of fluorescent probes both for the SNAP-tagged and the wild-type oxytocin receptors.

A new Tb-based luminescent time-resolved probe was developed in collaboration with Dr. Loic Charbonnière and Dr. Aline Nonat from the Laboratoire d'Ingénierie Moléculaire Appliquée à l'Analyse (Strasbourg.

The first selective non-peptide OTR ligands, derived from PF-3274167, allowed the establishment of a TR-FRET binding assay on the oxytocin receptor.

The turn-on approach was proposed for the detection of the non-modified oxytocin receptor on the surface of living cells. The project, carried out in collaboration with Dr. Andrey Klymchenko from the Laboratoire de Biophotonique et Pharmacologie (Strasbourg), resulted in the development of the Nile Red-based probes used to detect and quantify OTR at the cell surface without radioactive handle.

By changing the nature of the turn-on fluorophore to the near-infrared and ultra-bright squaraine, the second generation of the turn-probes was synthesized. With such a probe in hand we started the development of the screening test on wild-type GPCRs, which is currently in progress.

Finally, a new concept of the turn-on fluorescence response based on squaraine-dimers was proposed. Three squaraine-dimers were grafted onto the OTR ligand carbetocin and their potency was explored by confocal microscopy.

Chapter 2. Fluorescent probes for selectivity assays (profiling)

Development of multicolor TR-FRET binding assay

The characterization of a ligand-receptor binding event includes:

1) The determination of the ligand affinity for the receptor of interest (the dissociation constant K_d or the inhibition constant K_i).

2) The investigation of the ligand selectivity versus other receptors.

This requires the conducting of multiple receptor binding assays to fully characterize one ligand, which is time- and money-consuming.

The alternative would be to carry out multiple receptor binding assays in one test using separate detection channels (different optical filters in the case of TR-FRET technique). This would give access to affinities of the ligand for the target receptor and for concurrent receptors at once, in a single experiment. This alternative strategy is possible to implement taking into account the line-like emission of Tb (III) cryptate (the donor of the TR-FRET) which enables the energy transfer to multiple fluorophores at the same time, which emit in different spectral regions. The number of possible simultaneous detection channels is only limited by the width of the acceptor fluorescence spectra and the available optical filters.

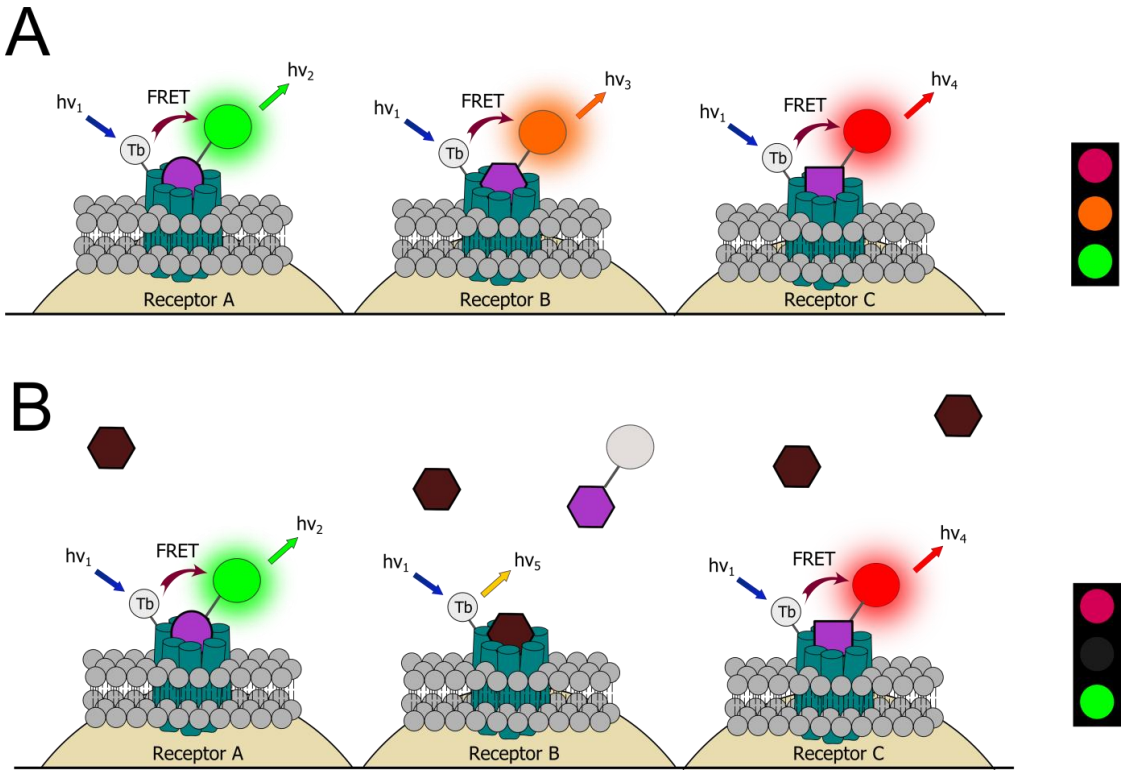

Figure 51. Principle of the multicolor binding assay for 3 receptors: the mixture of three receptors with their ligands (A) and the same mixture after the addition of a competitive ligand for receptor B (B).

It was decided to develop the multicolor approach in collaboration with the group of Dr. Thierry Durroux from the Institut de Génomique Fonctionnelle in Montpellier on the system of three receptors (Apelin, dopamine D_3 and vasopressin V_2) using three commercially available emission filters: green (520/15 nm), orange (605/15 nm) and red (665/35 nm).

The steps of the multicolor binding assay are the following:

1) Mixing of three types of cells each expressing one receptor of interest (each labeled with the same TR-FRET donor).

2) Incubation of cells with a mixture of three selective fluorescent tracers ("green" for D_3R, "orange" for V_2R and "red" for ApelinR).

3) Detection of three different FRET signals.

4) Addition of the increasing concentrations of a ligand-to-test.

5) Measuring the changes in each FRET signal induced by the competition between the ligand-to-test and the fluorescent tracers (Figure 51).

Having in hands selective "red" ligand **3.1** for the apelin receptor and "green" ligand **3.2** for the D_3 receptor (developed previously in the laboratory, structures will be published soon), we focused our attention on the synthesis of selective "orange" V_2R ligand. For this purpose we decided to introduce fluorophores onto the selective V_2 receptor ligand **3.3** (Figure 52) developed previously in the laboratory (Loison et al., 2012).

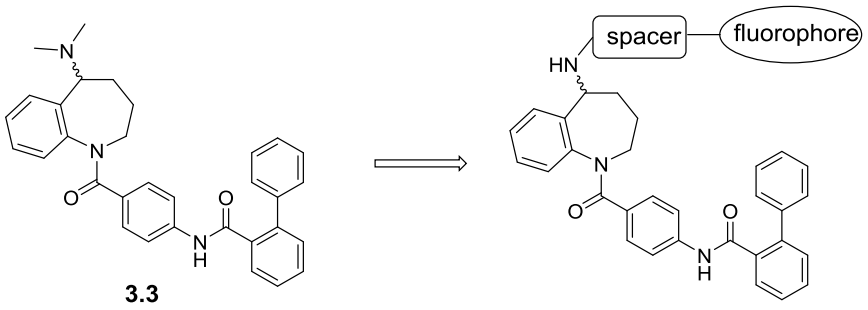

Figure 52. Selective V_2R ligand **3.3** and the envisaged fluorescent derivatives.

A benzazepine derivative **3.4** with a short spacer containing the triazole moiety was prepared following the described protocol (Loison et al., 2012) by Dr. Corinne Baehr (Figure 53). It was reported that the introduction of bulky fluorophores like DY-647 or Lumi-4-Tb via such a spacer did not influence the pharmacological properties of the ligand. Dr. Corinne

Baehr also performed the direct introduction of the long PEG8 spacer onto **3.3** to investigate the importance of the triazole moiety (Figure 53).

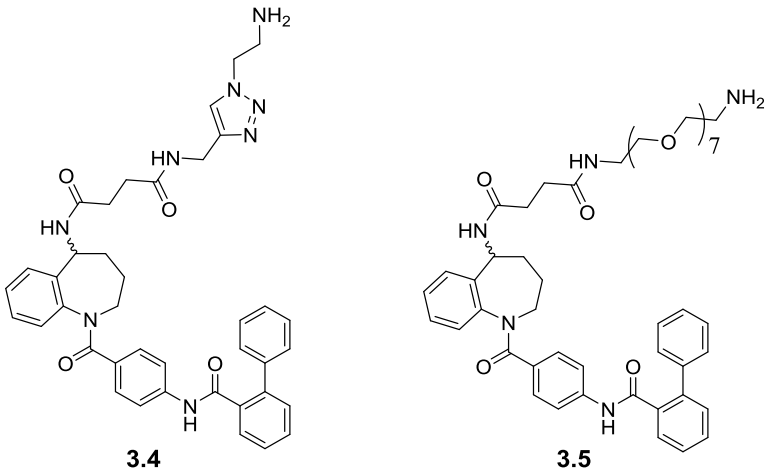

Figure 53. Benzazepine derivatives **3.4** and **3.5**.

The choice of the suitable "orange" fluorophore for the labelling of the V_2R ligands depended on three criteria:

1) The fluorophore should be an acceptor of the Lumi-4-Tb emission.
2) Its fluorescence should be detectable using the commercial "orange" filter (605/15).
3) The residual fluorescence of the "orange" ligand in the "green" and the "red" filters should be minimal.

It was decided to test fluorophores DY-590® (the derivative of sulforhodamine 101 with an emission maximum near 600 nm and a QY of 60% in water), *p*-Lissamine® rhodamine B (emission maximum at 590 nm and a QY of 33% in water) and QDot® 605 (which possess a narrow emission spectra with a maximum at 605 nm).

The introduction of DY-590® was performed by treatment of **3.4** or **3.5** with DY-590®-NHS-ester in the presence of DIEA in DMSO overnight (Scheme 24). The obtained fluorescent benzazepine derivatives **3.6** and **3.7** were purified by semi-preparative HPLC and characterized by LC-HRMS.

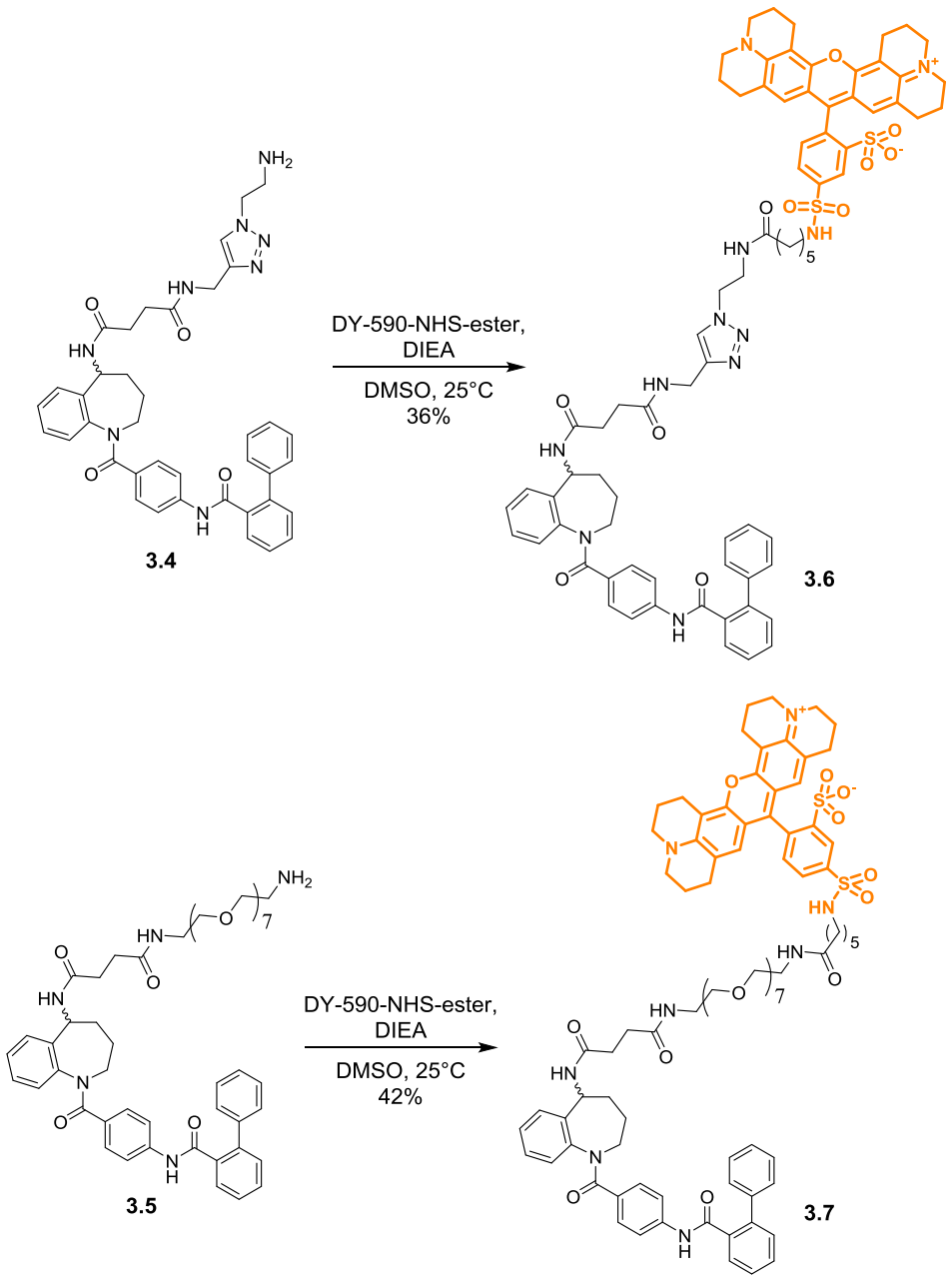

Scheme 24. Synthesis of DY-590®-labeled V_2R ligands **3.6** and **3.7**.

The *p*-Lissamine® rhodamine B (LRh) derivative of the benzazepine **3.3** with triazole moiety and a PEG4 spacer (Figure 54, compound **3.8**) was previously synthesized in the laboratory (Loison et al., 2012), so we decided to use this ligand for the evaluation of the LRh fluorophore. This ligand possesses high affinity for the V_2 receptor (4 nM) and an excellent selectivity versus other vasopressin receptors subtypes and the oxytocin receptor.

Finally, the biotin-labelled benzazepine derivatives **3.9** and **3.10** (Figure 54) were synthesized by Dr. Corinne Baehr as precursors for the labelling with QDots® 605, modified at the surface with streptavidin.

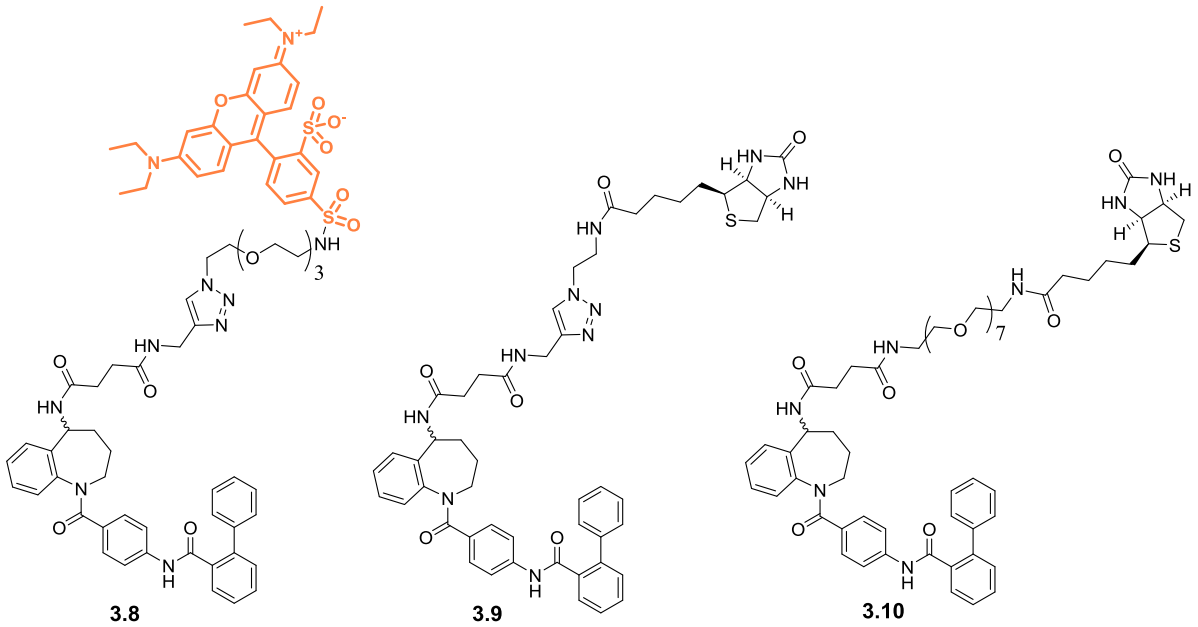

Figure 54. Structures of LRh-labeled benzazepine **3.8** and biotin-labeled benzazepines **3.9** and **3.10**.

The affinities of synthesized benzazepines (K_i) were evaluated by TR-FRET competition assay using fluorescein-labeled SNAP-V_2 receptors as acceptors of FRET and Lumi-4-Tb labeled compound **47** from Loison et al., 2012 (K_d = 6 nM) as competitor and luminescence donor (Table 17).

Table 17. Inhibition constants of **3.6**, **3.7**, **3.9** and **3.10** on V_2R when using **47** (Loison et al., 2012) as tracer and the representative curves for the competition.

Compound			Competition, TR-FRET (K_i, nM)
	Spacer	Label	V_2R
3.6	triazole	DY-590®	18.2
3.7	PEG	DY-590®	44.4
3.9	triazole	biotin	4.43
3.10	PEG	biotin	22.0

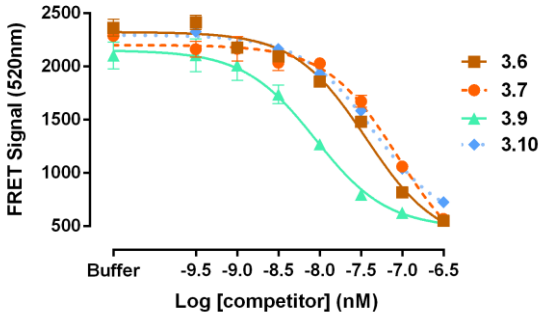

As it can be seen from Table 17, both DY-590® and biotin derivatives of benzazepine **3.4** with triazole-containing spacer (compounds **3.6** and **3.9**) possessed higher affinity for the V_2 receptor that the corresponding pegylated derivatives. This could be probably explained by the formation of hydrogen bonds with triazole, which stabilize the ligand-receptor complex and are apparently not possible with the PEG chain.

Thus, three V_2R ligands labeled with DY-590® (**3.6**), biotin (**3.9**), and LRh (**3.8**) were chosen for the preliminary tests which should reveal the most potent fluorophore for the multicolor binding assay.

The test was designed as following (Figure 55):

1) HEK 293 cells were seeded in 96-well plate and transfected either with the plasmid coding for the V_2 receptor (V_2R cells) or the pRK5 plasmid, which does not code for GPCRs (Mock cells).
2) The transfection medium was removed and all the plate was subjected to the labelling with Lumi-4-Tb-BG, except the columns "A" where the cells remained without FRET donor (only the buffer solution was added).
3) The solutions of **3.6**, **3.8**, **3.9** in TagLite buffer were prepared (at concentration 3 times higher than their K_i). We also used the classical "red" ligand for V_2R – compound **44** from Loison et al., 2012 in order to have a standard for the fluorescence signal in the "red" channel.
4) The plate was washed with TagLite buffer and the ligands **3.6**, **3.8**, **3.9** and **44** were added as shown in Figure 55: wells "D" = "donor" – without fluorescent ligands; wells "A" = "acceptor" – fluorescent ligands on unlabeled cells; wells "D+A" = "donor + acceptor" – fluorescent ligands on Lumi-4-Tb-labeled cells; wells "D+A+C" = "donor + acceptor + cold" – fluorescent ligands on Lumi-4-Tb-labeled cells in the presence of the "cold" competitor AVP. The plate with ligands was incubated for 1 hour at r.t.
5) After reading of the plate, QDots® 605 modified with streptavidin were added to the rows containing **3.9** and the plate was incubated at r.t. for another 5 min.

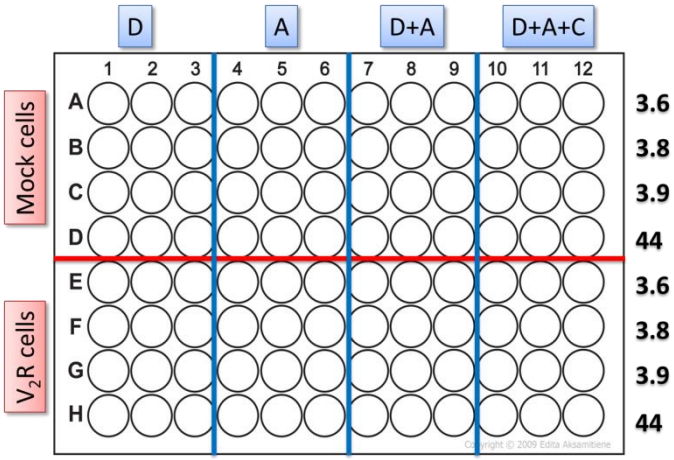

Figure 55. The scheme of the 96-well plate for the test for the choice of the "orange" fluorophore.

The following results were obtained for the DY-590® and LRh-labeled ligands (**3.6** and **3.8**, respectively):

- A strong specific signal was observed in the “orange” channel for **3.6** (Figure 56A) and a rather less intensive specific signal for **3.8**. (which was expected because of the lower quantum yield of the Lissamine® comparing to DY-590®)
- No residual fluorescence was observed in the “green” channel for both dyes (Figure 56C) and in the “red” channel for the Lissamine® derivative **3.8** (Figure 56B).
- A “contamination” of the “red” channel by the fluorescence of **3.6** was observed (Figure 56B), however the intensity was not important in comparison with the signal of the “red” dye **44** in this channel.

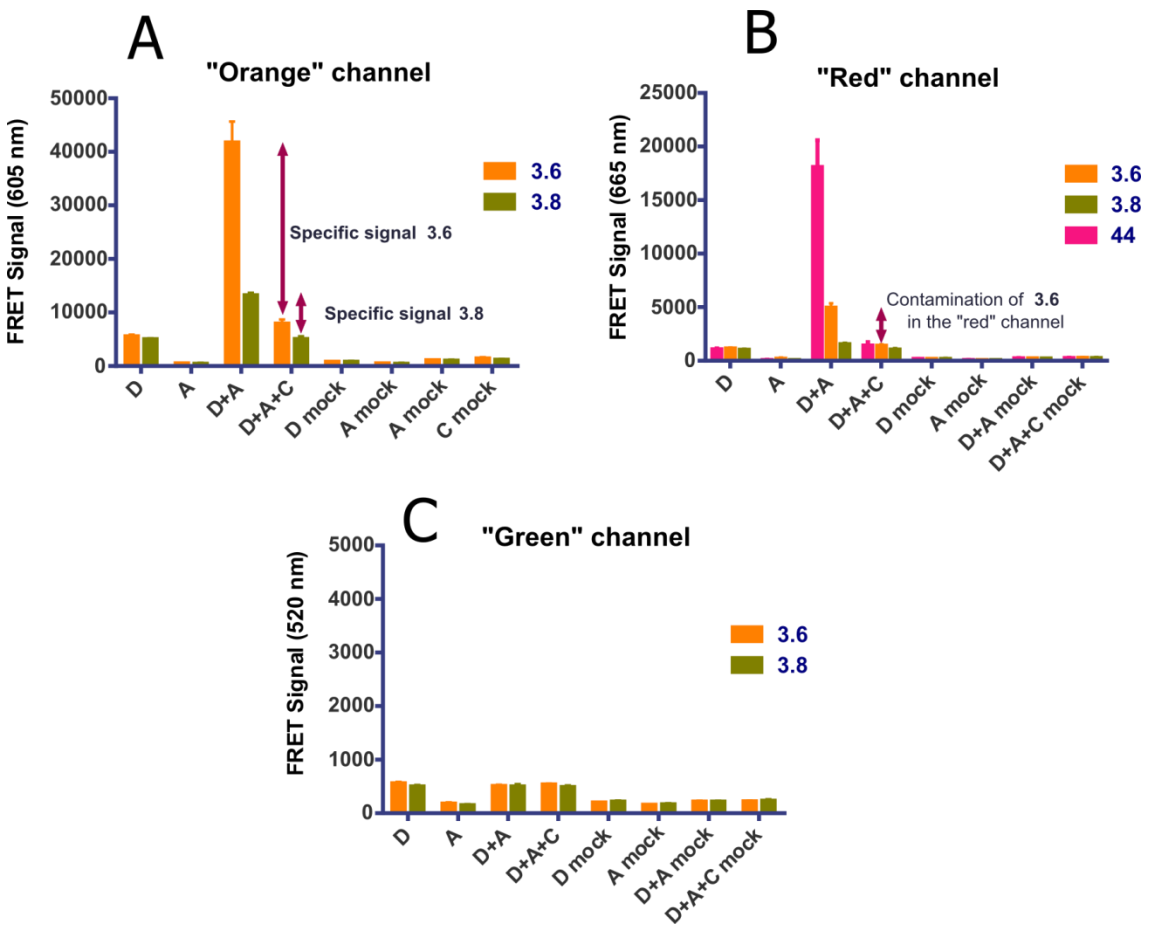

Figure 56. Results of the test for the choice of the "orange" ligand for **3.6** and **3.8**.

The rows containing the QDots®-modified ligand **3.9** were read on the plate reader in homogenous conditions and after each of 4 consecutive washing with TagLite buffer. The following results were obtained:

- ❖ No residual fluorescence from QDots® 605 was detected in both “green” and “red” channels (Figure 57B and C).
- ❖ Without washing, a strong non-specific signal was observed (Figure 57A), which could be also detected with a 150 µs delay (QDots® are characterized by long emissive lifetimes).
- ❖ However no competitive signal was detected (difference between D+A+C and D+A) which could be explained by the extremely large size of QDots® and by the non-stoichiometric binding ligand-QDots® (approximately 5 to 10 streptavidins per Qdot®).

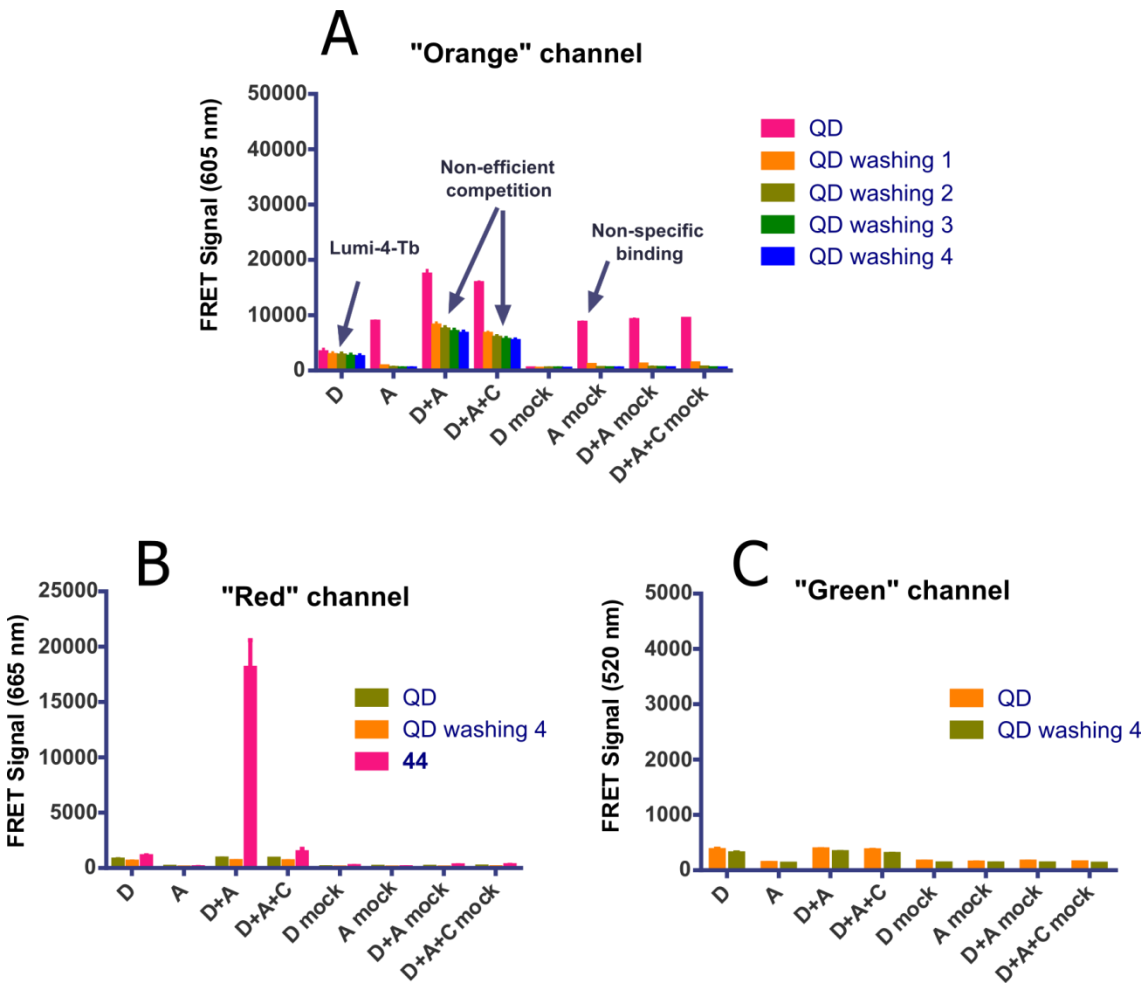

Figure 57. Results of the test for the choice of the "orange" ligand for **3.9** labeled with QDots® 605.

As a conclusion, in contrast to the Lissamine®-labeled ligand **3.8** which possessed a rather low specific fluorescence and to QDot® 605-labeled ligand **3.9**, presenting a weak fluorescence signal and a non-competitive binding to V_2R, benzazepine **3.6**, modified with DY-590® resulted in a strong specific fluorescence signal with almost negligible contamination in the "red" channel. Benzazepine **3.6** was chosen for the development of the multicolor binding test.

The nest step of our study was to test the possibility of detection of three specific binding events with a mixture of fluorescent ligands ("green" for D_3R, "orange" for V_2R and "red" for ApelinR) on a mixture of three cell lines expressing different receptors. The established protocol was the following:

1) HEK 293 cells were seeded in a 6-well plate and transfected separately with the plasmids coding for D_3R, V_2R or ApelinR (2 wells for each plasmid).

2) After 6 hours cells were detached, mixed in different proportions (maintaining the concentration of each cell line in final mixtures at 30 000 cells/well) and seeded in a 96-well plate according to scheme presented in Figure 58.
3) After 24 hours the medium was removed and the plate was subjected to the labelling with Lumi-4-Tb-BG.
4) The mixture of **3.1** ("red" ligand), **3.2** ("green" ligand), and **3.6** ("orange" ligand) at concentrations 3 times higher than their affinities was prepared.
5) The mixture of three "cold" competitors at concentrations 500 times higher than their affinities was prepared. We used AVP for V_2R, apelin-13 for ApelinR and BP 897 (Pilla et al., 1999) for D_3R.
6) The plate was washed with TagLite buffer and incubated with the mixtures of ligands for 1 hour at r.t. before reading.

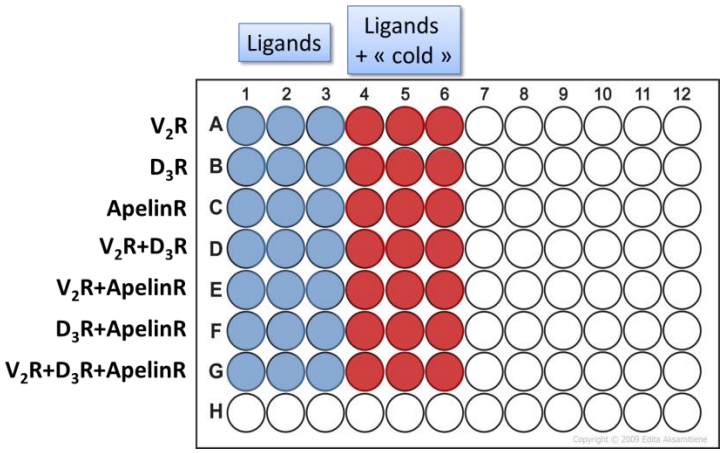

Figure 58. The scheme of the 96-well plate for the test on the cell mixture.

In this preliminary tests on the cell mixture the following results were obtained:

- The "green" D_3R ligand was easily detected in the mixture of fluorescent ligands on all the prepared cell mixtures (Figure 59A).
- The "red" ApelinR ligand also resulted in high specific signal in the mixtures of ApelinR-transfected cells (Figure 59C). Interestingly, due to the high brightness of the "red" ligand the residual fluorescence of the "orange" ligand in the "red" filter was negligible (compare histogram bars "V_2R" and "ApelinR" in Figure 59C).
- The "orange" V_2R ligand was also detected in the mixture, however the "orange" channel was unexpectedly contaminated by the residual fluorescence from the "green" D_3R ligand.

As a conclusion, the “red” and the “green” ligands can be easily detected in the mixtures of cells expressing three different receptor types. To extract the “pure” FRET values for the “orange” ligand, the percentage of the residual fluorescein fluorescence in the “orange” channel should be calculated for the optimized concentration of the three fluorescent competitors.

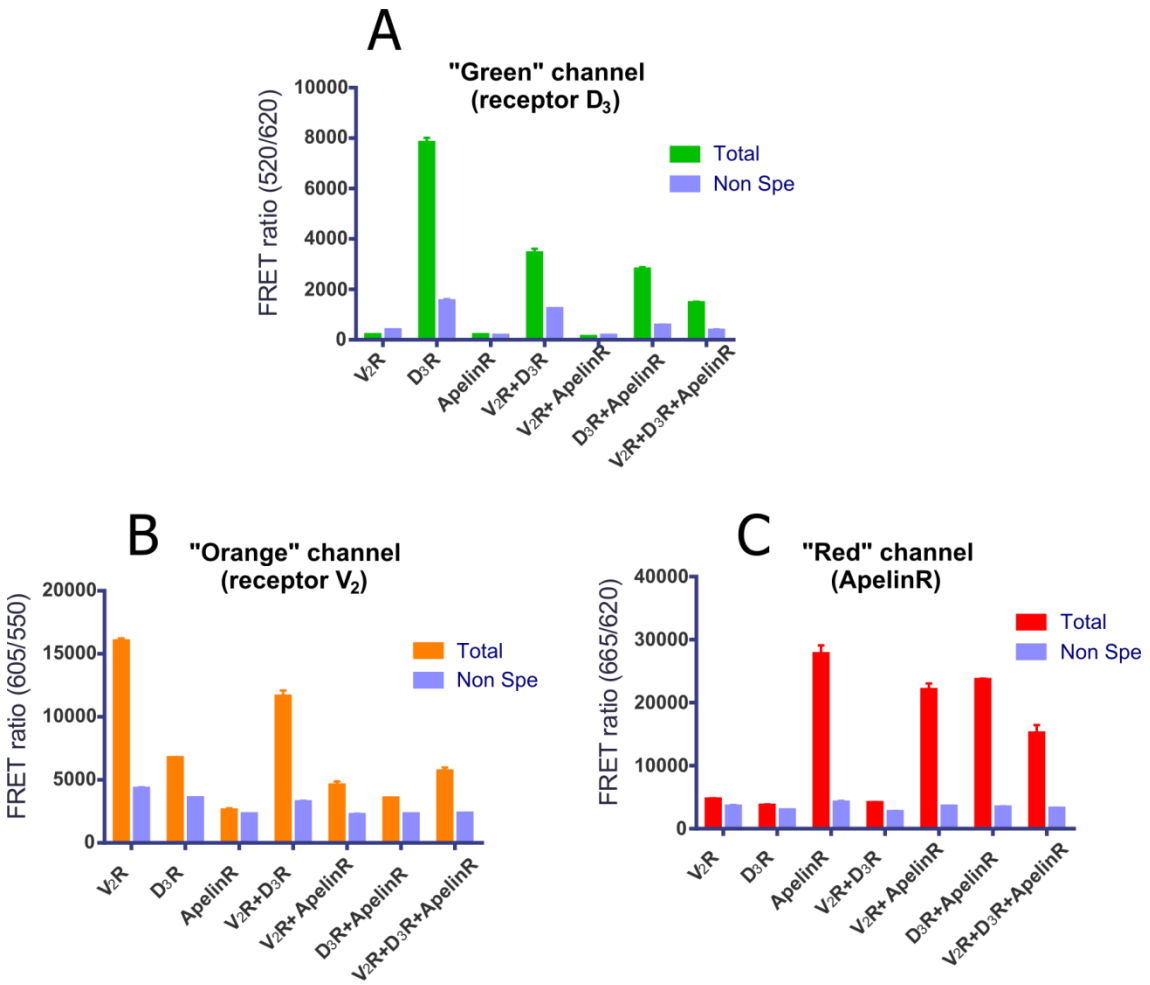

Figure 59. Detection of specific bindings in the mixture of fluorescent ligands on the mixture of cells expressing different receptors.

Conclusion and perspectives

The objective of the research project presented above, which was mainly conducted in the Institut de Génomique Fonctionnelle of Montpellier in collaboration with the group of Dr. Thierry Durroux, was to develop the first multicolor binding TR-FRET assay. Such a test will allow the simultaneous determination of the affinity of a GPCR ligand and of its selectivity versus receptors with high similarity. It is particularly important in the case of the oxytocin/vasopressin receptors which have high level of homology and many common non-specific ligands among both peptides or small organic molecules.

Having in hands previously synthesized effective "green" and "red" ligands, we performed preliminary tests which helped us to choose the most appropriate "orange" ligand between DY-590®, *p*-Lissamine® Rhodamine B and Qdots® 605.

The first assays on mixture of cells expressing three different GPCRs (D_3R, V_2R and ApelinR) ensured us that the three fluorescent tracers could be detected separately by using commercial emission filters. Further validation of the multicolor TR-FRET binding assay is currently ongoing in the IGF in Montpellier.

We envisage using the established TR-FRET multicolor binding assay for the HTS discovery of new selective and centrally active small organic ligands of the oxytocin receptor.

General conclusion and perspectives

The main objective of my research was to develop imaging and detections tools to study the oxytocin and the vasopressin receptors both *in vitro* and *in vivo* which will allow to deeply understand their role in autism spectrum disorders and, on the other hand, to accelerate the development of selective centrally active agonists for OTR as potential treatment of ASD.

During my thesis I contributed to the development of four precursors for the radiolabelling with ^{11}C and ^{18}F, two of which were successfully labelled and preliminary evaluated on the rat brain slices. We believe that these radioligands will allow performing the translational PET imaging from small animal (rat or mouse) to human and discovering new features of the OTR distribution and implication in the development of ASD.

Our fruitful collaborative work on the fluorescent ligands for OTR resulted in the development of first selective fluorescent OTR ligands for the TR-FRET binding assay, as well as red and far-red turn-on fluorescent ligands for the native oxytocin receptor. The formers have already enabled the establishment of the TR-FRET binding assay on the SNAP-fused OTR, which will evidently contribute to the discovery of new OTR ligands. On the other hand, our future objective is to develop an alternative binding assay on the native oxytocin receptor, using the extremely bright far-red turn-on squaraine-dimer.

Finally, I was glad to participate in the first steps of the development of the parallel affinity/selectivity multicolor binding assay, which, I am sure, will accelerate the evaluation of GPCR ligands, especially of the OT/AVP receptor's family.

Experimental part

Part I: PET radiotracers for the oxytocin and the vasopressin V_{1a} receptors

1. Chemical synthesis

1.1. General

Reagents were obtained from commercial sources and used without any further purification. Thin layer chromatography was performed on silica gel $60F_{254}$ plates. Flash chromatography was performed on silica gel (40 µm, Grace) or RP18 (25−40 µm, Merck) prepacked columns on a SPOT II ultima from Armen. Semi-preparative HPLC chromatography was performed on SunFire C18 column (5 µm, 19 × 150 mm) or SymmetryShield C18 column (7 µm, 19 × 300 mm) on Gilson PLC2020 with absorption detection. Analytical RP-HPLC separations were performed on Ascentis Express C18 column (2.7 µm, 4.6 mm × 75 mm) using a linear gradient (5% to 100% in 7.4 min, flow rate of 1.6 $mL \cdot min^{-1}$) of solvent B (0.1% TFA in CH_3CN, v/v) in solvent A (0.1% TFA in H_2O, v/v). Detection was set at 220 and 254 nm. ^1H NMR spectra were recorded at 400 and 500 MHz on a Bruker Advance spectrometer. Chemical shifts are reported in parts per million (ppm), coupling constants (J) are reported in hertz (Hz). Signals are described as s (singlet), d (doublet), t (triplet), m (multiplet), and brs (broad singlet). LC-MS spectra were obtained on a ZQ (Z quadripole) Waters/Micromass spectrometer equipped with an X-Terra C18 column (3.5 µm, 4.6 × 50 mm) using electrospray ionization mode (ESI). High resolution mass spectra (HRMS) were acquired on a Bruker MicroTof mass spectrometer, using electrospray ionization (ESI) and a time-of-flight analyzer (TOF).

1.2. [^{11}C]Carbetocin (CBT)

*Desmethyl carbetocin **1.9***

Solid-phase reactions were performed in polypropylene tubes equipped with polyethylene frits and polypropylene caps using an orbital agitator shaking device. Fmoc-protected Rink Amide NovaGel® resin was purchased from Novabiochem® and the overall yields for the solid-phase syntheses were calculated based on the initial loadings provided by the supplier (0.7 mmol/g).

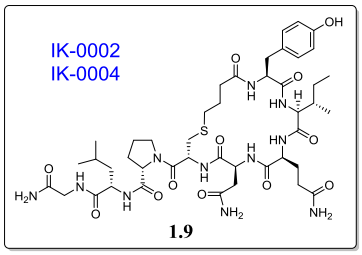

1.9

All Fmoc-protected amino acids (4 eq.) were coupled in *N*,*N*-dimethylformamide (DMF) for 45 min using HBTU (3.8 eq.) and HOBt (4 eq.) with *N*,*N*-diisopropylethylamine (DIEA) (12 eq.) as activating agents (Scheme 1). Fmoc-Cys(PG)-OH (5 eq.) was coupled in DMF for 45 min using HATU (4.9 eq.) with tetramethylpiperidine (10 eq.). 4-Bromobutyric acid (5 eq.) was coupled in DMF for 24 hours using DIC (5 eq.) and HOBt (5 eq.) as activating agents. The cleavages of Fmoc protecting groups were performed in 20% piperidine/DMF (2 times for 15 min).

The completion of couplings and Fmoc cleavages was monitored with the ninhydrin test (Kaiser et al., 1970), the TNBS test (Hancock and Battersby, 1976) or the chloranil test (Mařík et al., 2003) as well as by analytical HPLC (minicleavages of the resin with TFA/H_2O 95/5).

To remove the *S*-*tert*-butylsulfanyl protecting group the peptide was treated with tributylphosphine in DCM/DMF (1/1) with 5% H_2O under argon. The 4-methoxyltrityl (Mmt) protecting group was cleaved with 2% of trifluoroacetic acid in DCM with 5% TIS (6 times for 2 min).

The intermolecular cyclisation was performed with 2M NH_3 in a mixture of MeOH/THF (1/3) for 4 hours. The conjugate was cleaved from the resin by TFA/TIS/H_2O (95/2.5/2.5) treatment for 4 hours.

The crude **1.9** was purified by semi-preparative HPLC (Symmetry Shield column) eluted with solvent B in solvent A: 5% for 3 min, 5-25% in 15 min then 25-35% in 30 min. Yield 22%. HRMS (ESI): calc. for $C_{44}H_{68}N_{11}O_{12}S$ (M+H)+ = 974.47697; found (M+H)+ = 974.47679.

Optimization of the protocol for the desmethyl CBT alkylation

To a solution of **1.9** (1 mg, 1 eq.) in dry DMF (200 µL) dry K_2CO_3 (0.7 mg, 5 eq.) or dry NaOMe (1 mg, 18 eq.) was added. To the obtained suspension MeI (5 µL, around 80 eq.) was added. The reaction mixture was stirred either at r.t. or in the water bath heated to 50°C. The progress of the reaction was monitored by analytical HPLC (detection at 220 nm) using a linear gradient (5% to 100% in 20 min, flow rate of 1.6 mL·min^{-1}) of solvent B in solvent A. T_r (**1.9**) = 5.26–5.72 min, T_r (CBT) = 6.60–6.84 min.

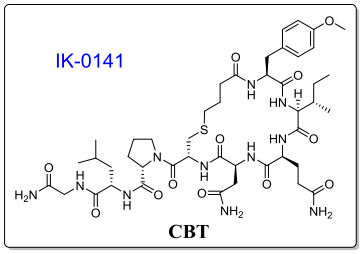

1.3. [^{11}C]Relcovaptan (SR49059)

*4-((tert-Butyldimethylsilyl)oxy)-3-methoxybenzene-1-sulfonyl chloride **1.20**.*

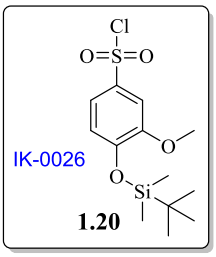

To a solution of **1.19** (1 mmol, 223 mg) in dry ACN (7 mL) under argon TBDMS-Cl (0.05 mmol, 7.5 mg) and MTBSTFA (5 mmol, 1.17 mL) were added. The reaction mixture was stirred at r.t. for 15 min. The volatiles were removed under vacuum and the residue was purified by flash chromatography eluted with heptane/EA (100:0 → 90:10, v/v) to provide **1.20** as a colorless liquid (335 mg, quant.). ^{1}H NMR (400 MHz, $CDCl_3$) δ 7.57 (dd, *J* = 8.5, 2.4 Hz, 1H), 7.44 (d, *J* = 2.3 Hz, 1H), 6.97 (d, *J* = 8.5 Hz, 1H), 3.90 (s, 3H), 1.00 (s, 9H), 0.21 (s, 6H). ^{13}C NMR (101 MHz, $CDCl_3$) δ 151.94, 151.45, 136.82, 121.54, 120.89, 110.29, 56.01, 25.66, 18.63, -4.35. BRMS (ESI): $(M+H)^+$ calcd: 337.07, found: 337.07.

*4-(Chlorosulfonyl)-2-methoxyphenyl acetate **2.21***

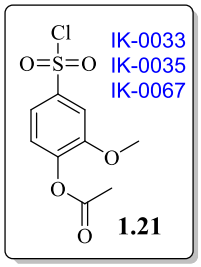

A solution of **1.19** (0.1 mmol, 22 mg) in a mixture of Ac_2O (1 mL) and AcOH (0.5 mL) was stirred at 110°C for 1hour. To the resulting mixture DCM (20 mL) and water (20 mL) were added and the organic layer was separated, washed twice with 1N solution of $NaHCO_3$ (20 mL), twice with water (20 mL), dried over Na_2SO_4. The volatiles were removed under high vacuum to give **2.21** as a yellow oil which crystallized rapidly (21 mg, 77%). ^{1}H NMR (400 MHz, $CDCl_3$) δ 7.67 (dd, *J* = 8.4, 2.2 Hz, 1H), 7.56 (d, *J* = 2.2 Hz, 1H), 7.27 (d, *J* = 8.4 Hz, 1H), 3.94 (s, 3H), 2.36 (s, 3H). ^{13}C NMR (101 MHz, $CDCl_3$) δ 168.02, 152.12, 145.48, 142.34, 124.08, 120.38, 110.81, 56.69, 20.70. mp = 83–84°C. BRMS (ESI): $(M+H)^+$ calcd: 264.99, found: 264.99.

*4-(N-(4-Chloro-2-(2-chlorobenzoyl)phenyl)sulfamoyl)-2-methoxyphenyl acetate **2.22***

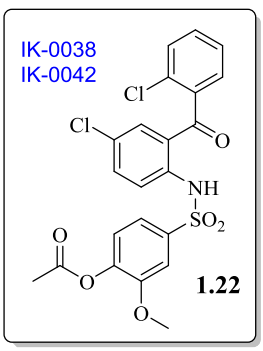

To a solution of **1.21** (0.21 mmol, 55 mg) and **1.18** (0.19 mmol, 51 mg) in dry DCM (4 mL) pyridine (400 µL) was added. The mixture was stirred at r.t. for 14 hours. The solvents were removed under vacuum and the residue was purified by flash chromatography eluted with heptane/EA (95:5 → 0:100, v/v) to produce **2.22** as yellow crystals (12 mg, 13%). ^{1}H NMR (400 MHz, $CDCl_3$) δ 10.89 (s, 1H), 7.84 (d, *J* = 8.9 Hz, 1H), 7.53 – 7.34 (m, 6H), 7.19 (d, *J* = 2.5 Hz, 1H), 7.16 – 7.10 (m,

1H), 7.08 (d, *J* = 8.3 Hz, 1H), 3.78 (s, 3H), 2.31 (s, 3H). ^{13}C NMR (101 MHz, $CDCl_3$) δ 198.07, 168.17, 151.88, 143.92, 138.88, 137.51, 137.44, 135.44, 133.81, 132.01, 131.09, 130.43, 129.09, 128.91, 127.24, 124.59, 123.57, 122.37, 120.37, 111.08, 56.44, 20.70. mp = 133–136°C. BRMS (ESI): $(M+H)^+$ calcd: 494.02, found: 494.02.

Potassium 4-(benzyloxy)-3-methoxybenzenesulfonate ***1.24***

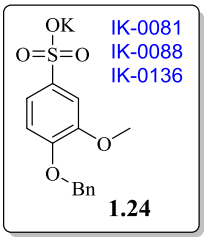

A solution of 25% KOH in water (4 mL H_2O, 1009 mg KOH) was added to a solution of **1.23** (3 mmol, 754 mg), 18-crown-6 (0.3 mmol, 79 mg) and BnBr (9 mmol, 1076 µL) in a mixture of DCM (8 mL) and H_2O (4 mL). The reaction mixture was stirred at r.t. over a week-end. A yellow precipitate was formed. The resulting mixture was acidified with 1N HCl then water (50 mL) and DCM (20 mL) were added to solubilize the precipitate. The solvents were removed under vacuum and the obtained mixture (should be heated well to solubilize) was purified by reverse phase flash chromatography eluted with H_2O/ACN (10:0 → 7:3 v/v) to give **1.24** as a white solid (372 mg, 37%). ^{1}H NMR (400 MHz, D_2O) δ 7.58 – 7.30 (m, 7H), 7.14 (d, *J* = 8.4 Hz, 1H), 5.25 (s, 2H), 3.90 (s, 3H). ^{13}C NMR (101 MHz, D_2O) δ 149.44, 148.55, 136.09, 135.58, 128.83, 128.51, 128.01, 118.99, 113.48, 109.30, 70.85, 55.96. mp = 302–303°C. BRMS (ESI): $(M-K)^-$ calcd: 293.0, found: 293.0.

4-(Benzyloxy)-N-(4-chloro-2-(2-chlorobenzoyl)phenyl)-3-methoxybenzenesulfonamide ***1.25***

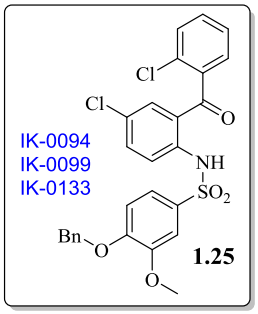

To a solution of **1.24** (0.27 mmol, 90 mg) in dry DMF (5 mL) $SOCl_2$ (0.81 mmol, 59 µL) was added. The reaction mixture was stirred at r.t. for 30 min, then DMF was removed under vacuum, the residual $SOCl_2$ was co-evaporated three times with toluene (was heated to solubilize completely) then dried under high vacuum overnight to get sulfochloride of **1.24**.

To a suspension of NaH (0.41 mmol, 16 mg of 60%, washed twice with toluene) in dry DMF (1 mL) at ice-water temperature under argon a solution of **1.18** (0.27 mmol, 72 mg) in dry DMF (2 mL) was added. The resulting mixture was stirred at ice-water temperature for 15 min then a solution of the sulfochloride (0.27 mmol, 85 mg) in a mixture of dry DMF (4 mL) and dry toluene (1 mL) was added dropwise. The reaction mixture was stirred at ice-water temperature for 2 hours then at r.t. for 2 hours monitored by HPLC. Water (50 mL) was added and the mixture was extracted twice with DCM (25 mL).

The combined organic fractions were washed twice with water (50 mL), then the solvent was removed under vacuum and the residue was purified by reverse phase flash chromatography eluted with ACN/H_2O (30:70 → 100:0 v/v in 30 min) to give **1.25** as a pale yellow solid (62 mg, 42%). ^{1}H NMR (400 MHz, $CDCl_3$) δ 10.81 (s, 1H), 7.80 (d, *J* = 8.9 Hz, 1H), 7.51 – 7.27 (m, 11H), 7.21 – 7.11 (m, 2H), 6.85 (d, *J* = 8.9 Hz, 1H), 5.15 (s, 2H), 3.83 (s, 3H). ^{13}C NMR (101 MHz, $CDCl_3$) δ 197.83, 152.43, 149.90, 139.24, 137.53, 135.96, 135.32, 133.61, 132.03, 131.13, 130.45, 128.91, 128.89, 128.58, 128.44, 127.38, 127.14, 124.33, 122.14, 121.40, 112.66, 110.06, 71.15, 56.41. mp = 65–68°C. BRMS (ESI): $(M-H)^-$ calcd: 540.0, found: 540.0.

(S)-1-(2-(4-(Benzyloxy)-N-(4-chloro-2-(2-chlorobenzoyl)phenyl)-3-methoxyphenylsulfon-amido)acetyl)pyrrolidine-2-carboxamide ***1.26***

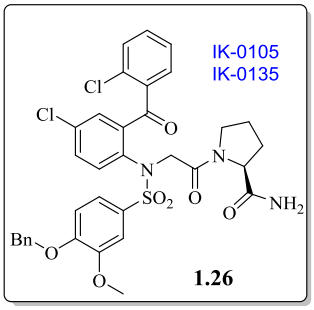

To a solution of **1.25** (0.11 mmol, 61 mg) in dry DMF (2 mL) K_2CO_3 (0.22 mmol, 31 mg) was added. The resulting mixture was stirred for 5 min then a solution of **1.16** (0.45 mmol, 120 mg; synthesized according to Villhauer et al., 2002) in dry DMF (3 mL) was added. The reaction mixture was stirred at r.t. overnight. Water (20 mL) was added and the mixture was extracted twice with DCM (20 mL). The organic layer was washed three times with water (20 mL) then with brine (20 mL), dried over Na_2SO_4. The volatiles were removed under vacuum to give **1.26** as a pale yellow solid (77 mg, quant.). ^{1}H NMR (500 MHz, DMSO-d_6, 100°C) δ 7.67 – 7.51 (m, 4H), 7.51 – 7.42 (m, 4H), 7.43 – 7.37 (m, 3H), 7.37 – 7.31 (m, 1H), 7.27 – 7.15 (m, 1H), 7.15 – 7.04 (m, 2H), 7.01 – 6.51 (m, 2H), 5.15 (s, 2H), 4.52 – 4.00 (m, 3H), 3.82 – 3.70 (m, 3H), 3.59 – 3.27 (m, 2H), 2.08 – 1.65 (m, 4H). ^{13}C NMR (126 MHz, DMSO-d_6, 100°C) δ 191.50, 172.60, 165.69, 151.47, 148.55, 140.04, 136.45, 136.06, 134.38, 134.00, 132.86, 132.25, 131.57, 131.09, 130.93, 130.22, 129.95, 129.71, 127.87, 127.41, 127.17, 126.53, 121.40, 112.54, 111.86, 70.10, 59.54, 55.70, 53.11, 45.69, 28.39, 23.78. mp = 81–84°C. BRMS (ESI): $(M+Na)^+$ calcd: 718.1, found: 718.0.

(S)-1-(2-(N-(4-Chloro-2-(2-chlorobenzoyl)phenyl)-4-hydroxy-3-methoxyphenylsulfonamido)acetyl)pyrrolidine-2-carboxamide ***1.14***

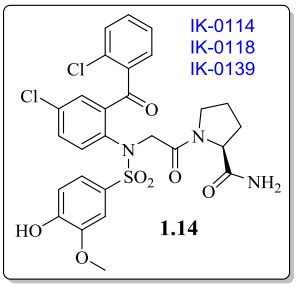

A solution of **1.26** (0.13 mmol, 92 mg) in EtOAc (5 mL) in a 25 mL flask with a magnetic stirrer was degased 3 times by water-jet pump. To the solution Pd/C (0.04 mmol, 42 mg) was added, the resulting mixture was degased 3 more times. The flask was filled with H_2 (atmospheric pressure) and the reaction mixture was stirred overnight. The resulting solution was degased three times then filtered over a Celite pad washed with EtOAc. The volatiles were removed under vacuum and the residue was purified by reverse phase flash chromatography eluted with ACN/H_2O (30:70 → 100:0 v/v in 30 min) to give **1.14** as a pale yellow solid (50 mg, 62%). ^{1}H NMR (400 MHz, $CDCl_3$) δ 7.70 (d, *J* = 8.6 Hz, 1H), 7.51 – 7.42 (m, 3H), 7.39 (dd, *J* = 8.6, 2.5 Hz, 1H), 7.35 – 7.27 (m, 3H), 7.23 – 7.15 (m, 2H), 6.90 – 6.68 (m, 2H), 5.47 (s, 1H), 4.82 – 4.31 (m, 3H), 3.83 (s, 3H), 3.78 – 3.60 (m, 1H), 3.53 – 3.40 (m, 1H), 2.40 – 2.25 (m, 1H), 2.12 – 1.87 (m, 3H). ^{13}C NMR (101 MHz, $CDCl_3$) δ 193.06, 173.61, 168.58, 150.12, 146.41, 140.83, 136.86, 136.70, 135.40, 134.88, 132.85, 132.73, 132.58, 132.31, 131.12, 130.84, 130.28, 126.83, 123.26, 113.98, 110.85, 60.35, 56.44, 55.13, 47.16, 27.97, 25.10. mp = 142–145 °C. BRMS (ESI): $(M-H)^-$ calcd: 604.1, found: 604.0.

(S)-1-((2R,3S)-5-Chloro-3-(2-chlorophenyl)-3-hydroxy-1-((4-hydroxy-3-methoxyphenyl)sulfonyl)indoline-2-carbonyl)pyrrolidine-2-carboxamide ***1.13***

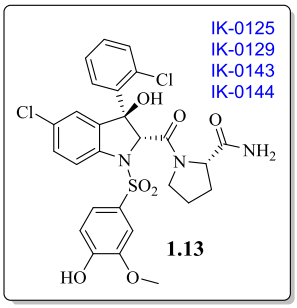

To a solution of **1.14** (0.079 mmol, 48 mg) in MeOH (5 mL) DBU (0.39 mmol, 59 µL) was added. The reaction mixture was stirred at r.t. for 2 days monitored by HPLC. The resulting stereoisomers were separated by three consecutives semi-preparative HPLC eluted with solvent B in solvent A:

A) 3 min at 20%, 3–6 min from 20 to 30%, 6–30 min from 30 to 45%, 30–33 min from 45 to 100%.

B) 3 min at 20%, 3–6 min from 20 to 30%, 6–30 min from 30 to 50%, 30–33 min from 50 to 100%.

C) 3 min at 20%, 3–6 min from 20 to 35%, 6–24 min from 35 to 46%, 24–27 min from 46 to 100%.

The fractions containing the desired compound (T_r = 4.29 min on the analytical HPLC with the 7.4 min linear gradient from 5% to 100% of solvent B in solvent A) were collected to give

after lyophilization **1.13** as a white powder (6.7 mg, 14%). ^{1}H NMR (500 MHz, DMSO-d_6) δ 9.82 (brs, 1H), 7.56 – 7.50 (m, 3H), 7.38 – 7.21 (m, 5H), 7.01 (s, 1H), 6.95 (d, J = 8.4 Hz, 1H), 6.74 – 6.20 (m, 3H), 5.34 (s, 1H), 3.94 – 3.84 (m, 1H), 3.80 (s, 3H), 3.75 – 3.66 (m, 1H), 3.53 (dd, J = 8.4, 3.0 Hz, 1H), 1.94 – 1.77 (m, 2H), 1.77 – 1.67 (m, 1H), 1.62 – 1.49 (m, 1H). ^{13}C NMR (126 MHz, DMSO-d_6) δ 172.13, 164.85, 151.63, 147.43, 140.79, 135.81, 135.53, 132.43, 130.61, 129.20, 128.62, 127.44, 126.32, 125.38, 124.61, 121.61, 115.04, 114.13, 111.70, 82.54, 74.39, 59.46, 55.80, 46.05, 27.88, 23.21. mp = 155–158 °C. HRMS (ESI): calc. for $C_{27}H_{24}Cl_2N_3O_7S$ $(M\text{-}H)^-$ = 604.07120; found $(M\text{-}H)^-$ = 604.07087.

*Alkylation of **1.13***

To a stirred solution of **1.13** (1 eq., 1 mg) in dry DMSO (200 µL) K_2CO_3 (22 eq., 5 mg) was added, followed by MeI (around 50 eq., 5 µL). The reaction mixture was stirred at 70°C (in a water bath) for 5 min. The progress of the reaction was monitored by analytical HPLC (detection at 220 nm) using a linear gradient of solvent B in solvent A (5% to 100% in 7.4 min, flow rate of 1.6 mL·min^{-1}). T_r (**1.13**) = 4.29 min, T_r (SR49059) = 4.63 min.

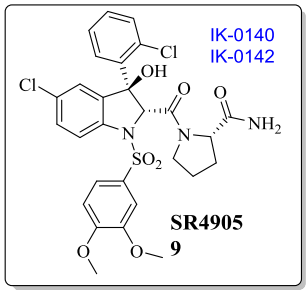

1.4. [^{11}C]PF-3274167

Methyl 2-(benzyloxy)acetate ***1.30***

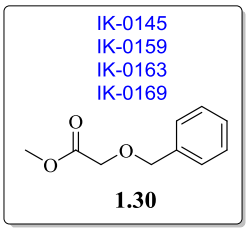

To a solution of methyl glycolate (5 mmol, 396 µL) in dry THF (25 mL) under argon at ice-water temperature NaH (5.25 mmol, 60% dispersion in oil, 210 mg) was added. The resulting mixture was stirred at ice-water temperature for 30 min, then NBu_4I (0.5 mmol, 185 mg) was added followed by BnBr (5 mmol, 610 µL). The reaction mixture was stirred at r.t. overnight then at 60°C overnight. Water (100 mL) was added and the mixture was extracted twice with DCM (50 mL). The combined organic fractions were washed twice with water (100 mL), then brine (100 mL). The volatiles were removed under vacuum and the residue was purified by reverse phase flash chromatography eluted with ACN/H_2O (from 20% to 100% in 30 min) to give **1.30** as a yellow oil (369 mg, 41%). ^{1}H NMR (400 MHz, $CDCl_3$) δ 7.41 – 7.27 (m, 5H), 4.64 (s, 2H), 4.11 (s, 2H), 3.77 (s, 3H). ^{13}C NMR (101 MHz, $CDCl_3$) δ 170.92, 137.19, 128.66, 128.22, 128.20, 73.53, 67.27, 51.99.

2-(Benzyloxy)acetohydrazide ***1.31***

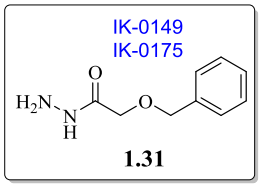

To a solution of **1.30** (2.5 mmol, 450 mg) in dry MeOH (20 mL) hydrazine monohydrate (3.7 mmol, 185 µL) was added. The reaction mixture was refluxed for 6 hours. The volatiles were removed under vacuum, co-evaporated 3 times with new portions of MeOH then dried under high vacuum for 5 hours to give **1.31** as a colorless oil (448 mg, quant.). ^{1}H NMR (400 MHz, $CDCl_3$) δ 7.41 – 7.27 (m, 5H), 4.56 (s, 2H), 4.06 (s, 2H). ^{13}C NMR (101 MHz, $CDCl_3$) δ 169.97, 136.75, 128.80, 128.47, 128.08, 73.86, 69.18. BRMS (ESI): $(M-H)^-$ calcd: 181.1, found: 181.0.

5-(3-((Benzyloxy)methyl)-5-(3-(2-chloro-4-fluorophenoxy)azetidin-1-yl)-4H-1,2,4-triazol-4-yl)-2-methoxypyridin-1-ium trifluoroacetate ***1.32***

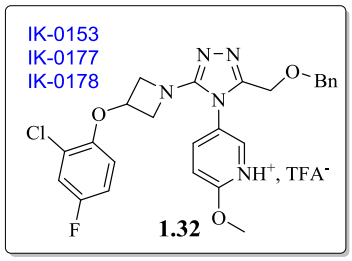

t-BuOK (1.44 mmol, 170 mg) was added to a solution of **1.28** (1.2 mmol, 441 mg; obtained according to the protocol described in Brown et al., 2006) in dry THF (17 mL) at 0°C. The resulting mixture was stirred for 5 min, then methyl iodide (1.44 mmol, 90 µL) was added. The reaction mixture was stirred at ice-water temperature for 15 min, then

water (150 mL) was added and the mixture was extracted twice with EtOAc (70 mL). The combined organic fractions were washed three times with water (150 mL), then with brine (150 mL), dried over Na_2SO_4 and the volatiles were removed *in vacuo*.

The residue was dissolved in dry THF (17 mL). To the obtained solution **1.31** (1.43 mmol, 257 mg) was added, followed by trifluoroacetic acid (0.59 mmol, 44 µL). The reaction mixture was stirred under reflux for 6 hours, then the volatiles were removed *in vacuo*. To the residue water (100 mL) was added and the mixture was extracted twice with DCM (50 mL). The organic layer was washed twice with water (100 mL), then with brine (100 mL) and dried over Na_2SO_4. The volatiles were removed *in vacuo* and the residue was purified by reverse phase flash chromatography using the gradient of 5 to100% of solvent B in solvent A in 30 min to give **1.32** as a yellow oil (300 mg, 41%). ^{1}H NMR (400 MHz, $CDCl_3$) δ 8.25 (d, *J* = 2.6 Hz, 1H), 7.66 (dd, *J* = 8.8, 2.6 Hz, 1H), 7.35 – 7.27 (m, 3H), 7.19 – 7.07 (m, 3H), 6.91 – 6.82 (m, 2H), 6.52 (dd, *J* = 9.0, 4.7 Hz, 1H), 5.02– 4.91 (m, 1H), 4.47 – 4.37 (m, 4H), 4.35 (s, 2H), 4.11 (dd, *J* = 9.3, 4.1 Hz, 2H), 4.02 (s, 3H). ^{13}C NMR (101 MHz, $CDCl_3$) δ 165.38, 157.52 (d, J = 244.5 Hz), 153.97, 148.64, 148.61, 146.29, 137.95, 136.46, 128.68, 128.36, 128.21, 124.20 (d, J = 10.5 Hz), 121.49, 118.36 (d, J = 26.2 Hz), 114.90 (d, J = 8.8 Hz), 114.50 (d, J = 22.8 Hz), 112.29, 72.86, 68.87, 60.66, 60.34, 54.49. BRMS (ESI): $(M+H)^+$ calcd: 496.2, found: 496.2.

5-(3-(3-(2-Chloro-4-fluorophenoxy)azetidin-1-yl)-5-(hydroxymethyl)-4H-1,2,4-triazol-4-yl)-2-methoxypyridin-1-ium trifluoroacetate ***1.27***

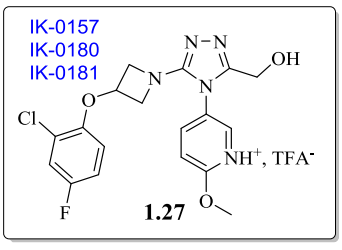

A solution of boron trichloride in DCM (1 M, 2.46 mmol, 2.46 mL) was added to a solution of **1.32** (0.49 mmol, 300 mg) in dry DCM (22 mL) cooled to ice-water temperature. The resulting mixture was stirred at ice-water temperature for 30 min then water (50 mL) and DCM (50 mL) were added. A solution of 10N NaOH was added dropwise until the pH of the aqueous phase reached 13. The organic layer was separated, washed with 1N solution of $NaHCO_3$ (50 mL), brine (50 mL), dried over Na_2SO_4 and the volatiles were removed *in vacuo*. The residue was purified by reverse phase flash chromatography using the gradient of 5 to100% of solvent B in solvent A in 30 min to afford **1.27** as a pale yellow solid (230 mg, 90%). mp = 143–145 °C. ^{1}H NMR (400 MHz, $CDCl_3$) δ 8.34 (d, *J* = 2.5 Hz, 1H), 7.84 (dd, *J* = 8.8, 2.5 Hz, 1H), 7.13 (dd, *J* = 7.9, 3.0 Hz, 1H), 6.94 (d, *J* = 8.8 Hz, 1H), 6.92 – 6.83 (m, 1H), 6.53 (dd, *J* = 9.0, 4.7 Hz, 1H), 5.03 – 4.92

(m, 1H), 4.53 (s, 2H), 4.47 – 4.35 (m, 2H), 4.18 – 4.07 (m, 2H), 4.02 (s, 3H). ^{13}C NMR (101 MHz, $CDCl_3$) δ 165.76, 157.56 (d, J = 244.6 Hz), 153.24, 148.56, 147.89, 146.32, 138.13, 124.28, 120.69, 118.39 (d, J = 26.1 Hz), 114.96 (d, J = 8.6 Hz), 114.54 (d, J = 22.8 Hz), 112.69, 68.89, 60.48, 54.60, 53.84. HRMS (ESI): calcd. for $C_{18}H_{18}ClFN_5O_3$ $(M+H)^+$ 406.10822; found 406.10746.

*Alkylation of **1.27***

To a solution of **1.27** (1 eq., 1 mg) in dry DMF (200 µL) NaH (13 eq., 1 mg, 60% dispersion in oil) was added. The solution was heated at 90°C for 1 min (in a water bath), then MeI (1 eq., 10 µL of 0.2 M solution in DMF) was added and the reaction mixture was stirred at 90°C for 5 min.

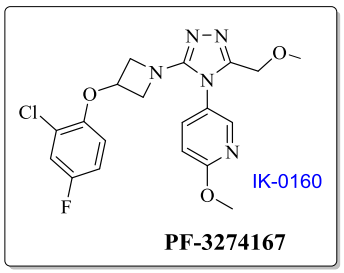

The progress of the reaction was monitored by analytical HPLC (detection at 220 nm) using a linear gradient of solvent B in solvent A (5% to 100% in 7.4 min, flow rate of 1.6 mL·min^{-1}). T_r (**1.27**) = 3.83 min, T_r (PF-3274167) = 4.19 min. BRMS (ESI): $(M+H)^+$ calcd: 420.1, found: 420.2.

1.5. [^{18}F] derivative of PF-3274167

5-(3-((2-(Benzyloxy)ethoxy)methyl)-5-(3-(2-chloro-4-fluorophenoxy)azetidin-1-yl)-4H-1,2,4-triazol-4-yl)-2-methoxypyridine ***1.36***

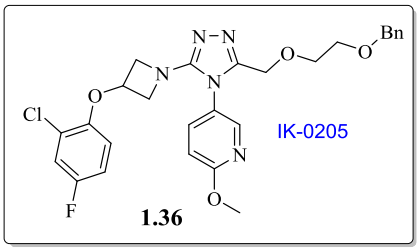

To a solution of **1.27** (0.12 mmol, 50 mg) in dry DMF (2 mL) KOH (0.74 mmol, 42 mg) was added. The resulting mixture was stirred at r.t. for 15 min, then a solution of benzyl 2-bromoethyl ether (0.15 mmol, 23.4 µL) in dry DMF (3 mL) was added. The reaction mixture was stirred at r.t. overnight. To the resulting mixture water (50 mL) was added and the mixture was extracted twice with DCM (50 mL). The organic layer was washed twice with water (100 mL), then with brine (100 mL) and dried over Na_2SO_4. The volatiles were removed under vacuum and the residue was purified by reverse phase flash chromatography using the gradient of 20 to 100% of ACN in H_2O in 30 min to give **1.36** as a pale yellow oil (37 mg, 56%). ^{1}H NMR (400 MHz, $CDCl_3$) δ 8.25 (d, *J* = 2.5 Hz, 1H), 7.68 (dd, *J* = 8.8, 2.5 Hz, 1H), 7.38 – 7.26 (m, 5H), 7.13 (dd, *J* = 8.0, 3.0 Hz, 1H), 6.88 (ddd, *J* = 9.0, 7.7, 3.0 Hz, 1H), 6.74 (d, *J* = 8.8 Hz, 1H), 6.51 (dd, *J* = 9.0, 4.7 Hz, 1H), 4.95 – 4.87 (m, 1H), 4.48 (s, 2H), 4.42 (s, 2H), 4.30 – 4.21 (m, 2H), 4.08 – 4.00 (m, 2H), 3.99 (s, 3H), 3.61 (dd, *J* = 6.0, 2.6 Hz, 2H), 3.56 (dd, *J* = 6.0, 2.6 Hz, 2H). ^{13}C NMR (101 MHz, $CDCl_3$) δ 165.01, 157.41 (d, *J* = 244.2 Hz), 149.21, 148.79, 148.76, 146.06, 138.13, 138.08, 128.58, 127.89, 127.88, 122.31, 124.16 (d, *J* = 10.5 Hz), 118.33 (d, *J* = 26.1 Hz), 114.71 (d, *J* = 8.7 Hz), 114.41 (d, *J* = 22.8 Hz), 112.02, 73.39, 69.67, 69.35, 68.89, 62.15, 59.97, 54.34. BRMS (ESI): $(M+H)^+$ calcd: 540.2, found: 540.1.

5-(3-(3-(2-Chloro-4-fluorophenoxy)azetidin-1-yl)-5-((2-hydroxyethoxy)methyl)-4H-1,2,4-triazol-4-yl)-2-methoxypyridin-1-ium trifluoroacetate ***1.37****.*

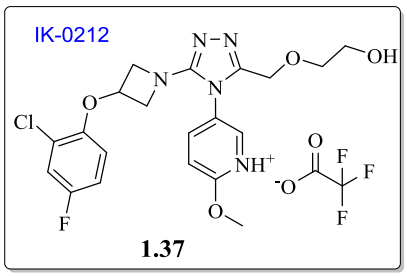

To a solution of **1.36** (0.068 mmol, 37 mg) in dry DCM (5 mL) at -78°C under argon a solution of boron trichloride (1M in DCM, 0.34 mmol, 343 µL) was added. The reaction mixture was stirred at -78°C for 30 min. Water (50 mL) was added and the resulting mixture was left to heat for r.t. The mixture was extracted with DCM (50 mL). The organic fraction was washed twice with water (50 mL), then with brine (50 mL), dried over Na_2SO_4 and the volatiles were removed under vacuum. The residue was purified by reverse phase

flash chromatography using the gradient of 30 to 100% of solvent B in solvent A in 30 min. The fractions containing the desired compound were concentrated under vacuum and lyophilized. The obtained compound was partially OH-trifluoroacetylated (65%, determined by RMN). It was decided to engage **1.37** into the next step without further purification as the trifluoroacetate was not stable in the conditions of the tosylation. 34 mg of **1.37** was obtained with the molar yield of 79%. ^{1}H NMR (400 MHz, $CDCl_3$) δ 8.35 – 8.31 (m, 0.35H), 8.31 – 8.26 (m, 0.65H), 7.88 – 7.80 (m, 0.35H), 7.76 – 7.67 (m, 0.65H), 7.16 – 7.10 (m, 1H), 6.97 – 6.84 (m, 2H), 6.54 (dd, *J* = 9.0, 4.7 Hz, 1H), 5.07 – 4.90 (m, 1H), 4.53 – 4.43 (m, 2H), 4.44 – 4.35 (m, 3.3H), 4.21 – 4.08 (m, 2H), 4.02 (s, 3H), 3.76 – 3.65 (m, 2H), 3.58 – 3.50 (m, 0.7H). ^{13}C NMR (101 MHz, $CDCl_3$) δ 165.78, 165.76, 161.12 (q, *J* = 38.3 Hz), 157.61 (d, *J* = 244.8 Hz), 157.12, 148.51, 148.48, 146.50, 146.42, 138.23, 137.92, 124.28, 124.19, 120.63, 118.40 (d, *J* = 26.2 Hz), 115.02 (d, *J* = 8.9 Hz), 114.57 (d, *J* = 22.9 Hz), 112.56, 112.52, 72.34, 68.82, 67.73, 66.42, 61.85, 61.72, 61.53, 60.51, 60.46, 54.62, 54.59. BRMS (ESI): $(M+H)^+$ calcd: 450.1, found: 450.0 (the trifluoroacetate was decomposed in the ionization source).

5-(3-(3-(2-Chloro-4-fluorophenoxy)azetidin-1-yl)-5-((2-(tosyloxy)ethoxy)methyl)-4H-1,2,4-triazol-4-yl)-2-methoxypyridin-1-ium trifluoroacetate ***1.34***

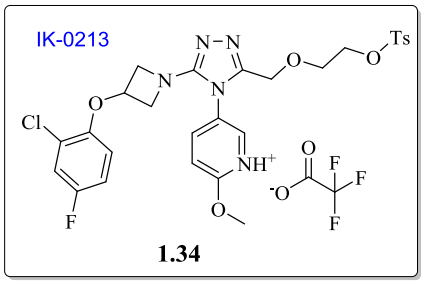

To a solution of **1.37** (0.066 mmol, 37 mg) in dry DCM (3 mL) cooled to ice-water temperature KOH (0.26 mmol, 15 mg) was added followed by Ts-Cl (0.72 mmol, 14 mg). The reaction mixture was stirred at ice-water temperature for 2 hours then at r.t. for 5 hours. Water (50 mL) was added and the resulting mixture was extracted with DCM (50 mL). The organic fraction was washed twice with water (50 mL), then with brine (50 mL), dried over Na_2SO_4 and the volatiles were removed under vacuum. The residue was purified by reverse phase flash chromatography using the gradient of 30 to100% of solvent B in solvent A in 30 min to give after the lyophilization **1.34** as a colorless oil (29 mg, 73%). ^{1}H NMR (400 MHz, $CDCl_3$) δ 8.20 (d, *J* = 2.6 Hz, 1H), 7.82 – 7.72 (m, 2H), 7.68 (dd, *J* = 8.8, 2.6 Hz, 1H), 7.38 – 7.30 (m, 2H), 7.12 (dd, *J* = 8.0, 3.0 Hz, 1H), 6.95 – 6.80 (m, 2H), 6.55 – 6.45 (m, 1H), 5.00 – 4.80 (m, 1H), 4.35 (s, 2H), 4.27 – 4.17 (m, 2H), 4.08 – 4.02 (m, 4H), 4.01 (s, 3H), 3.68 – 3.60 (m, 2H), 2.44 (s, 3H). HRMS (ESI): calcd. for $C_{27}H_{28}ClFN_5O_6S$ $(M+H)^+$ 604.14329; found 604.14256.

2-Fluoroethyl 4-methylbenzenesulfonate ***1.39***

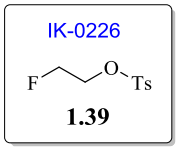

To a solution of 2-fluoroethan-1-ol (1 mmol, 59 µL) in dry DCM (10 mL) cooled to ice-water temperature KOH (3 mmol, 168 mg) and Ts-Cl (1.05 mmol, 204 mg) were added. The reaction mixture was stirred at ice-water temperature for 2 hours then at r.t. overnight. To the resulting mixture water (100 mL) and DCM (30 mL) were added. The organic layer was washed twice with water (50 mL), then with brine (50 µL), dried over Na_2SO_4, filtered and concentrated *in vacuo* to afford **1.39** as a colorless oil (196 mg, 90%). ^{1}H NMR (400 MHz, $CDCl_3$) δ 7.86 – 7.76 (m, 2H), 7.39 – 7.32 (m, 2H), 4.66 – 4.48 (m, 2H), 4.32 – 4.21 (m, 2H), 2.46 (s, 3H). ^{13}C NMR (101 MHz, $CDCl_3$) δ 145.27, 132.90, 130.08, 128.14, 80.68 (d, *J* = 173.8 Hz), 68.54 (d, *J* = 21.1 Hz), 21.80. BRMS (ESI): $(M+Na)^+$ calcd: 241.0, found: 241.2.

5-(3-(3-(2-Chloro-4-fluorophenoxy)azetidin-1-yl)-5-((2-fluoroethoxy)methyl)-4H-1,2,4-triazol-4-yl)-2-methoxypyridine ***1.33***

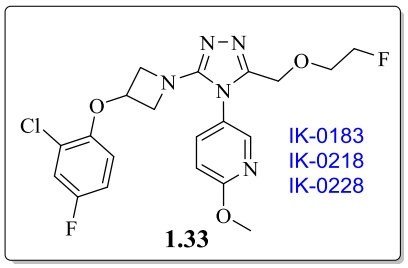

To a solution of **1.27** (0.038 mmol, 20 mg) in dry DMF (1 mL) cooled to ice-water temperature KOH (0.19 mmol, 11 mg) was added. The resulting mixture was stirred at ice-water temperature for 10 min, then **1.39** (0.058 mmol, 12.6 mg) was added. The reaction mixture was stirred at ice-water temperature for 3 hours, then at r.t. overnight. To the resulting mixture water (50 mL) was added and the mixture was extracted with DCM (50 mL). The organic fraction was washed twice with water (50 mL), then with brine (50 mL), dried over Na_2SO_4 and the volatiles were removed under vacuum. The residue was purified by reverse phase flash chromatography using the gradient of 30 to100% of solvent B in solvent A in 30 min. The fractions, containing the desired compound were concentrated under vacuum, extracted with DCM (50 mL) and the organic fraction was washed three times with a saturated solution of $NaHCO_3$ (50 mL), then with brine (50 mL), dried over Na_2SO_4 and the volatiles were removed under vacuum to give **1.33** as a colorless oil (15 mg, 69%). ^{1}H NMR (400 MHz, $CDCl_3$) δ 8.27 (d, *J* = 2.6 Hz, 1H), 7.72 (dd, *J* = 8.8, 2.6 Hz, 1H), 7.13 (dd, *J* = 8.0, 3.0 Hz, 1H), 6.95 – 6.82 (m, 2H), 6.53 (dd, *J* = 9.0, 4.7 Hz, 1H), 5.01 – 4.90 (m, 1H), 4.56 – 4.48 (m, 1H), 4.44 (s, 2H), 4.43 – 4.37 (m, 1H), 4.38 – 4.30 (m, 2H), 4.10 (dd, *J* = 9.3, 4.4 Hz, 2H), 4.01 (s, 3H), 3.74 – 3.66 (m, 1H), 3.66 – 3.58 (m, 1H). ^{13}C NMR (101 MHz, $CDCl_3$) δ 165.22, 157.50 (d, *J* = 244.5 Hz), 155.62, 148.83, 146.10, 137.95, 124.29 (d, *J* =

10.4 Hz), 122.15, 118.34 (d, *J* = 26.1 Hz), 114.93 (d, *J* = 8.8 Hz), 114.44 (d, *J* = 22.8 Hz), 112.22, 82.57 (d, *J* = 170.0 Hz), 69.54 (d, *J* = 19.4 Hz), 69.01, 62.18, 60.15, 54.41. HRMS (ESI): calcd. for $C_{20}H_{21}ClF_2N_5O_3$ $(M+H)^+$ 452.13010; found 452.13076.

2. Pharmacological evaluations of 1.33[11]

2.1. Determination of the affinity for OTR and the selectivity versus $V_{1a}R$, $V_{1b}R$ and V_2R.

A specific plasmid construction was engineered into the pCDNA3 vector with the SNAP-tag and the gene encoding for the oxytocin receptor (plasmid #412 from CisBio). HEK293 cells from ATCC were transfected with 5µg of plasmid by electroporation. 48 hours following the transfection, 800µg/mL of G418 was added to the medium. One week later, G418 was decreased to 500µg/mL and conserved in the medium until all non-transfected cells were died.

HEK293 cells expressing the SNAP-tag oxytocin receptor were cultured in MEM medium supplemented with 500µg/mL G418.

A functional test of the labeled receptor was performed by measuring intracellular calcium flux. For that, attached cells were incubated for 45 min at 37°C with 5µM of the fluorescent dye Indo1-AM in Hepes buffer supplemented with 0.1% BSA. After a wash step with PBS, cells were detached using Accutase® (PAA) and suspended in Hepes-BSA buffer. 200µL of a 0.5×10^6 cells/mL suspension were distributed in a 96-well plate.

Fluorescence of Indo1 was recorded at 401 and 475nm (excitation wavelength at 338 nm) for 3 minutes following the addition of oxytocin using FlexStation®III reader (Molecular Devices). A dose-response curve was generated by plotting normalized fluorescence ratio of Indo1 and oxytocin concentrations tested.

The same experiment was realized with HEK293 cells expressing the wild-type oxytocin receptor.

Calculated EC_{50} values for oxytocin were 8 nM for the SNAP-tag OTR, and 4 nM for the wild-type OTR, showing that the SNAP-tag fusion did not affect the oxytocin receptor function.

To label the SNAP-tag OTR cells, a solution of 100 nM Lumi4-Tb-BG (CisBio) was prepared in Tag-lite® buffer (CisBio). Attached cells were incubated with this solution for 1

[11] Performed by Christel Valencia (PCBIS, Illkirch).

hour in the incubator. Cells were then washed three times with Tag-lite® buffer, detached with Accutase® (PAA) and suspended in MEM medium.

To check the labeling efficiency, fluorescence of Lumi4-Tb at 615 nm (excitation wavelength at 337 nm) was recorded for labeled SNAP-tag OTR cells and for wild-type HEK293 cells labeled using the same protocol. Specific labeling of SNAP-tag OTR cells was obtained by the difference between total labeling (fluorescence at 615 nm of labeled SNAP-tag OTR cells) and non-specific labeling (fluorescence at 615 nm of labeled wild-type HEK293 cells.

The labeled cells were then aliquoted and frozen in liquid nitrogen until use.

For competition assays, 10 µL of a 1×10^6 cells/mL suspension in Tag-lite® buffer were distributed in each well of a 384-well plate (CORNING 3824). Increasing concentrations of **1.33** were diluted in 5 µL of Tag-lite® medium and added to the cells together with 5µL of a solution of fluorescent competitors (EP109DY at final concentration of 50 nM for OTR and $V_{1a}R$ and SL450DY at final concentration of 30 nM for V_2R).

The plate was incubated for 3 hours at room temperature before reading on the Envision plate reader (Perkin Elmer) with a classical HTRF® protocol (excitation at 337 nm, emission at 665 and 615 nm). The inhibition constants (K_i) were calculated using GraphPad Prism Software (GraphPad, San Diego, CA, USA).

2.2. *In vitro* functional assay

Cell treatment was performed as described in Weill et al., 2011. Briefly, HEK293 cells were loaded with 5 µM of the calcium-sensing dye Indo-1 acetoxy-methyl ester (Indo-1 AM) in Hepes buffer (10 mM Hepes, 137,5 mM NaCl, 1,25 mM $MgCl_2$, 1,25 mM $CaCl_2$, 6 mM KCl, 0,4 mM NaH_2PO_4 and 5,6 mM glucose, pH 7.4) supplemented with 1 mg/mL BSA, for 45 minutes at 37°C in the presence of 5% CO_2. After washing they were collected in Hepes-BSA buffer at 1.3×10^6 cells/ml and seeded into 384 well polystyrene plates (Greiner 781091) in order to get 50 000 cells/well and then centrifuged 5 min at 800 rpm.

Intracellular Ca^{2+} release measurement was performed by monitoring the fluorescence of the ratiometric calcium probe Indo-1 using the FlexStation® 3 microplate reader (Molecular Devices Corp., Palo Alto, CA, USA). Fluorescence (excitation at 338 nm, emissions recorded at 401 nm and 475 nm) was acquired at room temperature over a 3 minute period.

Fluorescence emission ratio (signal = (fluorescence measured at 401 nm)/(fluorescence measured at 475 nm)) was calculated in order to follow the calcium release. Minimum signal was obtained before the addition of the compound and maximum signal was given after the digitonin addition. Normalization was done using the following equation:

Normalized Signal = 100 × (signal – signal min)/(signal max – signal min)

Addition of the compound was performed using the FlexStation® 3 apparatus 30 s after the beginning of the reading.

For the antagonist assay, the compound at final concentrations from 0.3 nM to 30 µM was mixed with oxytocin (20 nM) before cell treatment.

In order to assess the maximum calcium level, addition of digitonin (Sigma Aldrich) (100 µM) was performed 110 s after compound treatment.

Dose-response curves were obtained by plotting the normalized signal of calcium release against the logarithmic values of compound concentration. The half maximal inhibitory concentration (IC_{50}) was calculated using GraphPad Prism Software (GraphPad, San Diego, CA, USA).

3. Radiolabelling[12]

3.1. [^{11}C]PF-3274167

Carbon-11 was produced via the $^{14}N(p,\alpha)^{11}C$ nuclear reaction (IBA Cyclone 18/9 cyclotron).

[^{11}C]CH_3I was produced using the gas phase conversion described by Larsen et al., 1997 in an automated synthesis module ScanSys. Thereby, [^{11}C]CO_2 was trapped on a molecular sieve (4 Å) and converted to [^{11}C]CH_4 within 120 s in the presence of Ni catalyst and hydrogen at 360°C. Subsequently, [^{11}C]CH_4 was reacted with elemental iodine at 720°C to get [^{11}C]CH_3I and recirculated for 300 s. [^{11}C]CH_3I was trapped online on HayeSep® D in a small glass column and finally released by heating to 190°C in a stream of He.

[^{11}C]CH_3I was trapped online in a reactor containing 1.25 mg of **1.27** and 2.2 mg of NaH in 300µL of DMF cooled to 10°C. The reactor was sealed and the reaction mixture heated to 90°C for 5 min. After cooling down to room temperature, the reaction mixture was quenched by the addition of 2.4 mL of the HPLC eluent (0.1 M H_3PO_4/CH_3CN : 60/40) and subsequently transferred to the injection loop of the HPLC system.

Pure [^{11}C]PF-3274167 was obtained after HPLC separation (Sunfire C18 5µm 10 x 250 mm) eluted with 0.1 M H_3PO_4/CH_3CN : 60/40 at 3 mL/min (detection at 254 nm). For biological use, the radiotracer was formulated via SPE techniques. The product was diluted in 40 mL of sterile water and loaded on a SEP-Pak tC18 cartridge (Waters, Milford, MA, USA). The loaded cartridge was rinsed with water and eluted with 1 mL of ethanol and 2 mL of water, and the final product was diluted with isotonic saline and sterilized by filtration (sterile filter Millex-GS, 0.22 mm). The radiochemical purity and specific activity of [^{11}C]PF-3274167 were assayed by analytical HPLC (MachereyeNagel EC 250/4.6 Nucleodur 100-5-C18ec C18 column; mobile phase H_2O/CH_3CN/TFA: 55/45/0.1%; flow rate 0.9 mL/min). The identity of [^{11}C]PF-3274167 was confirmed by co-injection with an authentic non-radioactive sample.

3.2. [^{18}F] 1.33

Just before the radiolabeling, the tosyl precursor **1.34** (1,85 mg) was mixed with NaH (0,27 mg) in 3 mL of DMSO and sonicated for 10 min in a Ultra-Sound cuve.

[12] Performed by Dr. Thierry Billard (CERMEP - Imagerie du vivant, Bron).

Fluorine-18 was produced via the $^{18}O(p,n)^{18}F$ nuclear reaction (IBA Cyclone 18/9 cyclotron). Tosyl/fluoro exchange was performed on a standard Neptis® synthesizer (Ora™): after initial fluoride preparation (collection, drying and kryptofix activation), the solution of tosyl precursor **1.34** was introduced, and the reaction mixture was heated at 150°C for 10 min. After dilution with 15 mL of water, the reaction mixture was passed through an activated C18 cartridge for pre-purification, and the crude product was eluted from the cartridge with 1.5 mL of methanol. Pure **[^{18}F]1.33** was obtained after separation on a preparative HPLC (C18 Symmetry Prep Waters 7 µm 7.8 x 300 mm) eluted with H_2O/CH_3CN/TFA: 65/35/0.1% at 3 mL/min (detection at 220 nm). For biological use, the radiotracer was formulated via SPE techniques (Lemaire et al., 1999). The product was diluted in 20 mL of sterile water and loaded on a SEP-Pak Light C18 cartridge (Waters, Milford, MA, USA). The loaded cartridge was rinsed with water and eluted with 1 mL of ethanol, and the final product was diluted with isotonic saline and sterilized by filtration (sterile filter Millex-GS, 0.22 mm). The radiochemical purity and specific activity of **[^{18}F]1.33** were assayed by analytical HPLC (MachereyeNagel EC 250/4.6 Nucleodur 100-5-C18ec C18 column; mobile phase H_2O/CH_3CN/TFA: 50/50/0.1%; flow rate, 0.9 mL/min). The identity of **[^{18}F]1.33** was confirmed by co-injection with an authentic non-radioactive sample.

4. *In vitro* autoradiography studies[13]

In vitro autoradiography was performed in rats (Male Sprague-Dawley, Charles River Laboratories). After euthanasia by inhaled isoflurane overdose, rat brains were carefully removed and immediately frozen in 2-methylbutane cooled with dry ice (-29°C). Coronal sections (30 mm thick) across hippocampus and striatum were cut using a -20°C cryostat (SM1850; Leica), thaw-mounted on glass slides, and allowed to air-dry before storage at -80°C until use. On the day of radiotracer synthesis, the slides were allowed to reach room temperature and then incubated for 20 min in Tris phosphate-buffered saline (138 mM NaCl, 2.7 mM KCl, pH adjusted to 7.6) containing 37 kBq/mL (1 mCi/mL) of the PET radiotracer ([^{11}C]PF3274167 or **[^{18}F]1.33**) . For competition experiments with [^{11}C]PF3274167, the slides were placed in the same buffer supplemented with unlabelled (or "cold") molecule (10 nM, 100 nM, or 1 µM of PF3274167). After incubation, slides were dipped in cold buffer (4°C) for 90 s and in distilled cold water (4°C) for 90 s, and then dried and placed on a phosphor

[13] Performed by Prof. Luc Zimmer (Lyon Neuroscience Research Center, Lyon and CERMEP-Imaging platform).

imaging plate for 60 min (BAS-5000; Fujifilm). Regions of interest (such as the striatum or the hippocampus) were visualized using Multigauge software (Fujifilm), according to the rat brain atlas (Paxinos and Watson, 1998).

Part II Chapter 1: Fluorescent probes for binding studies

1. Tb (III)–labeled ligands

1.1. Synthesis

General

Reagents were obtained from commercial sources and used without any further purification. Semi-preparative HPLC chromatography was performed on SunFire C18 column (5 µm, 19 × 150 mm) on Gilson PLC2020 with absorption detection. Analytical RP-HPLC separations were performed on Ascentis Express C18 column (2.7 µm, 4.6 mm × 75 mm) using a linear gradient (5% to 100% in 7.4 min, flow rate of 1.6 mL·min^{-1}) of solvent B (0.1% TFA in CH_3CN, v/v) in solvent A (0.1% TFA in H_2O, v/v). Detection was set at 220 and 254 nm. LC-MS spectra were obtained on a ZQ (Z quadripole) Waters/Micromass spectrometer equipped with an X-Terra C18 column (3.5 µm, 4.6 × 50 mm) using electrospray ionization mode (ESI). Mass spectra were acquired on a Bruker MicroTof mass spectrometer, using electrospray ionization (ESI) and a time-of-flight analyzer (TOF) or on a Autoflex II TOF/TOF Bruker mass spectrometer using matrix-assisted laser desorption/ionization technique (MALDI) and a time-of-flight analyzer (TOF).

Lys^{8}-CBT trifluoroacetate

Solid-phase reactions were performed in polypropylene tubes equipped with polyethylene frits and polypropylene caps using an orbital agitator shaking device. Fmoc-protected Rink Amide NovaGel® resin was purchased from Novabiochem® and the overall yields for the solid-phase syntheses were calculated based on the initial loadings provided by the supplier (0.7 mmol/g).

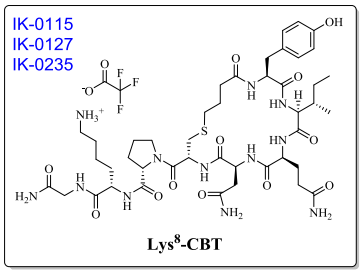

All Fmoc-protected amino acids (4 eq.) were coupled in *N*,*N*-dimethylformamide (DMF) for 45 min using HBTU (3.8 eq.) and HOBt (4 eq.) with *N*,*N*-diisopropylethylamine (DIEA) (12 eq.) as activating agents (Scheme 12). Fmoc-Cys(Mmt)-OH (5 eq.) was coupled in DMF for 45 min using HATU (4.9 eq.) with tetramethylpiperidine (10 eq.). 4-Bromobutyric acid (5 eq.) was coupled in DMF for 24 hours using DIC (5 eq.) and HOBt (5 eq.) as activating agents. The cleavages of Fmoc protecting groups were performed in 20% piperidine/DMF (2 times for 15 min).

The completion of couplings and Fmoc cleavages was monitored with the ninhydrin test (Kaiser et al., 1970), the TNBS test (Hancock and Battersby, 1976) or the chloranil test (Mařík et al., 2003) as well as by analytical HPLC (minicleavages of the resin with TFA/H_2O 95/5).

The Cys 4-methoxyltrityl (Mmt) protecting group was cleaved with 2% of trifluoroacetic acid in DCM with 5% TIS (6 times for 2 min).

The intermolecular cyclisation was performed with 2M NH_3 in a mixture of MeOH/THF (1/3) for 4 hours. The conjugate was cleaved from resin by TFA/TIS/H_2O (95/2.5/2.5) treatment for 4 hours.

The crude Lys^8-CBT was purified by semi-preparative HPLC chromatography (SunFire column) eluted with solvent B in solvent A: 5% for 3 min, 5-15% in 3 min then 15-23% in 14 min. Yield 32%. BRMS (ESI): calc. for $C_{45}H_{71}N_{12}O_{12}S$ $(M+H)^+$ = 1003.50; found $(M+H)^+$ = 1003.51.

*CBT conjugate **2.3***

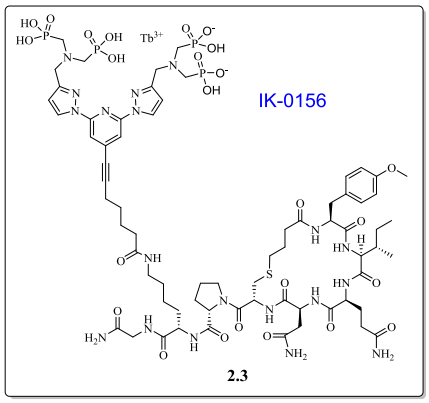

To a solution of Lys^8-CBT (1 eq, 12.9 mg) in 1 mL of 0.2 M $NaHCO_3$ buffer solution (pH 8.3) **2.1** (2 eq, 25 mg) in 1 mL of 0.2 M $NaHCO_3$ buffer was added. The reaction mixture was stirred at r.t. overnight monitored by HPLC. The resulting mixture was purified by semi-preparative HPLC eluted with solvent B in solvent A: 5 min at 5%, from 5 to 38% in 23 min, then from 38 to 100 % in 7 min to give **2.3** as a white solid (4.4 mg, 22%). T_r = 2.55 min (on the analytical HPLC column with a linear gradient of solvent B in solvent A: 5% to 100% in 7.4 min, flow rate of 1.6 mL·min^{-1}). BRMS (ESI+APCI): calc. for $C_{69}H_{102}N_{19}O_{25}P_4S$ $(M-H)^-$ = 1752.6; found $(M-H)^-$ = 1752.6.

*Tb(III) complex **2.5***[14]

To a solution of **2.3** in 0.01 M Tris-HCl buffer pH 7.4 (0.94 mL, 1.78 mM[15]) a solution of $TbCl_3$ (0.1 mM, 16.7 mL) was added. The reaction mixture was stirred at r.t. for 1 hour, then purified by semi-preparative HPLC eluted with ACN/1M triethylammonium acetate buffer pH 7 (0% - 50% in 23 min, then 50% to 100% in 7 min) to give **2.2** as a white solid (3.16 mg, quant.). BRMS (MALDI): calc. for $C_{69}H_{101}N_{19}O_{25}P_4STb^+$ = 1910.51; found = 1910.82.

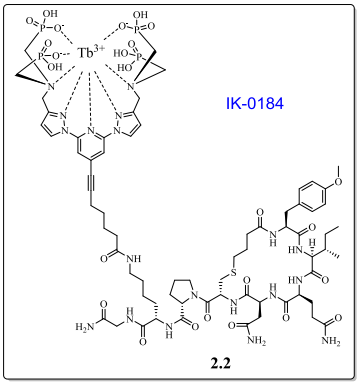

1.2. Determination of the affinity for OTR by radioligand binding assay[16]

The inhibition constant (K_i) for the human OTR was determined on membrane preparations from CHO cells stably expressing the receptor by competition binding assays. Binding experiments were performed at 30°C using [^{3}H]-AVP as the radioligand and 10 µg of CHO cell membrane proteins (K_d for [^{3}H]-AVP to the human OTR expressed in this system has been published previously and is 1.36 nM (Breton et al., 2001). Briefly, membranes were incubated in 50 mM Tris-HCl pH 7.4, 5 mM $MgCl_2$ supplemented with 1 mg/mL BSA (binding buffer) and with radiolabeled and displacing ligands for 30 min. Competition experiments were conducted using [^{3}H]-AVP (1-2 nM) and varying concentrations of the unlabeled ligand from 0.1 nM to 1 µM. Nonspecific binding was determined by adding unlabeled AVP (10 µM). Bound and free radioactivity were separated by filtration over Whatman GF/C filters pre-soaked in a 10 mg/mL BSA solution for 3-4 hours. The ligand binding data were analyzed by nonlinear least-squares regression using the computer program GraphPad Prism. All assays were performed in triplicate on at least three independent batches of cell membranes.

1.3. Fluorescence spectroscopy[17]

Absorption spectra were recorded on a Specord 205 Analytik Jena spectrometer. Steady-state emission spectra were recorded on a Horiba Jobin Yvon Fluorolog 3 working with a

[14] Performed by the author in IPHC (Strasbourg) with the help of Dr. Aline Nonat and Dr. Corinne Baehr.
[15] The concentration was determined from the evolution absorption and emission curves presented in Figure 20.
[16] Performed by Dr. Christiane Mendre and Dr. Bernard Mouillac (IGF, Montpellier).
[17] Performed by the author in IPHC (Strasbourg) with the help of Dr. Aline Nonat.

continuous 450W Xe lamp, exciting at 330 nm. All spectra were corrected for the instrumental functions. Luminescence quantum yields were measured according to conventional procedures, with diluted solutions (optical density < 0.05), using [TbL(H_2O)]Na (Φ = 31%, Weibel et al., 2004) in non-degassed water as references. Estimated errors are ±15%.

Luminescence lifetimes in H_2O and D_2O were measured in time-resolved mode by monitoring the luminescence decay (emission at 545 nm) using a Jobin Yvon FluoroHub single photon counting controller and a Xenon flash lamp as the excitation source. The decays were analyzed with DataStation v2.4.

The number of water molecules in the Tb(III) coordination sphere (q) was obtained using equation (1) (Beeby et al., 1999), were τ (H_2O) and τ (D_2O) respectively refer to the measured luminescence decay lifetimes (in ms) in water and deuterated water.

(1) $q = 5 \times ({}^{1}/_{\tau(H_2O)} - {}^{1}/_{\tau(D_2O)} - 0.06)$

1.4. FRET assays[18]

These assays were performed on HEK293 cells stably expressing OTR fused to GFP (GFP-OTR cells) or wild-type OTR (wtOTR cells). Briefly, cells were cultivated in DMEM medium supplemented with 10% FCS, 1% penicillin/streptomycin antibiotics and 50 µg/mL hygromycine H500. Confluent cells were dissociated and distributed in black 96-well plates (Costar 3686) at 100 000 cells/well.

Cells were incubated with increasing concentrations of **2.2** in HEPES buffer (without Na_2HPO_4) alone or with 10 µM of carbetocin for 30 min at room temperature.

Plates were then read in the Envision plate reader (Perkin Elmer) with laser excitation at 337 nM and acceptor emission measured at 510 nm, 150 µs delay, 500 µs integration. Data were analyzed using GraphPad Prism Software (GraphPad, San Diego, CA, USA).

[18] Performed by the author at PCBIS (Illkirch) with the help of Sophie Gioria.

2. First selective non-peptide fluorescent probes for the oxytocin receptor

2.1. Synthesis

General.

Reagents were obtained from commercial sources and used without any further purification. DY647-NHS was purchased from Dyomics GmbH (Jena, Germany), 5-SFX was purchased from Life Technologies Corp. (Carlsbad, USA. Thin-layer chromatography was performed on silica gel 60F254 plates. Merck silica gel (Kieselgel 60) was used for chromatography (230-400 mesh) columns. Flash chromatography was performed on silica gel (40 μm, Grace) or RP18 (25−40 μm, Merck) prepacked columns on a SPOT II ultima from Armen. Analytical RP-HPLC separations were performed on a C18 Ascentis Express (2.7 μm, 4.6 mm × 75 mm) using a linear gradient (5% to 100% of solvent B in solvent A in 7.4 min, flow rate of 1.6 mL·min^{-1}, detection at 220 nm, solvent A: 0.1% TFA in H_2O, v/v, solvent B: 0.1% TFA in CH_3CN, v/v). Semi-preparative RP-HPLC separations were performed on a SunFire C18 column (5 μm, 19 × 150 mm). Purified final compounds were eluted as single and symmetrical peaks (thereby confirming a purity of ≥ 95%). NMR spectra were recorded at 300 or 400 MHz on a Bruker Advance spectrometer. Chemical shifts are reported in parts per million (ppm), coupling constants (J) are reported in hertz (Hz). LC-MS spectra were obtained on a ZQ (Z quadripole) Waters/Micromass spectrometer equipped with an X-Terra C18 column (3.5 μm, 4.6 × 50 mm) using electrospray ionization mode (ESI). HRMS were acquired on a Bruker MicroTof mass spectrometer, using ESI and a TOF analyzer.

((Oxybis(ethane-2,1-diyl))bis(oxy))bis(ethane-2,1-diyl) bis(4-methylbenzenesulfonate) ***2.6***

To a solution of tetraethylene glycol (2 mmol, 388.5 mg) in dry DCM (15 mL) cooled to ice-water temperature KOH (6 mmol, 673 mg) and 4-toluenesulfonyl chloride (4 mmol, 778 mg) were added. The reaction mixture was stirred at ice-water temperature for 2 hours. Water (100 mL) and DCM (50 mL) were added. The organic fraction was separated, washed twice with water, brine, dried over Na_2SO_4 and the volatiles were removed under vacuum. The residue was purified by flash chromatography eluted with EA/heptane (5% - 100% in 30 min) to give **2.6** as a colorless oil (875 mg, 87%). ^{1}H NMR (400 MHz, $CDCl_3$) δ 7.79 (d, *J* = 8.2 Hz, 4H), 7.34 (d, *J* = 8.2 Hz, 4H), 4.18 – 4.11 (m, 4H),

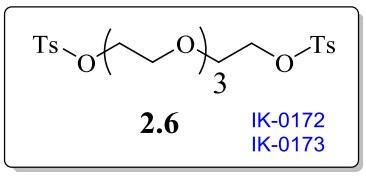

2.6 IK-0172 IK-0173

3.70 – 3.64 (m, 4H), 3.60 – 3.51 (m, 8H), 2.44 (s, 6H). ^{13}C NMR (101 MHz, $CDCl_3$) δ 144.94, 133.23, 129.97, 128.12, 70.91, 70.72, 69.39, 68.86, 21.77. BRMS (ESI): $(M+Na)^+$ calcd: 525.1, found: 525.0.

3,6,9,12,15,18,21-Heptaoxatricosane-1,23-diyl bis(4-methylbenzenesulfonate) ***2.7***

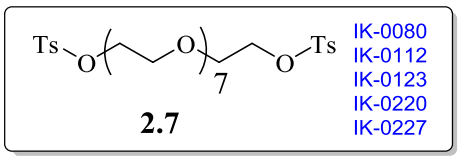

To a stirred solution of octaethylene glycol (1 mmol, 370.4 mg) in dry DCM (2 mL), cooled to ice-water temperature, KOH (8 mmol, 449 mg) and 4-toluenesulfonyl chloride (2 mmol, 381.3 mg) were added. The reaction mixture was stirred at ice-water temperature for 1 hour. The resulting mixture was quenched with water (50 mL) and extracted with DCM (3×20 mL). The combined organic fractions were washed with water (2×50 mL), brine (50 mL), dried over Na_2SO_4, and the volatiles were removed under vacuum. The residue was purified by column chromatography eluted with DCM/MeOH (97:3 v/v) to afford **2.7** as a colorless oil (482 mg, 71%). ^{1}H NMR (400 MHz, $CDCl_3$) δ 7.79 (d, *J* = 8.3 Hz, 4H), 7.34 (d, *J* = 8.2 Hz, 4H), 4.19 – 4.12 (m, 4H), 3.70 – 3.55 (m, 28H), 2.44 (s, 6H). ^{13}C NMR (101 MHz, $CDCl_3$) δ 144.92, 133.25, 129.97, 128.14, 70.91, 70.78, 70.73, 70.68, 69.39, 68.85, 21.78. BRMS (ESI): $(M+Na)^+$ calcd: 701.2, found: 701.2.

Tert-butyl N-[(tert-butoxy)carbonyl]-N-(2-{[(4-methylphenyl)sulfonyl]oxy}-((Oxybis (ethane-2,1-diyl))bis(oxy))bis(ethane-1-yl))carbamate ***2.8***

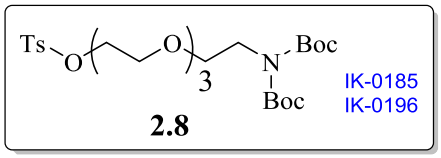

To a solution of **2.6** (2.7 mmol, 1376 mg) in dry DMF (20 mL) Cs_2CO_3 (10.9 mmol, 3.57 g) was added. The resulting mixture was cooled to ice-water temperature, then a solution of $NH(Boc)_2$ (1.37 mmol, 297 mg) in dry DMF (16 mL) was added dropwise over a period of 30 min. The reaction mixture was stirred at ice-water temperature for 3 hours then at r.t. overnight. To the resulting mixture water (50 mL) was added and the mixture was extracted with DCM (3×20 mL). The combined organic fractions were washed with water (3×50 mL), brine (50 mL), dried over Na_2SO_4. The volatiles were removed under vacuum and the residue was purified by reverse phase flash chromatography eluted with ACN/H_2O (3:7 - 10:0 v/v in 30 min). The fractions containing the desired compound were basified with 1N $NaHCO_3$, then ACN was evaporated and the residue was extracted with DCM. The volatiles were removed under vacuum to give **2.8** as a colorless oil (330 mg, 44%). ^{1}H NMR (400 MHz, $CDCl_3$) δ 7.79 (d, *J* = 8.3 Hz, 2H), 7.34 (d, *J* = 8.3 Hz, 2H), 4.21 – 4.09 (m, 2H), 3.77

(t, *J* = 6.2 Hz, 2H), 3.73 – 3.63 (m, 2H), 3.62 – 3.52 (m, 10H), 2.44 (s, 3H), 1.49 (s, 18H). ^{13}C NMR (101 MHz, $CDCl_3$) δ 152.78, 144.91, 133.20, 129.95, 128.12, 82.41, 70.88, 70.76, 70.68, 70.34, 69.41, 69.36, 68.83, 45.32, 28.20, 21.77. BRMS (ESI): $(M+Na)^+$ calcd: 570.2, found: 570.2.

Tert-butyl N-[(tert-butoxy)carbonyl]-N-(23-{[(4-methylphenyl)sulfonyl]oxy}-3,6,9,12,15,18,21-heptaoxa tricosan-1-yl)carbamate ***2.9***

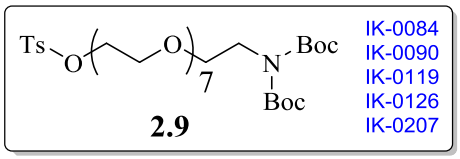

To a solution of **2.7** (0.31 mmol, 214 mg) in dry DMF (4 mL) Cs_2CO_3 (2.2 mmol, 725 mg) was added. The resulting mixture was stirred at ice-water temperature for 15 min then a solution of $NH(Boc)_2$ (0.18 mmol, 40.3 mg) in dry DMF (2 mL) was added dropwise over a period of 30 min. The reaction mixture was then stirred at ice-water temperature for 3 hours and at r.t. overnight. To the resulting mixture water (50 mL) was added and the mixture was extracted with DCM (3×20 mL). The combined organic fractions were washed with water (3×50 mL), brine (50 mL), dried over Na_2SO_4. The volatiles were removed under vacuum and the residue was purified by reverse phase flash chromatography eluted with ACN/H_2O (3:7 - 10:0 v/v in 30 min) to give **2.9** as a colorless oil (79 mg, 59%). ^{1}H NMR (400 MHz, $CDCl_3$) δ 7.80 (d, *J* = 8.3 Hz, 2H), 7.34 (d, *J* = 8.3 Hz, 2H), 4.20 – 4.11 (m, 2H), 3.78 (t, *J* = 6.2 Hz, 2H), 3.72 – 3.54 (m, 28H), 2.45 (s, 3H), 1.49 (s, 18H). ^{13}C NMR (101 MHz, $CDCl_3$) δ 152.79, 144.92, 133.25, 129.97, 128.14, 82.40, 77.36, 70.91, 70.77, 70.73, 70.68, 70.42, 70.39, 70.37, 69.44, 69.37, 68.85, 45.36, 28.21, 21.78. BRMS (ESI): $(M+Na)^+$ calcd: 746.3, found: 746.2.

Tert-butyl N-(23-bromo-3,6,9,12,15,18,21-heptaoxatricosan-1-yl)-N-[(tert-butoxy) carbonyl]carbamate ***2.10***

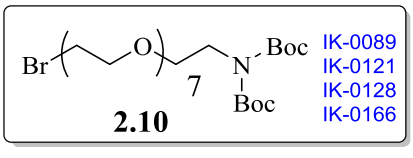

To a solution of **2.9** (0.10 mmol, 74 mg) in anhydrous DMF (5 mL) LiBr (0.15 mmol, 13.3 mg) was added. The reaction mixture was stirred at r.t. overnight then at 50°C for 12 hours followed by HPLC. To the resulting mixture DCM (20 mL) and water (20 mL) were added. The organic layer was separated, washed with water (3×20 mL), brine (20 mL) and the volatiles were removed under vacuum to give **2.10** as a colorless oil (62 mg, 96%). 1H NMR (400 MHz, CDCl3) δ 3.84 – 3.75 (m, 4H), 3.70 – 3.56 (m, 26H), 3.47 (t, J = 6.3 Hz,

2H), 1.49 (s, 18H). 13C NMR (101 MHz, CDCl3) δ 152.77, 82.39, 71.37, 70.81, 70.74, 70.70, 70.36, 69.43, 45.35, 30.43, 28.20. BRMS (ESI): $(M+Na)^+$ calcd: 654.2, found: 654.2.

1-(5-(3-(2-chloro-4-fluorophenoxy)azetidin-1-yl)-4-(6-methoxypyridin-3-yl)-4H-1,2,4-triazol-3-yl)-2,5,8,11-tetraoxatridecan-13-aminium trifluoroacetate ***2.11***

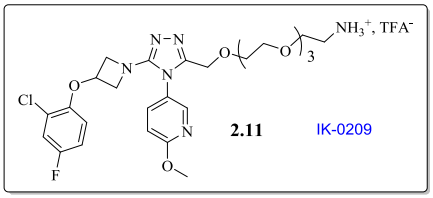

To a solution of **1.27** (0.038 mmol, 20 mg) in dry DMF (2.5 mL) under Ar at ice-water temperature KOH (0.29 mmol, 16.6 mg) was added. The resulting mixture was stirred for 15 min, then a solution of **2.8** (0.059 mmol, 32.4 mg) in dry DMF (2.5 mL) was added. The reaction mixture was stirred at ice-water temperature for 3 hours, then at r.t. overnight. To the resulting mixture water (50 mL) and DCM (50 mL) were added. The organic fraction was separated, washed with water (2×50 mL), brine (50 mL), dried over Na_2SO_4 and concentrated under vacuum. The residue was dissolved in dry DCM (2 mL) and treated with TFA (2 mL) for 30 min. The volatiles were removed under vacuum and the residue was purified by reverse phase flash chromatography eluted with solvent B in solvent A (30% to 100 % in 30 min) to afford **2.11** as a yellow oil (16 mg, 60%). ^{1}H NMR (400 MHz, DMSO-d_6) δ 8.35 (d, J = 2.5 Hz, 1H), 8.02 (brs, 3H), 7.90 (dd, J = 8.8, 2.5 Hz, 1H), 7.44 (dd, J = 8.3, 2.8 Hz, 1H), 7.17 – 7.04 (m, 1H), 7.00 (d, J = 8.8 Hz, 1H), 6.89 (dd, J = 9.1, 4.9 Hz, 1H), 5.14 – 5.00 (m, 1H), 4.34 (s, 2H), 4.25 – 4.15 (m, 2H), 3.91 (s, 3H), 3.86 (dd, J = 8.9, 4.3 Hz, 2H), 3.61 – 3.58 (m, 2H), 3.56 – 3.52 (m, 4H), 3.51 – 3.47 (m, 2H), 3.45 – 3.38 (m, 6H), 3.00 – 2.90 (m, 2H). ^{13}C NMR (101 MHz, DMSO-d_6) δ 163.94, 156.25 (d, J = 240.8 Hz), 149.21, 148.53, 148.51, 146.16, 138.83, 123.09, 122.07, 121.96, 117.61 (d, J = 26.6 Hz), 114.84 (d, J = 8.9 Hz), 114.83 (d, J = 22.6 Hz), 111.20, 69.78, 69.71, 69.68, 69.66, 69.44, 68.86, 68.36, 66.66, 61.75, 59.18, 53.86, 38.55. BRMS (ESI): $(M+H)^+$ calcd: 581.2, found: 581.2.

1-(5-(3-(2-chloro-4-fluorophenoxy)azetidin-1-yl)-4-(6-methoxypyridin-3-yl)-4H-1,2,4-triazol-3-yl)-2,5,8,11,14,17,20,23-octaoxapentacosan-25-aminium trifluoroacetate ***2.12***

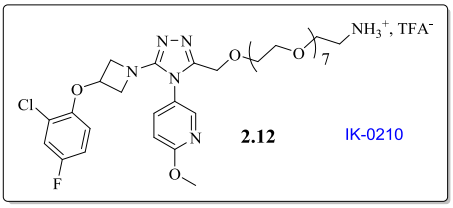

To a solution of **1.27** (0.038 mmol, 20 mg) in dry DMF (2.5 mL) under Ar at ice-water temperature KOH (0.29 mmol, 16.6 mg) was added. The resulting mixture was stirred for 15 min, then a solution of **2.10** (0.059 mmol, 37.4 mg) in dry DMF (2.5 mL) was added. The

reaction mixture was stirred at ice-water temperature for 3 hours, then at r.t. overnight. To the resulting mixture water (50 mL) and DCM (50 mL) were added. The organic fraction was separated, washed with water (2×50 mL), brine (50 mL), dried over Na_2SO_4 and concentrated under vacuum. The residue was dissolved in dry DCM (2 mL) and treated with TFA (2 mL) for 30 min. The volatiles were removed under vacuum and the residue was purified by reverse phase flash chromatography eluted with solvent B in solvent A (30% to 100 % in 30 min) to afford **2.12** as a colorless oil (10 mg, 30%). ^{1}H NMR (400 MHz, DMSO-d_6) δ 8.39 (d, J = 2.4 Hz, 1H), 8.14 – 7.82 (m, 4H), 7.46 (dd, J = 8.3, 3.0 Hz, 1H), 7.17 – 7.07 (m, 1H), 7.01 (d, J = 8.8 Hz, 1H), 6.90 (dd, J = 9.1, 4.9 Hz, 1H), 5.15 – 5.02 (m, 1H), 4.35 (s, 2H), 4.32 – 4.22 (m, 2H), 3.94 – 3.89 (m, 5H), 3.63 – 3.59 (m, 2H), 3.58 – 3.53 (m, 4H), 3.53 – 3.45 (m, 18H), 3.44 – 3.39 (m, 6H), 3.02 – 2.90 (m, 2H). ^{13}C NMR (101 MHz, DMSO-d_6) δ 164.13, 156.27 (d, J = 240.7 Hz), 148.94, 148.44, 148.41, 146.41, 138.98, 122.37, 122.04, 121.94, 117.62 (d, J = 26.5 Hz), 114.84 (d, J = 8.6 Hz), 114.82 (d, J = 22.6 Hz), 111.20, 69.76, 69.71, 69.66, 69.63, 69.40, 68.93, 68.29, 66.64, 61.53, 59.42, 53.87, 38.52. BRMS (ESI): $(M+H)^+$ calcd: 757.3, found: 757.2.

*General procedure for the coupling of fluorescein and DY647 onto compounds **2.11** and **2.12***. A solution of 5-SFX (1 eq.) or DY647-NHS (1 eq.) in anhydrous DMSO was added to a solution of **2.11** or **2.12** (0.9 eq.) in anhydrous DMSO, followed by DIEA (10 eq.). The reaction mixture was stirred at room temperature for 2 hours (**2.13** and **2.14**) or for 1 hour (**2.15** and **2.16**). The completion of the reaction was monitored by analytical RP-HPLC. The labeled compounds were isolated by HPLC using a linear gradient of solvent B in solvent A. Fractions containing the products of interest were lyophilized and further checked by analytical RP-HPLC.

*Fluorescein-labeled compound **2.13***. Yellow powder (350 nmol, 37%). RP-HPLC purity: >95%; T_r = 4.38 min. HRMS (ESI): calcd for $C_{53}H_{57}ClFN_7O_{13}$ $(M+2H)^{2+}/2$ 526.6843, found 526.6855.

*Fluorescein-labeled compound **2.14***. Yellow powder (574 nmol, 57%). RP-HPLC purity: >95%; T_r = 4.39 min. HRMS (ESI): calcd for $C_{61}H_{73}ClFN_7O_{17}$ $(M+2H)^{2+}/2$ 614.7368, found 614.7391.

*DY647-labeled compound **2.15***. Blue powder (150 nmol, 15%). RP-HPLC purity: >95%; T_r = 3.94 min. HRMS (ESI): calcd for $C_{58}H_{71}ClFN_8O_{13}S_2$ $(M+H)^+$ 1205.4255, found 1205.4251.

DY647-labeled compound ***2.16****.* Blue powder (480 nmol, 48%). RP-HPLC purity: >95%; T_r = 3.97 min. HRMS (ESI): calcd for $C_{66}H_{88}ClFN_8O_{17}S_2$ $(M+2H)^{2+}/2$ 691.2691, found 691.2696.

2.2. TR-FRET binding assays[19]

These assays were performed as previously described (Zwier et al., 2010). Briefly, HEK293 cells were cultivated in DMEM medium supplemented with 10% FCS and 1% penicillin/streptomycin antibiotics. As described in Cottet et al., 2011, confluent cells were dissociated and plated in black 96-well plates previously coated with poly-ornithine (diluted at 0.1 mg/mL in sterile water, incubated 30 min at 37 °C, washed with sterile PBS). The cells were treated with Lipofectamine 2000® complex of plasmid DNA coding for the OT, V_{1a}, V_{1b} or V_2 receptors fused to the SNAP-tag suicide enzyme in Opti-MEM® medium. Plates were incubated for 48 hours (OTR) or 24 hours (V_{1a}R, V_{1b}R or V_2R) at 37 °C and 5% CO_2. Expressed receptors fused to the SNAP-tag were then labeled with luminescent donor (BG-Lumi4-Tb) at 100 nM in 100 µL/well of Tag-lite® labelling medium, for 1 hour at 37 °C. Cells were then washed 3 times with Tag-lite® medium and then incubated with the fluorescent ligands. For saturation assays, increasing concentrations of fluorescent ligands were diluted in 100 µL of Tag-lite® medium. For competition assays, a fixed concentration of fluorescent ligand (equal to its K_d) was mixed with an increasing concentration of "cold" competitor ligand (OT, OTA or **31a**) in Tag-lite® medium. Plates were read in an HTRF®-compatible multi-well plate reader with a classic HTRF® protocol (excitation at 340 nM, donor emission measured at 620 nm and acceptor emission at 665 nm (DY647) or 520 nm (Fluor), 150 µs delay, 500 µs integration). To determine the incubation time necessary to reach the equilibrium, FRET and luminescence signals were measured after various times of incubation. Dissociation (saturation) and inhibition (competition) constants were determined when equilibrium is reached by fitting experimental data with Graphpad Prism 6 (GraphPad Software). For competition we used a 1 hour incubation at room temperature or a 4 hours long incubation at 4°C to prevent receptor internalization when OT is used.

[19] Performed by the author in IGF (Montpellier) with the help of Thiéric Rodriguez and Dr. Thierry Durroux.

3. Turn-on Nile red-based probes for OTR

3.1. Synthesis

General

Reagents were obtained from commercial sources and used without any further purification. Flash chromatography was performed on silica gel (40 μm, Grace) or RP18 (25−40 μm, Merck) prepacked columns on a SPOT II ultima from Armen. Semi-preparative HPLC chromatography was performed on SunFire C18 column (5 μm, 19 × 150 mm) or SymmetryShield C18 column (7 μm, 19 × 300 mm) on Gilson PLC2020. Analytical RP-HPLC separations were performed on Ascentis Express C18 column (2.7 μm, 4.6 mm × 75 mm) using a linear gradient (5% to 100% in 7.4 min, flow rate of 1.6 mL/min) of solvent B (0.1% TFA in CH_3CN, v/v) in solvent A (0.1% TFA in H_2O, v/v). Detection was set at 220 and 254 nm. NMR spectra were recorded at 400 and 500 MHz on a Bruker Advance spectrometer. Chemical shifts are reported in parts per million (ppm), coupling constants (*J*) are reported in hertz (Hz). Signals are described as s (singlet), d (doublet), t (triplet), m (multiplet), and brs (broad singlet). LC-MS spectra were obtained on a ZQ (Z quadripole) Waters/Micromass spectrometer equipped with an X-Terra C18 column (3.5 μm, 4.6 × 50 mm) using electrospray ionization mode (ESI). High resolution mass spectra (HRMS) were acquired on a Bruker MicroTof mass spectrometer, using electrospray ionization (ESI) and a time-of-flight analyzer (TOF).

Tert-butyl N-(23-azido-3,6,9,12,15,18,21-heptaoxatricosan-1-yl)-N-[(tert-butoxy) carbonyl]carbamate ***2.17***

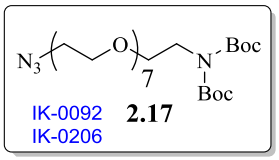

IK-0092 IK-0206 **2.17**

To a solution of **2.9** (0.19 mmol, 136 mg) in dry DMF (5 mL) sodium azide (0.28 mmol, 18.3 mg) was added. The reaction mixture was stirred at 50°C for 5 hours. To the resulting mixture water (50 mL) was added and the mixture was extracted with ethyl acetate (2×20 mL). The combined organic fractions were washed with water (3×20 mL), brine (20 mL) and concentrated under vacuum to give **2.17** as a colorless oil (104 mg, 93%). ^{1}H NMR (400 MHz, $CDCl_3$) δ 3.78 (t, *J* = 6.2 Hz, 2H), 3.70 – 3.57 (m, 28H), 3.39 (t, *J* = 5.1 Hz, 2H), 1.50 (s, 18H). ^{13}C NMR (101 MHz, $CDCl_3$) δ 152.79, 82.40, 70.87, 70.84, 70.80, 70.75, 70.38, 70.19, 69.45, 50.87, 45.37, 28.21. BRMS (ESI): $(M+Na)^+$ calcd: 617.3, found: 617.2.

Tert-butyl N-(23-amino-3,6,9,12,15,18,21-heptaoxatricosan-1-yl)-N-[(tert-butoxy)carbonyl]carbamate ***2.18***

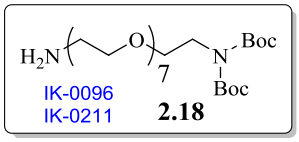

A mixture of **2.17** (0.16 mmol, 98 mg) and triphenylphosphine polymer-bound (1.4 mmol/g loading, 0.66 mmol, 461 mg) in THF/H_2O 4/1 (5 mL) was stirred at r.t. over a week-end. The resulting mixture was filtered and the volatiles were removed under vacuum to give **2.18** as a colorless oil (93 mg, quant.). ^{1}H NMR (400 MHz, $CDCl_3$) δ 3.77 (t, *J* = 6.2 Hz, 2H), 3.69 – 3.55 (m, 28H), 2.92 (t, *J* = 5.1 Hz, 2H), 1.49 (s, 18H), 1.42 (s, 2H). ^{13}C NMR (101 MHz, $CDCl_3$) δ 152.77, 82.39, 72.03, 70.68, 70.65, 70.59, 70.49, 70.34, 69.39, 45.33, 41.59, 28.19. BRMS (ESI): $(M+H)^+$ calcd: 569.4, found: 569.4.

Tert-butyl N-[(tert-butoxy)carbonyl]-N-[23-(2-{[8-(diethylamino)-12-oxo-12H-10-oxa-5-azatetraphen-3-yl]oxy}acetamido)-3,6,9,12,15,18,21-heptaoxatricos ***2.19***

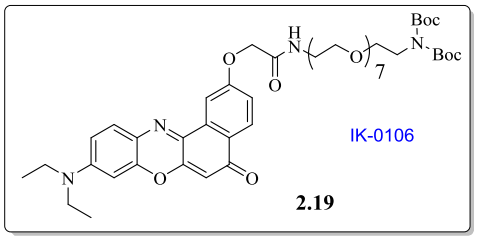

To a stirred solution of NR-COOH[20] (0.15 mmol, 61.4 mg) and **2.18** (0.15 mmol, 89 mg) in DMF anhydre (0.5 mL) a solution of PyBOP (0.31 mmol, 162.9 mg) in DMF anhydre (0.5 mL) and DIEA (0.63 mmol, 103.5 µL) were added. The reaction mixture was stirred at r.t. for 30 min. To the obtained mixture water (50 mL) was added and the mixture was extracted with DCM (2×20 mL). The combined organic fractions were washed with water (2×50 mL), brine (50 mL), dried over Na_2SO_4. The volatiles were removed under vacuum and the residue was purified by reverse phase flash chromatography eluted with ACN/H_2O (30% - 100% v/v in 30 min) to give **2.19** as a dark taffy (63 mg, 43%). ^{1}H NMR (400 MHz, DMSO-d_6) δ 8.27 (t, *J* = 5.6 Hz, 1H), 8.07 (d, *J* = 8.7 Hz, 1H), 8.00 (d, *J* = 2.3 Hz, 1H), 7.61 (d, *J* = 9.1 Hz, 1H), 7.31 (dd, *J* = 8.7, 2.3 Hz, 1H), 6.83 (dd, *J* = 9.1, 2.2 Hz, 1H), 6.66 (d, *J* = 2.2 Hz, 1H), 6.21 (s, 1H), 4.69 (s, 2H), 3.62 (t, *J* = 5.8 Hz, 2H), 3.56 – 3.40 (m, 34H), 1.42 (s, 18H), 1.16 (t, *J* = 6.9 Hz, 6H). ^{13}C NMR (101 MHz, DMSO-d_6) δ 181.32, 167.16, 160.22, 152.11, 151.81, 150.88, 146.49, 138.16, 133.47, 130.89, 127.26, 125.37, 123.95, 117.72, 110.15, 107.33, 104.12, 96.03, 81.67, 69.74, 69.56, 69.52, 68.84, 68.34, 67.00, 44.92, 44.43, 38.31, 27.54, 12.42. BRMS (ESI): $(M+Na)^+$ calcd: 965.5, found: 965.4.

[20] Synthesized by the group of Dr. Andrey Klymchenko (LBP, Illkirch) according to the protocol described in Kashida and Asanuma, 2012.

1-((9-(diethylamino)-5-oxo-5H-benzo[a]phenoxazin-2-yl)oxy)-2-oxo-6,9,12,15,18,21,24-heptaoxa-3-azahexacosan-26-aminium trifluoroacetate ***2.20***

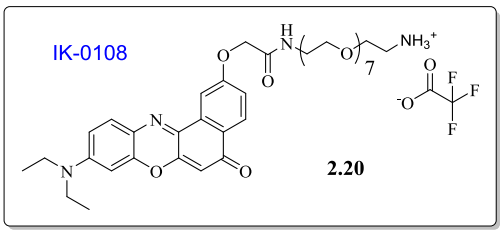

To a solution of **2.19** (0.06 mmol, 57 mg) in DCM (3 mL) TFA (2 mL) was added. The reaction mixture was stirred at r.t. for 30 min. The volatiles were removed under vacuum. To the residue water (5 mL) was added and the resulting mixture was lyophilized to give **2.20** as a dark taffy (59 mg, quant.). ^{1}H NMR (400 MHz, D_2O) δ 7.50 (d, *J* = 8.7 Hz, 1H), 7.02 – 6.83 (m, 2H), 6.80 (d, *J* = 9.3 Hz, 1H), 6.52 (d, *J* = 9.3 Hz, 1H), 5.97 (s, 1H), 5.61 (s, 1H), 4.22 (s, 2H), 3.83 – 3.54 (m, 28H), 3.54 – 3.45 (m, 2H), 3.44 – 3.27 (m, 4H), 3.27 – 3.11 (m, 2H), 1.18 (t, *J* = 6.8 Hz, 6H). ^{13}C NMR (101 MHz, D_2O) δ 172.36, 161.42, 154.81, 153.46, 148.83, 134.74, 133.28, 129.40, 129.01, 125.87, 124.84, 120.08, 115.61, 107.49, 104.47, 98.30, 84.14, 72.15, 72.12, 72.07, 72.03, 71.99, 71.96, 71.31, 68.87, 68.66, 48.19, 41.61, 41.27, 14.59. BRMS (ESI): $(M+2H)^{2+}/2$ calcd: 744.4, found: 744.4.

3-{[23-(2-{[8-(diethylamino)-12-oxo-12H-10-oxa-5-azatetraphen-3-yl]oxy}acetamido)-3,6,9,12,15,18,21-heptaoxatricosan-1-yl]carbamoyl}propanoic acid ***2.21***

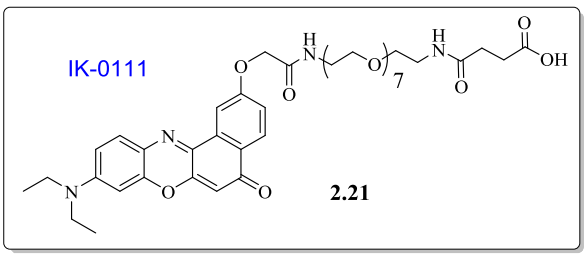

To a solution of **2.20** (0.053 mmol, 52 mg) in dry MeOH (5 mL) succinic anhydride (0.159 mmol, 15.9 mg) was added followed by DIEA (0.27 mmol, 44.2 µL). The reaction mixture was stirred at r.t. for 4 h, then water (20 mL) and DCM (20 mL) were added and the mixture was acidified with 1N HCl to pH 1. The organic layer was separated, washed with 1N HCl (2×20 mL), brine (20 mL) dried over Na_2SO_4. The volatiles were removed under vacuum to give **2.21** as a dark taffy (39 mg, 86%). ^{1}H NMR (400 MHz, DMSO-d_6) δ 12.04 (brs, 1H), 8.27 (t, *J* = 5.5 Hz, 1H), 8.07 (d, *J* = 8.6 Hz, 1H), 8.00 (s, 1H), 7.89 (t, *J* = 5.0 Hz, 1H), 7.61 (d, *J* = 9.1 Hz, 1H), 7.38 – 7.24 (m, 1H), 6.90 – 6.74 (m, 1H), 6.66 (s, 1H), 6.21 (s, 1H), 4.69 (s, 2H), 3.58 – 3.42 (m, 30H), 3.41 – 3.35 (m, 4H), 3.23 – 3.09 (m, 2H), 2.40 (t, *J* = 6.8 Hz, 2H), 2.30 (t, *J* = 6.8 Hz, 2H), 1.16 (t, *J* = 6.9 Hz, 6H). ^{13}C NMR (101 MHz, DMSO-d_6) δ 181.33, 173.78, 170.99, 167.18, 160.22, 151.82, 150.88, 146.49, 138.15, 133.47, 130.89, 127.26, 125.38, 123.95, 117.73, 110.16, 107.32, 104.12, 96.02, 69.74, 69.68, 69.55, 69.08, 68.83, 67.00, 44.44, 38.55, 38.31, 29.90, 29.10, 12.42. BRMS (ESI): $(M+2H)^{2+}/2$ calcd: 844.4, found: 844.4.

NR-PEG-CBT

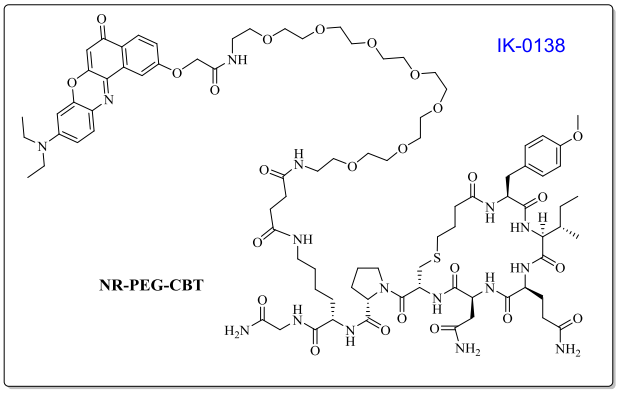

To a stirred solution of **2.21** (0.01 mmol, 9 mg) and Lys[8]-CBT (0.015 mmol, 16.7 mg) in dry DMF (1 mL) a solution of PyBOP (0.027 mmol, 14.2 mg) in dry DMF (1 mL) was added, followed by DIEA (0.086 mmol, 14.2 µL). The reaction mixture was stirred at r.t. for 40 min. The resulting mixture was purified by semi-preparative HPLC (SunFire column) eluted with solvent B in solvent A (5 min at 20% then 20 - 50% in 30 min) to give after lyophilization NR-PEG-CBT as a dark violet powder (7.8 mg, 40%). HRMS (ESI): calcd for $C_{87}H_{128}N_{16}O_{25}S$ $(M+2H)^{2+}/2$ 914.4479, found: 914.4479.

23-(4-(6-(2-(3-([1,1'-biphenyl]-4-yl)-5-methyl-4H-1,2,4-triazol-4-yl)-3-methylphenoxy)hexyl)piperazin-1-yl)-3,6,9,12,15,18,21-heptaoxatricosan-1-aminium trifluoroacetate ***2.22***

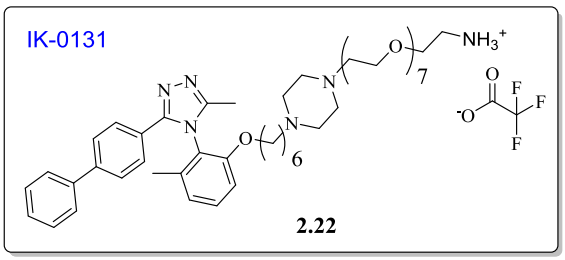

To a solution of EP (0.043 mmol, 22 mg) and K_2CO_3 (0.086 mmol, 12 mg) in dry DMF (1 mL) a solution of **2.10** (0.103 mmol, 65 mg) in dry DMF (1 mL) was added. The reaction mixture was stirred at 50°C overnight. To the resulting mixture water (20 mL) was added and the mixture was extracted with DCM (2×20 mL). The combined organic fractions were washed with brine (50 mL) and the volatiles were removed under vacuum. The residue was dissolved in 2 mL of DMSO and purified by semi-preparative flash chromatography eluted with solvent B in solvent A (3 min at 5%, then from 5 to 30% in 5 min, then from 30 to 55% in 25 min). The fractions containing the desired compound were concentrated under vacuum and the residue was dissolved in DCM (1 mL). The solution was treated with TFA (1 mL) for 30 min, then the volatiles were removed under vacuum and the residue was lyophilized from H_2O/ACN mixture to give **2.22** as a colorless oil (17 mg, 40%). ^{1}H NMR (400 MHz, MeOD) δ 7.68 – 7.57 (m, 4H), 7.54 – 7.40 (m, 5H), 7.40 – 7.32 (m, 1H), 7.11 (d, *J* = 8.4 Hz, 1H), 7.02 (d, *J* = 7.7 Hz, 1H), 4.14 – 3.95 (m, 2H), 3.87 – 3.77 (m, 2H), 3.76 – 3.70 (m, 2H), 3.70 – 3.57 (m, 24H), 3.45 (brs, 8H), 3.28 – 3.23 (m, 2H), 3.17 – 3.10 (m, 2H), 3.03 – 2.95 (m, 2H), 2.28 (s, 3H), 1.98 (s, 3H), 1.70 – 1.52 (m, 4H), 1.31 – 1.22 (m, 4H). ^{13}C NMR (101 MHz,

MeOD) δ 155.86, 144.66, 140.78, 138.16, 133.03, 130.10, 129.24, 128.91, 128.41, 127.99, 126.20, 124.22, 112.04, 71.41, 71.39, 71.35, 71.30, 71.26, 71.23, 71.15, 70.82, 69.80, 67.81, 66.90, 57.71, 57.34, 50.89, 50.84, 40.52, 29.64, 27.11, 26.65, 25.01, 17.30, 10.35. BRMS (ESI): $(M+H)^+$ calcd: 861.6, found: 861.2.

NR-PEG-EP

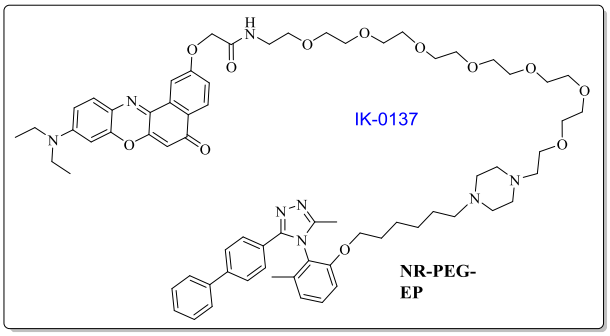

To a solution of **2.22** (0.017 mmol, 17 mg) and NR-COOH (0.017 mmol, 6.8 mg) in dry DMF (2 mL) PyBOP (0.043 mmol, 23 mg) was added followed by NEt_3 (0.139 mmol, 23 µL). The reaction mixture was stirred at r.t. for 2 hours. The resulting mixture was purified by semi-preparative HPLC eluted with solvent B in solvent A (5 min at 20%, then from 20 to 36% in 3 min, then from 36 to 50% in 17 min) to give after lyophilization NR-PEG-EP as a dark violet powder (7.8 mg, 36%). HRMS (ESI): calcd for $C_{70}H_{92}N_8O_{12}$ $(M+2H)^{2+}/2$ 618.34174, found: 618.34299.

NR-CBT

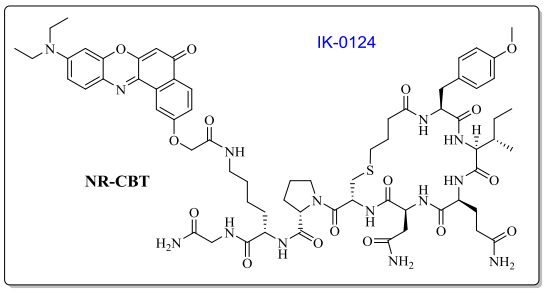

To a stirred solution of NR-COOH (0.016 mmol, 6.2 mg) and Lys^8-CBT (0.016 mmol, 17.7 mg) in dry DMF (1 mL) a solution of PyBOP (0.04 mmol, 21 mg) in dry DMF (0.5 mL) was added followed by DIEA (0.128 mmol, 21 µL). The reaction mixture was stirred at r.t. for 2 hours. The resulting mixture was purified by semi-preparative HPLC (SunFire column) eluted with solvent B in solvent A (20% for 6 min, then 20% - 40% in 10 min, then 40% - 43% in 25 min) to give after lyophilization NR-CBT as a violet solid (11 mg, 50%). HRMS (ESI): calcd for $C_{67}H_{89}N_{14}O_{16}S$ $(M+H)^+$ 1377.63017, found: 1377.62826.

LRh-CBT

To a stirred solution of **2.23** (5.6 µmol, 3.2 mg) and Lys[8]-CBT (5.6 µmol, 6.3 mg) in dry DMF (0.5 mL) NEt_3 (28.2 µmol, 4µL) was added. The reaction mixture was stirred at r.t. overnight. The resulting mixture was purified by semi-preparative HPLC (SunFire column) eluted with solvent B in solvent A (20 to 35% in 8 min then 35 - 65% in 30 min) to give after lyophilization LRh-CBT as a deep violet solid (3.6 mg, 41%). HRMS (ESI): calcd for $C_{72}H_{99}N_{14}O_{18}S_3$ $(M+H)^+$ 1543.64240, found: 1543.64210.

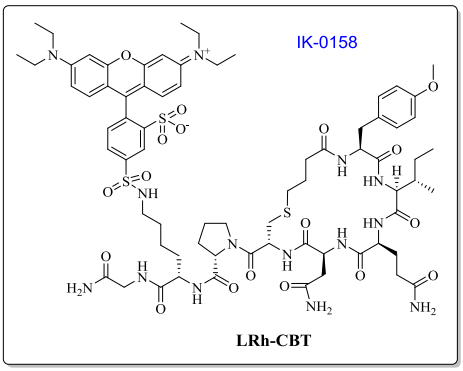

3.2. Pharmacological characterization

Determination of the affinity by radioligand binding assay[21]

The inhibition constants (K_i) of turn-on compounds for human OTR were determined on membrane preparations from CHO cells stably expressing the receptor by competition binding assays. Binding experiments were performed at 30°C using [^{3}H]-AVP as the radioligand and 10 µg of CHO cell membrane proteins (K_d for [^{3}H]-AVP to the human OTR expressed in this system has been published previously and is 1.36 nM (Breton et al., 2001)). Briefly, membranes were incubated in 50 mM Tris-HCl pH 7.4, 5 mM $MgCl_2$ supplemented with 1 mg/mL BSA (binding buffer) and with radiolabeled and displacing ligands for 30 min. Competition experiments were conducted using [^{3}H]-AVP (1-2 nM) and varying concentrations of the unlabeled ligands from 0.1 nM to 1 µM. Nonspecific binding was determined by adding unlabeled AVP (10 µM). Bound and free radioactivity were separated by filtration over Whatman GF/C filters pre-soaked in a 10 mg/mL BSA solution for 3-4 h. The ligand binding data were analyzed by nonlinear least-squares regression using the computer program GraphPad Prism. All assays were performed in triplicate on at least three independent batches of cell membranes.

[21] Performed by Dr. Christiane Mendre and Dr. Bernard Mouillac (IGF, Montpellier).

In vitro functional assay (calcium measurement)[22]

Cell treatment was performed as described in Weill et al., 2011. Briefly, HEK293 cells were loaded with 5 µM of the calcium-sensing dye Indo-1 acetoxy-methyl ester (Indo-1 AM) in Hepes buffer (10 mM Hepes, 137,5 mM NaCl, 1,25 mM $MgCl_2$, 1,25 mM $CaCl_2$, 6 mM KCl, 0,4 mM NaH_2PO_4 and 5,6 mM glucose, pH 7.4) supplemented with 1 mg/mL BSA, for 45 minutes at 37°C in the presence of 5% CO_2. After washing they were collected in Hepes-bovine serum albumin buffer at 1.3×10^6 cells/ml and seeded into 384 well polystyrene plates (Greiner 781091) in order to get 50 000 cells/well and then centrifuged 5 min at 800 rpm.

Intracellular Ca^{2+} release measurement was performed by monitoring the fluorescence of the ratiometric calcium probe Indo-1 using the FlexStation® 3 microplate reader (Molecular Devices Corp., Palo Alto, CA, USA). Fluorescence (excitation at 338 nm, emissions recorded at 401 nm and 475 nm, which excluded any spectral overlap with Nile Red-based probes) was acquired at room temperature over a 3 minute kinetic period.

Fluorescence emission ratio (signal = (fluorescence measured at 401 nm)/(fluorescence measured at 475 nm)) was calculated in order to follow the calcium release. Minimum signal was obtained before addition of compound treatment and maximum signal was given after digitonin addition. Normalization was done using the following equation:

Normalized Signal = 100 × (signal – signal min)/(signal max – signal min)

Addition of compounds was performed by using the FlexStation® 3 apparatus 30s after the beginning of readings.

For the agonist assay, compounds were tested at final concentrations ranging from 0.03 nM to 3 µM. For the antagonist assay, compounds at final concentrations from 0.3 nM to 30µM were mixed with oxytocin (20 nM) before cell treatment.

In order to assess the maximum calcium level, addition of digitonin (Sigma Aldrich) (100 µM) was performed 110 s after compound treatment.

Dose-response curves were obtained by plotting the normalized signal of calcium release against the logarithmic values of compound concentration. The half maximal inhibitory concentration (IC_{50}) and the half maximal effective concentration (EC_{50}) were calculated for each tested compound.

[22] Performed by Christel Valencia (PCBIS, Illkirch).

Measurements of receptor expression levels[23]

[^{3}H]-AVP binding to whole cells was performed as follows : HEK OTR+ cells were seeded into 24-well plates pretreated with poly-ornithine and incubated into Dulbecco's Modified Eagle's medium (DMEM) supplemented with 10% fetal calf serum, 100U/mL penicillin/streptomycin and 500 µg/mL of G418 at 37°C in a humidified 5% CO_2 atmosphere. After 48h seeding, the plates were placed on ice and cells were washed three times with 250 µL ice-cold HBS (HEPES buffer pH 7.4, 2.2 mM $MgCl_2$, 1 mg/mL BSA, 0.1 mM phenylalanine). For saturation studies, cells were incubated 3.5 hours at 4°C with HBS containing increasing [^{3}H]-AVP concentrations (from 0.2 to 20 nM). An excess of unlabeled AVP (2 µM) was also added in the medium to determine the non-specific binding. After 4 washings with ice-cold HBS, the cells were lysed 15 min at 37°C with 400 µL of 0.1 M NaOH. Then 100 µL of 0.4 M acetic acid was added. The lysates were transferred into scintillation vials and their radioactivity determined. The specific binding was calculated as the difference between the total binding and the non-specific binding. Scatchard analysis expressing the ratio of Bound/Free versus Bound with the software Kell Ligand allows the determination of the maximum number of receptor sites. Statistics were performed on three experiments.

Protein quantification was determined using the BCA method (Smith et al., 1985).

3.3. Cell culture and preparation of lipid vesicles

Cell culture[24]

HEK293 (OTR-) and HEK pIRESneo3-OXTR (OTR+) cells were cultured in Eagle's minimal essential medium (MEM, Invitrogen 21090) with 10% heat-inactivated fetal bovine serum, 100 U/mL of penicillin, 100 µg/mL of streptomycin, 2 M of glutamine and 500µg/mL of G418 in the case of OTR+ cells at 37 °C in a humidified 5% CO_2 atmosphere. Cell concentration of 3-5×10^5 cells/mL was maintained by removal of a portion of the culture and replacement with fresh medium twice a week.

For fluorescence spectroscopy experiments, cells were detached by treatment with Accutase® solution (Aldrich). After MEM removal, cells were washed twice with HBS. Accutase® solution was added and the cells were incubated for 3 min at room temperature.

[23] Performed by Dr. Christiane Mendre and Dr. Bernard Mouillac (IGF, Montpellier).
[24] Performed by the author in LBP (Illkirch) with the help of Rémy Kreder.

The solution of detached cells was then diluted with HBS, transferred to Falcon tubes and centrifuged at 900 rpm for 5 min. The washing procedure was repeated one more time and the cells were suspended in HBS at 50×10^6 cells/mL.

For confocal microscopy studies, cells were seeded onto a chambered cover glass (IBiDi) at a density of 5×10^4 cells/IBiDi. Cells were washed two times by gentle rinsing with HBS, then 0.8 mL of fresh HBS was added followed by 0.2 mL of HBS solution of fluorescent ligand. If not mentioned, the incubation time was 5 min at 25°C.

Lipid vesicles[25]

Dioleoylphosphatidylcholine (DOPC) was purchased from Sigma-Aldrich. Large unilamellar vesicles (LUVs) were obtained by the extrusion method, as previously described (Hope et al., 1985). Briefly, a suspension of multilamellar vesicles was extruded by using a Lipex Biomembranes extruder (Vancouver, Canada). The size of the filters was first 0.2 μm (7 passages) and thereafter 0.1 μm (10 passages). This generates monodisperse LUVs with a mean diameter of 0.11 μm as measured with a Malvern Zetamaster 300 (Malvern, U.K.).

3.4. Fluorescence spectroscopy and microscopy

Absorption spectra were recorded on a Cary 4000 spectrophotometer (Varian) and fluorescence spectra on a FluoroLog 3 (Jobin Yvon, Horiba) spectrofluorometer. Fluorescence emission spectra were systematically recorded at 520 nm excitation wavelength at 20°C. All spectra were corrected from the fluorescence of the corresponding blank (suspension of cells or lipid vesicles without the probe) and for instrumental effects. Fluorescence quantum yields (QY) were measured using Nile Red in 1,4-dioxane as a reference (QY = 70%; Sackett and Wolff, 1987). Fluorescence confocal microscopy experiments[26] were performed on a Leica TCS SPE-II microscope with a HXC PL APO 63x/1.40 OIL CS objective. For confocal images, NR-PEG-CBT, NR-PEG-EP and NR-CBT were excited at 488 nm, LRh-CBT at 561 nm.

[25] Performed by Rémy Kreder (LBP, Illkirch)
[26] Performed by the author with the help of Rémy Kreder.

4. Turn-on squaraine-based probes for OTR

4.1. Synthesis

General

Reagents were obtained from commercial sources and used without any further purification. Flash chromatography was performed on RP18 (25−40 μm, Merck) prepacked columns on a SPOT II ultima from Armen. Semi-preparative HPLC chromatography was performed on SunFire C18 column (5 μm, 19 × 150 mm) on Gilson PLC2020. Analytical RP-HPLC separations were performed on Ascentis Express C18 column (2.7 μm, 4.6 mm × 75 mm) using a linear gradient (5% to 100% in 7.4 min, flow rate of 1.6 mL/min) of solvent B (0.1% TFA in CH_3CN, v/v) in solvent A (0.1% TFA in H_2O, v/v). Detection was set at 220 and 254 nm. NMR spectra were recorded at 500 MHz on a Bruker Advance spectrometer. Chemical shifts are reported in parts per million (ppm), coupling constants (*J*) are reported in hertz (Hz). Signals are described as s (singlet), d (doublet), t (triplet), m (multiplet), and brs (broad singlet). LC-MS spectra were obtained on a ZQ (Z quadripole) Waters/Micromass spectrometer equipped with an X-Terra C18 column (3.5 μm, 4.6 × 50 mm) using electrospray ionization mode (ESI). High resolution mass spectra (HRMS) were acquired on a Bruker MicroTof mass spectrometer, using electrospray ionization (ESI) and a time-of-flight analyzer (TOF).

(Z)-4-((1-(1-ammonio-25-oxo-3,6,9,12,15,18,21-heptaoxa-24-azaoctacosan-28-yl)-3,3-dimethyl-3H-indol-1-ium-2-yl)methylene)-2-(((Z)-1-ethyl-3,3-dimethylindolin-2-ylidene)methyl)-3-oxocyclobut-1-en-1-olate trifluoroacetate ***2.25***

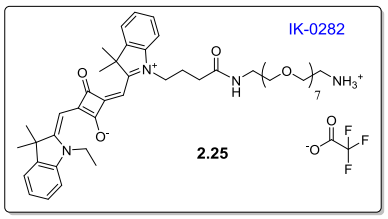

To a stirred solution of SQ-COOH[27] (1 eq., 17 mg, 0.0333 mmol) and **2.24** (1.5 eq., 23.4 mg, 0.0499 mmol) in dry DMF (1 mL) PyBOP (1.5 eq., 26 mg, 0.0499 mmol) and DIEA (8 eq., 34.4 mg, 44 μL, 0.266 mmol) were added. The reaction mixture was stirred at room temperature overnight. The resulting mixture was purified by reverse phase flash chromatography eluted with solvent B in solvent A (from 30% to 100% in 30 min). The volatiles were removed under vacuum and the residue was dissolved in DCM (1 mL) and treated with TFA (1 mL) for 30 min. The volatiles were removed under vacuum and the residue was lyophilized from ACN/H_2O mixture to give

[27] Prepared by Rémy Kreder (LBP, Illkirch)

2.25 as a dark taffy (15 mg, 46%). ^{1}H NMR (500 MHz, DMSO-d_6) δ 7.97 (t, J = 5.4 Hz, 1H), 7.82 (brs, 3H), 7.56 – 7.45 (m, 2H), 7.39 – 7.27 (m, 4H), 7.20 – 7.11 (m, 2H), 5.84 – 5.77 (m, 2H), 4.20 – 3.99 (m, 4H), 3.61 – 3.57 (m, 2H), 3.57 – 3.52 (m, 4H), 3.51 – 3.46 (m, 20H), 3.43 – 3.36 (m, 2H), 3.26 – 3.15 (m, 2H), 3.00 – 2.93 (m, 2H), 2.25 (t, J = 7.1 Hz, 2H), 1.99 – 1.87 (m, 2H), 1.73 – 1.62 (m, 12H), 1.32 – 1.19 (m, 3H). ^{13}C NMR (126 MHz, DMSO-d_6) δ 180.66, 178.73, 178.45, 171.28, 169.01, 168.78, 142.23, 141.69, 141.58, 141.43, 128.01, 127.95, 123.74, 123.64, 122.27, 122.22, 110.24, 110.12, 86.04, 85.75, 69.75, 69.66, 69.62, 69.55, 69.07, 66.67, 54.89, 48.74, 42.51, 38.63, 38.54, 38.00, 31.83, 26.53, 26.41, 22.52, 11.73. BRMS (ESI): $(M+H)^+$ calcd: 861.5, found: 861.5.

(Z)-4-((1-(1-carboxy-3,29-dioxo-7,10,13,16,19,22,25-heptaoxa-4,28-diazadotriacontan-32-yl)-3,3-dimethyl-3H-indol-1-ium-2-yl)methylene)-2-(((Z)-1-ethyl-3,3-dimethylindolin-2-ylidene)methyl)-3-oxocyclobut-1-en-1-olate ***2.26***

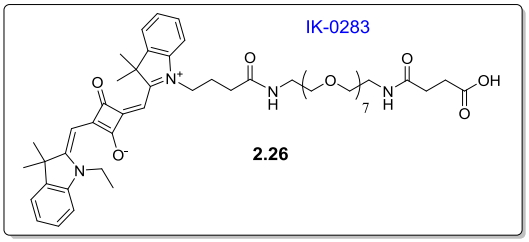

To a solution of **2.25** (1 eq., 15 mg, 0.0154 mmol) in dry MeOH (1 mL) succinic anhydride (5 eq., 7.7 mg, 0.0769 mmol) was added followed by DIEA (10 eq., 19.9 mg, 25.4 μL, 0.154 mmol). The reaction mixture was stirred at r.t. for 1 hour. MeOH was evaporated under vacuum and the residue was purified by semi-preparative HPLC eluted with solvent B in solvent A (from 30% to 100% in 30 min) to give **2.26** as a dark taffy (10.4 mg, 70%). ^{1}H NMR (500 MHz, DMSO-d_6) δ 8.01 – 7.93 (m, 1H), 7.92 – 7.84 (m, 1H), 7.57 – 7.47 (m, 2H), 7.40 – 7.28 (m, 4H), 7.22 – 7.12 (m, 2H), 5.87 – 5.74 (m, 2H), 4.23 – 3.99 (m, 4H), 3.63 – 3.27 (m, 28H), 3.25 – 3.12 (m, 4H), 2.40 (t, J = 6.8 Hz, 2H), 2.30 (t, J = 6.8 Hz, 2H), 2.28 – 2.20 (m, 2H), 1.98 – 1.86 (m, 2H), 1.68 (s, 12H), 1.28 (t, J = 7.1 Hz, 3H). ^{13}C NMR (126 MHz, DMSO-d_6) δ 180.59, 178.84, 178.59, 173.80, 171.21, 171.00, 169.01, 168.72, 142.27, 141.68, 141.59, 141.42, 127.99, 127.95, 123.71, 123.62, 122.28, 122.22, 110.23, 110.10, 86.02, 85.73, 69.76, 69.58, 69.54, 69.10, 69.08, 48.73, 42.47, 38.57, 38.54, 37.97, 31.80, 29.91, 29.12, 26.53, 26.41, 22.50, 11.73. HRMS (ESI): calcd for $C_{52}H_{74}N_4O_{13}$ $(M+2H)^{2+}/2$ 481.26262, found: 481.26232.

SQ-PEG-CBT

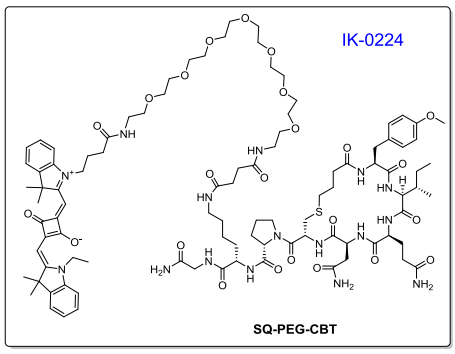

To a stirred solution of **2.26** (1.1 eq., 0.01 mmol, 10 mg) and Lys[8]-CBT (1 eq., 0.0948 mmol, 10.5 mg) in dry DMF (1 mL) a solution of PyBOP (2.7 eq., 0.026 mmol, 13.5 mg) in dry DMF (1 mL) was added followed by DIEA (9 eq., 0.083 mmol, 13.7 µL). The reaction mixture was stirred at room temperature for 40 min. The resulting mixture was purified by semi-preparative HPLC eluted with solvent B in solvent A (5 min at 20% then 5-35 min from 20 to 50%) to give SQ-PEG-CBT as a dark taffy (5.3 mg, 30%). HRMS (ESI): calcd for $C_{97}H_{142}N_{16}O_{24}S$ $(M+2H)^{2+}/2$ 973.50518, found: 973.50242.

4.2. Pharmacological characterizations[28]

For saturation assays, 10 µL of a 1×10^6 cells/mL suspension of defreezed Lumi4-Tb-SNAP-OTR cells in Tag-lite® buffer were distributed in each well of a 384-well plate (CORNING 3824). Increasing concentrations of SQ-PEG-CBT were diluted in 5 µL of Tag-lite® medium and added to the cells together with 5µL of Tag-lite® buffer (total binding) or 5µL of an oxytocin solution at final concentration of 10 µM (non-specific binding).

The plate was incubated for 3 hours at room temperature before reading on the Envision plate reader (Perkin Elmer) with a classical HTRF® protocol (excitation at 337 nm, emission at 665 and 615 nm). The dissociation constant (K_d) was calculated using GraphPad Prism Software (GraphPad, San Diego, CA, USA).

4.3. Cell culture and preparation of lipid vesicles

Cell culture

HEK293 pIRESneo3-OXTR (wtOTR) and HEK293 pIREShyg3-SP-GFP-OXTR (GFP-OTR) cells were cultured in Eagle's minimal essential medium (MEM, Invitrogen 21090) with 10% heat-inactivated fetal bovine serum, 100 U/mL of penicillin, 100 µg/mL of streptomycin, 2 M of glutamine and 500µg/mL of G418 for wtOTR cells or 50µg/mL of

[28] Performed by Christel Valencia (PCBIS, Illkirch)

hygromycin B for GFP-OTR cells at 37 °C in a humidified 5% CO_2 atmosphere. 70-80% cell confluence was maintained by removal of a portion of the culture and replacement with fresh medium twice a week.

For fluorescence spectroscopy experiments (Figure 40A), cells were detached by treatment with a trypsin solution (Aldrich). The solution of detached cells was diluted with MEM, transferred to Falcon tubes and centrifuged at 900 rpm for 5 min. Cells were then washed twice with PBS. Finally, cells were suspended in Leibovitz's L-15 medium (no phenol red) at 10^6 cells/mL.

For confocal microscopy studies, cells were seeded onto a chambered cover glass (IBiDi) at a density of 5×10^4 cells/IBiDi. Cells were washed two times by gentle rinsing with PBS, then a solution of SQ-PEG-CBT or NR-PEG-CBT in 1 mL of Leibovitz's L-15 medium (no phenol red) was added.

Lipid vesicles[29]

Dioleoylphosphatidylcholine (DOPC) was purchased from Sigma-Aldrich. Large unilamellar vesicles (LUVs) were obtained by the extrusion method, as previously described (Hope et al., 1985). Briefly, a suspension of multilamellar vesicles was extruded by using a Lipex Biomembranes extruder (Vancouver, Canada). The size of the filters was first 0.2 μm (7 passages) and thereafter 0.1 μm (10 passages). This generates monodisperse LUVs with a mean diameter of 0.11 μm as measured with a Malvern Zetamaster 300 (Malvern, U.K.).

4.4. Fluorescence spectroscopy and microscopy

Absorption spectra were recorded on a Cary 4000 spectrophotometer (Varian) and fluorescence spectra on a FluoroMax 3 (Jobin Yvon, Horiba) spectrofluorometer. Fluorescence spectra were systematically recorded at 600 nm excitation wavelength at 20°C. All spectra were corrected for instrumental effects. Fluorescence quantum yields (QY) were measured using DID in MeOH as a reference (QY = 33%; Texier et al., 2009).

Fluorescence confocal microscopy experiments were performed on a Leica TCS SPE-II microscope with a HXC PL APO 63x/1.40 OIL CS objective. GFP excitation was performed with 488 nm 10 mW laser (30% intensity), the excitation of SQ-PEG-CBT was performed with 635 nm 18 mW laser (30% intensity). Photobleaching experiments were conducted by

[29] Performed by Rémy Kreder (LBP, Illkirch)

exciting NR-PEG-CBT with 488 nm laser at 100% intensity and SQ-PEG-CBT with 635 nm laser at 25% intensity. Timelaps experiments of 50 frames (2 scans par frame, minimal time between frames) were performed.

4.5. Turn-on assay on wild-type OTR[30]

For fluorescence spectroscopy experiments, wtOTR cells were detached by treatment with Accutase® solution (Aldrich). The solution of detached cells was then diluted with MEM, transferred to Falcon tubes and centrifuged at 1500 rpm for 5 min. The washing procedure with HEPES was performed twice. The cells were suspended in HEPES buffer at 10^6 cells/mL.

The cell suspension was placed in a fluorescence glass cuvette with a stirring bar and solutions of SQ-PEG-CBT alone or with 10 µM of CBT were added. Fluorescence measurements were performed on a FluoroLog 3 (Jobin Yvon, Horiba). Fluorescence spectra were recorded at 600 nm excitation wavelength at 20°C and were corrected for instrumental effects and for the fluorescence of the corresponding blank (suspension of cells alone or with 10 µM of CBT).

Fluorescence intensity at 655 nm as a function of ligand concentration was plotted using GraphPad Prism Software (GraphPad, San Diego, CA, USA).

[30] Performed by the author with the help of Sophie Gioria (PCBIS, Illkirch).

5. Squaraine-dimers as a new concept of fluorogenic probes

5.1. Solid-phase synthesis of squaraine-dimers

General

Reagents were obtained from commercial sources and used without any further purification. Semi-preparative HPLC chromatography was performed on SunFire C18 column (5 µm, 19 × 150 mm) on Gilson PLC2020 with absorption detection. Analytical RP-HPLC separations were performed on Ascentis Express C18 column (2.7 µm, 4.6 mm × 75 mm) using a linear gradient (5% to 100% in 7.4 min, flow rate of 1.6 $mL \cdot min^{-1}$) of solvent B (0.1% TFA in CH_3CN, v/v) in solvent A (0.1% TFA in H_2O, v/v). Detection was set at 220 and 254 nm. High resolution mass spectra (HRMS) were acquired on a Bruker MicroTof mass spectrometer, using electrospray ionization (ESI) and a time-of-flight analyzer (TOF).

General procedure for the synthesis of squaraine-dimers

Solid-phase reactions were performed in polypropylene tubes equipped with polyethylene frits and polypropylene caps using an orbital agitator shaking device. Wang resin was purchased from Novabiochem® and the overall yields for the solid-phase syntheses were calculated based on the initial loadings provided by the supplier (0.86 mmol/g).

Fmoc-NH-PEG3-COOH (Scheme 20) was synthesized as previously described (Soriano et al., 2009) with additional HPLC purification.

Fmoc-β-Ala-OH (10 eq.) was introduced after the symmetrical anhydride formation with DIC (5 eq.) in DMF in the presence of DMAP (0.1 eq.). The reaction was left for 1 hour at room temperature.

All Fmoc-protected amino acids (1.5 eq.) and SQ-COOH[31] (2.5 eq.) or SQpeg-COOH[32] (2.5 eq.) were coupled in DMF for 45 min using PyBOP (1 eq. corresponding to the amino-acid used) with DIEA (8 eq.) as activating agent (Scheme 21 and Scheme 22). Fmoc-α-sulfo-β-alanine (2 eq.) was coupled in a mixture of NMP and DMF for 45 min using PyBOP (2 eq.) with DIEA (8 eq.) as previously described (Romieu et al., 2008).

The cleavages of Fmoc protecting groups were performed in 20% piperidine/DMF (2 times for 15 min).

[31] Synthesized by Rémy Kreder (LBP, Illkirch)
[32] Synthesized by Dr. Mayeul Collot (LBP, Illkirch)

The completion of couplings and Fmoc cleavages was monitored with the ninhydrin test (Kaiser et al., 1970) and the TNBS test (Hancock and Battersby, 1976) as well as by analytical HPLC (minicleavages of the resin with TFA/H_2O 95/5).

The chains were cleaved from the solid phase by treatment with TFA/H_2O 95/5 for 3 hours, then the volatiles were removed under vacuum.

*Squaraine-dimer **2.27***

Crude product was purified by semi-preparative HPLC chromatography eluted with solvent B in solvent A: 20% for 5 min, then from 20% to 65% in 25 min. Yield 12%. HRMS (ESI): calc. for $C_{113}H_{157}N_{15}O_{25}$ $(M+2H)^{2+}/2$ 1062.07376; found 1062.07301.

*Squaraine-dimer **2.28***

Crude product was purified by semi-preparative HPLC chromatography eluted with solvent B in solvent A: 20% for 5 min, then from 20% to 60% in 25 min. Yield 28%. HRMS (ESI): calc. for $C_{127}H_{186}N_{15}O_{33}$ $(M+3H)^{3+}/3$ 816.44458; found 816.44457.

*Squaraine-dimer **2.29***

Crude product was purified by semi-preparative HPLC chromatography eluted with solvent B in solvent A: 20% for 5 min, then from 20% to 65% in 25 min. Yield 16%. HRMS (ESI): calc. for $C_{116}H_{163}N_{16}O_{29}S$ $(M+3H)^{3+}/3$ 758.71642; found 758.71766.

General procedure for the conjugation with Lys^8-CBT

To a solution of **2.27**, **2.28** or **2.29** (1 eq.) and Lys^8-CBT (1.5 eq.) in dry DMF (0.5 mL/µmol) PyBOP (2.5 eq.) was added followed by DIEA (18 eq.). The reaction mixture was stirred at room temperature for 30 min. The resulting mixture was purified by semi-preparative HPLC eluted with solvent B in solvent A (20% for 5 min, then from 20% to 60% in 30 min) and then lyophilized to afford **2.30**, **2.31** or **2.32** as dark powders.

*Conjugate **2.30***

Yield 49%. HRMS (ESI): calc. for $C_{158}H_{226}N_{27}O_{36}S$ $(M+3H)^{3+}/3$ 1036.54682; found 1036.54737.

*Conjugate **2.31***

Yield 61%. HRMS (ESI): calc. for $C_{172}H_{255}N_{27}O_{44}S$ $(M+4H)^{4+}/4$ 858.70668; found 858.70597.

*Conjugate **2.32***

Yield 54%. HRMS (ESI): calc. for $C_{161}H_{232}N_{28}O_{40}S_2$ $(M+4H)^{4+}/4$ 815.41055; found 815.41105.

5.2. Fluorescence spectroscopy

Absorption spectra were recorded on a Cary 4000 spectrophotometer (Varian) and fluorescence spectra on a FluoroMax 3 (Jobin Yvon, Horiba) spectrofluorometer. Fluorescence spectra were systematically recorded at 600 nm excitation wavelength at 20°C. All spectra were corrected for instrumental effects. Fluorescence quantum yields (QY) were measured using DID in MeOH as a reference (QY = 33%; Texier et al., 2009).

5.3. Pharmacological characterizations[33]

For saturation assays, 10 µL of a 1×10^6 cells/mL suspension of defreezed Lumi4-Tb-SNAP-OTR cells in Tag-lite® buffer were distributed in each well of a 384-well plate (CORNING 3824). Increasing concentrations of **2.30**, **2.31** or **2.32** were diluted in 5 µL of Tag-lite® medium and added to the cells together with 5µL of Tag-lite® buffer (total binding) or 5µL of a carbetocin solution at final concentration of 10 µM (non-specific binding).

The plate was incubated for 3 hours at room temperature before reading on the Envision plate reader (Perkin Elmer) with a classical HTRF® protocol (excitation at 337 nm, emission at 665 and 615 nm). The dissociation constants (K_d) were calculated using GraphPad Prism Software (GraphPad, San Diego, CA, USA).

5.4. Cell culture and preparation of lipid vesicles

Cell culture

HEK293 pIRESneo3-OXTR (wtOTR) or HEK293 pIREShyg3-SP-GFP-OXTR (GFP-OTR) cells were cultured in Eagle's minimal essential medium (MEM, Invitrogen 21090) with 10% heat-inactivated fetal bovine serum, 100 U/mL of penicillin, 100 µg/mL of streptomycin, 2 M of glutamine and 500 µg/mL of G418 for wtOTR or 50µg/mL of

[33] Performed by Christel Valencia (PCBIS, Illkirch)

hygromycin B for GFP-OTR at 37 °C in a humidified 5% CO_2 atmosphere. 70-80% cell confluence was maintained by removal of a portion of the culture and replacement with fresh medium twice a week.

For microscopy studies, cells were seeded onto a chambered cover glass (IBiDi) at a density of 5×10^4 cells/IBiDi. Cells were washed two times by gentle rinsing with PBS, then solutions of fluorescent ligands in 1 mL of Leibovitz's L-15 medium (no phenol red) were added.

Lipid vesicles[34]

Dioleoylphosphatidylcholine (DOPC) was purchased from Sigma-Aldrich. Large unilamellar vesicles (LUVs) were obtained by the extrusion method, as previously described (Hope et al., 1985). Briefly, a suspension of multilamellar vesicles was extruded by using a Lipex Biomembranes extruder (Vancouver, Canada). The size of the filters was first 0.2 μm (7 passages) and thereafter 0.1 μm (10 passages). This generates monodisperse LUVs with a mean diameter of 0.11 μm as measured with a Malvern Zetamaster 300 (Malvern, U.K.).

5.5. Confocal microscopy and FLIM

Fluorescence confocal microscopy experiments were performed on a Leica TCS SPE-II microscope with a HXC PL APO 63x/1.40 OIL CS objective. GFP excitation was performed with 488 nm 10 mW laser (30% intensity), the excitation of SQ-PEG-CBT was performed with 635 nm 18 mW laser (30% intensity). Image treatment was proceeded using ImageJ (Wayne Rasband, National Institute of Mental Health, Bethesda). The graphs were plotted using GraphPad Prism Software (GraphPad, San Diego, CA, USA).

Time-correlated single-photon-counting (TCSPC) FLIM[35] was performed on a custom two-photon system laser-scanning setup based on an Olympus IX70 inverted microscope (Olympus, Japan) with an Olympus 60×1.2NA water immersion objective as previously described (Fritz et al., 2008). Two-photon excitation at 800 nm was provided by a mode-locked titanium-sapphire laser (Tsunami; Spectra Physics, CA), and the laser power was adjusted to give count rates with peaks up to 10^6 photons/s. Imaging was carried out with a laser-scanning system using two fast galvanometer mirrors (model 6210; Cambridge

[34] Prepared by Rémy Kreder (LBP, Illkirch)
[35] Performed by the author with the help of Dr. Ludovic Richert (LBP, Illkirch)

Technology, MA), operating in the descanned fluorescence collection mode. The fluorescence was directed to a fiber-coupled Avalanche photodetector (APD) (SPCM-AQR-14-FC; PerkinElmer, Canada), which was connected to a time-correlated single-photon-counting module (SPC830; Becker and Hickl, Germany), which operates in the reversed start-stop mode. Typically, the samples were scanned continuously for about 60 s to achieve appropriate photon statistics to analyze the fluorescence decays. Data were analyzed with a commercial software package (SPCImage V3.2; Becker and Hickl, Germany), which uses an iterative reconvolution method to recover the lifetimes from the fluorescence decays.

5.6. Time-resolved measurements [36]

Time-resolved fluorescence measurements were performed with the time-correlated, single-photon counting technique using the excitation pulses at 310 nm provided by a pulse-picked frequency-tripled Ti-sapphire laser (Tsunami, Spectra Physics) pumped by a Millenia X laser (Spectra Physics). The fluorescence decays were collected at the magic angle (54.7°) of the emission polarizer in order to avoid any artifact due to vertically polarized excitation beam. The single-photon events were detected with a microchannel plate photomultiplier (Hamamatsu) coupled to a pulse preamplifier HFAC (Becker-Hickl) and recorded on a SPC-130 board (Becker-Hickl). Time-resolved data were analyzed by the maximum entropy method (Pulse 5 software) (Brochon, 1994; Livesey and Brochon, 1987). In all cases, the χ^2 values were close to 1 and the weighted residuals as well as their autocorrelation were distributed randomly around 0, indicating an optimal fit.

[36] Performed by the author with the help of Dr. Ludovic Richert (LBP, Illkirch)

Part II Chapter 2: Fluorescent probes for selectivity assays (profiling)

1. Synthesis

General

Reagents were obtained from commercial sources and used without any further purification. Semi-preparative HPLC chromatography was performed on SunFire C18 column (5 µm, 19 × 150 mm) on Gilson PLC2020. Analytical RP-HPLC separations were performed on Ascentis Express C18 column (2.7 µm, 4.6 mm × 75 mm) using a linear gradient (5% to 100% in 7.4 min, flow rate of 1.6 mL/min) of solvent B (0.1% TFA in CH_3CN, v/v) in solvent A (0.1% TFA in H_2O, v/v). Detection was set at 220 and 254 nm. High resolution mass spectra (HRMS) were acquired on a Bruker MicroTof mass spectrometer, using electrospray ionization (ESI) and a time-of-flight analyzer (TOF).

*DY-590-labeled compound **3.6***

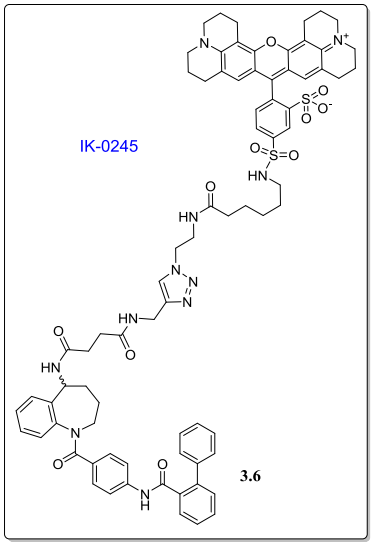

A solution of **3.4** in dry DMSO (734 nmol, 20 µL of 0.0122 M) was added to a solution of DY-590-NHS (245 nmol) in dry DMSO (100 µL) followed by NEt_3 (12 µmol, 2 µL). The reaction mixture was stirred at r.t. overnight. The resulting mixture was purified by semi-preparative HPLC eluted with solvent B in solvent A (20-35% in 5 min, then 35-50% in 23 min; detection at 590 nm) to give after lyophilization **3.6** as a purple solid (88 nmol, 36%). HRMS (ESI): calcd for $C_{76}H_{81}N_{11}O_{11}S_2$ $(M+2H)^{2+}/2$ 693.77792, found: 693.77840.

*DY-590-labeled compound **3.7***

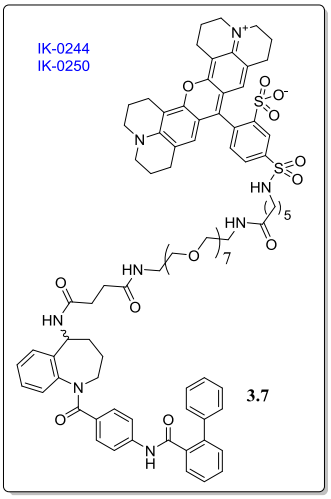

A solution of **3.5** in dry DMSO (734 nmol, 60 µL of 0.0122 M) was added to a solution of DY-590-NHS (245 nmol) in dry DMSO (100 µL) followed by NEt_3 (12 µmol, 2 µL). The reaction mixture was stirred at r.t. overnight. The resulting mixture was purified by semi-preparative HPLC eluted with solvent B in solvent A (20-35% in 5 min, then 35-48% in 23 min; detection at 590 nm) to give after lyophilization **3.7** as a purple solid (102 nmol, 42%). HRMS (ESI):

calcd for $C_{87}H_{106}N_8O_{18}S_2$ $(M+2H)^{2+}/2$ 807.35333, found: 807.35342.

2. Affinity of the ligands 3.6, 3.7, 3.9 and 3.10 for V_2R (TR-FRET competition assay)[37]

These assays were performed as previously described (Zwier et al., 2010). Briefly, HEK293 cells were cultivated in DMEM medium supplemented with 10% FCS and 1% penicillin/streptomycin antibiotics. As described in Cottet et al., 2011, confluent cells were dissociated and plated in black 96-well plates previously coated with poly-ornithine (diluted at 0.1 mg/mL in sterile water, incubated 30 min at 37 °C, washed with sterile PBS). The cells were treated with Lipofectamine 2000® complex of plasmid DNA coding for the V_2 receptor fused to the SNAP-tag suicide enzyme in Opti-MEM® medium. Plates were incubated for 24 hours at 37 °C and 5% CO_2. Expressed receptors fused to SNAP-tag were then labeled with FRET acceptor (BG-Fluorescein) at 100 nM in 100 µL/well of Tag-lite® labelling medium, for 1 hour at 37 °C. Cells were then washed 3 times with Tag-lite® medium and then incubated with increasing concentrations of ligands **3.6**, **3.7**, **3.9** or **3.10** in Tag-lite® medium in the presence of a fixed concentration (equal to its K_d) of luminescence donor **47**. Plates were read in an HTRF®-compatible multi-well plate reader with a classic HTRF® protocol (excitation at 340 nM, donor emission measured at 620 nm and acceptor emission at 520 nm, 150 µs delay, 500 µs integration). To determine the incubation time necessary to reach the equilibrium, FRET and luminescence signals were measured after various times of incubation. Inhibition constants were determined when equilibrium is reached by fitting experimental data with Graphpad Prism 6 (GraphPad Software).

3. Multicolor binding assays

3.1 Test for the choice of the "orange" fluorophore

Confluent cells were dissociated and plated in black 96-well plates previously coated with poly-ornithine (diluted at 0.1 mg/mL in sterile water, incubated 30 min at 37 °C, washed with sterile PBS). The cells were treated with Lipofectamine 2000® complex of either plasmid DNA coding for the V_2 receptor fused to the SNAP-tag suicide enzyme or pRK5 plasmid DNA, which does not code for GPCRs (Mock cells) in Opti-MEM® medium (see Figure 55). Plates were incubated for 24 hours at 37 °C and 5% CO_2.

[37] Performed by the author in IGF (Montpellier) with the help of Thiéric Rodriguez.

Opti-MEM was removed and cells in all the plate except columns "A" were labeled with FRET donor BG-Lumi-4-Tb at 100 nM in 100 µL/well of Tag-lite® labelling medium, for 1 hour at 37 °C. Cells in columns "A" were treated in the same manner with Tag-lite® labelling medium.

Cells were then washed 3 times with Tag-lite® medium and incubated with ligands **3.6**, **3.8**, **3.9** or **44** (at the concentration equal to $3\times K_d$) in Tag-lite® medium with or without the "cold" competitor AVP, according to the scheme presented in Figure 55 for 1 hour at r.t.

Plate was read in PHERAstar FS multi-well plate reader with a modified HTRF® protocol (excitation at 340 nM, donor emission measured at 550 nm and acceptor emission at 605 nm, 150 µs delay, 500 µs integration).

Next, the rows "3.9" were incubated for 5 min with a 12 nM solution of QDots® 605-streptavidin in Tag-lite® medium. The plate was read with the modified HTRF® protocol, presented above, then cells were then washed 4 times with Tag-lite® medium and read after each washing step.

Data were analyzed with Graphpad Prism 6 (GraphPad Software).

3.2 Test on the mixture of three receptors[38]

Confluent cells were dissociated and plated in a 6 well plate at 0.65 mln cells/well. Cells were treated with Lipofectamine 2000® complex of plasmid DNA coding for the V_2, the Apelin or the D_3 receptors fused to the SNAP-tag suicide enzyme in Opti-MEM® medium (2 wells for each plasmid). Plates were incubated for 6 hours at 37 °C and 5% CO_2.

Cells were dissociated, mixed in the required proportions in DMEM maintaining the concentration of each cell line in final mixtures at 30 000 cells/well and plated in a black 96 well plate (previously coated with poly-ornithine) according to Figure 58. Plates were incubated for 24 hours at 37 °C and 5% CO_2.

DMEM was removed and cells were labeled with FRET donor BG-Lumi-4-Tb at 100 nM in 100 µL/well of Tag-lite® labelling medium, for 1 h at 37 °C.

Cells were then washed 3 times with Tag-lite® medium and incubated with a mixture of ligands **3.1**, **3.2** and **3.6** (at the concentration equal to $3\times K_d$) in Tag-lite® medium with or without the mixture of "cold" competitors AVP, apelin-13 and BP 897 (at the concentration equal to $500\times K_d$) for 1 hour at r.t.

[38] Performed by the author in IGF (Montpellier) with the help of Amandine Falco.

Plate was read in PHERAstar FS multi-well plate reader with three HTRF® protocols ("green": excitation at 340 nM, donor emission at 620 nm, acceptor emission at 520 nm; "orange": excitation at 340 nM, donor emission at 550 nm, acceptor emission at 605 nm; "red": excitation at 340 nM, donor emission at 620 nm, acceptor emission at 665 nm; 150 µs delay, 500 µs integration).

Data were analyzed using GraphPad Prism 6 Software (GraphPad, San Diego, CA, USA).

References

A

Albizu, L., Teppaz, G., Seyer, R., Bazin, H., Ansanay, H., Manning, M., Mouillac, B., and Durroux, T. (2007). Toward efficient drug screening by homogeneous assays based on the development of new fluorescent vasopressin and oxytocin receptor ligands. J. Med. Chem. *50*, 4976–4985.

Anagnostou, E., Soorya, L., Chaplin, W., Bartz, J., Halpern, D., Wasserman, S., Wang, a T., Pepa, L., Tanel, N., Kushki, A., et al. (2012). Intranasal oxytocin versus placebo in the treatment of adults with autism spectrum disorders: a randomized controlled trial. Mol. Autism *3*, 16.

Andari, E., Duhamel, J.-R., Zalla, T., Herbrecht, E., Leboyer, M., and Sirigu, A. (2010). Promoting social behavior with oxytocin in high-functioning autism spectrum disorders. Proc. Natl. Acad. Sci. U. S. A. *107*, 4389–4394.

Arletti, R., and Bertolini, A. (1987). Oxytocin acts as an antidepressant in two animal models of depression. Life Sci. *41*, 1725–1730.

Arpin-Bott, M.P., Kaissling, B., Waltisperger, E., Rabhi, M., Saussine, P., Freund-Mercier, M.J., and Stoeckel, M.E. (2002). Historadioautographic Localization of Oxytocin and V1a Vasopressin Binding Sites in the Kidney of Developing and Adult Rabbit, Mouse and Merione and of Adult Human. Nephron Exp. Nephrol. *10*, 196–208.

Arunkumar, E., Forbes, C.C., Noll, B.C., and Smith, B.D. (2005a). Squaraine-derived rotaxanes: sterically protected fluorescent near-IR dyes. J. Am. Chem. Soc. *127*, 3288–3289.

Arunkumar, E., Ajayaghosh, A., and Daub, J. (2005b). Selective calcium ion sensing with a bichromophoric squaraine foldamer. J. Am. Chem. Soc. *127*, 3156–3164.

Attilakos, G., Psaroudakis, D., Ash, J., Buchanan, R., Winter, C., Donald, F., Hunt, L.P., and Draycott, T. (2010). Carbetocin versus oxytocin for the prevention of postpartum haemorrhage following caesarean section: the results of a double-blind randomised trial. BJOG *117*, 929–936.

Attwood, T.K., and Findlay, J.B. (1994). Fingerprinting G-protein-coupled receptors. Protein Eng. *7*, 195–203.

B

Baldwin, J.M. (1993). The probable arrangement of the helices in G protein-coupled receptors. EMBO J. *12*, 1693–1703.

Baldwin, J.M. (1994). Structure and function of receptors coupled to G proteins. Curr. Opin. Cell Biol. *6*, 180–190.

Bales, K.L., Kim, A.J., Lewis-Reese, A.D., and Sue Carter, C. (2004). Both oxytocin and vasopressin may influence alloparental behavior in male prairie voles. Horm. Behav. *45*, 354–361.

Barberis, C., Mouillac, B., and Durroux, T. (1998). Structural bases of vasopressin/oxytocin receptor function. J. Endocrinol. *156*, 223–229.

Barberis, C., Morin, D., Durroux, T., Mouillac, B., Guillon, G., Seyer, R., Hibert, M., Tribollet, E., and Manning, M. (1999). Molecular pharmacology of AVP and OT receptors and therapeutic potential. Drug News Perspect. *12 (5)*, 279–292.

Barlos, K., Gatos, D., Hatzi, O., Koch, N., and Koutsogianni, S. (1996). Synthesis of the very acid-sensitive Fmoc-Cys(Mmt)-OH and its application in solid-phase peptide synthesis. Int. J. Pept. Protein Res. *47*, 148–153.

Baumgartner, T., Heinrichs, M., Vonlanthen, A., Fischbacher, U., and Fehr, E. (2008). Oxytocin shapes the neural circuitry of trust and trust adaptation in humans. Neuron *58*, 639–650.

Beaino, W., and Trifilieff, E. (2010). Thiopalmitoylated peptides from the peripheral nervous system myelin p0 protein: synthesis, characterization, and neuritogenic properties. Bioconjug. Chem. *21*, 1439–1447.

Beckwith, B.E., Petros, T. V, Bergloff, P.J., and Staebler, R.J. (1987). Vasopressin analogue (DDAVP) facilitates recall of narrative prose. Behav. Neurosci. *101*, 429–432.

Beeby, A., Clarkson, I.M., Dickins, R.S., Faulkner, S., Parker, D., Royle, L., de Sousa, A.S., Williams, J. a. G., and Woods, M. (1999). Non-radiative deactivation of the excited states of europium, terbium and ytterbium complexes by proximate energy-matched OH, NH and CH oscillators: an improved luminescence method for establishing solution hydration states. J. Chem. Soc. Perkin Trans. 2 *2*, 493–504.

Berezin, M.Y., and Achilefu, S. (2010). Fluorescence lifetime measurements and biological imaging. Chem. Rev. *110*, 2641–2684.

Berque-Bestel, I., Soulier, J.-L., Giner, M., Rivail, L., Langlois, M., and Sicsic, S. (2003). Synthesis and characterization of the first fluorescent antagonists for human 5-HT4 receptors. J. Med. Chem. *46*, 2606–2620.

Bester-Meredith, J.K., Young, L.J., and Marler, C.A. (1999). Species differences in paternal behavior and aggression in peromyscus and their associations with vasopressin immunoreactivity and receptors. Horm. Behav. *36*, 25–38.

Beverina, L., and Salice, P. (2010). Squaraine Compounds: Tailored Design and Synthesis towards a Variety of Material Science Applications. European J. Org. Chem. *2010*, 1207–1225.

Birnbaumer, M. (2000). Vasopressin receptors. Trends Endocrinol. Metab. *11*, 406–410.

Birnbaumer, M., Seibold, A., Gilbert, S., Ishido, M., Barberis, C., Antaramian, A., Brabet, P., and Rosenthal, W. (1992). Molecular cloning of the receptor for human antidiuretic hormone. Nature *357*, 333–335.

Bisceglia, R., Jenkins, J.M., Wigg, K.G., O'Connor, T.G., Moran, G., and Barr, C.L. (2012). Arginine vasopressin 1a receptor gene and maternal behavior: evidence of association and moderation. Genes. Brain. Behav. *11*, 262–268.

Bonnet, D., Durroux, T., Hibert, M., Mouillac, B., Pflimlin, E., and Rodriguez, T. (2014). Labeled Ligands of the Oxytocin Receptor. Int. Pat. Appl. WO 2014056852 A1.

Borthwick, A.D. (2010). Oral oxytocin antagonists. J. Med. Chem. *53*, 6525–6538.

Bosch, O.J., Krömer, S.A., and Neumann, I.D. (2006). Prenatal stress: opposite effects on anxiety and hypothalamic expression of vasopressin and corticotropin-releasing hormone in rats selectively bred for high and low anxiety. Eur. J. Neurosci. *23*, 541–551.

Breton, C., Chellil, H., Kabbaj-Benmansour, M., Carnazzi, E., Seyer, R., Phalipou, S., Morin, D., Durroux, T., Zingg, H., Barberis, C., et al. (2001). Direct Identification of Human Oxytocin Receptor-binding Domains Using a Photoactivatable Cyclic Peptide Antagonist: Comparison with the Human V1a Vasopressin Receptor. J. Biol. Chem. *276*, 26931–26941.

Briddon, S.J., and Hill, S.J. (2007). Pharmacology under the microscope: the use of fluorescence correlation spectroscopy to determine the properties of ligand-receptor complexes. Trends Pharmacol. Sci. *28*, 637–645.

Briddon, S.J., Middleton, R.J., Cordeaux, Y., Flavin, F.M., Weinstein, J.A., George, M.W., Kellam, B., and Hill, S.J. (2004). Quantitative analysis of the formation and diffusion of A1-adenosine receptor-antagonist complexes in single living cells. Proc. Natl. Acad. Sci. United States Am. *101* , 4673–4678.

Brochon, J.C. (1994). Maximum entropy method of data analysis in time-resolved spectroscopy. Methods Enzymol. *240*, 262–311.

Brouard, R., Bossmar, T., Fournié-Lloret, D., Chassard, D., and Akerlund, M. (2000). Effect of SR49059, an orally active V1a vasopressin receptor antagonist, in the prevention of dysmenorrhoea. BJOG *107*, 614–619.

Brown, A., Brown, T.B., Calabrese, A., Ellis, D., Puhalo, N., Ralph, M., and Watson, L. (2010). Triazole oxytocin antagonists: Identification of an aryloxyazetidine replacement for a biaryl substituent. Bioorg. Med. Chem. Lett. *20*, 516–520.

Brown, A.D., Calabrese, A.A., and Ellis, D. (2006). Substituted Triazole Derivatives as Oxytocin Antagonists. US Pat. App. 2006/0160786 A1.

Bünzli, J.-C.G. (2010). Lanthanide luminescence for biomedical analyses and imaging. Chem. Rev. *110*, 2729–2755.

C

Cabrera-Vera, T.M., Vanhauwe, J., Thomas, T.O., Medkova, M., Preininger, A., Mazzoni, M.R., and Hamm, H.E. (2003). Insights into G protein structure, function, and regulation. Endocr. Rev. *24*, 765–781.

Caffé, A.R., and van Leeuwen, F.W. (1983). Vasopressin-immunoreactive cells in the dorsomedial hypothalamic region, medial amygdaloid nucleus and locus coeruleus of the rat. Cell Tissue Res. *233*, 23–33.

Caffé, A.R., van Leeuwen, F.W., and Luiten, P.G. (1987). Vasopressin cells in the medial amygdala of the rat project to the lateral septum and ventral hippocampus. J. Comp. Neurol. *261*, 237–252.

Caldwell, H.K., and Albers, H.E. (2004). Effect of photoperiod on vasopressin-induced aggression in Syrian hamsters. Horm. Behav. *46*, 444–449.

Caldwell, H.K., Lee, H.-J., Macbeth, A.H., and Young, W.S. (2008). Vasopressin: behavioral roles of an "original" neuropeptide. Prog. Neurobiol. *84*, 1–24.

Campbell, A. (2008). Attachment, aggression and affiliation: the role of oxytocin in female social behavior. Biol. Psychol. *77*, 1–10.

Champagne, F., Diorio, J., Sharma, S., and Meaney, M.J. (2001). Naturally occurring variations in maternal behavior in the rat are associated with differences in estrogen-inducible central oxytocin receptors. Proc. Natl. Acad. Sci. U. S. A. *98*, 12736–12741.

Chaviaras, S., Mak, P., Ralph, D., Krishnan, L., and Broadbear, J.H. (2010). Assessing the antidepressant-like effects of carbetocin, an oxytocin agonist, using a modification of the forced swimming test. Psychopharmacology (Berl). *210*, 35–43.

Chen, H., Farahat, M.S., Law, K.-Y., and Whitten, D.G. (1996). Aggregation of Surfactant Squaraine Dyes in Aqueous Solution and Microheterogeneous Media: Correlation of Aggregation Behavior with Molecular Structure. J. Am. Chem. Soc. *118*, 2584–2594.

Chung, S., Funakoshi, T., and Civelli, O. (2008). Orphan GPCR research. Br. J. Pharmacol. *153 Suppl* , S339–46.

Chung, S.-J., Zheng, S., Odani, T., Beverina, L., Fu, J., Padilha, L.A., Biesso, A., Hales, J.M., Zhan, X., Schmidt, K., et al. (2006). Extended squaraine dyes with large two-photon absorption cross-sections. J. Am. Chem. Soc. *128*, 14444–14445.

Consiglio, A.R., Borsoi, A., Pereira, G.A.M., and Lucion, A.B. (2005). Effects of oxytocin microinjected into the central amygdaloid nucleus and bed nucleus of stria terminalis on maternal aggressive behavior in rats. Physiol. Behav. *85*, 354–362.

Cooper, M., Metz, J., de Wit, H., Cook, E., Lorenz, J., and Brown, T. (1998). Interclass drug effects and changes in regional brain glucose metabolism. Psychopharmacol. Bull. *34*, 229–232.

Corbani, M., Trueba, M., Stoev, S., Murat, B., Mion, J., Boulay, V., Guillon, G., and Manning, M. (2011). Design, synthesis, and pharmacological characterization of fluorescent peptides for imaging human V1b vasopressin or oxytocin receptors. J. Med. Chem. *54*, 2864–2877.

Cottet, M., Faklaris, O., Zwier, J.M., Trinquet, E., Pin, J.-P., and Durroux, T. (2011). Original Fluorescent Ligand-Based Assays Open New Perspectives in G-Protein Coupled Receptor Drug Screening. Pharmaceuticals *4*, 202–214.

Cottet, M., Faklaris, O., Falco, A., Trinquet, E., Pin, J.-P., Mouillac, B., and Durroux, T. (2013). Fluorescent ligands to investigate GPCR binding properties and oligomerization. Biochem. Soc. Trans. *41*, 148–153.

Cunningham, V.J., Parker, C.A., Rabiner, E.A., Gee, A.D., and Gunn, R.N. (2005). PET studies in drug development: Methodological considerations. Drug Discov. Today Technol. *2*, 311–315.

Curley, J.P., Jensen, C.L., Franks, B., and Champagne, F.A. (2012). Variation in maternal and anxiety-like behavior associated with discrete patterns of oxytocin and vasopressin 1a receptor density in the lateral septum. Horm. Behav. *61*, 454–461.

D'Cunha, T.M., King, S.J., Fleming, A.S., and Lévy, F. (2011). Oxytocin receptors in the nucleus accumbens shell are involved in the consolidation of maternal memory in postpartum rats. Horm. Behav. *59*, 14–21.

D

Daly, C.J., and McGrath, J.C. (2003). Fluorescent ligands, antibodies, and proteins for the study of receptors. Pharmacol. Ther. *100*, 101–118.

Das, S., Thomas, K.G., Thomas, K.J., Madhavan, V., Liu, D., Kamat, P. V., and George, M. V. (1996). Aggregation Behavior of Water Soluble Bis(benzothiazolylidene)squaraine Derivatives in Aqueous Media. J. Phys. Chem. *100*, 17310–17315.

Datta, A., Mandal, D., Pal, S.K., and Bhattacharyya, K. (1997). Intramolecular Charge Transfer Processes in Confined Systems. Nile Red in Reverse Micelles. J. Phys. Chem. B *101*, 10221–10225.

Davis, D.M., and Birch, D.J. (1996). Extrinsic fluorescence probe study of human serum albumin using Nile red. J. Fluoresc. *6*, 23–32.

Degorce, F., Card, A., Soh, S., Trinquet, E., Knapik, G.P., and Xie, B. (2009). HTRF: A technology tailored for drug discovery - a review of theoretical aspects and recent applications. Curr. Chem. Genomics *3*, 22–32.

Demchenko, A.P. (2009). Introduction to Fluorescence Sensing (Springer).

Dempster, E.L., Burcescu, I., Wigg, K., Kiss, E., Baji, I., Gadoros, J., Tamás, Z., Kennedy, J.L., Vetró, A., Kovacs, M., et al. (2007). Evidence of an association between the vasopressin V1b receptor gene (AVPR1B) and childhood-onset mood disorders. Arch. Gen. Psychiatry *64*, 1189–1195.

Deshayes, S., and Divita, G. (2013). Fluorescence technologies for monitoring interactions between biological molecules in vitro. Prog. Mol. Biol. Transl. Sci. *113*, 109–143.

DeVries, A.C., Young, W.S., and Nelson, R.J. (1997). Reduced aggressive behaviour in mice with targeted disruption of the oxytocin gene. J. Neuroendocrinol. *9*, 363–368.

Dixon, R.A., Kobilka, B.K., Strader, D.J., Benovic, J.L., Dohlman, H.G., Frielle, T., Bolanowski, M.A., Bennett, C.D., Rands, E., Diehl, R.E., et al. (1986). Cloning of the gene and cDNA for mammalian beta-adrenergic receptor and homology with rhodopsin. Nature *321*, 75–79.

Domes, G., Heinrichs, M., Kumbier, E., Grossmann, A., Hauenstein, K., and Herpertz, S.C. (2013). Effects of intranasal oxytocin on the neural basis of face processing in autism spectrum disorder. Biol. Psychiatry *74*, 164–171.

Drake, M.T., Shenoy, S.K., and Lefkowitz, R.J. (2006). Trafficking of G protein-coupled receptors. Circ. Res. *99*, 570–582.

Dunphy, M.P.S., and Lewis, J.S. (2009). Radiopharmaceuticals in preclinical and clinical development for monitoring of therapy with PET. J. Nucl. Med. *50 Suppl 1*, 106S–21S.

Durroux, T. (2005). Principles: a model for the allosteric interactions between ligand binding sites within a dimeric GPCR. Trends Pharmacol. Sci. *26*, 376–384.

Dziuba, D., Benhida, R., and Burger, A. (2011). A Mild and Efficient Protocol for the Protection of 3-Hydroxychromones Under Phase-Transfer Catalysis. Synthesis (Stuttg). *2011*, 2159–2164.

E

Ebner, K., Wotjak, C.T., Landgraf, R., and Engelmann, M. (2002). Forced swimming triggers vasopressin release within the amygdala to modulate stress-coping strategies in rats. Eur. J. Neurosci. *15*, 384–388.

Egashira, N., Tanoue, A., Matsuda, T., Koushi, E., Harada, S., Takano, Y., Tsujimoto, G., Mishima, K., Iwasaki, K., and Fujiwara, M. (2007). Impaired social interaction and reduced anxiety-related behavior in vasopressin V1a receptor knockout mice. Behav. Brain Res. *178*, 123–127.

Egloff, P., Hillenbrand, M., Klenk, C., Batyuk, A., Heine, P., Balada, S., Schlinkmann, K.M., Scott, D.J., Schütz, M., and Plückthun, A. (2014). Structure of signaling-competent neurotensin receptor 1 obtained by directed evolution in Escherichia coli. Proc. Natl. Acad. Sci. U. S. A. *111*, E655–62.

Engelmann, M., Ludwig, M., and Landgraft, R. (1994). Simultaneous monitoring of intracerebral release and behavior: endogenous vasopressin improves social recognition. J. Neuroendocrinol. *6*, 391–395.

Engstrøm, T., Barth, T., Melin, P., and Vilhardt, H. (1998). Oxytocin receptor binding and uterotonic activity of carbetocin and its metabolites following enzymatic degradation. Eur. J. Pharmacol. *355*, 203–210.

F

Fabio, K., Guillon, C., Lacey, C.J., Lu, S.-F., Heindel, N.D., Ferris, C.F., Placzek, M., Jones, G., Brownstein, M.J., and Simon, N.G. (2011). Synthesis and evaluation of potent and selective human V1a receptor antagonists as potential ligands for PET or SPECT imaging. Bioorg. Med. Chem. *20*, 1337–1345.

Farina Lipari, E., and Valentino, B. (1993). Immunohistochemical research on vasopressin in the accessory hypothalamic nuclei. Ital. J. Anat. Embryol. *98*, 207–214.

Farina Lipari, E., Valentino, B., and Lipari, D. (1995). Immunohistochemical research on oxytocin in the hypothalamic accessory nuclei. Ital. J. Anat. Embryol. *100*, 189–193.

Feldman, R., Weller, A., Zagoory-Sharon, O., and Levine, A. (2007). Evidence for a neuroendocrinological foundation of human affiliation: plasma oxytocin levels across pregnancy and the postpartum period predict mother-infant bonding. Psychol. Sci. *18*, 965–970.

Feldman, R., Gordon, I., Schneiderman, I., Weisman, O., and Zagoory-Sharon, O. (2010). Natural variations in maternal and paternal care are associated with systematic changes in oxytocin following parent-infant contact. Psychoneuroendocrinology *35*, 1133–1141.

Ferguson, J.N., Young, L.J., Hearn, E.F., Matzuk, M.M., Insel, T.R., and Winslow, J.T. (2000). Social amnesia in mice lacking the oxytocin gene. Nat. Genet. *25*, 284–288.

Ferguson, J.N., Aldag, J.M., Insel, T.R., and Young, L.J. (2001). Oxytocin in the medial amygdala is essential for social recognition in the mouse. J. Neurosci. *21*, 8278–8285.

Ferris, C.F., and Potegal, M. (1988). Vasopressin receptor blockade in the anterior hypothalamus suppresses aggression in hamsters. Physiol. Behav. *44*, 235–239.

Ferris, C.F., Foote, K.B., Meltser, H.M., Plenby, M.G., Smith, K.L., and Insel, T.R. (1992). Oxytocin in the amygdala facilitates maternal aggression. Ann. N. Y. Acad. Sci. *652*, 456–457.

Filmore, D. (2004). It's a GPCR world. Mod. Drug Discov. 24–27.

Francis, D.D., Young, L.J., Meaney, M.J., and Insel, T.R. (2002). Naturally occurring differences in maternal care are associated with the expression of oxytocin and vasopressin (V1a) receptors: gender differences. J. Neuroendocrinol. *14*, 349–353.

Francis, S.M., Sagar, a, Levin-Decanini, T., Liu, W., Carter, C.S., and Jacob, S. (2014). Oxytocin and vasopressin systems in genetic syndromes and neurodevelopmental disorders. Brain Res. 1–20.

Frantz, M.-C., Rodrigo, J., Boudier, L., Durroux, T., Mouillac, B., and Hibert, M. (2010). Subtlety of the structure-affinity and structure-efficacy relationships around a nonpeptide oxytocin receptor agonist. J. Med. Chem. *53*, 1546–1562.

Frasch, A., Zetzsche, T., Steiger, A., and Jirikowski, G.F. (1995). Reduction of plasma oxytocin levels in patients suffering from major depression. Adv. Exp. Med. Biol. *395*, 257–258.

Fredriksson, R., Lagerström, M.C., Lundin, L.-G., and Schiöth, H.B. (2003). The G-protein-coupled receptors in the human genome form five main families. Phylogenetic analysis, paralogon groups, and fingerprints. Mol. Pharmacol. *63*, 1256–1272.

Freeman, S.M., Inoue, K., Smith, A.L., Goodman, M.M., and Young, L.J. (2014). The neuroanatomical distribution of oxytocin receptor binding and mRNA in the male rhesus macaque (Macaca mulatta). Psychoneuroendocrinology *45*, 128–141.

Fritschy, J.-M., and Hartig, W. (2001). Immunofluorescence. eLS.

Fritz, J. V, Didier, P., Clamme, J.-P., Schaub, E., Muriaux, D., Cabanne, C., Morellet, N., Bouaziz, S., Darlix, J.-L., Mély, Y., et al. (2008). Direct Vpr-Vpr interaction in cells monitored by two photon fluorescence correlation spectroscopy and fluorescence lifetime imaging. Retrovirology *5*, 87.

G

Gautier, A., Juillerat, A., Heinis, C., Corrêa, I.R., Kindermann, M., Beaufils, F., and Johnsson, K. (2008). An engineered protein tag for multiprotein labeling in living cells. Chem. Biol. *15*, 128–136.

Gee, A.D. (2003). Neuropharmacology and drug development. Br. Med. Bull. *65*, 169–177.

Gimpl, G., and Fahrenholz, F. (2001). The oxytocin receptor system: structure, function, and regulation. Physiol. Rev. *81*, 629–683.

Goekoop, J.G., de Winter, R.P.F., de Rijk, R., Zwinderman, K.H., Frankhuijzen-Sierevogel, A., and Wiegant, V.M. (2006). Depression with above-normal plasma vasopressin: validation by relations with family history of depression and mixed anxiety and retardation. Psychiatry Res. *141*, 201–211.

Gold, P.W., Goodwin, F.K., and Reus, V.I. (1978). Vasopressin in affective illness. Lancet *1*, 1233–1236.

Gordon, I., Vander Wyk, B.C., Bennett, R.H., Cordeaux, C., Lucas, M. V., Eilbott, J.A., Zagoory-Sharon, O., Leckman, J.F., Feldman, R., and Pelphrey, K.A. (2013). Oxytocin enhances brain function in children with autism. Proc. Natl. Acad. Sci. U. S. A. *110*, 20953–20958.

Gravati, M., Busnelli, M., Bulgheroni, E., Reversi, A., Spaiardi, P., Parenti, M., Toselli, M., and Chini, B. (2010). Dual modulation of inward rectifier potassium currents in olfactory neuronal cells by promiscuous G protein coupling of the oxytocin receptor. J. Neurochem. *114*, 1424–1435.

Greenspan, P., and Fowler, S.D. (1985). Spectrofluorometric studies of the lipid probe, nile red. J. Lipid Res. *26*, 781–789.

Grewen, K.M., Girdler, S.S., Amico, J., and Light, K.C. (2005). Effects of partner support on resting oxytocin, cortisol, norepinephrine, and blood pressure before and after warm partner contact. Psychosom. Med. *67*, 531–538.

Griebel, G., Simiand, J., Serradeil-Le Gal, C., Wagnon, J., Pascal, M., Scatton, B., Maffrand, J.-P., and Soubrie, P. (2002). Anxiolytic- and antidepressant-like effects of the non-peptide vasopressin V1b receptor antagonist, SSR149415, suggest an innovative approach for the treatment of stress-related disorders. Proc. Natl. Acad. Sci. U. S. A. *99*, 6370–6375.

Grigor'eva, M.E., and Golubeva, M.G. (2010). Oxytocin: Structure, synthesis, receptors, and basic effects. Neurochem. J. *4*, 75–83.

Grimm, J.B., Heckman, L.M., and Lavis, L.D. (2013). The chemistry of small-molecule fluorogenic probes. Prog. Mol. Biol. Transl. Sci. *113*, 1–34.

Guastella, A.J., Howard, A.L., Dadds, M.R., Mitchell, P., and Carson, D.S. (2009). A randomized controlled trial of intranasal oxytocin as an adjunct to exposure therapy for social anxiety disorder. Psychoneuroendocrinology *34*, 917–923.

Guastella, A.J., Kenyon, A.R., Alvares, G.A., Carson, D.S., and Hickie, I.B. (2010). Intranasal arginine vasopressin enhances the encoding of happy and angry faces in humans. Biol. Psychiatry *67*, 1220–1222.

Guastella, A.J., Kenyon, A.R., Unkelbach, C., Alvares, G.A., and Hickie, I.B. (2011). Arginine Vasopressin selectively enhances recognition of sexual cues in male humans. Psychoneuroendocrinology *36*, 294–297.

Gutkowska, J., Jankowski, M., Lambert, C., Mukaddam-Daher, S., Zingg, H.H., and McCann, S.M. (1997). Oxytocin releases atrial natriuretic peptide by combining with oxytocin receptors in the heart. Proc. Natl. Acad. Sci. U. S. A. *94*, 11704–11709.

Gutzler, S.J., Karom, M., Erwin, W.D., and Albers, H.E. (2010). Arginine-vasopressin and the regulation of aggression in female Syrian hamsters (Mesocricetus auratus). Eur. J. Neurosci. *31*, 1655–1663.

H

Hall, M.D., and Pike, V.W. (2011). Avoiding barriers to PET radioligand development: cellular assays of brain efflux transporters. J. Nucl. Med. *52*, 338–340.

Hanaoka, K. (2010). Development of responsive lanthanide-based magnetic resonance imaging and luminescent probes for biological applications. Chem. Pharm. Bull. *58*, 1283–1294.

Hancock, W., and Battersby, J. (1976). A new micro-test for the detection of incomplete coupling reactions in solid-phase peptide synthesis using 2, 4, 6-trinitrobenzene-sulphonic acid. Anal. Biochem. *264*, 260–264.

Harikumar, K.G., Clain, J., Pinon, D.I., Dong, M., and Miller, L.J. (2005). Distinct molecular mechanisms for agonist peptide binding to types A and B cholecystokinin receptors demonstrated using fluorescence spectroscopy. J. Biol. Chem. *280*, 1044–1050.

Harris, H.W., Zeidel, M.L., Jo, I., and Hammond, T.G. (1994). Characterization of purified endosomes containing the antidiuretic hormone-sensitive water channel from rat renal papilla. J. Biol. Chem. *269*, 11993–12000.

Hawtin, S.R., Wesley, V.J., Simms, J., Argent, C.C.H., Latif, K., and Wheatley, M. (2005). The N-terminal juxtamembrane segment of the V1a vasopressin receptor provides two independent epitopes required for high-affinity agonist binding and signaling. Mol. Endocrinol. *19*, 2871–2881.

Hayoz, D., Bizzini, G., Noël, B., Depairon, M., Burnier, M., Fauveau, C., Rouillon, A., Brouard, R., and Brunner, H.R. (2000). Effect of SR 49059, a V1a vasopressin receptor antagonist, in Raynaud's phenomenon. Rheumatology *39*, 1132–1138.

Van Heertum, R.L., and Tikofsky, R.S. (2003). Positron emission tomography and single-photon emission computed tomography brain imaging in the evaluation of dementia. Semin. Nucl. Med. *33*, 77–85.

Heim, C., Young, L.J., Newport, D.J., Mletzko, T., Miller, A.H., and Nemeroff, C.B. (2009). Lower CSF oxytocin concentrations in women with a history of childhood abuse. Mol. Psychiatry *14*, 954–958.

Hibert, M.F., Trumpp-Kallmeyer, S., Bruinvels, A., and Hoflack, J. (1991). Three-dimensional models of neurotransmitter G-binding protein-coupled receptors. Mol. Pharmacol. *40*, 8–15.

Hollander, E., Novotny, S., Hanratty, M., Yaffe, R., DeCaria, C.M., Aronowitz, B.R., and Mosovich, S. (2003). Oxytocin infusion reduces repetitive behaviors in adults with autistic and Asperger's disorders. Neuropsychopharmacology *28*, 193–198.

Holmes, C.L., Landry, D.W., and Granton, J.T. (2003). Science review: Vasopressin and the cardiovascular system part 1- receptor physiology. Crit. Care *7*, 427–434.

Hope, M.J., Bally, M.B., Webb, G., and Cullis, P.R. (1985). Production of large unilamellar vesicles by a rapid extrusion procedure: characterization of size distribution, trapped volume and ability to maintain a membrane potential. Biochim. Biophys. Acta *812*, 55–65.

Hurlemann, R., Patin, A., Onur, O.A., Cohen, M.X., Baumgartner, T., Metzler, S., Dziobek, I., Gallinat, J., Wagner, M., Maier, W., et al. (2010). Oxytocin enhances amygdala-dependent, socially reinforced learning and emotional empathy in humans. J. Neurosci. *30*, 4999–5007.

I

Inder, W.J., Donald, R.A., Prickett, T.C., Frampton, C.M., Sullivan, P.F., Mulder, R.T., and Joyce, P.R. (1997). Arginine vasopressin is associated with hypercortisolemia and suicide attempts in depression. Biol. Psychiatry *42*, 744–747.

Insel, T.R., and Hulihan, T.J. (1995). A gender-specific mechanism for pair bonding: oxytocin and partner preference formation in monogamous voles. Behav. Neurosci. *109*, 782–789.

Insel, T.R., and Shapiro, L.E. (1992). Oxytocin receptor distribution reflects social organization in monogamous and polygamous voles. Proc. Natl. Acad. Sci. U. S. A. *89*, 5981–5985.

Insel, T.R., and Young, L.J. (2000). Neuropeptides and the evolution of social behavior. Curr. Opin. Neurobiol. *10*, 784–789.

Ioffe, V.M., Gorbenko, G.P., Kinnunen, P.K.J., Tatarets, A.L., Kolosova, O.S., Patsenker, L.D., and Terpetschnig, E. a (2007). Tracing lysozyme-lipid interactions with long-wavelength squaraine dyes. J. Fluoresc. *17*, 65–72.

J

Ji, T.H., Grossmann, M., and Ji, I. (1998). G Protein-coupled Receptors: I. Diversity of Receptor-Ligand Interactions. J. Biol. Chem. *273*, 17299–17302.

Jin, D., Liu, H.-X., Hirai, H., Torashima, T., Nagai, T., Lopatina, O., Shnayder, N. a, Yamada, K., Noda, M., Seike, T., et al. (2007). CD38 is critical for social behaviour by regulating oxytocin secretion. Nature *446*, 41–45.

Jores, K., Haberland, A., Wartewig, S., Mäder, K., and Mehnert, W. (2005). Solid Lipid Nanoparticles (SLN) and Oil-Loaded SLN Studied by Spectrofluorometry and Raman Spectroscopy. Pharm. Res. *22*, 1887–1897.

Jose, J., and Burgess, K. (2006). Benzophenoxazine-based fluorescent dyes for labeling biomolecules. Tetrahedron *62*, 11021–11037.

K

Kaiser, E., Colescott, R., Bossinger, C., and Cook, P. (1970). Color test for detection of free terminal amino groups in the solid-phase synthesis of peptides. Anal. Biochem.

Kanamori, T., Kuwayama, K., Tsujikawa, K., Miyaguchi, H., Iwata, Y.T., and Inoue, H. (2011). Synthesis and identification of urinary metabolites of 4-iodo-2,5-dimethoxyphenethylamine. J. Forensic Sci. *56*, 1319–1323.

Kanner, L. (1943). Autistic disturbances of affective contact. Nerv. Child *2*, 217–250.

Karpenko, I.A., Kreder, R., Valencia, C., Villa, P., Mendre, C., Mouillac, B., Mély, Y., Hibert, M., Bonnet, D., and Klymchenko, A.S. (2014). Red fluorescent turn-on ligands for imaging and quantifying G protein-coupled receptors in living cells. Chembiochem *15*, 359–363.

Kashida, H., and Asanuma, H. (2012). Preparation of supramolecular chromophoric assemblies using a DNA duplex. Phys. Chem. Chem. Phys. *14*, 7196–7204.

Kendrick, K.M., Da Costa, A.P., Broad, K.D., Ohkura, S., Guevara, R., Lévy, F., and Keverne, E.B. (1997). Neural control of maternal behaviour and olfactory recognition of offspring. Brain Res. Bull. *44*, 383–395.

Kim, J.-G., and Jang, D. (2007). Mild and Efficient Indium Metal Catalyzed Synthesis of Sulfonamides and Sulfonic Esters. Synlett *2007*, 2501–2504.

Kimura, T., Tanizawa, O., Mori, K., Brownstein, M.J., and Okayama, H. (1992). Structure and expression of a human oxytocin receptor. Nature *356*, 526–529.

Klenerova, V., Krejci, I., and Sida, P. (2009). Modulatory effects of oxytocin and carbetocin on stress-induced changes in rat behavior in the open-field. J. Physiol. 57–62.

Kolakowski, L.F. (1994). GCRDb: a G-protein-coupled receptor database. Receptors Channels *2*, 1–7.

Kosaka, H., Munesue, T., Ishitobi, M., Asano, M., Omori, M., Sato, M., Tomoda, A., and Wada, Y. (2012). Long-term oxytocin administration improves social behaviors in a girl with autistic disorder. BMC Psychiatry *12*, 110.

Kosfeld, M., Heinrichs, M., Zak, P.J., Fischbacher, U., and Fehr, E. (2005). Oxytocin increases trust in humans. Nature *435*, 673–676.

Koshimizu, T.-A., Nakamura, K., Egashira, N., Hiroyama, M., Nonoguchi, H., and Tanoue, A. (2012). Vasopressin v1a and v1b receptors: from molecules to physiological systems. Physiol. Rev. *92*, 1813–1864.

Krieger, F., Mourot, A., Araoz, R., Kotzyba-Hibert, F., Molgó, J., Bamberg, E., and Goeldner, M. (2008). Fluorescent agonists for the Torpedo nicotinic acetylcholine receptor. Chembiochem *9*, 1146–1153.

Kruse, A.C., Ring, A.M., Manglik, A., Hu, J., Hu, K., Eitel, K., Hübner, H., Pardon, E., Valant, C., Sexton, P.M., et al. (2013). Activation and allosteric modulation of a muscarinic acetylcholine receptor. Nature *504*, 101–106.

Kucherak, O.A., Oncul, S., Darwich, Z., Yushchenko, D.A., Arntz, Y., Didier, P., Mély, Y., and Klymchenko, A.S. (2010). Switchable nile red-based probe for cholesterol and lipid order at the outer leaflet of biomembranes. J. Am. Chem. Soc. *132*, 4907–4916.

Kuder, K., and Kieć-Kononowicz, K. (2008). Fluorescent GPCR ligands as new tools in pharmacology. Curr. Med. Chem. *15*, 2132–2143.

L

Lacivita, E., Leopoldo, M., Masotti, A.C., Inglese, C., Berardi, F., Perrone, R., Ganguly, S., Jafurulla, M., and Chattopadhyay, A. (2009). Synthesis and characterization of environment-sensitive fluorescent ligands for human 5-HT1A receptors with 1-arylpiperazine structure. J. Med. Chem. *52*, 7892–7896.

Lakowicz, J.R. (2006). Principles of Fluorescence Spectroscopy (Springer).

Landgraf, R., Gerstberger, R., Montkowski, A., Probst, J.C., Wotjak, C.T., Holsboer, F., and Engelmann, M. (1995). V1 vasopressin receptor antisense oligodeoxynucleotide into septum reduces vasopressin binding, social discrimination abilities, and anxiety-related behavior in rats. J. Neurosci. *15*, 4250–4258.

Landgraf, R., Frank, E., Aldag, J.M., Neumann, I.D., Sharer, C.A., Ren, X., Terwilliger, E.F., Niwa, M., Wigger, A., and Young, L.J. (2003). Viral vector-mediated gene transfer of the vole V1a vasopressin receptor in the rat septum: improved social discrimination and active social behaviour. Eur. J. Neurosci. *18*, 403–411.

Larsen, P., Ulin, J., Dahlstrøm, K., and Jensen, M. (1997). Synthesis of [11C]iodomethane by iodination of [11C]methane. Appl. Radiat. Isot. *48*, 153–157.

Lavis, L.D., and Raines, R.T. (2008). Bright ideas for chemical biology. ACS Chem. Biol. *3*, 142–155.

Lee, P.H. (2000). Development of a Homogeneous High Throughput Fluorescence Polarization Assay for G Protein-Coupled Receptor Binding. J. Biomol. Screen. *5*, 415–419.

Lee, H.-J., Caldwell, H.K., Macbeth, A.H., and Young, W.S. (2008). Behavioural studies using temporal and spatial inactivation of the oxytocin receptor. Prog. Brain Res. *170*, 73–77.

Lefkowitz, R.J., and Shenoy, S.K. (2005). Transduction of receptor signals by beta-arrestins. Science *308*, 512–517.

Lemaire, C., Plenevaux, A., Aerts, J., Fiore, G. Del, Brihaye, C., Bars, D. Le, Comar, D., and Luxen, A. (1999). Solid phase extraction—an alternative to the use of rotary evaporators for solvent removal in the rapid formulation of PET radiopharmaceuticals. J Label. Comp Radiopharm *42*, 63–75.

Leopoldo, M., Lacivita, E., Berardi, F., and Perrone, R. (2009). Developments in fluorescent probes for receptor research. Drug Discov. Today *14*, 706–712.

Levin, J.I., Du, M.T., and Park, K. (2004). Practical Sulfonylation of Amines with 4-Hydroxybenzenesulfonyl Chloride. Synth. Commun. *34:15*, 2773–2781.

Li, Z., and Conti, P.S. (2010). Radiopharmaceutical chemistry for positron emission tomography. Adv. Drug Deliv. Rev. *62*, 1031–1051.

Lim, M.M., and Young, L.J. (2004). Vasopressin-dependent neural circuits underlying pair bond formation in the monogamous prairie vole. Neuroscience *125*, 35–45.

Lin, Y., and Smrcka, A. V (2011). Understanding molecular recognition by G protein βγ subunits on the path to pharmacological targeting. Mol. Pharmacol. *80*, 551–557.

Livesey, A.K., and Brochon, J.C. (1987). Analyzing the distribution of decay constants in pulse-fluorimetry using the maximum entropy method. Biophys. J. *52*, 693–706.

Lloyd, M.T., Mayer, A.C., Subramanian, S., Mourey, D.A., Herman, D.J., Bapat, A. V, Anthony, J.E., and Malliaras, G.G. (2007). Efficient solution-processed photovoltaic cells based on an anthradithiophene/fullerene blend. J. Am. Chem. Soc. *129*, 9144–9149.

Loison, S., Cottet, M., Orcel, H., Adihou, H., Rahmeh, R., Lamarque, L., Trinquet, E., Kellenberger, E., Hibert, M., Durroux, T., et al. (2012). Selective Fluorescent Nonpeptidic Antagonists For Vasopressin V(2) GPCR: Application To Ligand Screening and Oligomerization Assays. J. Med. Chem. *55*, 8588–8602.

Van Londen, L., Goekoop, J.G., van Kempen, G.M., Frankhuijzen-Sierevogel, A.C., Wiegant, V.M., van der Velde, E.A., and De Wied, D. (1997). Plasma levels of arginine vasopressin elevated in patients with major depression. Neuropsychopharmacology *17*, 284–292.

Lourenco, C.M., DaSilva, J.N., Warsh, J.J., Wilson, A.A., and Houle, S. (1999). Imaging of cAMP-specific phosphodiesterase-IV: comparison of [11C]rolipram and [11C]Ro 20-1724 in rats. Synapse *31*, 41–50.

Loving, G.S., Sainlos, M., and Imperiali, B. (2010). Monitoring protein interactions and dynamics with solvatochromic fluorophores. Trends Biotechnol. *28*, 73–83.

Loyens, E., Vermoesen, K., Schallier, A., Michotte, Y., and Smolders, I. (2012). Proconvulsive effects of oxytocin in the generalized pentylenetetrazol mouse model are mediated by vasopressin 1a receptors. Brain Res. *1436*, 43–50.

Ludolph, B., Eisele, F., and Waldmann, H. (2002). Solid-phase synthesis of lipidated peptides. J. Am. Chem. Soc. *124*, 5954–5955.

M

Ma, Z., Du, L., and Li, M. (2014). Toward Fluorescent Probes for G-Protein-Coupled Receptors (GPCRs). J. Med. Chem.

Manning, M., Misicka, A., Olma, A., Bankowski, K., Stoev, S., Chini, B., Durroux, T., Mouillac, B., Corbani, M., and Guillon, G. (2012). Oxytocin and Vasopressin Agonists and Antagonists as Research Tools and Potential Therapeutics. J. Neuroendocrinol. *24*, 609–628.

Mařík, J., Song, A., and Lam, K. (2003). Detection of primary aromatic amines on solid phase. Tetrahedron Lett. *44*, 4319–4320.

Markova, L.I., Malinovskii, V.L., Patsenker, L.D., and Häner, R. (2012). Synthesis and properties of squaraine-modified DNA. Org. Biomol. Chem. *10*, 8944–8947.

Marrero, M.B., Schieffer, B., Paxton, W.G., Heerdt, L., Berk, B.C., Delafontaine, P., and Bernstein, K.E. (1995). Direct stimulation of Jak/STAT pathway by the angiotensin II AT1 receptor. Nature *375*, 247–250.

Mawhinney, T.P., and Madson, M.A. (1982). N-Methyl-N-(tert-butyldimet hylsily) trifluoro acetamide and Related N-tert -Butyldimethylsilyl Amides as Protective Silyl Donor. J. Org. Chem. *47*, 3336–3339.

Mayer, J., and Heil, J. (1995). An alternative solid-phase approach to C1-oxytocin. Tetrahedron Lett. *36*, 7387–7390.

Melamed, E., Lahar, M., and Atlas, D. (1976). Direct localisation of β-adrenoceptor sites in rat cerebellum by a new fluorescent analogue of propranolol. Nature *261*, 420–422.

Meyer-Lindenberg, A., Domes, G., Kirsch, P., and Heinrichs, M. (2011). Oxytocin and vasopressin in the human brain: social neuropeptides for translational medicine. Nat. Rev. Neurosci. *12*, 524–538.

Michalet, X., Weiss, S., and Jäger, M. (2006). Single-molecule fluorescence studies of protein folding and conformational dynamics. Chem. Rev. *106*, 1785–1813.

Miller, J., Kumar, D., Mann, J.J., and Parsey, R. V. (2008a). Applications of Positron Emission Tomography in Neuropsychiatric Pharmaceutical Drug Development. Curr. Radiopharm. *1*, 12–16.

Miller, P.W., Long, N.J., Vilar, R., and Gee, A.D. (2008b). Synthesis of 11C, 18F, 15O, and 13N Radiolabels for Positron Emission Tomography. Angew. Chemie Int. Ed. *47*, 8998–9033.

Mouillac, B., Manning, M., and Durroux, T. (2008). Fluorescent agonists and antagonists for vasopressin/oxytocin G protein-coupled receptors: usefulness in ligand screening assays and receptor studies. Mini Rev. Med. Chem. *8*, 996–1005.

Murphy, P.S., McCarthy, T.J., and Dzik-Jurasz, a S.K. (2008). The role of clinical imaging in oncological drug development. Br. J. Radiol. *81*, 685–692.

N

Nadler, A., and Schultz, C. (2013). The power of fluorogenic probes. Angew. Chem. Int. Ed. Engl. *52*, 2408–2410.

Nathans, J., and Hogness, D.S. (1983). Isolation, sequence analysis, and intron-exon arrangement of the gene encoding bovine rhodopsin. Cell *34*, 807–814.

Nchimi-Nono, K., Wegner, K.D., Lindén, S., Lecointre, A., Ehret-Sabatier, L., Shakir, S., Hildebrandt, N., and Charbonnière, L.J. (2013). Activated phosphonated trifunctional chelates for highly sensitive lanthanide-based FRET immunoassays applied to total prostate specific antigen detection. Org. Biomol. Chem. *11*, 6493–6501.

Nephew, B. (2012). Behavioral Roles of Oxytocin and Vasopressin. Neuroendocrinol. Behav. InTech, Rijeka.

Nephew, B.C., and Bridges, R.S. (2008). Central actions of arginine vasopressin and a V1a receptor antagonist on maternal aggression, maternal behavior, and grooming in lactating rats. Pharmacol. Biochem. Behav. *91*, 77–83.

Nephew, B.C., Bridges, R.S., Lovelock, D.F., and Byrnes, E.M. (2009). Enhanced maternal aggression and associated changes in neuropeptide gene expression in multiparous rats. Behav. Neurosci. *123*, 949–957.

Neumann, I.D., and Landgraf, R. (2012). Balance of brain oxytocin and vasopressin: implications for anxiety, depression, and social behaviors. Trends Neurosci. 1–11.

Neumann, I.D., Torner, L., and Wigger, A. (2000). Brain oxytocin: differential inhibition of neuroendocrine stress responses and anxiety-related behaviour in virgin, pregnant and lactating rats. Neuroscience *95*, 567–575.

O

Ocampo Daza, D., Lewicka, M., and Larhammar, D. (2012). The oxytocin/vasopressin receptor family has at least five members in the gnathostome lineage, inclucing two distinct V2 subtypes. Gen. Comp. Endocrinol. *175*, 135–143.

Or, Y.S., Clark, R.F., and Luly, J.R. (1991). Cysteine alkylation in unprotected peptides: synthesis of a carbavasopressin analog by intramolecular cysteine alkylation. J. Org. Chem. *56*, 3146–3149.

P

Palakurthy, N.B., and Mandal, B. (2011). Sulfonamide synthesis using N-hydroxybenzotriazole sulfonate: an alternative to pentafluorophenyl (PFP) and trichlorophenyl (TCP) esters of sulfonic acids. Tetrahedron Lett. *52*, 7132–7134.

Palczewski, K. (2000). Crystal Structure of Rhodopsin: A G Protein-Coupled Receptor. Science (80-.). *289*, 739–745.

Park, J.H., Morizumi, T., Li, Y., Hong, J.E., Pai, E.F., Hofmann, K.P., Choe, H.-W., and Ernst, O.P. (2013). Opsin, a structural model for olfactory receptors? Angew. Chem. Int. Ed. Engl. *52*, 11021–11024.

Parker, N., Turk, M.J., Westrick, E., Lewis, J.D., Low, P.S., and Leamon, C.P. (2005). Folate receptor expression in carcinomas and normal tissues determined by a quantitative radioligand binding assay. Anal. Biochem. *338*, 284–293.

Paxinos, G., and Watson, C. (1998). Atlas of the Developing Mouse Brain: At E17.5, PO, and, Page 6 (Academic Press).

Pedersen, C.A., and Prange, A.J. (1979). Induction of maternal behavior in virgin rats after intracerebroventricular administration of oxytocin. Proc. Natl. Acad. Sci. U. S. A. *76*, 6661–6665.

Pietrowsky, R., Fehm-Wolfsdorf, G., Born, J., and Fehm, H.L. (1988). Effects of DGAVP on verbal memory. Peptides *9*, 1361–1366.

Pilla, M., Perachon, S., Sautel, F., Garrido, F., Mann, A., Wermuth, C.G., Schwartz, J.C., Everitt, B.J., and Sokoloff, P. (1999). Selective inhibition of cocaine-seeking behaviour by a partial dopamine D3 receptor agonist. Nature *400*, 371–375.

Pisoni, D.D.S., de Abreu, M.P., Petzhold, C.L., Rodembusch, F.S., and Campo, L.F. (2013). Synthesis, photophysical study and BSA association of water-insoluble squaraine dyes. J. Photochem. Photobiol. A Chem. *252*, 77–83.

Pitkow, L.J., Sharer, C.A., Ren, X., Insel, T.R., Terwilliger, E.F., and Young, L.J. (2001). Facilitation of affiliation and pair-bond formation by vasopressin receptor gene transfer into the ventral forebrain of a monogamous vole. J. Neurosci. *21*, 7392–7396.

Polucci, P., Magnaghi, P., Angiolini, M., Asa, D., Avanzi, N., Badari, A., Bertrand, J., Casale, E., Cauteruccio, S., Cirla, A., et al. (2013). Alkylsulfanyl-1,2,4-triazoles, a new class of allosteric valosine containing protein inhibitors. Synthesis and structure-activity relationships. J. Med. Chem. *56*, 437–450.

Postina, R., Kojro, E., and Fahrenholz, F. (1996). Separate Agonist and Peptide Antagonist Binding Sites of the Oxytocin Receptor Defined by Their Transfer into the V2 Vasopressin Receptor. J. Biol. Chem. *271*, 31593–31601.

Premont, R.T., and Gainetdinov, R.R. (2007). Physiological roles of G protein-coupled receptor kinases and arrestins. Annu. Rev. Physiol. *69*, 511–534.

R

Rajagopal, K., Lefkowitz, R.J., and Rockman, H.A. (2005). When 7 transmembrane receptors are not G protein-coupled receptors. J. Clin. Invest. *115*, 2971–2974.

Rapozzi, V., Beverina, L., Salice, P., Pagani, G. a, Camerin, M., and Xodo, L.E. (2010). Photooxidation and Phototoxicity of pi-extended squaraines. J. Med. Chem. *53*, 2188–2196.

Rasmussen, S.G.F., Choi, H.-J., Fung, J.J., Pardon, E., Casarosa, P., Chae, P.S., Devree, B.T., Rosenbaum, D.M., Thian, F.S., Kobilka, T.S., et al. (2011). Structure of a nanobody-stabilized active state of the β(2) adrenoceptor. Nature *469*, 175–180.

Reichardt, C. (1994). Solvatochromic Dyes as Solvent Polarity Indicators. Chem. Rev. *94*, 2319–2358.

Riddell, D.C., Mallonee, R., Phillips, J.A., Parks, J.S., Sexton, L.A., and Hamerton, J.L. (1985). Chromosomal assignment of human sequences encoding arginine vasopressin-neurophysin II and growth hormone releasing factor. Somat. Cell Mol. Genet. *11*, 189–195.

Rijkers, D.T.S., Kruijtzer, J.A.W., Killian, J.A., and Liskamp, R.M.J. (2005). A convenient solid phase synthesis of S-palmitoyl transmembrane peptides. Tetrahedron Lett. *46*, 3341–3345.

Rilling, J.K., Demarco, A.C., Hackett, P.D., Thompson, R., Ditzen, B., Patel, R., and Pagnoni, G. (2011). Effects of intranasal oxytocin and vasopressin on cooperative behavior and associated brain activity in men. Psychoneuroendocrinology *37*, 447–461.

Rimmele, U., Hediger, K., Heinrichs, M., and Klaver, P. (2009). Oxytocin makes a face in memory familiar. J. Neurosci. *29*, 38–42.

Romieu, A., Brossard, D., Hamon, M., Outaabout, H., Portal, C., and Renard, P.-Y. (2008). Postsynthetic derivatization of fluorophores with alpha-sulfo-beta-alanine dipeptide linker. Application to the preparation of water-soluble cyanine and rhodamine dyes. Bioconjug. Chem. *19*, 279–289.

Rosenbaum, D.M., Rasmussen, S.G.F., and Kobilka, B.K. (2009). The structure and function of G-protein-coupled receptors. Nature *459*, 356–363.

Rosenbaum, D.M., Zhang, C., Lyons, J.A., Holl, R., Aragao, D., Arlow, D.H., Rasmussen, S.G.F., Choi, H.-J., Devree, B.T., Sunahara, R.K., et al. (2011). Structure and function of an irreversible agonist-β(2) adrenoceptor complex. Nature *469*, 236–240.

Ros-Lis, J. V, Martínez-Máñez, R., and Soto, J. (2002). A selective chromogenic reagent for cyanide determination. Chem. Commun. (Camb). 2248–2249.

Ros-Lis, J. V, García, B., Jiménez, D., Martínez-Máñez, R., Sancenón, F., Soto, J., Gonzalvo, F., and Valldecabres, M.C. (2004). Squaraines as fluoro-chromogenic probes for thiol-containing compounds and their application to the detection of biorelevant thiols. J. Am. Chem. Soc. *126*, 4064–4065.

Roux, B.T., and Cottrell, G.S. (2014). G protein-coupled receptors: what a difference a "partner" makes.

Royer, C. a (2006). Probing protein folding and conformational transitions with fluorescence. Chem. Rev. *106*, 1769–1784.

Rozenfeld, R., and Devi, L. a (2010). Receptor heteromerization and drug discovery. Trends Pharmacol. Sci. *31*, 124–130.

S

Sackett, D.L., and Wolff, J. (1987). Nile red as a polarity-sensitive fluorescent probe of hydrophobic protein surfaces. Anal. Biochem. *167*, 228–234.

Scherer, D., Dörfler, R., Feldner, A., Vogtmann, T., Schwoerer, M., Lawrentz, U., Grahn, W., and Lambert, C. (2002). Two-photon states in squaraine monomers and oligomers. Chem. Phys. *279*, 179–207.

Schönberger, M., Leggett, C., Kim, S.W., and Hooker, J.M. (2010). Synthesis of [11C]SSR149415 and preliminary imaging studies using positron emission tomography. Bioorg. Med. Chem. Lett. *20*, 3103–3106.

Sekiguchi, H., Muranaka, K., Osada, A., Ichikawa, S., and Matsuda, A. (2010). Efficient synthesis of Hsp90 inhibitor dimers as potential antitumor agents. Bioorg. Med. Chem. *18*, 5732–5737.

Shafeekh, K.M., Soumya, M.S., Rahim, M. a, Abraham, A., and Das, S. (2014). Synthesis and characterization of near-infrared absorbing water soluble squaraines and study of their photodynamic effects in DLA live cells. Photochem. Photobiol. *90*, 585–595.

Shi, C., Shin, Y.-O., Hanson, J., Cass, B., Loewen, M.C., and Durocher, Y. (2005). Purification and characterization of a recombinant G-protein-coupled receptor, Saccharomyces cerevisiae Ste2p, transiently expressed in HEK293 EBNA1 cells. Biochemistry *44*, 15705–15714.

Shorr, R., and Heald, S. (1982). The beta-adrenergic receptor: rapid purification and covalent labeling by photoaffinity crosslinking. Proc. Natl. Acad. Sci. U. S. A. *256*, 5820–5826.

Silvestri, F., Irwin, M.D., Beverina, L., Facchetti, A., Pagani, G.A., and Marks, T.J. (2008). Efficient squaraine-based solution processable bulk-heterojunction solar cells. J. Am. Chem. Soc. *130*, 17640–17641.

Skrundz, M., Bolten, M., Nast, I., Hellhammer, D.H., and Meinlschmidt, G. (2011). Plasma oxytocin concentration during pregnancy is associated with development of postpartum depression. Neuropsychopharmacology *36*, 1886–1893.

Smith, A.L., Freeman, S.M., Stehouwer, J.S., Inoue, K., Voll, R.J., Young, L.J., and Goodman, M.M. (2012). Synthesis and evaluation of C-11, F-18 and I-125 small molecule radioligands for detecting oxytocin receptors. Bioorg. Med. Chem. *20*, 2721–2738.

Smith, A.L., Freeman, S.M., Voll, R.J., Young, L.J., and Goodman, M.M. (2013a). Carbon-11 N-methyl alkylation of L-368,899 and in vivo PET imaging investigations for neural oxytocin receptors. Bioorg. Med. Chem. Lett. *23*, 902–906.

Smith, A.L., Freeman, S.M., Voll, R.J., Young, L.J., and Goodman, M.M. (2013b). Investigation of an F-18 oxytocin receptor selective ligand via PET imaging. Bioorg. Med. Chem. Lett. *23*, 5415–5420.

Smith, P., Krohn, R., and Hermanson, G. (1985). Measurement of protein using bicinchoninic acid. Anal. Biochem. *150*, 76–85.

Snowdon, C.T., Pieper, B.A., Boe, C.Y., Cronin, K.A., Kurian, A. V, and Ziegler, T.E. (2010). Variation in oxytocin is related to variation in affiliative behavior in monogamous, pairbonded tamarins. Horm. Behav. *58*, 614–618.

Soriano, A., Ventura, R., Molero, A., Hoen, R., Casadó, V., Cortés, A., Fanelli, F., Albericio, F., Lluís, C., Franco, R., et al. (2009). Adenosine A2A receptor-antagonist/dopamine D2 receptor-agonist bivalent ligands as pharmacological tools to detect A2A-D2 receptor heteromers. J. Med. Chem. *52*, 5590–5602.

Sreejith, S., Divya, K.P., and Ajayaghosh, A. (2008). A near-infrared squaraine dye as a latent ratiometric fluorophore for the detection of aminothiol content in blood plasma. Angew. Chem. Int. Ed. Engl. *47*, 7883–7887.

Sridharan, R., Zuber, J., Connelly, S.M., Mathew, E., and Dumont, M.E. (2014). Fluorescent approaches for understanding interactions of ligands with G protein coupled receptors. Biochim. Biophys. Acta *1838*, 15–33.

Srivastava, A., Yano, J., Hirozane, Y., Kefala, G., Gruswitz, F., Snell, G., Lane, W., Ivetac, A., Aertgeerts, K., Nguyen, J., et al. (2014). High-resolution structure of the human GPR40 receptor bound to allosteric agonist TAK-875. Nature.

Stacey, M., Lin, H.H., Gordon, S., and McKnight, A.J. (2000). LNB-TM7, a group of seven-transmembrane proteins related to family-B G-protein-coupled receptors. Trends Biochem. Sci. *25*, 284–289.

Steinwall, M., Bossmar, T., Brouard, R., Laudanski, T., Olofsson, P., Urban, R., Wolff, K., Le-Fur, G., and Akerlund, M. (2005). The effect of relcovaptan (SR 49059), an orally active vasopressin V1a receptor antagonist, on uterine contractions in preterm labor. Gynecol. Endocrinol. *20*, 104–109.

Stevenson, E.L., and Caldwell, H.K. (2012). The vasopressin 1b receptor and the neural regulation of social behavior. Horm. Behav. *61*, 277–282.

Sugimoto, T., Saito, M., Mochizuki, S., Watanabe, Y., Hashimoto, S., and Kawashima, H. (1994). Molecular cloning and functional expression of a cDNA encoding the human V1b vasopressin receptor. J. Biol. Chem. *269*, 27088–27092.

T

Takayanagi, Y., Yoshida, M., Bielsky, I.F., Ross, H.E., Kawamata, M., Onaka, T., Yanagisawa, T., Kimura, T., Matzuk, M.M., Young, L.J., et al. (2005). Pervasive social deficits, but normal parturition, in oxytocin receptor-deficient mice. Proc. Natl. Acad. Sci. U. S. A. *102*, 16096–16101.

Taylor, S.E., Saphire-Bernstein, S., and Seeman, T.E. (2010). Are plasma oxytocin in women and plasma vasopressin in men biomarkers of distressed pair-bond relationships? Psychol. Sci. *21*, 3–7.

Terrillon, S., Cheng, L.L., Stoev, S., Mouillac, B., Barberis, C., Manning, M., and Durroux, T. (2002). Synthesis and characterization of fluorescent antagonists and agonists for human oxytocin and vasopressin V1a receptors. J. Med. Chem. *45*, 2579–2588.

Texier, I., Goutayer, M., Da Silva, A., Guyon, L., Djaker, N., Josserand, V., Neumann, E., Bibette, J., and Vinet, F. (2009). Cyanine-loaded lipid nanoparticles for improved in vivo fluorescence imaging. J. Biomed. Opt. *14*, 054005.

Theodore, W.H. (2000). PET: cerebral blood flow and glucose metabolism--pathophysiology and drug effects. Adv. Neurol. *83*, 121–130.

Thibonnier, M., Auzan, C., Madhun, Z., Wilkins, P., Berti-Mattera, L., and Clauser, E. (1994). Molecular cloning, sequencing, and functional expression of a cDNA encoding the human V1a vasopressin receptor. J. Biol. Chem. *269*, 3304–3310.

Thibonnier, M., Preston, J.A., Dulin, N., Wilkins, P.L., Berti-Mattera, L.N., and Mattera, R. (1997). The human V3 pituitary vasopressin receptor: ligand binding profile and density-dependent signaling pathways. Endocrinology *138*, 4109–4122.

Thibonnier, M., Berti-Mattera, L.N., Dulin, N., Conarty, D.M., and Mattera, R. (1998). Signal transduction pathways of the human V1-vascular, V2-renal, V3-pituitary vasopressin and oxytocin receptors. Prog. Brain Res. *119*, 147–161.

Thibonnier, M., Conarty, D.M., Preston, J.A., Plesnicher, C.L., Dweik, R.A., and Erzurum, S.C. (1999). Human vascular endothelial cells express oxytocin receptors. Endocrinology *140*, 1301–1309.

Treibs, A., and Jacob, K. (1965). Cyclotrimethine Dyes Derived from Squaric Acid. Angew. Chemie Int. Ed. English *4*, 694–694.

U

Urban, J.D., Clarke, W.P., von Zastrow, M., Nichols, D.E., Kobilka, B., Weinstein, H., Javitch, J.A., Roth, B.L., Christopoulos, A., Sexton, P.M., et al. (2007). Functional selectivity and classical concepts of quantitative pharmacology. J. Pharmacol. Exp. Ther. *320*, 1–13.

Uvnäs-Mobcrg, K., Widström, A.-M., Nissen, E., and Björvell, H. (1990). Personality traits in women 4 days postpartum and their correlation with plasma levels of oxytocin and prolactin. J. Psychosom. Obstet. Gynecol. *11*, 261–273.

V

Du Vigneaud, V., Ressler, C., and Trippett, S. (1953). The sequence of amino acids in oxytocin, with a proposal for the structure of oxytocin. J. Biol. Chem. *205*, 949–957.

Villhauer, E.B., Brinkman, J.A., Naderi, G.B., Dunning, B.E., Mangold, B.L., Mone, M.D., Russell, M.E., Weldon, S.C., and Hughes, T.E. (2002). 1-[2-[(5-Cyanopyridin-2-yl)amino]ethylamino]acetyl-2-(S)-pyrrolidinecarbonitrile: A Potent, Selective, and Orally Bioavailable Dipeptidyl Peptidase IV Inhibitor with Antihyperglycemic Properties. J. Med. Chem. *45*, 2362–2365.

W

Wacker, D., Wang, C., Katritch, V., Han, G.W., Huang, X.-P., Vardy, E., McCorvy, J.D., Jiang, Y., Chu, M., Siu, F.Y., et al. (2013). Structural features for functional selectivity at serotonin receptors. Science *340*, 615–619.

Wagnon, J., Serradeil-Le Gal, C., Tonnerre, B., Plouzane, C., and Nisato, D. (1992). Dérives d'indoline portant une fonction amidique, leur préparation, les compositions plarmaceutiques en contenant. European Patent 0 526 348 A1.

Waller, A., Simons, P.C., Biggs, S.M., Edwards, B.S., Prossnitz, E.R., and Sklar, L. a (2004). Techniques: GPCR assembly, pharmacology and screening by flow cytometry. Trends Pharmacol. Sci. *25*, 663–669.

Wang, T. (2013). The complexity of G-protein coupled receptor-ligand interactions. Sci. China Chem. *56*, 1344–1350.

Wang, S., Li, N., Pan, W., and Tang, B. (2012). Advances in functional fluorescent and luminescent probes for imaging intracellular small-molecule reactive species. TrAC Trends Anal. Chem. *39*, 3–37.

Warne, T., Serrano-Vega, M.J., Baker, J.G., Moukhametzianov, R., Edwards, P.C., Henderson, R., Leslie, A.G.W., Tate, C.G., and Schertler, G.F.X. (2008). Structure of a beta1-adrenergic G-protein-coupled receptor. Nature *454*, 486–491.

Weibel, N., Charbonnière, L.J., Guardigli, M., Roda, A., and Ziessel, R. (2004). Engineering of highly luminescent lanthanide tags suitable for protein labeling and time-resolved luminescence imaging. J. Am. Chem. Soc. *126*, 4888–4896.

Weill, N., Valencia, C., Gioria, S., Villa, P., Hibert, M., and Rognan, D. (2011). Identification of Nonpeptide Oxytocin Receptor Ligands by Receptor-Ligand Fingerprint Similarity Search. Mol. Inform. *30*, 521–526.

Wersinger, S.R., Ginns, E.I., O'Carroll, A.-M., Lolait, S.J., and Young, W.S. (2002). Vasopressin V1b receptor knockout reduces aggressive behavior in male mice. Mol. Psychiatry *7*, 975–984.

Van West, D., Del-Favero, J., Aulchenko, Y., Oswald, P., Souery, D., Forsgren, T., Sluijs, S., Bel-Kacem, S., Adolfsson, R., Mendlewicz, J., et al. (2004). A major SNP haplotype of the arginine vasopressin 1B receptor protects against recurrent major depression. Mol. Psychiatry *9*, 287–292.

Wigger, A., Sánchez, M.M., Mathys, K.C., Ebner, K., Frank, E., Liu, D., Kresse, A., Neumann, I.D., Holsboer, F., Plotsky, P.M., et al. (2004). Alterations in central neuropeptide expression, release, and receptor binding in rats bred for high anxiety: critical role of vasopressin. Neuropsychopharmacology *29*, 1–14.

Winslow, J.T., and Insel, T.R. (2002). The social deficits of the oxytocin knockout mouse. Neuropeptides *36*, 221–229.

Winslow, J.T., Hastings, N., Carter, C.S., Harbaugh, C.R., and Insel, T.R. (1993). A role for central vasopressin in pair bonding in monogamous prairie voles. Nature *365*, 545–548.

Wombacher, R., and Cornish, V.W. (2011). Chemical tags: applications in live cell fluorescence imaging. J. Biophotonics *4*, 391–402.

X

Xu, F., Wu, H., Katritch, V., Han, G.W., Jacobson, K.A., Gao, Z.-G., Cherezov, V., and Stevens, R.C. (2011a). Structure of an agonist-bound human A2A adenosine receptor. Science *332*, 322–327.

Xu, J., Corneillie, T.M., Moore, E.G., Law, G.-L., Butlin, N.G., and Raymond, K.N. (2011b). Octadentate cages of Tb(III) 2-hydroxyisophthalamides: a new standard for luminescent lanthanide labels. J. Am. Chem. Soc. *133*, 19900–19910.

Y

Yang, J., and Zhang, Y. (2014). GPCRSD: a database for experimentally solved GPCR structures. (http://zhanglab.ccmb.med.umich.edu/GPCRSD/).

Yang, Y., Zhao, Q., Feng, W., and Li, F. (2013). Luminescent chemodosimeters for bioimaging. Chem. Rev. *113*, 192–270.

Yuan, L., Lin, W., Zheng, K., He, L., and Huang, W. (2013). Far-red to near infrared analyte-responsive fluorescent probes based on organic fluorophore platforms for fluorescence imaging. Chem. Soc. Rev. *42*, 622–661.

Z

Zanos, P., Georgiou, P., Wright, S.R., Hourani, S.M., Kitchen, I., Winsky-Sommerer, R., and Bailey, A. (2014). The oxytocin analogue carbetocin prevents emotional impairment and stress-induced reinstatement of opioid-seeking in morphine-abstinent mice. Neuropsychopharmacology *39*, 855–865.

Zhang, J., Zhang, K., Gao, Z.-G., Paoletta, S., Zhang, D., Han, G.W., Li, T., Ma, L., Zhang, W., Müller, C.E., et al. (2014). Agonist-bound structure of the human P2Y12 receptor. Nature *509*, 119–122.

Zheng, H., Loh, H.H., and Law, P.-Y. (2010). Agonist-selective signaling of G protein-coupled receptor: mechanisms and implications. IUBMB Life *62*, 112–119.

Zwier, J.M., Roux, T., Cottet, M., Durroux, T., Douzon, S., Bdioui, S., Gregor, N., Bourrier, E., Oueslati, N., Nicolas, L., et al. (2010). A fluorescent ligand-binding alternative using Tag-lite® technology. J. Biomol. Screen. *15*, 1248–1259 .

Iuliia KARPENKO

Conception, synthèse et évaluation de sondes fluorescentes et de radioligands TEP des récepteurs de l'ocytocine et de la vasopressine

Laboratoire d'Innovation Thérapeutique
UMR 7200 CNRS - Unistra

Résumé

Les récepteurs de l'ocytocine et de la vasopressine sont connus pour être impliqués dans la modulation d'effets centraux complexes comme l'amour, l'attachement mère-enfant, l'altruisme, la générosité et la confiance. Récemment le récepteur de l'ocytocine a été proposé comme une cible thérapeutique potentielle pour le traitement des troubles du spectre autistique, les troubles du développement humain caractérisés par des anormalités dans la communication, les interactions sociales et le comportement répétitif.

Afin de mieux comprendre le rôle des récepteurs de l'ocytocine et de la vasopressine dans les troubles du spectre autistique, d'éclaircir des nouveaux traits de sa pharmacologie et d'établir des méthodes du criblage à haut débit sur les récepteurs sauvages, nous avons développé des traceurs pour la tomographie par émission des positons ainsi que des sondes fluorescentes pour la famille ocytocine/vasopressine des RCPG. Les ligands fluorescents ont été utilisés pour établir un test de liaison TR-FRET pour l'OTR et pour initier le développement du test alternatif sur les récepteurs sauvages. Les radiotraceurs TEP seront bientôt testés chez la souris et chez le singe pour évaluer leurs performances pour la détection des récepteurs de l'ocytocine centraux avant d'envisager des études chez l'Homme.

Mots-clés : RCPG, ocytocine, vasopressine, TEP, radiotraceurs, fluorescence, sondes fluorescentes, TR-FRET, criblage à haut débit.

Abstract

The oxytocin and the vasopressin G protein-coupled receptors are known to be involved in the modulation of complex social behaviors such as love, mother-child attachment, altruism, generosity and trust. Recently, the oxytocin receptor was proposed as a potential target for the treatment of autism spectrum disorders (ASD), neurodevelopmental disorders which are characterized by difficulties in communication, social functioning and repetitive behavior.

In order to better understand the role of the oxytocin and the vasopressin receptors in ASD, to reveal new features in its pharmacology and signaling and to establish high-throughput screening method on wild-type G protein-coupled receptors, we developed imaging probes for the oxytocin-vasopressin receptors family, namely radiotracers for positron emission tomography and optical probes for fluorescence detection and imaging. The fluorescent ligands have been used to establish TR-FRET binding assay for OTR and to initiate the development the screening assay for the wild-type oxytocin receptor. The PET radiotracers will be shortly tested in mice and monkeys to evaluate their potency in detecting the central oxytocin receptors.

Key-words: GPCR, oxytocin, vasopressin, PET, radiotracers, fluorescence, fluorescent probes, TR-FRET, high-throughput screening.